2015

Characterization of Bacterial Metabolites Involved in Host Pathogen Resistance

Kavita J. Rangan

CHARACTERIZATION OF BACTERIAL METABOLITES INVOLVED IN HOST PATHOGEN RESISTANCE

A Thesis Presented to the Faculty of

The Rockefeller University

in Partial Fulfillment of the Requirements for

the degree of Doctor of Philosophy

by

Kavita J. Rangan

June 2015

CHARACTERIZATION OF BACTERIAL METABOLITES INVOLVED IN HOST PATHOGEN RESISTANCE

Kavita J. Rangan, Ph.D.

The Rockefeller University 2015

The intestinal microbiome can mediate host resistance to enteric pathogens by modulating host immunity or by directly inhibiting pathogen growth and virulence. Although the abundance and diversity of bacterial metabolites in the intestine is appreciated, the majority of intestinal bacteria and bacterial products have not been characterized in the context of microbiota-mediated pathogen resistance. In this thesis, we describe two projects aimed at developing new methodologies to study how intestinal bacteria, and the metabolites they generate, inhibit bacterial pathogenesis.

In Chapters 2 and 3, we use a chemical reporter strategy to analyze fatty acid protein modifications in bacteria. Dietary and bacterially-produced fatty acids can modulate the virulence of various pathogens, such as *Salmonella typhimurium*, possibly through covalent protein modification. We demonstrate that alkynyl-functionalized fatty acids can be metabolized and covalently attached to known fatty-acylated proteins in *E. coli*. Proteomic analysis of modified proteins revealed an unconventional fatty-acid modification on the metabolic enzyme YjgF, highlighting the utility of this method for the discovery of novel sites of fatty-acylation. Using these reporters, we also explored the effects of fatty acids on *S. typhimurium* virulence. Our results in *S. typhimurium* underscored the extensive fatty acid metabolism of this pathogen as compared to *E. coli*,

and revealed a potential fatty acid modification on the virulence factor HilA. In addition, we demonstrated that alkynyl-functionalized short chain fatty acids, like natural fatty acids, can inhibit the secretion of *Salmonella* virulence factors *in vitro*. Overall, our results suggest that alkynyl-functionalized fatty acids may be useful for analyzing *Salmonella* metabolism and virulence.

In Chapter 4, we describe a *C. elegans* model system that we used to investigate the effects of *Enterococcus faecium* on bacterial pathogenesis. Probiotic strains of *E. faecium* can inhibit the virulence of several intestinal pathogens, including *Salmonella typhimurium*, but it is unknown if *E. faecium* directly targets pathogens or modulates host immunity. Through a combination of genetic, biochemical, and proteomic approaches, we identified a secreted peptidoglycan hydrolase (SagA) from *E. faecium* that confers protection against *Salmonella* pathogenesis. Our results indicate that SagA does not directly inhibit pathogen growth, but instead remodels peptidoglycan *in vivo* to enhance host resistance to pathogenesis. We define specific peptidoglycan fragments that are sufficient for mediating host protection, and show that this protection requires the host gene *tol-1*. Notably, introduction of SagA into a non-protective intestinal bacteria, *E. faecalis*, is sufficient to mediate host protection in *C. elegans* as well as germ-free mice, suggesting that SagA acts through evolutionarily conserved host pathways. We hypothesize that SagA-generated peptidoglycan fragments may strengthen intestinal barrier integrity through local innate immune activation to confine pathogens to the intestinal lumen. Our results suggest that commensal bacteria can restrict intestinal pathogens by directly modifying microbial-associated molecular patterns in the intestine.

Overall, the projects described in this thesis underscore the role of bacterial metabolites, such as fatty acids and peptidoglycan fragments, in restricting intestinal pathogens.

For my parents.

ACKNOWLEDGEMENTS

I would like to thank my advisor, Howard Hang, for his continued mentorship over the last 7 years. I feel like I've seen the lab, and the people in it, transition so much. Thanks to the "original" Hang lab members, especially: Paul Dossa, Markus Grammel, Ann Raghavan, Kelvin Tsou, Jacob Yount, and Ming-zi Zhang for being fantastic colleagues and friends. They made the lab a fun and uniquely vibrant place for many years. I'd also like to thank the current members of the lab, especially Tao Peng and Xiaoqiu Yuan for their friendship and support.

I greatly appreciate the guidance, support, and insight of my committee members, Cori Bargmann, Vince Fischetti, and Daniel Mucida. In particular, I would like to thank Cori Bargmann and the entire Bargmann lab. They have always met me with warmth and friendship, and have helped me along the way in both work and spirit. I'd also like to thank Eric Pamer, for graciously agreeing to be on my committee and review my thesis.

Immeasurable thanks to my family and friends, whose support and love have made the completion of graduate school possible. To my friend, Taro Ohkawa, who is a meticulous scientist, and a patient teacher. His mentorship in college was a huge impetus for me to pursue graduate school. Thank you to my grandmother, Ammama, who is a contendable force in this world, and lives her life with tremendous strength. I'd also like to thank my brothers, Adi, Gau, and Keshav, whose thoughtfulness and individuality I cherish. I cannot thank my parents enough; they have always supported me unconditionally and have taught me everything. They live by a beautiful life philosophy,

and continually inspire me. Finally, thank you to my loving husband, Donovan Ventimiglia, who is an extraordinary thinker, teacher, and my best friend. I feel so lucky to be in his wolf pack.

TABLE OF CONTENTS

LIST OF FIGURES

CHAPTER 1.

CHAPTER 2.

CHAPTER 3.

CHAPTER 4.

LIST OF TABLES

CHAPTER 2.

CHAPTER 4.

CHAPTER 1. Mechanisms of pathogen restriction by the intestinal microbiome

Composed of over 10^{13} cells from some 300 different species, the human intestinal microbiome regulates host nutrition and metabolism, immune system maturation and homeostasis[1], and resistance to enteric pathogens[2-4]. Despite individual heterogeneity in microbial composition, trends in community structure can be correlated with host health and disease[5]. Microbial dysbiosis is associated with various diseases, including: allergy[6], diabetes[7], obesity[8], and inflammatory bowel disease[9]. The importance of the microbiome in pathogen restriction is broadly demonstrated in germ-free and antibiotic-treated animals, which exhibit chronic colitis and an increased susceptibility to bacterial pathobionts and pathogens[10-12].

Over the last decade, various mechanisms of pathogen restriction by the intestinal microbiome have been elucidated. These fall generally into two categories, namely: (1.) The modulation of host immunity to restrict pathogens and (2.) The direct inhibition of pathogen growth and virulence (Figure 1.1). In this Chapter, we will discuss these modes of commensal-mediated pathogen restriction, with a focus on the molecular and genetic bacterial factors involved.

Mechanisms of pathogen restriction through host immunomodulation.

Recognition of microbial-associated molecular patterns (MAMPs) by both intestinal epithelial cells and lymphoid cells is required for proper immune system development and response to bacterial pathogens[13]. MAMPs are conserved microbial

factors, such as bacterial cell-surface components, that elicit innate immune responses upon recognition by pattern recognition receptors. Toll-like receptors, Nod-like receptors, and C-type lectin receptors all respond to MAMPs derived from commensal bacteria and pathogens alike.

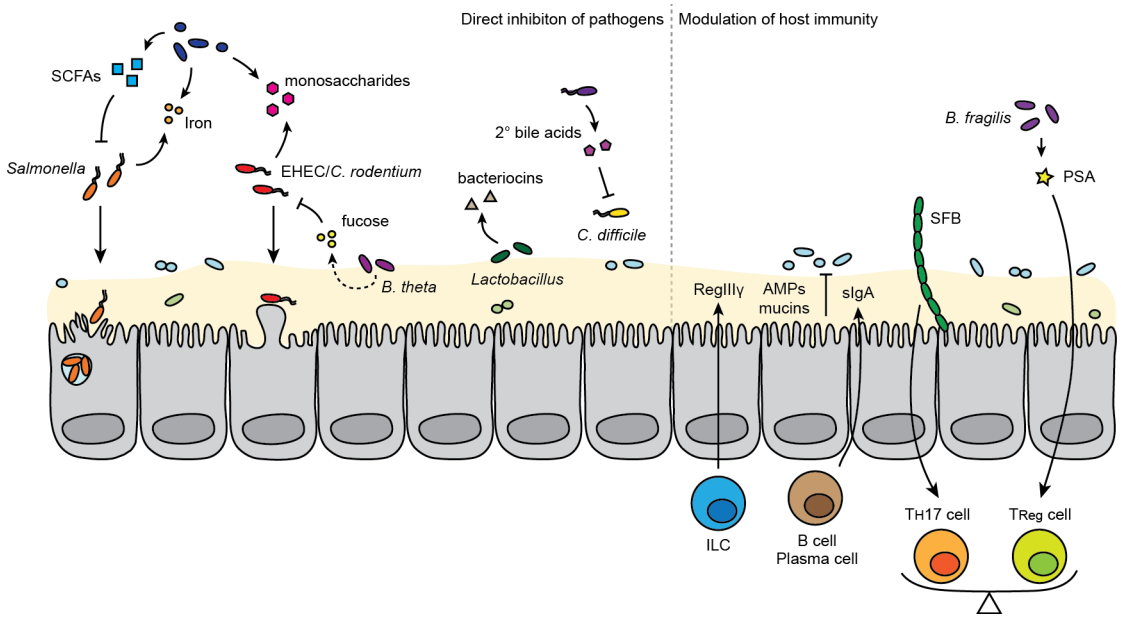

Figure 1.1. An overview of microbiota-mediated pathogen restriction mechanisms. A schematic of different mechanisms by which intestinal bacteria can inhibit bacterial pathogens. On the left-hand side, mechanisms of direct pathogen inhibition are illustrated. These include: competition over nutrients such as iron and specific monosaccharides; the production of metabolites including short-chain fatty acids (SCFAs)[14-16], fucose[17], and secondary (2°) bile acids[18] that can inhibit pathogen growth and virulence pathways; as well as the production of antimicrobials such as bacteriocins[19,20]. On the right-hand side, indirect mechanisms of pathogen inhibiton, through host immune modulation, are depicted. These include: MAMP-induced enhancement of epithelial barrier function, involving the secretion of antimicrobial proteins (AMPs), mucins, and secretory IgA (sIgA)[21,22]; induction of pro-inflammatory T_H17 cell differentiation[23]; as well as the induction of anti-inflammatory T_{Reg} cell proliferation[24-26].

The activation of these pattern recognition receptors leads to a variety of downstream immune responses. Toll-like receptor (TLR) signaling in response to a diversity of microbial factors leads to NF-κB activation and the production of pro-inflammatory cytokines, antimicrobial proteins, and T_H1-type immunity[27]. NOD1 and NOD2 are peptidoglycan recognition receptors that activate NF-κB and MAPK pathways to promote autophagosome formation, T_H2-type immunity, as well as the production of pro-inflammatory cytokines and antimicrobial proteins[28]. Other Nod-like receptors (NLRs) sense a variety of bacterial factors and are involved primarily in inflammasome formation[29]. C-type lectin receptors (CLRs) are largely involved in fungal immunity, however mucus sensing by Dectin-1 is important for immune homeostasis[30]. In addition, CLRs recognize mycobacterial surface sugars, leading to the production of pro-inflammatory cytokines and T_H17 development. The basal immune responses elicited by these receptors in response to intestinal bacteria helps maintain immune system homeostasis[31].

Bacterial surface components including lipo-polysaccharide, lipo-teichoic acid, peptidoglycan, capsular polysaccharides, flagellin, and surface proteins can all be recognized by pattern recognition receptors to modulate intestinal immunity[32]. For example, lipo-teichoic acids from commensal *Lactobacillus* are recognized by TLR-2, and stimulate pro-inflammatory immune responses[33,34]. In contrast, NOD2 recognition of *Lactobacillus* peptidoglycan stimulates an anti-inflammatory response that alleviates chemically-induced colitis[35]. TLR-5 recognition of bacterial flagellin by dendritic cells leads to production of the antimicrobial peptide RegIIIγ, which limits colonization of vancomycin-resistant *Enterococcus*[36,37]. Surface layer protein A (SlpA) produced by

Lactobacillus acidophilus is recognized by the C-type lectin receptor DC-SIGN on dendritic cells, although it is not known how this affects host response to pathogens[38].

Hyper-activation of pattern recognition receptors may be prevented by controlling the localization and abundance of receptors, as well as by specific negative regulators of the downstream pathways. Variability in the specific bacterial cell-surface components that are recognized may also tailor host immune responses to pathogenic or commensal bacteria.

One important downstream response of microbial pattern recognition is the modulation of epithelial barrier function[21]. Secreted mucins, antimicrobial proteins, and secretory IgA (sIgA), all serve to exclude bacteria from a sterile zone maintained close to the surface of intestinal epithelial cells[22]. Recognition of intestinal bacterial MAMPs helps to maintain this barrier. For example, administration of lipo-polysaccharide and peptidoglycan can restore the mucous barrier in germ-free mice, and protect against chemically-induced colitis[39]. Intestinal bacteria can specifically enhance the production of various components necessary for maintaining barrier function. For example, *in vitro*, *Lactobacillus* can enhance epithelial cell secretion of the mucin Muc3[40]. In mice, commensal bacteria taken up by dendritic cells induce IgA production to enhance barrier function[41].

An important aspect of epithelial barrier function is the production of antimicrobial peptides[42]. Toll-like receptor recognition of commensal bacteria by Paneth cells leads to the production of antimicrobial proteins, including the C-type lectins RegIIIβ and RegIIIγ[43,44]. This, in turn, restricts penetration through the mucosa by both pathogenic and commensal bacteria[44,45]. Specific bacteria and bacterial components can

induce the production of RegIIIγ and other antimicrobial proteins. For example, mono-colonization of mice with just *Bacteroides thetaiotaomicron* can increase the expression of RegIIIγ[43]. As mentioned earlier, TLR-5 recognition of flagellin can also enhance RegIIIγ production[36,37]. Recognition of flagellin from the commensal *E. coli* strain Nissle 1917 also induces the production of another antimicrobial protein, β-defensin-2, by epithelial cells *in vitro*[46,47]. NOD2 recognition of peptidoglycan leads to the secretion of another type of antimicrobial protein, α-defensin, and is required for the inhibition of *Listeria monocytogenes* infection in mice[48].

The regulation of tight junctions and epithelial cell turnover by intestinal bacteria also serves to enhance epithelial barrier integrity. *In vitro*, *Lactobacillus plantarum* can enhance the expression of epithelial cell tight junction proteins[49,50], and reduce damage to the epithelia caused by enterohemorrhagic *E. coli* (EHEC) infection[51]. In mice, indole produced by intestinal bacteria can also enhance the expression of tight junction proteins, and protect against chemically-induced colitis[52,53]. *Lactobacillus rhamnosus* secretes two putative peptidoglycan hydrolases, p75 and p40, that activate Akt to inhibit apoptosis and enhance epithelial cell proliferation[54,55]. In mice, acetate production by *Bifidobacterium longum* also prevents epithelial cell apoptosis as well as Shiga toxin translocation to inhibit EHEC pathogenesis[56,57].

Intestinal bacteria can also promote the development and differentiation of innate lymphoid cells, IgA-producing cells, and T cells. T_H17 cells and T_{Reg} cells are important T cell subsets that mediate pro-inflammatory and anti-inflammatory responses in the intestine respectively. Specific intestinal bacteria can skew the ratio of these two cell types, which can differentially affect bacterial pathogenesis. For example, adhesion of

segmented filamentous bacteria (SFB) to intestinal epithelial cells induces the differentiation of T_H17 cells, which leads to the production of pro-inflammatory cytokines, antimicrobial peptides, and secretion of IgA. These responses cumulatively inhibit *C. rodentium* infection[23]. Specific microbial products present in the lumen, such as ATP, can also drive the differentiation of T_H17 cells[58]. Intestinal bacteria can also induce the proliferation of anti-inflammatory T_{Reg} cells. For example, dendritic cell presentation of the *Bacteroides fragilis* capsular polysaccharide, polysaccharide A, promotes the development of anti-inflammatory T_{Reg} cells, which protect against both chemically- and bacterially-induced colitis[24-26]. *Bifidobacterium infantis* can also increase T_{Reg} cell numbers to inhibit *Salmonella typhimurium*-mediated inflammation although the microbial factors involved are unknown[59].

Mechanisms of direct pathogen inhibition by intestinal bacteria.

Besides modulating host immunity, intestinal bacteria can restrict enteric pathogens through metabolic competition, direct killing, or the inhibition of pathogen virulence mechanisms. The effects of metabolic competition on pathogen colonization can be observed in the case of *Citrobacter rodentium* infection of mice[60]. *C. rodentium* transiently colonizes the intestines of wild-type mice, but persistently colonizes the intestines of germ-free mice. This differential colonization is due to metabolic competition over monosaccharides. Mono-colonization of mice with intestinal bacteria that fully rely on monosaccharide metabolism, limits *C. rodentium* use of this essential nutrient, and hence limits colonization. In a similar fashion, the combined sugar

metabolism of commensal *E. coli* strains HS and Nissle 1917 has been suggested to inhibit EHEC colonization in mice[61].

Iron is an essential, but limiting nutrient in the intestine. For this reason, many intestinal bacteria produce iron-chelating siderophores to increase iron uptake. Host-secreted antimicrobial proteins, such as lipocalin-2, restrict bacterial growth by binding and inactivating diverse bacterial siderophores. However, bacterial pathogens, including *Salmonella enterica*, evade lipocalin-2-mediated growth inhibition by producing modified siderophores that cannot be bound by lipocalin-2 [62,63]. In this context, *E. coli* Nissle 1917, which expresses four iron uptake systems resistant to lipocalin-2, competes against *Salmonella* for iron to limit *Salmonella* colonization and subsequent inflammation[64].

In addition to limiting pathogen growth through metabolic competition, some intestinal bacteria can specifically kill pathogens by producing bacteriocidal compounds. Metagenomics analysis of the intestine has revealed an abundance of natural products, including antibiotics, encoded by intestinal bacteria[65]. The role of antibiotics generated *in vivo*, however, is unclear. A well-characterized class of bacterially-encoded antimicrobials are bacteriocins. Bacteriocins are diverse lytic peptides that are generally of narrow-spectrum activity against related bacterial species[66]. *Lactobacillus* species encode a variety of bacteriocins[19,20], and some, such as plantaricin, which is produced by *Lactobacillus plantarum*, are expressed in the intestine[67]. In the context of intestinal infection, the bacteriocin Abp118 produced by *Lactobacillus salivarus* has been shown to inhibit *Listeria monocytogenes* infection in mice[68]. Another bacteriocin, thurucin CD,

which is produced by *Bacillus thuringensis*, limits *Clostridium difficile* proliferation in an *in vitro* human distal colon model while largely maintaining the intestinal microbiota[69,70].

Intestinal bacteria can also directly affect pathogen virulence mechanisms. Pathogens regulate the expression of virulence genes by sensing various environmental factors, some of which can be modified by intestinal bacteria. For example, expression of the *Shigella flexneri* Type-3 secretion system involved in host cell invasion is regulated by oxygen availability. *S. flexneri* senses a local increase in oxygen availability close to the intestinal epithelial surface, and in response, increases virulence gene expression[71]. Intestinal bacteria that adhere to the mucosa, such as *Lactobacillus rhamnosus*[72] could potentially inhibit *Shigella* invasion by consuming local oxygen.

The concentration of different metabolites can also affect pathogen virulence. For example, the expression of fucosidases by *Bacteroides thetaiotaomicron* cleaves fucose from host mucins. EHEC senses fucose levels through the FusKR two-component system, and in response decreases the expression of virulence genes required for the formation of attaching and effacing lesions (AE lesions)[17]. Bacterial fermentation in the intestine results in the secretion of diverse short-chain fatty acids. Short-chain fatty acids can directly modulate the virulence of various pathogens, possibly through covalent protein modification. For example, *Salmonella enterica* decreases the expression of a Type-3 secretion system required for host cell invasion in response to the short-chain fatty acids butyrate and propionate[14-16]. In mice, acetate production by *Bifidobacterium breve* inhibits the production of Shiga toxin by EHEC [73]. Secreted factors from *B. thetaiotaomicron* can also inhibit EHEC Shiga toxin expression, although the mechanisms underlying this inhibition are unknown[74]. The products of bacterial

metabolism can also inhibit pathogen growth directly. For example, *Clostridium scindens* generates secondary bile acids that inhibit *C. difficile* growth in mice[18]. In some cases, microbiota-generated metabolites can enhance pathogen virulence. For example, succinate produced by *B. thetaiotaomicron*, can be consumed by *C. difficile* to enhance intestinal colonization[75]. In the case of *Citrobacter rodentium,* succinate specifically enhances Type-3 secretion system expression, and hence virulence[76].

Pathogen sensing of inter-species quorum sensing molecules, such as N-acyl homoserine lactones (AHLs), has been proposed as a possible mechanism by which intestinal bacteria could modulate virulence. Both EHEC and *Salmonella* encode the transcription factor required for AHL recognition, SdiA, but lack the machinery to synthesize AHLs[77,78]. In the case of EHEC, AHLs repress the expression of virulence genes involved in the formation of AE lesions, but enhance the expression of acid-resistance genes[79]. Consistent with this, SdiA is required for EHEC colonization of the cow rumen, but has no affect on intestinal colonization. Curiously, AHLs are largely not found in the intestine[80,81], making the relevance of AHL-mediated quorum sensing in the intestine unclear. Intestinal bacteria may respond to other quorum sensing pathways, however, as intestinal delivery of auto-inducer-2 can alter microbiome reconstitution after antibiotic treatment[82].

Strategies of pathogen-mediated competition.

Just as the microbiome employs numerous strategies to restrict pathogens, bacterial pathogens have evolved a variety of strategies to compete with the microbiome.

Many of the characterized strategies revolve around generating a distinct niche and/or gaining access to unique nutrients. In a simple sense, adhesion to the surface of intestinal epithelial cells by enteropathogenic *E. coli* and *C. rodentium*, or invasion into host cells by *Salmonella* could be viewed as a means to evade competing intestinal bacteria. The utilization of unique nutrients is another way to avoid competition with the microbiota. For example, pathogenic strains of *E. coli* consume a unique subset of mucus-derived sugars as compared to commensal strains of *E. coli*[83].

Pathogen-induced inflammation is a mechanism to disrupt the microbiome[84] and release unique metabolites, giving pathogens a growth advantage. For example, *Salmonella*-induced intestinal inflammation leads to the generation of tetrathionate. Tetrathionate respiration by *Salmonella* confers a growth advantage over other intestinal bacteria that rely on fermentation[85]. In the inflamed intestine, ethanolamine utilization by both *Salmonella*[86] and pathogenic *E. coli*[87] can also enhance colonization[88]. Inflammation can also lead to the outgrowth of non-pathogenic members of the microbiota. For instance, nitrate released in the inflamed intestine is used in anaerobic respiration by commensal *E. coli* strains[89]. The effect of such shifts in microbiota composition on bacterial pathogenesis is unclear.

Pathogens can also directly kill intestinal bacteria. For example, *Salmonella enterica* produces the bacteriocin Colicin Ib, which can kill *E. coli* in the inflamed intestine[90]. *Vibrio cholera* uses a Type-6 secretion system to deliver antimicrobial effectors to intestinal bacteria, such as *E. coli*[91]. Self-immunity to this secretion system is required for intestinal colonization, which suggests that *V. cholera* employs Type-6 secretion *in vivo*[92].

Introduction to the work presented in this thesis.

The examples outlined in this Chapter highlight the dynamic nature of bacterial interactions in the intestine. Different model systems can emphasize the various contributions of host, commensal, and pathogen within this niche. Clarifying specific commensal determinants of pathogen restriction requires integrating *in vitro* and *in vivo* approaches.

In the following chapters, we describe two projects aimed at developing new methodologies to study how intestinal bacteria restrict bacterial pathogenesis. In Chapters 2 and 3, we use a chemical reporter strategy to analyze long-chain and short-chain fatty acid protein modifications in bacteria. In Chapter 2, we assess the utility of these reporters in *E. coli* for the visualization and identification of fatty-acid modified proteins. In Chapter 3, we apply this method to explore the effects of long-chain and short-chain fatty acids on *Salmonella* pathogenesis *in vitro*. In Chapter 4, we describe a *C. elegans* model system that we use to investigate the effects of *Enterococcus faecium* on *Salmonella* pathogenesis.

CHAPTER 2. Visualization and large-scale profiling of protein fatty-acylation in bacteria using bio-orthogonal chemical reporters.

INTRODUCTION.

Fatty acids are important metabolites that modulate the activity of microbes and host cells *in vivo*. Intestinal bacteria are exposed to millimolar concentrations of short-chain fatty acids[93], which are generated from microbial fermentation. In contrast, free long-chain fatty acids derived from ingested fats are present at micromolar concentrations[94]. For intracellular bacterial pathogens, fatty acids can be a key nutrient source. For example, *M. tuberculosis* relies heavily on host fatty acids as a carbon source, and mutants of fatty acid metabolism are attenuated in mice[95]. Other pathogens, such as *Salmonella*, are generalists, exploiting a wide variety of host carbon sources[96,97]. The shift from an extracellular to intracellular lifestyle is cued by changes in a variety of factors, including pH, antimicrobial peptides, and the concentration of various cations and nutrients[98,99]. The modulation of bacterial physiology and virulence in response to fatty acids, however, is not well understood. Besides altering metabolic flux, exposure to fatty-acids can regulate cell function through the post-translational modification of proteins.

Long-chain fatty acylation of proteins can modulate protein localization, folding, as well as interactions with other proteins. In bacteria, the canonical form of protein lipidation is sequence-specified and results in N-terminal tri-acylation (Figure 2.1a) [100,101]. In *E. coli* K-12, such bacterial lipoproteins are predicted to constitute approximately 2% of the proteome. These lipoproteins are a functionally diverse subset of membrane-

associated proteins that are involved in various cellular processes including membrane maintenance, transport, and signal transduction. Many lipoproteins have also been implicated in the virulence and immune evasion mechanisms of bacterial pathogens, and have been found to enhance antigenicity, adhesion, and antibiotic resistance in a variety of pathogens[102]. In addition, lipoproteins can stimulate host innate immunity through recognition by TLR-1, TLR-2, and TLR-6. Despite their clinical relevance and role in numerous essential membrane processes, the majority of bacterial lipoproteins remain uncharacterized. This is due, in part, to a lack of robust and convenient tools for the detection and large-scale analysis of lipoproteins in bacteria.

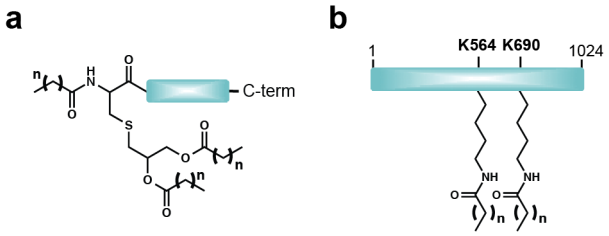

Figure 2.1. Long-chain fatty acid protein modifications in *E. coli.*
a. Schematic of a bacterial lipoprotein modification in *E. coli*. An N-terminal cysteine is modified with a thioether-linked diacyl glyceryl moiety and an amide-linked palmitate. n=15-18. **b.** Schematic of *E. coli* hemolysin A (HlyA) fatty-acylation. Two internal lysine residues (K564 and K690) are fatty-acylated by HlyC through an amide linkage. n=14. For both (a.) and (b.), the blue bar represents protein.

The most well-characterized form of protein lipidation in bacteria is the generation of N-terminally tri-acylated lipoproteins. Although the precise modification can vary across species, the general pathway is largely conserved. This enzymatic pathway has been best-characterized in *E. coli*, which exhibits a 15-18 carbon chain-

length preference[101] (Figure 2.1a). Post-translational protein lipidation is directed by an N-terminal signal sequence comprising a lipobox motif with an invariant cysteine (Cys) residue. This lipobox motif is well-conserved, enabling the prediction of lipoproteins from primary amino-acid sequence across bacterial genomes. Lipobox-containing proteins are translocated through the inner membrane, where the enzyme Lgt installs a diacylglyceryl moiety, derived from membrane phospholipids, onto the lipobox Cys residue through a thioether linkage. The signal sequence of this prolipoprotein is cleaved by Lsp, and the newly generated N-terminus is fatty-acylated by Lnt. Mature lipoproteins are then selectively sorted to the inner or outer membrane by secondary recognition elements.

Although this pathway is the predominant form of protein lipidation in *E. coli*, maturation of the toxin hemolysin (HlyA) and related RTX family exotoxins occurs through a unique protein fatty-acylation pathway (Figure 2.1b) [103]. Hemolysin is fatty-acylated via an amide linkage on two internal lysine residues by the dedicated acyl-transferase, HlyC. HlyC is cotranscribed with HlyA, and requires acyl-ACP as a donor, exhibiting chain-length preference through enhanced affinity for myristoyl-ACP. The prevalence of other non-canonical mechanisms of lipidation is not known and requires further investigation.

At the start of this study, existing methods available for the identification and analysis of long-chain fatty acid protein modifications in bacteria were limited to radioactive labeling and bioinformatic approaches. Labeling with radioactive fatty acids has low sensitivity and is not amenable to large-scale proteomic studies. Bioinformatic predictions are limited to lipoproteins containing a recognizable N-terminal lipobox

signal motif. As aforementioned, this motif directs the canonical form of protein lipidation in Gram-negative bacteria, but the prevalence of non-canonical mechanisms of lipidation is not known, making proteomic analysis essential for exploring the diversity of lipid-modified proteins in bacteria. The large-scale analysis of short-chain fatty acid protein modifications has been focused primarily on lysine acetylation[104,105]. Proteomic profiling of lysine acetylation has been achieved through acetyl-lysine antibody pull-down followed by mass spectrometry. However, protein modifications on alternative residues or with alternative short-chain fatty acids have not yet been systematically assessed.

Bio-orthogonal chemical reporter strategies have been used to characterize and discover fatty-acylated proteins in several eukaryotic systems[106]. Briefly, a bio-orthogonal chemical reporter refers to any functionalized reporter that can be covalently reacted to a secondary detection tag through a non-cellular reaction. In particular, the Hang laboratory has developed alkyne-functionalized fatty acid reporters that can be specifically reacted to azide-modified detection tags through Cu(I)-catalyzed cycloaddition (Figure 2.2a-c). Once fed to cells, alkynyl-fatty acids are metabolized and installed onto endogenous protein targets. Modified proteins can then be either visualized using a fluorescent detection tag (Figure 2.2a), or isolated with a biotin secondary tag (Figure 2.2b). At the time of this study, these reporters had not been used to explore the diversity of endogenously expressed bacterial fatty-acylated proteins. Given that the enzymatic machinery required for fatty acid processing and protein modification is different between eukaryotes and bacteria, the utility of alkynyl-fatty acid reporters in bacteria needed to be assessed.

Our goal in this study was to determine if alkynyl-fatty acid reporters could be used to visualize and identify fatty-acid modified proteins in bacteria. We first focused on characterizing long-chain fatty acid chemical reporters in *E. coli*. Because bacterial lipoproteins are a well-characterized class of fatty-acid modified proteins, we could validate these reporters using known and predicted lipoproteins.

RESULTS.

To assess the incorporation of long-chain fatty acid chemical reporters onto proteins in *E. coli*, we metabolically labeled *E. coli* K12 with alkynyl-fatty acid (alk-FA) reporters of varying chain lengths (alk-12, alk-14, and alk-16). Bacterial cell lysates were then reacted with the fluorophore azido-rhodamine (Figure 2.2a) via Cu(I)-catalyzed azide-alkyne cycloaddition (CuAAC) (Figure 2.2c). Alk-FA-modified proteins were visualized by in-gel fluorescence, revealing selective and chain-length dependent labeling of proteins (Figure 2.3a). Since alk-14 qualitatively labeled *E. coli* proteins most efficiently, we focused on further characterizing this fatty acid reporter. Alk-14 was rapidly incorporated into proteins (Figure 2.3c) and labeling was robust at low micromolar dosing (Figure 2.3b). For all subsequent experiments, we labeled cells with 20 μM alk-14. At this dose, alk-14 had no effect on *E. coli* growth rate (Figure 2.3d). To determine if alk-14 is incorporated into known lipoproteins, we generated a C-terminally His_6-tagged construct of the lipoprotein NlpE[107]. This construct was driven by an IPTG-inducible promoter, and expressed in *E. coli* BL21(DE3). In-gel fluorescence

visualization of purified NlpE-His_6 showed specific labeling of NlpE-His_6 by alk-14 (Figure 2.3e).

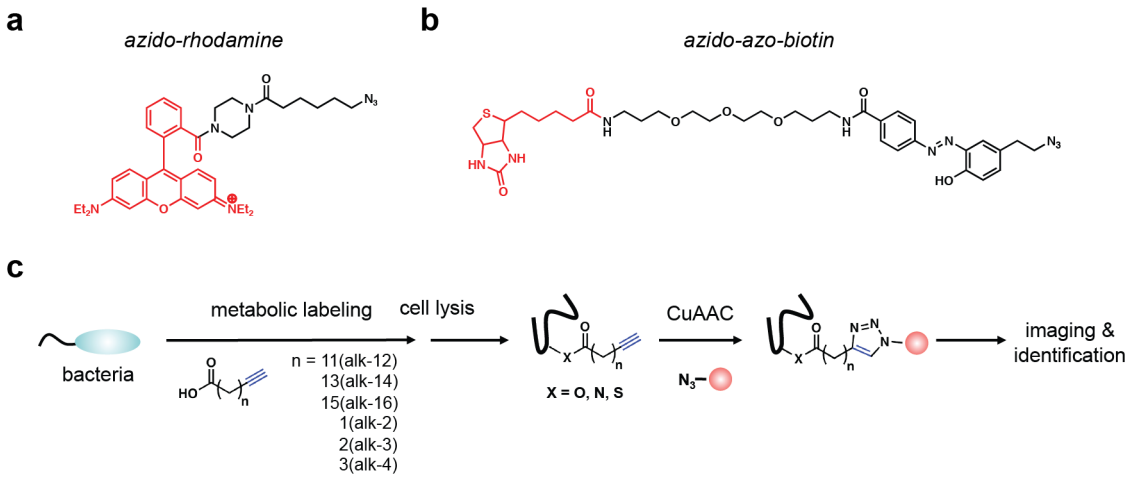

Figure 2.2. Bio-orthogonal labeling strategy for the analysis of fatty-acid modified proteins.

a. Structure of azido-rhodamine. Rhodamine (highlighted in red) allows imaging by in-gel fluorescence. **b.** Structure of azido-azo-biotin. Biotin (highlighted in red) allows protein pull-down with streptavidin beads (see Figure 3a) for subsequent protein identification. The azo-benzene moiety allows specific protein elution from streptavidin beads using sodium dithionite. **c.** Strategy for the covalent modification and analysis of fatty acid modified proteins. Bacteria are metabolically labeled with alkyne-functionalized fatty acids (alk-12, alk-14, alk-16, alk-2, alk-3, or alk-4). Cells are lysed, and modified proteins are reacted with azido-functionalized detection tags (a.) and (b.) by Cu(I)-catalyzed azide-alkyne cycloaddition (CuAAC) for subsequent imaging or pull-down studies.

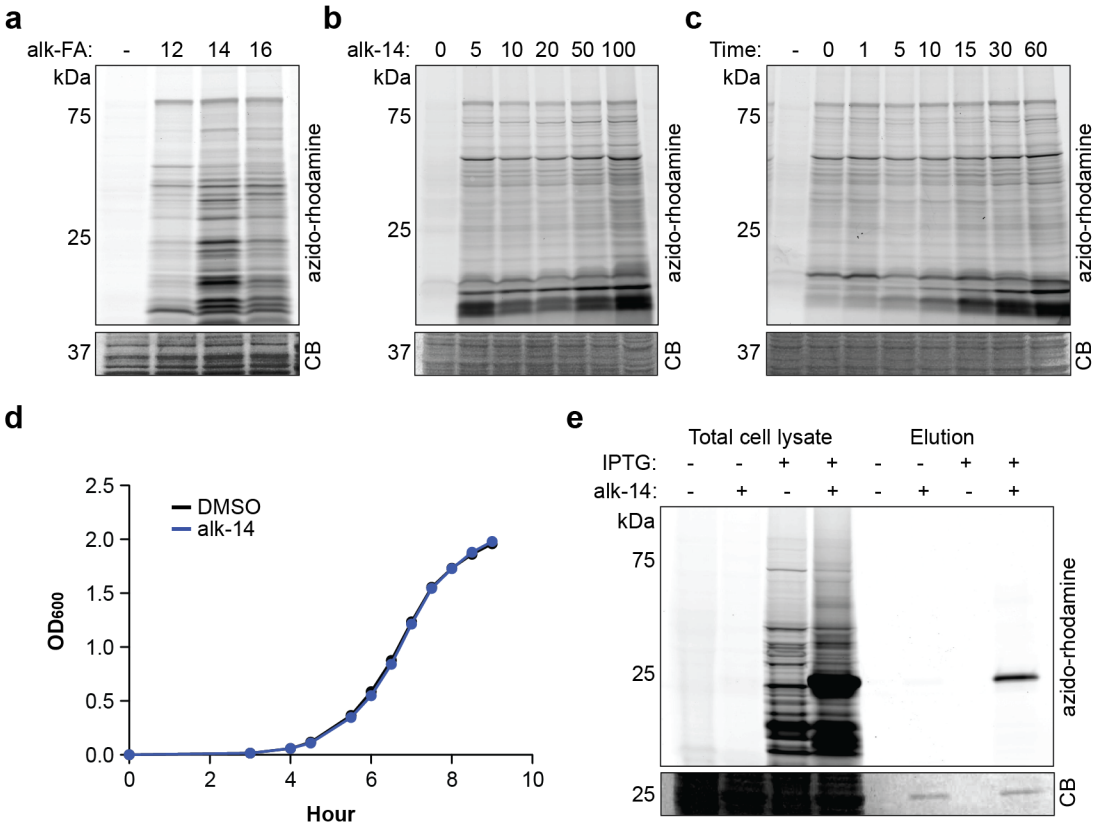

Figure 2.3. Characterization of alk-14 labeling in *E. coli*.

a. Profile of *E. coli* proteins labeled with alkyne-fatty acids (alk-FA) of varying chain length separated by SDS-PAGE. Modified proteins were imaged by rhodamine fluorescence. Alk-FA were used at 20 μM. (-) indicates DMSO control treatment. Coomassie blue (CB) indicates protein loading. **b.** Labeling of *E. coli* proteins with varying doses of alk-14. From left to right, *E. coli* were labeled with 0, 5, 10, 20, 50 and 100 μM of alk-14. **c.** Time dependence of alk-14 labeling of *E. coli*. *E. coli* were labeled for 0-60 minutes with 20μM alk-14. Note: pelleting and washing of cells before lysis took ~10 minutes, during which time, alk-14 incorporation occurs. **d.** Growth curves of *E. coli* treated with 20μM alk-14 (blue line) or DMSO control (black line). Data averaged from three experiments. Error bars (not visible) represent ± standard deviation. **e.** alk-14 labeling of *E. coli* expressing the His_6-tagged lipoprotein NlpE under an IPTG-inducible promoter. Total cell lysate and elution after His_6 purification are shown.

Figure 2.4. Enrichment and identification of fatty acid modified proteins

a. Strategy for the pull-down and identification of acyl-modified proteins. Bacteria are metabolically labeled with alkyne-fatty acids. Cells are lysed, and proteins are reacted with azido-azo-biotin by Cu(I)-catalyzed azide-alkyne cycloaddition (CuAAC). Biotin-modified proteins are enriched upon binding to streptavidin beads. Proteins are specifically eluted off of streptavidin beads with sodium dithionite, and separated by SDS-PAGE. Proteins are then subjected to in-gel trypsin digestion for proteomics analysis. **b.** Alk-14-labeled proteins retrieved from *E. coli* using the azido-azo-biotin affinity tag. *E. coli* expressed IPTG-inducible NlpE-His_6 as a control for lipoprotein pull-down. Cells were metabolically labeled under inducing and non-inducing conditions with 20 μM alk-14 and labeled lysates were reacted with azido-rhodamine for in-gel visualization (left). The remaining lysate was reacted with azido-azo-biotin, and labeled proteins were captured on streptavidin beads. Captured proteins were eluted with $Na_2S_2O_4$ and total eluant was visualized by Coomassie blue (CB) (right). The red star indicates an eluted band corresponding to the predicted molecular weight of NlpE. **c.** alk-2 and alk-14 labeled proteins retrieved from *E. coli* using the azido-azo-biotin affinity tag. Cells were metabolically labeled with 5 mM alk-2 or 20 μM alk-14. 20 μg of labeled lysates were reacted with az-Rho for in-gel visualization (left). The remaining lysate was reacted with azido-azo-biotin, and labeled proteins were captured on streptavidin beads. Captured proteins were eluted with $Na_2S_2O_4$ and total eluant was visualized by CB (right).

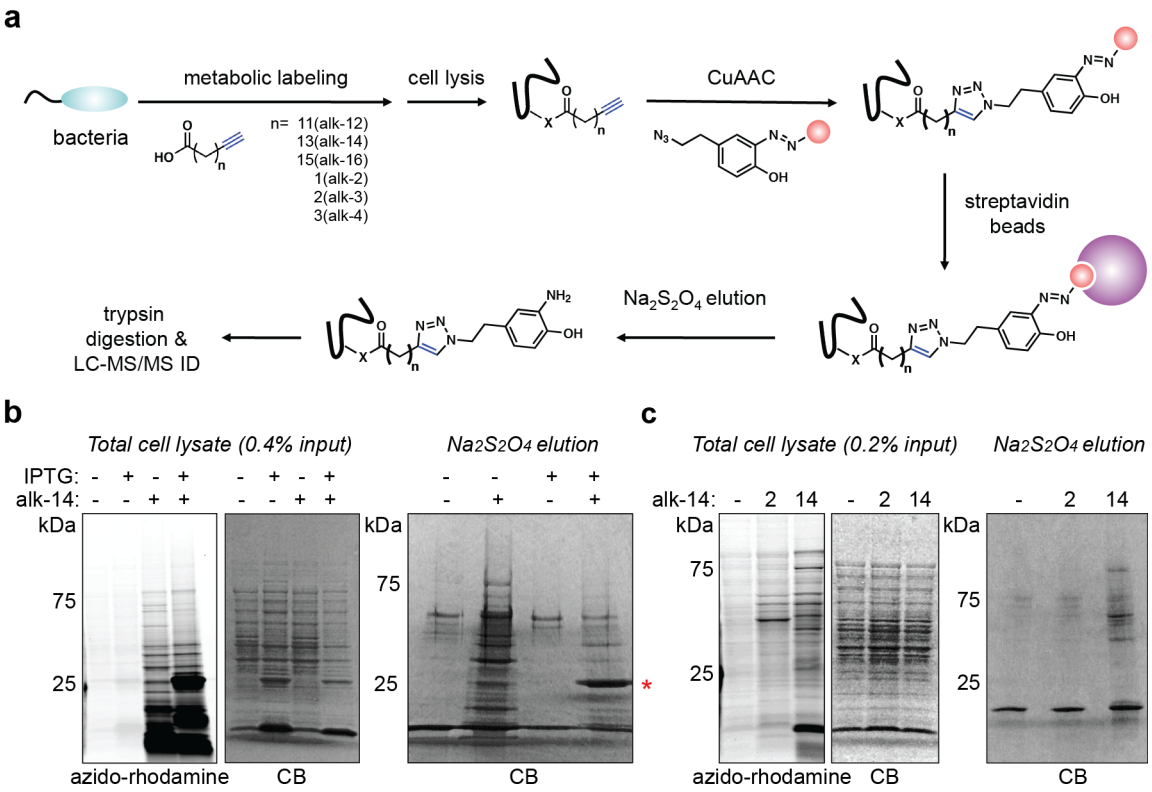

Figure 2.4. Enrichment and identification of fatty acid modified proteins

Having established by fluorescence visualization that alk-14 labels a diversity of proteins, and is incorporated into a known lipoprotein, we sought to use alk-14 for the large-scale enrichment and identification of fatty acid modified proteins. To do this, we reacted alk-14-labeled *E. coli* cell lysates with a cleavable azido-azo-biotin affinity tag[108] (Figure 2.2b and 2.4a). This secondary tag allows for the enrichment of biotinylated proteins with streptavidin beads. Enriched modified proteins are then selectively eluted with sodium dithionite ($Na_2S_2O_4$), and recovered proteins are separated by SDS-PAGE for gel-based proteomics.

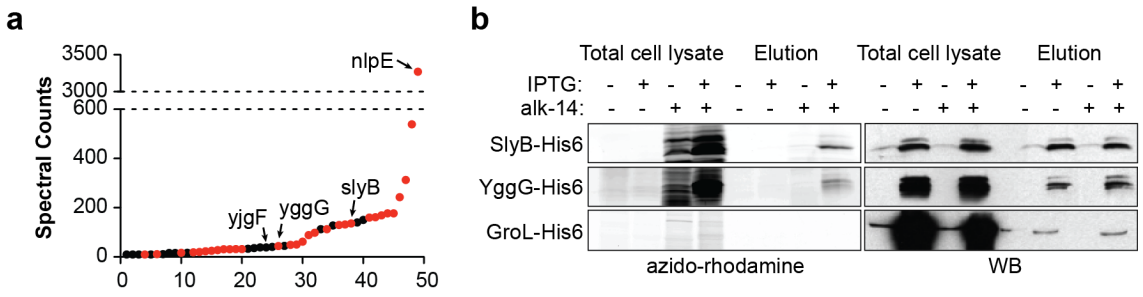

Figure 2.5. Summary of alk-14 modified proteins identified in *E. coli*.

a. High confidence proteins identified by LC-MS/MS from experiments described in Figure 3b and c. The y-axis represents the sum of peptide-spectral counts from the three proteomics runs. The x-axis represents arbitrary protein number. Predicted lipoproteins are highlighted in red. Proteins validated as alk-14-modified in this study are indicated. Induction of NlpE-His_6 in Experiment 2 is reflected in the high number of spectral counts for this protein. **b.** alk-14 labeling of C-terminally His_6-tagged lipoproteins SlyB and YggG. His_6-tagged GroL was used as a negative control. Proteins were expressed from an IPTG-inducible promoter. Total cell lysates and elutions from the His_6-purifications are shown. Anti-His_6 Western blot (WB) indicates protein loading.

As a positive control for lipoprotein recovery, we labeled *E. coli* expressing NlpE-His_6 under both inducing and non-inducing conditions. Coomassie blue visualization of the $Na_2S_2O_4$-eluted proteins showed that NlpE-His6 was strongly recovered in the IPTG-induced sample as compared to the non-induced sample (Figure 2.4b). In a separate experiment, we labeled *E. coli* with either alk-14 or an alkynyl-acetic acid analog, alk-2[109], to determine if protein labeling and pull-down was generic to any alkyne-functionalized reporter (Figure 2.4c). As compared to alk-14, alk-2 did not efficiently label bacterial proteins by fluorescence profiling, and few proteins were recovered after $Na_2S_2O_4$-elution (Figure 2.4c).

Proteomics analysis of the three alk-14 labeled samples yielded 45 high confidence alk-14 labeled candidate proteins, of which 69% were known or predicted lipoproteins, based on prediction by LipoP[110] (Figure 2.5a, Appendix 1). An additional 51 candidates were identified with medium confidence, of which only 12% were predicted lipoproteins (Appendix 2). As expected, NlpE was substantially enriched in the IPTG-induced samples. In addition to recovering predicted lipoprotein candidates, we also selectively recovered acyl-carrier protein (AcpP) from alk-14 labeled samples, suggesting that alk-14 is accepted into the fatty acid synthesis pathway. Of the 150 proteins identified from the alk-2 labeled sample, only 3% were predicted lipoproteins, indicating that lipoprotein labeling is specific to alk-14 and not due to general labeling of proteins by alkynyl-functionalized substrates (Appendix 3). Although our lab has shown that alk-2 can be installed into sites of histone lysine acetylation in mammalian cells[109], only 23% of the alk-2 proteins we identified in *E. coli* were previously reported to be lysine acetylated. This suggests that alk-2 is not be a robust acetic-acid analogue in *E. coli*, and

may reflect differences in substrate specificity of the acetylation machinery between eukaryotes and prokaryotes.

We next validated alk-14 labeling on additional proteins selectively recovered from alk-14 labeled *E. coli*. We confirmed alk-14 labeling of SlyB, a known lipoprotein, and YggG, a predicted but unverified lipoprotein, by fluorescence detection of C-terminally His_6-tagged constructs after affinity purification (Figure 2.5b). Non-specific labeling due to over-expression is unlikely since no labeling was observed with the over-expressed non-lipidated protein, GroL-His6 (Figure 2.5b).

One of the proteins identified in our alk-14 samples not predicted to be a lipoprotein was YjgF, a highly conserved protein found in all domains of life involved in branched chain amino acid synthesis[111]. To verify alk-14 labeling of YjgF, we generated an N-terminally His_6-tagged YjgF construct (His_6-YjgF). Attachment of an N-terminal His_6-tag helps rule out the possibility that YjgF bears an unrecognized N-terminal signal peptide, since the N-terminus is cleaved after lipoprotein modification. We were able to robustly detect and purify His_6-YjgF by His_6 affinity, indicating retention of the N-terminal His_6-tag. Alk-14 modification was verified by in-gel fluorescence detection of purified His_6-YjgF (Figure 2.6a). YjgF contains one internal cysteine (Cys) residue at position 107, as a potential site of alk-14 modification that is conserved in many bacterial homologs of YjgF. To determine if Cys107 is the site of alk-14 modification, we generated a Cys107 to Serine mutant (His_6-YjgF-C107S). We observed no alk-14 labeling of His6-YjgF-C107S by in-gel fluorescence detection, suggesting that YjgF is indeed fatty acid modified at this residue (Figure 2.6a).

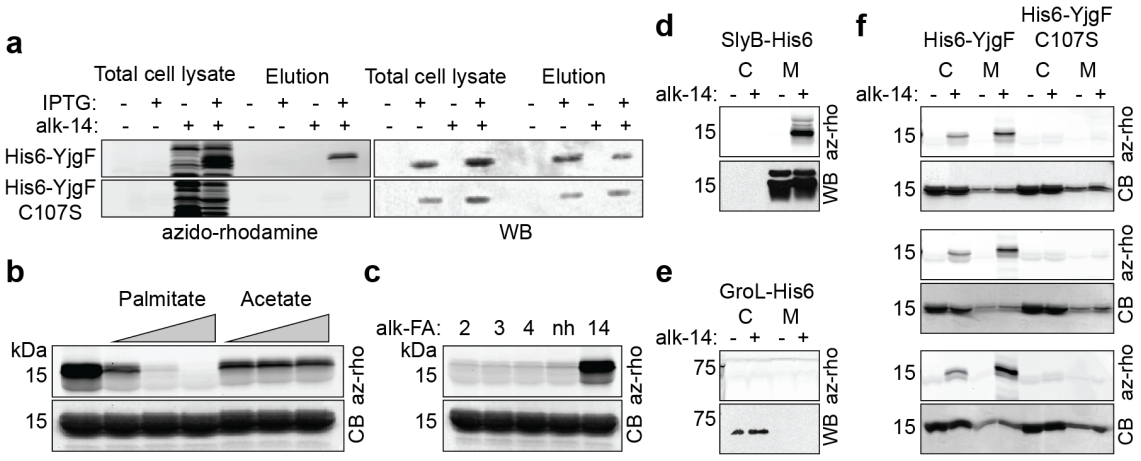

Figure 2.6. Characterization of YjgF fatty acid modification.

a. alk-14 labeling of His_6-tagged YjgF on Cysteine107. Mutation of Cysteine107 to Serine abrogates alk-14 labeling. Both wild-type YjgF and YjgF C107S were expressed from an IPTG-inducible promoter. Total cell lysates and elutions from the His_6-purifications are shown. Anti-His_6 Western blot (WB) indicates protein loading. **b.** Dose-dependent competition of alk-14 labeling on His_6-purified His_6-YjgF by palmitate, but not sodium acetate. Palmitate was used at increasing concentrations of 20 μM, 200 μM, and 400 μM. Sodium acetate was used at increasing concentrations of 200 μM, 2 mM, and 4 mM. Coomassie blue (CB) shows protein loading. **c.** His_6-YjgF is not labeled by short-chain fatty acid reporters alk-2, alk-3, or alk-4, nor by a non-hydrolyzable alk-16 analogue (nh). alk-2, alk-3, and alk-4 were used at 5 mM, nh and alk-14 were used at 20 μM. **d.** Cellular fractionation of alk-14 labeled *E. coli* expressing SlyB-His_6, **e.** GroL-His_6, **f.** His_6-YjgF, or His_6-YjgF C107S. Cells were lysed by osmotic shock, and lysates were separated into cytoplasmic (C) or membrane (M) fractions. Samples were reacted with azido-rhodamine, and His_6-tagged proteins were purified on Ni-NTA beads. Eluant was separated by SDS-PAGE, and gels were analyzed by in-gel fluorescence. Anti-His_6 Western blot (WB) or Coomassie blue (CB) staining indicate protein loading. SlyB-His6 and GroL-His6 serve as controls for cellular fractionation and alk-14 labeling. Three independent replicates of cellular fractionation of His_6-YjgF and His_6-YjgF C107S are shown.

To determine whether the alk-14 labeling we observe on YjgF is reflective of long-chain fatty acid modification, we performed competition experiments of alk-14 labeling with palmitic acid or sodium acetate. Alk-14 labeling on His6-YjgF was effectively competed away with increasing amounts of palmitic acid, but not with sodium acetate (Figure 2.6b), suggesting that YjgF is covalently modified with a long-chain fatty acid metabolite. Consistent with this, His6-YjgF was not labeled by short-chain fatty acid analogues alk-2, alk-3, or alk-4[109] (Figure 2.6c).

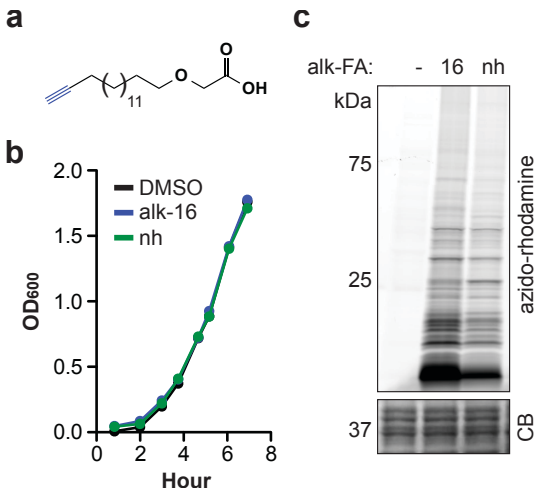

Figure 2.7. *E. coli* growth and protein labeling with a non-hydrolyzable alkynyl-fatty acid analogue.

a. Structure of alk-16nh. **b.** Growth curve of *E. coli* labeled with DMSO (control), alk-16, or alk-16nh (nh). **c.** Fluorescence profile of *E. coli* proteins modified by alk-16 or alk-16nh. By fluorescence, alk-16 and alk-16nh label similar protein profiles to a similar extent. (-) indicates DMSO control.

To evaluate whether any processing of alk-14 is necessary for covalent attachment to YjgF, we assessed labeling of His6-YjgF with the non-hydrolyzable long-chain fatty acid analogue alk-16nh[112] (Figure 2.7a). Alk-16nh has an oxygen replacing the

β-carbon, thereby theoretically preventing both degradation and elongation of fatty acid chain length. However, alk-16nh should still be incorporated into both membrane phospholipids[113] and proteins, since it can still be CoA-modified. Alk-16nh did not affect *E. coli* growth and labeled a similar protein profile as alk-16 (Figure 2.7b-c), which is consistent with our results that the majority of proteins labeled with long-chain fatty acid reporters in *E. coli* are *bona fide* lipoproteins. However, in-gel fluorescence visualization of alk-16nh labeling showed no labeling of purified His6-YjgF (Figure 2.6c), suggesting that some chain-length processing of alk-14 is necessary before modification of YjgF.

To determine if fatty-acid modification alters YjgF membrane association, we fractionated alk-14 labeled *E. coli* expressing either His6-YjgF of His6-YjgF-C107S into cytoplasmic and membrane fractions. Using SlyB and GroL as membrane-associated, and cytoplasmic controls respectively (Figure 2.6d-e), we were confident that our fractionation method robustly separated these protein populations. We found that His6-YjgF and His6-YjgF-C107S fractionated similarly to both the cytoplasmic and membrane compartments (Figure 2.6f). Likewise, alk-14-modified YjgF was found in both the cytoplasmic and membrane-bound fractions, although it was consistently more enriched in the membrane-associated fraction (Figure 2.6f). This suggests that fatty acid modification of Cys107 does not influence the localization of YjgF to membranes.

Although several structural studies have been conducted on YjgF family proteins[114-117], the biochemical activity of YjgF has only recently been elucidated. YjgF deaminates reactive enamine/imine intermediates formed in pyridoxal 5' phosphate-dependent reactions important to branched-chain amino acid biosynthesis[118,119]. YjgF

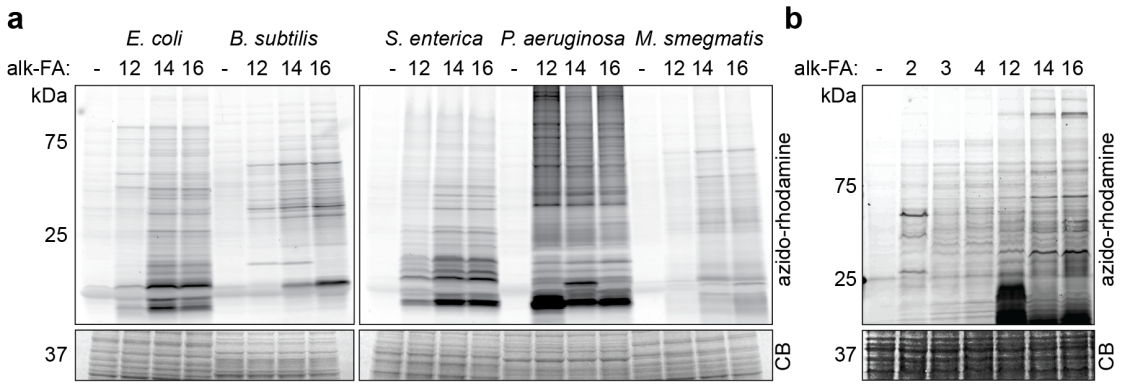

Figure 2.8. Profiling of fatty-acid modified proteins across bacterial species. **a.** Fluorescence profiling of alk-FA-modified proteins in various bacteria. *E. coli, B. subtilis, S. typhimurium, P. aeruginosa,* and *M. smegmatis* were labeled with 20 μM of alk-12, alk-14, or alk-16 for 30 minutes in LB media. Cell lysates were reacted with azido-rhodamine, then separated by SDS-PAGE and visualized by in-gel fluorescence. Coomassie blue (CB) staining indicates protein loading. **b.** Fluorescence profiling of short-chain fatty-acid-modified proteins in *E. coli*. alk-2, alk-3, and alk-4 were used at 5 mM, while alk-12, alk-14, and alk-16 were used at 20 μM.

converts imines to alpha-keto-acids, releasing ammonia, which may decrease the levels of toxic metabolites in the cell. Important to this enzymatic function is the coordination of water in the active site of YjgF to attack the imine[118]. Binding of alpha-keto butyrate[117] and the coordination of water by YjgF family proteins have been confirmed by structural studies[115]. Cys107 is involved in the hydrogen bonding necessary for the coordination of water. Therefore, the modification of Cys107 with a fatty acid metabolite would likely alter or abolish enzymatic function of YjgF. This may be a mechanism to regulate YjgF activity, and suggests an interesting coupling of amino acid and fatty acid metabolism that warrants future investigation.

Having established that alk-14 is a useful tool in *E. coli* for the visualization and large-scale identification of lipoproteins, we sought to generally evaluate the utility of long-chain fatty acid reporters across various bacterial species. We labeled Gram-negative bacteria (*Salmonella enterica* and *Pseuodomonas aeruginosa)*, Gram-positive bacteria (*Bacillus subtilis)*, and mycobacteria (*Mycobacteria smegmatis)* with alk-12, alk-14, and alk-16 (Figure 2.8a). By in-gel fluorescence visualization, we saw robust labeling and distinct fluorescence profiles amongst the bacteria evaluated (Figure 2.8a). This suggests that long-chain alkynyl-fatty acid reporters may be useful in different bacterial species to study fatty acid protein modifications.

Our analysis of alk-2 labeling in *E. coli* suggested that this reporter is not robustly incorporated as an acetic acid analogue onto proteins. To evaluate protein labeling by other short-chain fatty acid reporters, we compared protein profiles of *E. coli* labeled with alk-2, alk-3, and alk-4 by fluorescence visualization (Figure 2.8b). Alk-3 and alk-4 labeled similar protein profiles, distinct from alk-2 (Figure 2.8b), suggesting that these reporters are incorporated onto different proteins than alk-2. Future proteomics analyses on alk-3 and alk-4 modified proteins may lend insight into the effects of short-chain fatty acids on bacterial physiology.

SUMMARY.

In this Chapter, we have demonstrated that the long-chain fatty acid reporter alk-14 can be used to visualize and identify lipoproteins in *E. coli*. The discovery of lipobox-independent fatty-acid modification on YjgF highlights the strength of this methodology

for identifying novel lipid-modified proteins. Future investigation into the effects of this modification on YjgF enzyme activity is of interest. Our survey of alk-FA labeling in other bacterial species suggests that this method may be a general strategy for evaluating bacterial lipoproteins.

ACKNOWLEDGEMENTS AND CONTRIBUTIONS.

Thanks to Guillaume Charron, who synthesized alk-12, alk-14, alk-16, and alk-16nh; to Yu-Ying Yang, who synthesized azido-azo-biotin, alk-2, alk-3, and alk-4; and to Paul Dossa, who synthesized azido-rhodamine. In addition, thanks to The Rockefeller Proteomics Facility who ran all samples for LC-MS/MS analysis. Finally, thank you to Ming-zi Zhang, John Wilson, and Jacob Yount for advice on click chemistry and proteomics.

MATERIALS AND METHODS.

Strains.

E. coli K12 strain EC100, *E. coli* DH5α, *E. coli* BL21 (DE3), *Salmonella enterica* serovar *typhimurium* strain IR715, *Pseudomonas aeruginosa* strain PAO1, and *Bacillus subtilis* 168 were grown in LB media (BD Difco) at 37 °C. *Mycobacterium smegmatis* strain mc2155 was grown in LB was supplemented with 0.05% Tween-80. When necessary, ampicillin was used at 100 μg/ml.

Chemicals.

All chemicals were obtained either from Sigma-Aldrich, MP Biomedicals, Alfa Aesar, TCI, Fluka, or Acros and were used as received unless otherwise noted. Azido- and alkynyl-fatty acids, azido-rhodamine and azido-diazo-biotin were previously synthesized[108,109,112,120].

Fluorescence labeling and visualization of alkynyl-fatty acid modified proteins.

Metabolic labeling of bacteria with alkynyl-fatty acids:

For metabolic labeling, bacterial cultures of OD_{600} = 1.7-2.0 (absorbance was determined by SpectraMax M2) were labeled with 20 μM alk-12, alk-14, alk-16, or alk-16nh (from a 50 mM stock in DMSO) or 5 mM alk-2, alk-3, or alk-4 (from a 200 mM stock of alk-FA Na^+ salt in water). As a negative control, the same volume of DMSO or water was added in lieu of alkynyl-fatty acid. Cells were incubated at 37 °C for time indicated and pelleted at 5000 g for 5 minutes. Cells were washed with PBS (2x), and then lysed as described below or flash frozen and stored at -80 °C for future lysis.

Preparation of cell lysates:

Cell pellets were lysed in 0.1% SDS buffer (50 mM triethanolamine (TEA), 150 mM NaCl, 0.1% SDS, 1X EDTA-free protease inhibitor cocktail (Roche), 5 mM PMSF from a 250 mM stock in EtOH, 0.1 μl benzonase (Sigma)) by sonicating pellet for 10 seconds, then incubating on ice for 10 minutes. 5 μl of 10 mg/ml lysozyme (in ddH_2O) (Sigma) was added to each sample. Samples were incubated on ice for 30 minutes. Then, 12% SDS buffer (in 50 mM TEA, 150 mM NaCl) was added to bring final SDS

concentration to 4%. Cells were sonicated in 5 second intervals until the lysates were clear. Cell lysates were centrifuged at 1000 g for 5 min to remove cell debris and supernatant was collected. Protein concentration was determined by BCA assay (Pierce). Typical protein concentration obtained was between 3-5 mg/ml.

CuAAC reaction:

50 μg of cell lysate was brought up to 45 μl volume in 4% SDS buffer (50 mM TEA, 150 mM NaCl, 4% SDS). 5 μl of click chemistry reagents were added to the lysate as a master mix: azido-rhodamine: 0.1 mM, from a 10 mM stock solution in DMSO; tris(2-carboxyethyl)phosphine hydrochloride (TCEP): 1 mM, from a 50 mM freshly prepared stock solution in ddH2O; tris[(1-benzyl-1H-1,2,3-triazol-4-yl)methyl]amine (TBTA): 0.1 mM, from a 2 mM stock in 4:1 tert-butanol:DMSO; and $CuSO_4$-$5H_2O$: 1 mM, from a 50 mM freshly prepared stock in ddH2O.

Samples were incubated at room temperature for 1 hour. After incubation, proteins were precipitated by chloroform/methanol precipitation as follows: 4X MeOH, 1.5X chloroform, and 3X ddH2O by volume were added to CuAAC reaction and vortexed. Samples were centrifuged at 20,000 g for 1 minute and the aqueous layer was removed. Samples were washed two times with 4X methanol, mixing gently by inversion, centrifuging at 20,000 g for 1 minute, then decanting off the supernatant each time. Protein pellets were air-dried, then resuspended by sonication in 35 μl buffer and 15 μl 4X SDS sample buffer (250 mM 0.5M Tris-Cl pH 6.8, 8% SDS, 40% glycerol, 0.4% bromo-phenol blue, 20% 2-mercaptoethanol), and heated at 95 °C for 5 minutes. 20 μg of

protein corresponding to 20 µl was loaded per lane for separation by SDS-PAGE (Bio-Rad Criterion Tris-HCl 4%-20% gel).

Visualization by in-gel fluorescence:

Proteins separated by SDS-PAGE were visualized by in-gel scanning using an Amersham Biosciences Typhoon 9400 variable mode imager (excitation 532 nm, 580 nm filter, 30 nm band-pass).

Growth curves.

Comparing growth with alk-14 vs. DMSO: *E. coli* was grown overnight at 37 °C, in 2 ml of LB media. This culture was diluted 1:1000 in fresh LB media containing either 20 μM alk-14 (as a 50 mM stock in DMSO) or an equal volume of DMSO. 1 ml aliquots of the culture were removed at given time points, and OD_{600} was measured. Each condition (alk-14 and DMSO) was done in triplicate.

Comparing growth with alk-16 vs. alk-16nh: *E. coli* was grown overnight at 37 °C, in 2 ml of LB media. This culture was diluted 1:1000 in fresh LB media containing either 20 μM alk-16 or alk-16nh (as a 50 mM stock in DMSO). 1 ml aliquots of the culture were removed at given time points, and OD_{600} was measured.

Plasmids used in this study.

Table 2.1. Cloning primers used in this study. The given genes were PCR amplified out of the *E. coli* genome using these primer sets.

Gene name	Primer sequences
nlpE	FW: aaaggatccaatggtgaaaaaagcgatag RV: tttgaattcttctgccccaaactactgcaa
slyB	FW: aaaggatccatgattaaacgcgtattgg RV: tttctcgaggcgcggagaaacggtcacc
yggG	FW: aaaggatccaatgaaaattcgcgcctta RV: tttgaattcttcttaatcccatccgcgc
groL	FW: aaagaattcaatggcagctaaagacgtaa RV: tttaagcttcatcatgccgcccatgc
yjgF	FW: aaaggatccaagcaaaactatcgcgacg RV: tttctgcagttagcgacgaacagcgatc

The nlpE PCR product was cut with BamH1 and EcoR1; slyB was cut with Xho1 and BamH1; yggG was cut with BamH1 and EcoR1; and groEL was cut with EcoR1 and HinD3. PCR products were ligated to the pET21a vector cut with corresponding restriction enzymes, yielding C-terminal His6-tagged proteins. The yjgF PCR product was cut with BamH1 and Pst1 and was ligated to the pETDUET-1 vector cut with BamH1 and Pst1, yielding an N-terminal His6-tagged protein. All ligations were transformed into EC100 chemically competent cells for sequencing of plasmid DNA.

Sequence-verified constructs were then transformed into BL21(DE3) chemically competent cells for expression.

His6-YjgFC107S was constructed from His6-yjgF in the pET-DUET-1 vector using the Stratagene site directed mutagenesis kit (Agilent) as per the manufacturer's protocol with the following mutagenesis primer set:

FW: cccggcacgttcttctgttgaagttgcccg

RV: cgggcaacttcaacagaagaacgtgccggg

Analysis of His6-tagged proteins.

For labeling and over-expression of proteins, BL21 (DE3) cultures were inoculated 1:100 with overnight cultures, and grown for 2 hours or until culture OD_{600} ~ 0.4. Cultures were induced with 1 mM IPTG and labeled with 20 μM of alk-14 or alk-16nh, or 5 mM of alk-2, alk-3, or alk-4 for 4 hr. Non-induced and non-labeled controls were included for each experiment. Cells were pelleted at 5000 g for 5 minutes and washed 2X with PBS. Cells were lysed and reacted with azido-rhodamine via CuAAC as described above. His6-tagged proteins were purified from cell lysates on a small-scale using Ni-NTA agarose beads (Qiagen) as per the manufacturer's protocol. Total lysates and eluants were analyzed either by Commassie blue staining or by Western blot using anti-His6 HRP conjugated polyclonal antibody (Bethyl Laboratories) at a 1:10,000 dilution.

Palmitic acid and sodium acetate competition of YjgF labeling.

LB media supplemented with varying amounts of palmitic acid (from a 100mM stock in DMSO) or sodium acetate (from a 1M stock in water) was inoculated at a 1:100 dilution of an overnight culture of *E. coli* carrying His6-yjgF. This culture was grown shaking at 37 °C to OD_{600} = 0.4. 1mM IPTG was added to induce expression of His6-yjgF, and cells were grown for 15 minutes. Then, 20μM alk-14 was added and cells were labeled for 3 h 45 m. Cells were lysed and reacted with azido-rhodamine via CuACC as described above. His6-YjgF was purified from cell lysates as described above. Total lysates and eluants were analyzed by in-gel rhodamine fluorescence and Coomassie blue staining.

Subcellular fractionation.

IPTG induced, alk-14 labeled *E. coli* expressing GroL-His6, SlyB-His6, His6-YjgF, or His6-YjgF C107S were pelleted at 5000 g for 10 m. Cells were washed once in 30mM Tris buffer pH 8.1 then re-suspended in 20% sucrose (w/v) in 30mM Tris (pH 8.1). 100 μg lysozyme was added and samples were incubated on ice for 30 minutes. Distilled water with 1X EDTA-free protease inhibitor cocktail (Roche), 5 mM PMSF (from a 250 mM stock in EtOH), and 0.1 μl benzonase (Sigma) was added and samples were sonicated in 5 second bursts 5 times. Samples were then centrifuged at 5000 g for 10 m to remove unlysed cells. Supernatant was then centrifuged at 20,800g for 1.5 hour. Supernatant was collected as the cytoplasmic fraction. The pellet was washed twice in water, centrifuging 1.5 hours at 20,800g after each wash, then lysed in 4% SDS buffer. This was considered the membrane fraction. Protein concentration was determined by BCA assay (Pierce). Samples were then reacted with azido-rhodamine via CuACC, then

separated by SDS-PAGE. Gels were scanned for in-gel fluorescence, then stained with Coomassie blue. A parallel gel was run to perform a Western Blot using polyclonal anti-His6 HRP conjugated antibody at a 1:10,000 dilution.

Azido-biotin labeling and enrichment of alk-14 modified proteins for MS ID.

Metabolic Labeling:

E. coli Experiments 1 and 2: An overnight culture of *E. coli* carrying pET21a-NlpE-His6 was diluted 1:1000 in fresh LB and grown until OD_{600} = 0.4. Cells were induced with 1 mM IPTG, 20 μM alk-14 was added to the culture, and cultures were grown for 4 hours. Non-induced samples were also prepared. DMSO controls for alk-14 labeling were also prepared for both induced and non-induced cultures.

E. coli Experiment 3: LB was inoculated 1:1000 from an overnight culture of *E. coli* and cells were grown in LB media to OD_{600} = 1.8. 20 μM alk-14 (from a 50 mM stock in DMSO) or 5 mM alk-2 (from 200 mM stock of alk-2 Na^+ salt in water) were added to the media and cells were labeled for 30 min. A DMSO control for alk-FA labeling was also prepared.

CuAAC reaction:

Cell lysates (10 – 20 mg) were brought up to a volume of 8.9 ml with a final SDS concentration of 2%. To this, 200 μl of 5 mM azido-diazo-biotin; 200 μl of 50 mM TCEP; 500 μl of 2 mM TBTA; and 200 μl of 50 mM $CuSO_4$ were added, and samples were incubated for 1.5 hours at room temperature. After incubation, proteins were

precipitated by chloroform/methanol precipitation as described: 4x MeOH, 1.5X chloroform, and 3X ddH2O were added to reaction, and samples were vortexed vigorously. Samples were centrifuged at 5200 g for 30 minutes, and the aqueous layer was removed. Samples were washed two times with 4X methanol, by vortexing vigorously, centrifuging at 5200 g for 30 minutes, then decanting off the supernatant each time. Protein pellets were air-dried, then resuspended in 1 ml 4% SDS buffer and 20 μl 0.5 M EDTA pH 8. Protein concentration was estimated by BCA assay.

Streptavidin bead capture:

CuAAC reacted proteins (5-15 mg) were added to PBS-washed high-capacity streptavidin agarose beads (Thermo scientific) (beads in a 50% Brij buffer slurry, 100 μl per 5 mg protein). Beads were incubated with cell lysates for 1 hour at room temperature with rocking. Beads were then washed 2X with 10 ml of 0.1% SDS in PBS, 3X with 10 ml PBS, 2X with 50 mM ABC, then incubated for 30 minutes with freshly made 8 M urea solution (500 μL 8 M urea, 25 μl 200 mM TCEP, 25 μl 400 mM iodoacetamide). Beads were washed 2X with 50 mM ABC, then transferred to a dolphin tube with 1 ml ABC. Proteins were eluted off beads in two steps with a total of 400 μl freshly prepared elution buffer (0.5% SDS, 25 mM $Na_2S_2O_4$ in 50 mM ABC) by rocking for 1 hour at room temperature, then for 30 minutes. Eluant was concentrated using a Microcon YM-10 centrifugal filter (Millipore) as per manufacturers protocol. Microcon filters were rinsed twice with 50 μl 1% SDS/75 mM BME to collect all sample, and samples were dried by vacuum at room temperature. Samples were resuspended in 25 μl LDS buffer (1X LDS (Invitrogen), 5% BME), boiled for 5 minutes at 95 ºC, spun at 1000 g for 1

minute, then separated by SDS-PAGE. Gels were stained with Coomassie blue and destained overnight (40% methanol, 10% acetic acid, 50% water)

Sample preparation for MS ID:

Each gel lane was cut into 8 slices. Slices were minced, and pieces were washed once in 50 mM ABC, twice in 1:1 50 mM ABC to acetonitrile (ACN), and once in ACN. Slices were dried by speed-vac. 2 μg of trypsin in 50 mM ABC was added to each gel slice, and slices were incubated overnight at 37 ºC. Proteins released from the gel were collected, and gel slices were washed in 1:1 50 mM ABC:ACN + 0.1% TFA twice, collecting the supernatant each time. The pooled supernatant was dried by speed-vac then resuspended in 25 μl 0.1% TFA in water for analysis by LC-MS/MS, performed at the Rockefeller University Proteomics Facility.

Analysis of MS data:

Peptides were identified using SEQUEST version 28 (revision 13) and X!Tandem searched against either the EcoProt *E. coli* complete proteome with 10 ppm precursor mass and 1 Da fragment mass tolerance. Cysteines were considered constantly modified by carboxyamidomethylation. Allowable variable modifications in Sequest included oxidation on methionine and tryptophan, deamidation of asparagine and glutamine. Allowable variable modifications in X!Tandem were the same with the addition of amino acid cyclization with an N-terminal glutamine or iodoacetamide-capped cysteine (-NH3), or glutamic acid (-OH) resulting in N-terminal pyrrolidone carboxylic acids. Sequest and X!Tandem data was then imported into Scaffold for Peptide Prophet filtering. Peptides

with ≥95% likelihood of correct assignment were accepted. Proteins matched with 2 or more tryptic peptides were accepted; for those proteins, non-tryptic peptides were also accepted. From these data compiled by Scaffold, high and medium confidence thresholds were assigned by spectral counts, High confidence was assigned as >10 spectral counts and >10 fold enrichment above unlabeled control, and medium confidence was assigned as >5 spectra counts and >5 fold enrichment above the unlabeled control.

CHAPTER 3. Analysis of fatty acid protein modifications in *Salmonella enterica*.

INTRODUCTION.

Salmonella enterica is the causative agent of gastroenteritis and typhoid fever worldwide[98,121]. During infection, *Salmonella* migrates from the lumen of the intestine to inside host cells. Broadly, two pathogenicity islands, termed SPI-1 and SPI-2, mediate the invasion into host cells and subsequent adaptation to the intracellular environment. SPI-1 and SPI-2 each encode Type-3 secretion systems to inject bacterial effector proteins into host cells. The injection of SPI-1 effector proteins causes transient actin remodeling to induce *Salmonella* internalization, as well as transient inflammation. Passive mechanisms of invasion, such as disruption of tight junctions or phagocytosis by dendritic cells[122,123], do not cause as much inflammation. SPI-2 effectors proteins are involved in intracellular survival mechanisms including the formation of a *Salmonella*-containing vacuole (SCV).

A variety of environmental cues regulate the gene expression changes necessary to facilitate the transition from extracellular to intracellular niche[99,124]. Many two-component systems are involved in sensing changes in pH, oxidative stress, and the concentration of different metabolites to regulate gene expression. Among these, the PhoP/Q two-component system is activated upon acidic pH and Mg^{2+} starvation, and is required for intracellular survival[125]. PhoP is thought to regulate, directly or indirectly, the expression of ~5% of the genome, particularly genes involved in virulence processes including: outer membrane modification to evade immune detection[126], antimicrobial peptide resistance, and expression of the SPI-2 Type-3 secretion system[127].

Concomitantly, PhoP/Q represses genes involved in invasion of host cells[128,129], as this process is presumably no longer required. PhoP/Q also regulates the expression of lipoproteins including SlyB, an outer membrane lipoprotein that negatively regulates PhoP/Q[130].

Both long-chain and short-chain fatty acids can modulate *Salmonella* virulence. For example, unsaturated, but not saturated, long-chain fatty acids directly repress PhoQ activity[131]. Short-chain fatty acids secreted by intestinal bacteria regulate *Salmonella* SPI-1 gene expression in a chain-length dependent manner. Specifically, acetate enhances invasion through activation of SPI-1 gene expression[16], while propionate and butyrate[14] are inhibitory. The mechanisms underlying this differential regulation by short-chain fatty acids are not well characterized, although post-translational modification of the SPI-1 transcriptional regulator HilD with a propionate-derived metabolite has been suggested[15].

In bacteria, the diversity and function of short-chain fatty acid protein modifications has only recently been explored[104,105]. In particular, multiple recent proteomics studies have highlighted the extent of lysine acetylation[132-135]. This widespread reversible modification regulates key cellular processes including transcription, translation, protein folding, and central metabolism. Lysine acetylation of protein active sites or interaction surfaces can modulate protein function. For example, in *E. coli*, acetylation of the response regulator RcsB inhibits its ability to bind target DNA, preventing transcription[136]. In *Salmonella enterica*, the widespread acetylation of metabolic enzymes regulates the flow of central carbon metabolism[134]. Besides protein acetylation, the modification of proteins with other short-chain fatty acids also occurs.

For example, lysine propionylation on the propionyl-CoA synthetase PrpE inhibits its function[137]. Other short-chain fatty acid-derived metabolites, such as malonate[138] and succinate[139-141], can also modify proteins. However, the prevalence and diverse functions of these modifications are not known.

The enzymatic machinery involved in short-chain fatty acid protein modifications is best characterized for acetylation. Lysine acetylation can be either enzyme-mediated or non-enzymatic. In enzyme-mediated lysine acetylation, the protein acetyltransferase YfiQ (Pat) transfers an acetyl group from acetyl-CoA onto protein targets. In non-enzymatic lysine acetylation, acetyl phosphate, generated by acetate kinase (Ack), transfers its acetyl group onto lysine[135,142]. Acetylation via either mechanism is subject to enzyme-mediated de-acetylation by the de-acetylase CobB[143]. Another form of enzyme-mediated acetylation is N-terminal acetylation. This seemingly rare constitutive modification occurs only on a handful of ribosomal proteins and requires specific N-terminal acetyltransferases. The enzymes involved in other short-chain fatty acid modifications are not known. However, Pat and CobB appear to be relatively promiscuous, as both protein propionylation[137] and succinylation[139] can be mediated by these enzymes.

Having demonstrated the utility of alkynyl-long-chain fatty acid reporters for the analysis of lipoproteins in *E. coli,* we explored protein fatty-acylation in *Salmonella enterica* serovar *typhimurium* (*S. typhimurium)* in response to different virulence-stimulating *in vitro* culture conditions. In addition, we evaluated the utility of alkynyl-short-chain fatty acid reporters to study the inhibitory effects of short-chain fatty acids on *Salmonella* pathogenicity.

RESULTS.

To investigate virulence-associated changes in lipoprotein expression, we labeled *S. typhimurium* with alk-14 in LB, MgM, and MgM+ media. We chose these media as a simple way to mimic virulence states representative of SPI-1 and SPI-2 activation. In LB, *S. typhimurium* basally expresses SPI-1 genes, and secretes SPI-1 effectors into the culture supernatant (Figure 3.1a). MgM is a low pH (5.0), low Mg^{2+} (10 μM) minimal media designed to mimic the intracellular environment[144]. In this media, the PhoP/Q two-component system is activated, and the SPI-1 locus is suppressed (Figure 3.1a). To isolate PhoP/Q Mg^{2+} specific responses, we also labeled *Salmonella* in a modified MgM media we call MgM+. This media is modified to be neutral pH (7.2) and high Mg^{2+} (10 mM). In this media, although SPI-1 effector secretion was inhibited, we did detect expression of the effector SopE2 by Western blot in cell lysates (Figure 3.1a), suggesting that transcription of the SPI-1 locus was not inhibited. To verify activation of PhoP/Q in MgM media specifically, we performed one proteomics experiment using *S. typhimurium* expressing FLAG-tagged MgtB[145], which is a PhoP-activated Mg^{2+} transporter[146]. By Western blot, we detected MgtB-FLAG expression only in *Salmonella* grown in MgM media (Figure 3.1b). Alk-14-labeled *S. typhimurium* cell lysates were reacted with azido-rhodamine for in-gel fluorescence profiling and with azido-azo-biotin for affinity enrichment and gel-based proteomics (Figure 3.1b).

Proteomics analysis of the three alk-14 labeled LB samples yielded 250 high confidence candidate proteins, ~5.5 times as many as identified from *E. coli* (Appendix 4). Curiously, only 10% of these high confidence proteins were predicted to be

lipoproteins (Figure 3.1c). This is in contrast to the *E. coli* dataset, where ~70% of the high confidence proteins labeled by alk-14 were predicted lipoproteins (Figure 3.1c). Instead, 49% of the high confidence proteins we recovered from *S. typhimurium* were metabolic enzymes, in contrast to the 13% identified from our *E. coli* dataset (Figure 3.1c). These included enzymes involved in both fatty acid catabolism and biosynthesis, suggesting the metabolism of alk-14 and the subsequent incorporation of an alk-14-derived metabolite into further metabolic pathways (Figure 3.2). The metabolism of alk-14 into shorter-chain acyl-CoA derivatives was suggested by labeling of the acetyl-coA synthetase, Acs, as well as numerous enzymes in the TCA cycle, glyoxlate shunt, pyruvate dehydrogenase, and gluconeogenesis/glycolysis pathways (Figure 3.2). Covalent modification of the enzymes in these pathways with an alkyne-acetyl analogue is likely, given that lysine acetylation has been previously reported on several of these enzymes as a means to regulate carbon flux[134]. Indeed, ~15% of the proteins we identified are known to be acetylated. The abundant labeling of these enzymes could also represent covalent intermediates of enzyme activity. The extensive metabolism of alk-14 by *Salmonella* but not *E. coli*, may be due to the highly diverse and redundant metabolic activity unique to *Salmonella*, which is thought to represent an adaptation to pathogenicity[96,97].

Despite the metabolic processing of alk-14, we recovered the protein YjgF from our alk-14 labeled LB samples, suggesting that fatty acid modification of YjgF is conserved (Appendix 4). YjgF shares 94% sequence identity between *E. coli* and *S. typhimurium*, and the site of modification, Cys107, is conserved. To validate alk-14 labeling of *S. typhimurium* YjgF, we generated a C-terminally His6-tagged construct of

Salmonella YjgF (YjgF-His6), and expressed it in *E. coli* BL21 (DE3) for labeling and purification. By in-gel fluorescence visualization, we saw alk-14 labeling of purified YjgF-His6 (Figure 3.1d), confirming that *S. typhimurium* YjgF is fatty acid modified.

Proteomics analysis of our MgM and MgM+ datasets revealed a breakdown of alk-14 into numerous metabolic pathways, similar to that seen in the LB dataset (Appendices 5 and 6). From the MgM+ samples, we identified the SPI-1 effector proteins SipA, SipB, and SopB (Appendix 5), which is consistent with the expression of SopE2 we observed in MgM+ cell lysates. In contrast, we did not identify any SPI-1 effector proteins from the MgM dataset (Appendix 6). Activation of PhoP/Q in MgM media was evidenced by the identification of PhoP itself, as well as PhoP-activated proteins PhoN, MgtB, OmpX, and SlyB[147] (Appendix 6). Interestingly, we recovered the SPI-1 transcriptional regulator HilA from our MgM dataset (Appendix 6). PhoP/Q represses expression of the SPI-1 locus through the inhibition of HilA[128]. The direct modification of HilA with a fatty acid derived metabolite could be a mechanism of inhibition. Activation of HilA requires the integration of several inputs upstream of the transcriptional regulators HilE, HilC, HilD, and RtsA[124]. The activity of HilD, which positively regulates HilA, has been shown to be inhibited by propionate, but not acetate[15]. Post-translational modification of HilD with either propionate or acetate[134] may mediate this regulation. The covalent modification of both HilD and HilA with fatty acid derived metabolites could serve to fine-tune the regulation of SPI-1 expression by short-chain fatty acids.

Figure 3.1. Summary of alk-14 modified proteins identified in *S. typhimurium*.
a. Profile of proteins secreted by *S. typhimurium* in different media visualized by Coomassie blue staining (CB). Effector proteins are secreted in LB and BHI media, but not MgM+, MgM, or N-minimal (Nmin) media. Anti-HA Western blot (WB) of SopE2-CPG2-HA from cell lysates of the same cultures. SopE2 is a SPI-1 effector protein required for host cell invasion. SopE2 is not expressed in MgM or N+ media. Ponceau staining (Pon) shows loading control. **b.** Representative gels of alk-14-labeled proteins retrieved from *S. typhimurium* using the azido-azo-biotin affinity tag. *S. typhimurium* were grown in LB, MgM+ or MgM media. Cells were metabolically labeled with 20 μM alk-14 and labeled lysates were reacted with azido-rhodamine for in-gel visualization (left). The remaining lysate was reacted with azido-azo-biotin, and labeled proteins were captured on streptavidin beads. Captured proteins were eluted with $Na_2S_2O_4$ and total eluant was visualized by Coomassie blue (CB) (right). Anti-FLAG WB shows expression of MgtB-FLAG in MgM media, but not MgM+ or LB media. For a list of proteins identified, see Appendices 4-6. **c.** Pie charts of high-confidence candidate proteins recovered from alk-14 labeling in LB for *E. coli* as compared to *S. typhimurium*. Proportion of predicted lipoproteins (aqua), metabolic enzymes (purple) or other proteins (grey) is as indicated. **d.** Alk-14 labeling of *S. typhimurium* YjgF-His_6. YjgF was cloned from *S. typhimurium* and expressed with a C-terminal His_6-tag in *E. coli* BL21(DE3) under an IPTG-inducible promoter. Total cell lysates and elutions from the His_6-purifications are shown. Coomassie blue (CB) indicates protein loading.

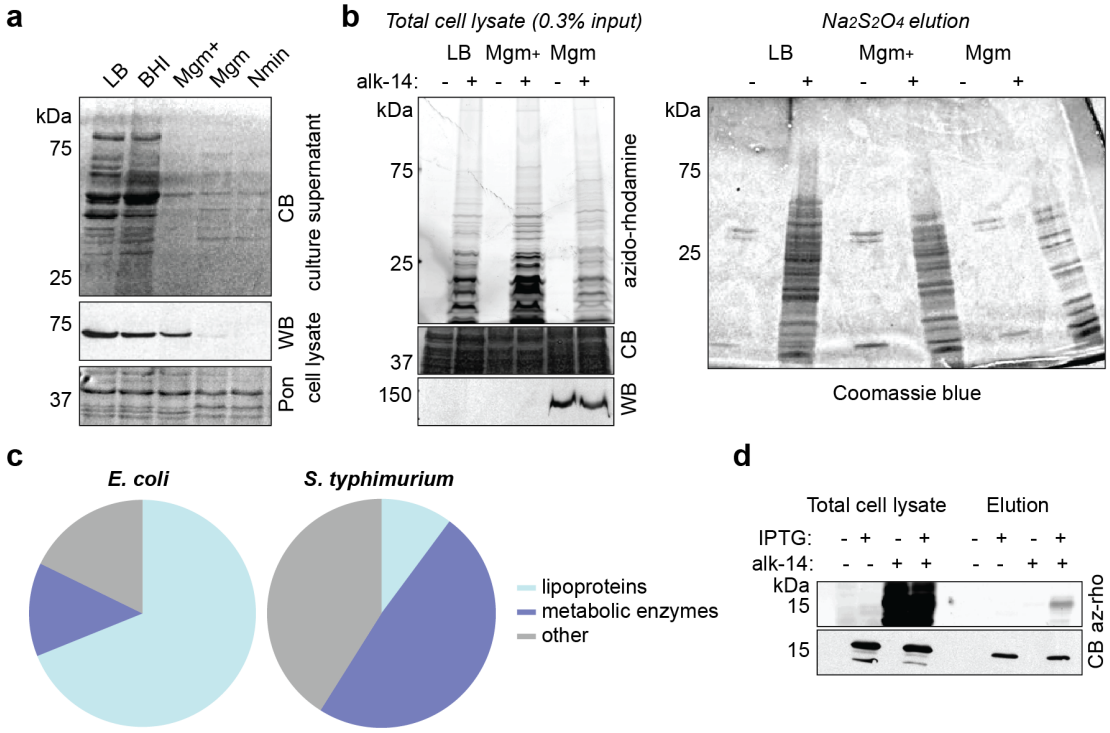

Figure 3.1. Summary of alk-14 modified proteins identified in *S. typhimurium*.

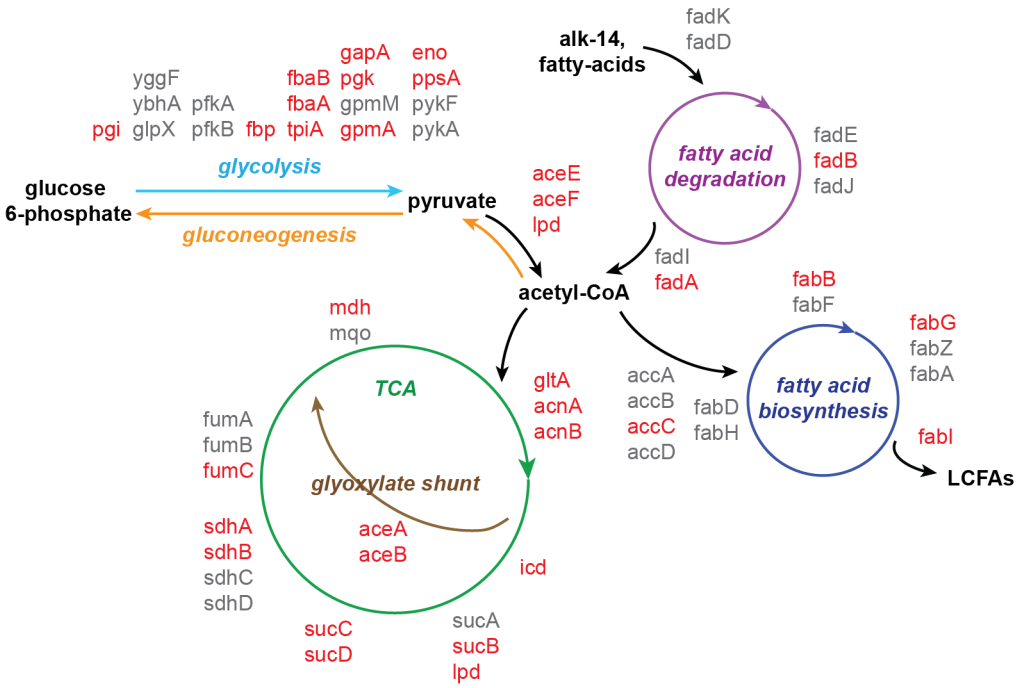

Figure 3.2. Metabolism of alk-14 by *S. typhimurium*

Schematic showing alk-14-labeled enzymes involved in central metabolism identified in the *S. typhimurium* LB proteomics dataset. All enzymes in the fatty acid degradation, fatty acid biosynthesis, TCA cycle, glyoxylate shunt, and glycolysis/gluconeogenesis pathways are shown. Enzymes recovered with high confidence in alk-14 samples are highlighted in red. alk-14 theoretically feeds into the fatty acid degradation pathway as indicated.

To take a more direct approach to assess the protein modifications possibly underlying the regulation of the SPI-1 locus by short-chain fatty acids, we first assessed whether alk-3 and alk-4 could mimic the inhibitory effects of short-chain fatty acids on SPI-1 effector secretion. We analyzed SPI-1 effector secretion *in vitro* in the presence of alk-3 or alk-4[109] (Figure 3.3a and b). By Coomassie blue staining, we observed a dose-dependent reduction in secretion for both alk-3 and alk-4, which is consistent with the inhibitory effects on SPI-1 secretion by propionate and butyrate respectively (Figure

3.3b). To measure secretion rate, we used a *Salmonella* reporter strain previously developed by the Hang laboratory that expresses SopE2-CPG2-HA under its endogenous promoter[148]. Secreted CPG2 cleaves a dye presented in the media, resulting in a color change that allows quantification of secretion rate. Measuring SopE2-CPG2-HA secretion confirmed dose-dependent inhibition of secretion by alk-3 and alk-4 (Figure 3.3c). Fluorescence visualization of alk-3 and alk-4 modified proteins in the culture supernatant revealed modification of several effector proteins (Figure 3.3b). In alk-3 and alk-4 labeled cell lysates, we observed an abundance of modified proteins (Figure 3.3a). Future proteomics analysis of these labeled proteins may give insight into the inhibitory effect of short-chain fatty acid reporters. Although alk-2-labeling in *E. coli* suggests that it does not function as an acetic acid analogue, it will be interesting to re-evaluate alk-2 labeling in *Salmonella*, and determine if it can enhance SPI-1 secretion.

Figure 3.3. Protein labeling and inhibition of SPI-1 effector secretion by short-chain fatty acids.

a. Fluorescence profiling of alk-4ONa and alk-3ONa-modified proteins in *S. typhimurium* cell lysates. Cells were metabolically labeled with an increasing dose of either alk-4ONa or alk-3ONa in LB media (an increasing dose of 3 mM, 5 mM, 10 mM, and 20 mM was used for each reporter). 5 mM and 20 mM NaCl were used as a control for salt addition. (-) indicates water control. Coomassie blue (CB) indicates protein loading. **b.** Fluorescence profile (top) and Coomassie blue staining (bottom) of SPI-1 protein secretion in culture. Increasing dose of alk-4ONa and alk-3ONa inhibits the secretion of SPI-1 effector proteins, while an increasing dose of NaCl has no effect on secretion. **c-e.** SopE2-CPG2-HA secretion assays from culture supernatants of cells exposed to increasing doses of **c.** NaCl, **d.** alk-4ONa, and **e.** alk-3ONa. SopE2-CPG2-HA secretion decreases in a dose dependent manner with alk4ONa and alk-3ONa, but not with NaCl.

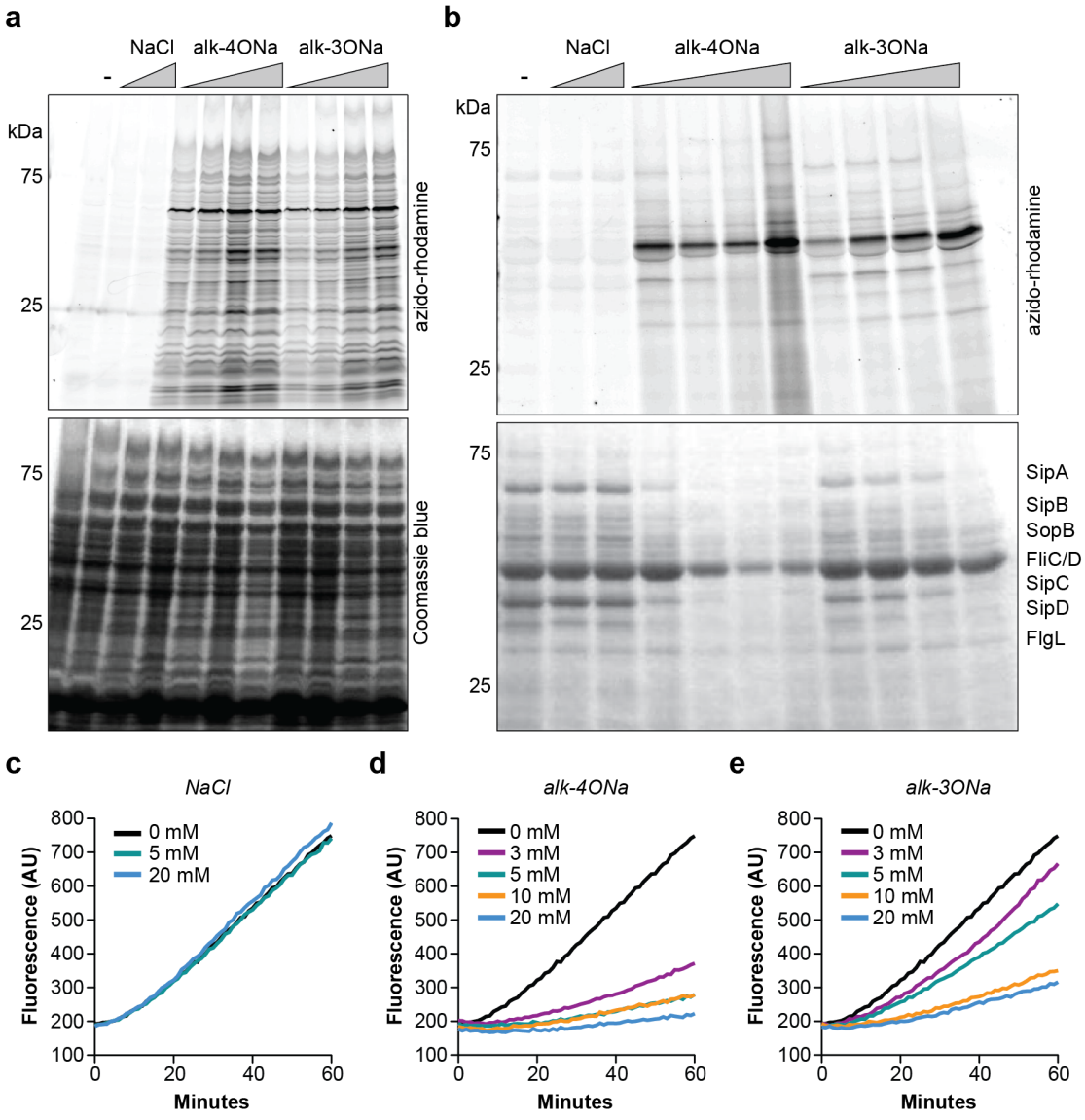

Figure 3.3. Protein labeling and inhibition of SPI-1 effector secretion by short-chain fatty acids.

SUMMARY.

Our studies in *Salmonella* have emphasized the metabolic differences between *E. coli* and *Salmonella* that make lipoprotein characterization in *Salmonella* using alk-14 difficult. The study of alk-14 metabolism by *Salmonella* could be a viewed as a cautionary tale for using this reporter in the analysis of bacterial lipoproteins. Alternatively, alkyne-functionalized fatty acid reporters could be used in pulse-chase experiments to study lipid metabolism, turnover, or enzyme specificity, as it affects protein modification. Such experiments would be complementary to metabolic studies that use ^{13}C-isotope labeling. Future studies requiring a lipoprotein-specific reporter in *Salmonella* could evaluate the utility of alk-16nh[112], which theoretically cannot engage fatty acid metabolic pathways.

Our alk-14 proteomics analysis in *Salmonella* nonetheless suggests an intriguing fatty-acid modification on HilA that warrants future investigation. Future work characterizing the effects of short-chain fatty acid protein modifications on virulence using the reporters alk-3 and alk-4 seems to be a promising avenue, as these reporters function similarly to propionate and butyrate in inhibiting SPI-1 mediated effector secretion. In fact, recent work by Jerry Zhang from the Hang laboratory has confirmed that alk-14, alk-3, and alk-4 all label HilA, although the precise modification(s) and how they affect protein function remain to be determined.

ACKNOWLEDGEMENTS AND CONTRIBUTIONS.

Thanks to Guillaume Charron, who synthesized alk-14; to Yu-Ying Yang, who synthesized azido-azo-biotin, alk-3, and alk-4; and to Paul Dossa, who synthesized azido-rhodamine. Thanks to The Rockefeller Proteomics Facility who ran all samples for LC-MS/MS analysis. In addition, thanks to Eduardo Groisman for gifting us the MgtB-FLAG *S. typhimurium* strain, and to Jacob Yount for the *S. typhimurium* SopE2-CPG2-HA strain. Thank you to Jacob Yount, Markus Grammel, and Paul Dossa for advice on *Salmonella* secretion assays and general microbiology. Finally, thanks to Jerry Zhang, who is currently studying the effects of short-chain fatty acids on *Salmonella* SPI-1 secretion and HilA function.

MATERIALS AND METHODS.

Strains.

E coli DH5α, *E. coli* BL21-RIL(DE3), and *Salmonella enterica* serovar *typhimurium* strain IR715 were grown in LB (BD Difco). *S. typhimurium* strain MgtB-FLAG was a gift from Eduardo Groisman[145].

Plasmids used in this study.

The *S. typhimurium* strain carrying SopE2-CPG2-HA was generated by Jacob Yount[148]. SopE2-CPG2-HA is encoded on the pWSK29 vector, which carries ampicillin resistance.

pET21a-YjgFStm-His6: YjgF was PCR amplified out of the *S. typhimurium* genome using the following primer set:

FW: AAAGGATCCAATGAGCAAAACTATTGCGACGG

RV: TTTGAATTCTTGCGACGAACAGCGATCGCTTCA

The PCR product was cut with BamH1 and EcoR1 and ligated to cut pET21a vector. pET21a-YjgFStm-His6 was transformed into *E. coli* DH5α for sequencing, and the sequence-verified construct was transformed into *E. coli* BL21-RIL(DE3) for expression.

Metabolic labeling and click chemistry methods for alkynyl-fatty acid labeled protein visualization and proteomics are essentially the same as outlined in Chapter 1 Materials and Methods, with the following modifications:

Salmonella typhimurium Experiments 1, 2, and 3: Overnight cultures of *S. typhimurium* were diluted 1:1000 into fresh LB and grown up to OD_{600} = 1.4. For labeling in LB, culture was pelleted, washed @X in LB, resuspended in fresh LB with 20 μM alk-14 (or DMSO as negative control) and labeled for 4 hours. For labeling in MgM or MgM+ media, cultures were pelleted then washed 2X in MgM media[144] (100 mM Tris-HCl, 5 mM KCl, 7.5 mM $(NH_4)_2SO_4$, 1 mM KH_2PO_4, 0.5 mM K_2SO_4, 38 mM glycerol, 10 μM $MgCl_2$, 0.1% casamino acids, pH 5) or MgM+ media (100 mM Tris-HCl, 5 mM KCl, 7.5 mM $(NH_4)_2SO_4$, 1 mM KH_2PO_4, 0.5 mM KH_2PO_4, 38 mM glycerol, 10 mM $MgCl_2$, 0.1%

casamino acids, pH 7), resuspended in either MgM or MgM+ with 20 μM alk-14 (or DMSO as negative control) and labeled for 4 hours.

After LC-MS/MS, peptides were searched against the S. *typhimurium* 14028 complete proteome found on Uniprot.

SPI-1 protein secretion assays.

SPI-1 secretion in different media: 2 ml of LB, BHI, MgM, MgM+, or N-minimal media[149] (0.1 mM Tris-HCl, 5mM KCl, 7.5 mM (NH4)2SO4, 0.5 mM K2SO4, 1 mM KH2PO4, 0.2% glucose, 38 mM glycerol, 10 μM MgCl2, 0.1% casamino acids, pH 7.4) was inoculated 1:30 with an overnight culture of *S. typhimurium* expressing SopE2-CPG2-HA. Cultures were grown for 4 hours, shaking at 37 °C, the pelleted at 7000 g for 5 minutes. 1 ml of culture supernatant was precipitated with trichloro acetic acid (TCA) at a final concentration of 10% overnight at 4 °C. Precipitated proteins were pelleted at 20,800 g for 30 minutes, rinsed 2 times in acetone, then air-dried. Proteins were then separated by SDS-PAGE and visualized by Coomassie blue staining. A parallel gel was run for anti-HA (Clonetech) Western blot and Ponceau staining.

SPI-1 secretion in the presence of alk-3, alk-4, or NaCl: For each condition, 2 mL of LB was inoculated 1:30 with an overnight culture of *S. typhimurium*. Varying concentrations of alk-3, alk-4 or NaCl was added to media. Cultures were processed as described above. Proteins were separated by SDS-PAGE and visualized by rhodamine fluorescence and Coomassie blue staining.

SopE2-CPG2-HA assay.

The SopE2-CPG2-HA secretion assay was performed as described by Yount et al[148]. Varying doses of alk-3, alk-4 or NaCl were added to each secretion reaction.

CHAPTER 4. Characterization of a bacterial secreted peptidoglycan hydrolase that enhances host resistance to *Salmonella*.

INTRODUCTION.

As discussed in Chapter 1, the intestinal microbiome mediates host resistance to enteric pathogens through a variety of direct and indirect protection mechanisms. Recent concerns over the spread of antibiotic resistance, as well as enhanced pathogen virulence after antibiotic-induced dysbiosis[150,151], have made the development of probiotic therapies an attractive alternative to antibiotics. Indeed, the clinical potential of microbiota-based therapies against infectious disease is now being explored. Available treatments are still limited, however, with fecal transplantation for *Clostridium difficile* infection being the only FDA-approved therapy[152,153]. Transitioning to more targeted therapeutics requires a better understanding of the specific protection mechanisms of individual bacterial species.

The characterization of beneficial bacterial species has been facilitated by germ-free and gnotobiotic animal models. Although these models reduce the complexity of the microbiota, they do not reduce the complexity of the host immune system, which has co-evolved with, and is regulated by, the intestinal microbiome. We reasoned that a more simplified animal model could be useful as an initial screening platform to identify new commensal factors relevant to inhibiting bacterial pathogenesis. These candidate commensal factors could then be tested for activity in more complex mammalian models.

We chose to develop *C. elegans* as a model host for the mechanistic exploration of commensal-pathogen interactions in the intestine. *C. elegans* has been used extensively as a model organism for studying evolutionarily conserved aspects of innate immunity and microbial pathogenesis[154,155]. *C. elegans* lacks an adaptive immune response, as well as innate immune cells. Instead, the *C. elegans* innate immune system comprises both constitutive and induced signaling pathways, many with homology to mammalian innate immune components. In response to intestinal infection, *C. elegans* mounts pathogen-specific immune responses[156,157], which can lead to behavioral changes[158] as well as the expression of antimicrobial and stress response effectors. The mechanisms of pathogen recognition, however, have not been characterized. The *C. elegans* genome lacks a diversity of putative TLRs or NLRs; however, it encodes over 250 C-type lectin domain containing proteins[159], which may function as pattern recognition receptors.

Despite differences in host immunity, several human pathogens, including *Salmonella enterica*[160,161], are pathogenic to *C. elegans*. After being ingested, *Salmonella* establishes a persistent luminal infection in *C. elegans,* ultimately resulting in death. In non-typhoid human infections, the majority of *Salmonella* persist extracellularly in the intestine[98]. Transient inflammation associated with invasion is thought to give the luminal population a competitive advantage over other intestinal bacteria[162]. In *C. elegans,* the requirement of *Salmonella* virulence factors involved in host cell invasion and intracellular replication is unclear[163]. Internalization of *Salmonella* by the intestinal epithelia has been reported, but bacteria were found mostly contained within autophagosomes and are subsequently degraded[164]. It is possible, then, that *Salmonella*

virulence determinants during infection of *C. elegans* instead reflect conserved adaptations to extracellular intestinal life required in non-systemic diarrheal disease.

Broadly speaking, the *C. elegans* intestinal milieu is thought to have a similar physiology to the mammalian small intestine[165]. The intestinal epithelium is composed of polarized cells with apical microvilli. Cells are connected by apical junctions, which are homologous to mammalian tight junctions[166]. Coating the microvilli is a peritrophic matrix/glycocalyx[167] containing unstructured proteoglycans[168,169] that is functionally similar to the mammalian intestinal mucosa, acting as a barrier and filter. The basolateral basement membrane is composed of extracellular matrix proteins, including homologues of laminin and type IV collagen[170]. The intestinal lumen has a pH ranging from ~6 to ~4 from pharynx to tail[171], and comprises lysozymes, digestive enzymes, and antimicrobial peptides secreted by the intestinal epithelia.

In the laboratory, *C. elegans* do not have an endogenous intestinal microbiota, and instead feed on a monoculture of *E. coli* OP50[172]. However, many species of bacteria are able to colonize the worm intestine. In the wild, *C. elegans* harbor live bacteria and yeasts in their intestine[173], although the extent and composition of a stable *C. elegans* intestinal microflora is unknown. Interestingly, aerobically grown *Enterococcus faecium* can colonize the *C. elegans* intestine without causing apparent disease[174]. For this reason, we chose to focus on *E. faecium* as a model "commensal" in our studies.

Enterococci are facultatively anaerobic, lactic acid bacteria, formerly classified as Group D *Streptococci*[175]. *Enterococci* are part of the intestinal microbiome of diverse animal species[176,177] including: mammals, reptiles, birds, lamprey[178], snails[179], and flies. For this reason, *Enterococci* are regarded as primordial founding members of the

intestinal microbiome. In humans, *E. faecium* and *E. faecalis* constitute the predominant species of colonizing *Enterococci*. Although found throughout the small and large intestine, *E. faecium* and *E. faecalis* numbers are concentrated in the jejunum, ileum, and caecum[180].

In animals including chickens, pigs, dogs, and mice, probiotic strains of *E. faecium* have been shown to inhibit the pathogenesis of various enteric pathogens, including *Salmonella enterica*[181,182]. A variety of mechanisms have been proposed, including: secretion of antimicrobial bacteriocins[183], modulation of host immunity[184], and prevention of pathogen adhesion[185]; but the relevant *in vivo* protection mechanisms have remained unclear. Nevertheless, *E. faecium* is included in veterinary probiotic formulations against diarrheal disease. In humans, the utility of *E. faecium* as a therapeutic is limited due to its potential to acquire pathogenicity after antibiotic treatment in nosocomial infections[186,187]. Decoupling the beneficial effects of *E. faecium* from the risks associated with using *E. faecium* as a probiotic could greatly increase its therapeutic potential.

In this study, we aimed to develop *C. elegans* as a model system to characterize *E. faecium*-mediated restriction of *Salmonella* pathogenesis. We hoped that in the absence of an endogenous microbiota and host adaptive immune system, we would be able to distill commensal-pathogen interactions relevant to more complex mammalian models. Thus, our *C. elegans* model system would provide a bridge between *in vitro* studies and mouse models, to discover and characterize the conserved bacterial factors underlying *E. faecium* probiotic function.

RESULTS.

For our experiments, we used *Salmonella enterica* serovar *typhimurium* strain IR715 (*S. typhimurium*) as a model pathogen. This strain is a naladixic acid resistant variant of strain 14028, and both strains are comparably pathogenic to *C. elegans* (Figure 4.1a). To investigate whether *E. faecium* can inhibit *Salmonella* pathogenesis in *C. elegans*, we developed a pulsed treatment-infection assay (Figure 4.1c). The standard *C. elegans Salmonella* infection model is one of continuous re-infection[188], but *Salmonella* is known to persistently colonize the worm intestine[160], and can shorten lifespan even after just 1 hour of infection (Figure 4.1b). We reasoned that a pulsed infection time would maximize our chances of recapitulating dynamic commensal-pathogen interactions in the worm intestine, and perhaps highlight more subtle protection mechanisms that constant re-infection could obscure. After surveying a few different treatment and infection time windows, we decided on a 1 day treatment - 1 day infection regimen (Figure 4.1c). In our assay, worms were treated with different bacteria on agar plates for 1 day, then infected with *S. typhimurium* on agar plates for another day (Figure 4.1c). Worms were then transferred onto *E. coli* OP50 agar plates for the remainder of the assay, and survival was scored. Control worms were fed *E. coli* OP50 for all stages of the assay.

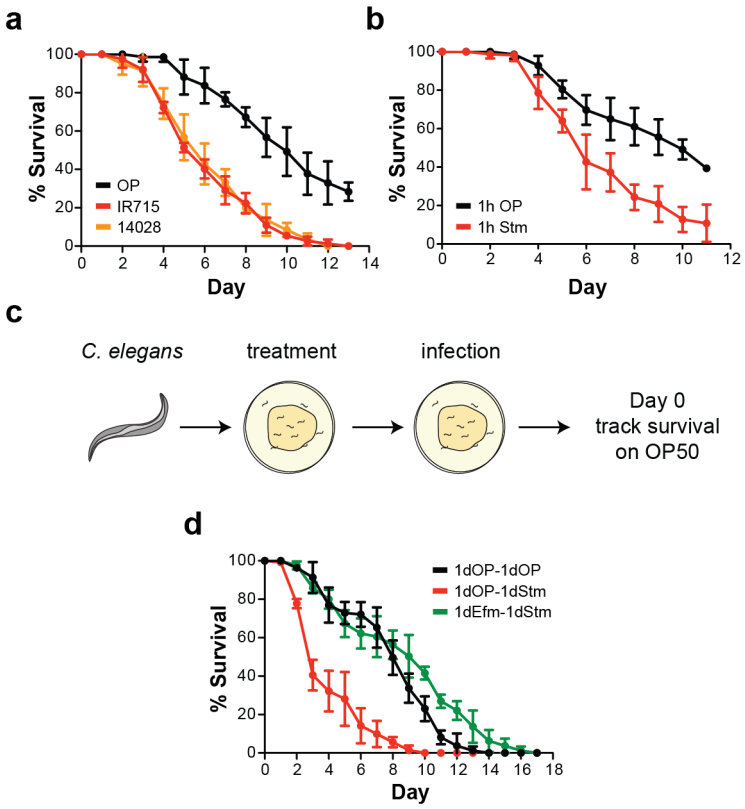

Figure 4.1. A pulsed treatment infection assay for analyzing *E. faecium*-mediated inhibition of *Salmonella* pathogenesis.

a. Survival curve of *Salmonella* pathogenesis in a continuous infection assay. Worms were fed *E. coli* OP50, *S. typhimurium* strain IR715 or *S. typhimurium* strain 14028. **b.** Survival curve after 1 hour pulsed *Salmonella* infection. Worms were fed *E. coli* OP50 or *S. typhimurium* on BHI agar plates for 1 hour before transfer to *E. coli* OP50-NGM plates for the remainder of the assay. **c.** Schematic of pulsed treatment-infection assay. See text for details. **d.** Pulsed treatment-infection assay with a 1 day treatment and 1 day infection. Legend indicates treatment-infection. Abbreviations: *E. coli* OP50 (OP); *S. typhimurium* (Stm); *E. faecium* (Efm). For a, b, and d, data points represent mean ± standard deviation for 3 plates of 30 worms each.

In this assay, *C. elegans* survival was increased in worms fed *E. faecium* prior to infection with *S. typhimurium* as compared to worms fed *E. coli* OP50 (Figure 4.1d).

Because *E. faecium* grows poorly on standard nematode growth medium, we performed the treatment and infection steps on BHI agar, which is commonly used to assess the effects of *Enterococcus* on *C. elegans* survival. However, continuous feeding on *E. coli* OP50 grown on BHI agar has been reported to be pathogenic to worms[174]. *E. faecium* treatment prior to 1 day of feeding on *E. coli* OP50 grown on BHI prolonged survival, indicating an inhibition of intrinsic *E. coli* OP50 pathogenesis (Figure 4.2b). However, we did not observe a decrease in survival when worms were fed *E. coli* OP50 prior to *Salmonella* infection as compared to non-pathogenic *Bacillus subtilis* 168 (Figure 4.2c). This suggests that in a pulsed treatment format, *E. coli* OP50 only marginally contributes to pathogenesis in our assay.

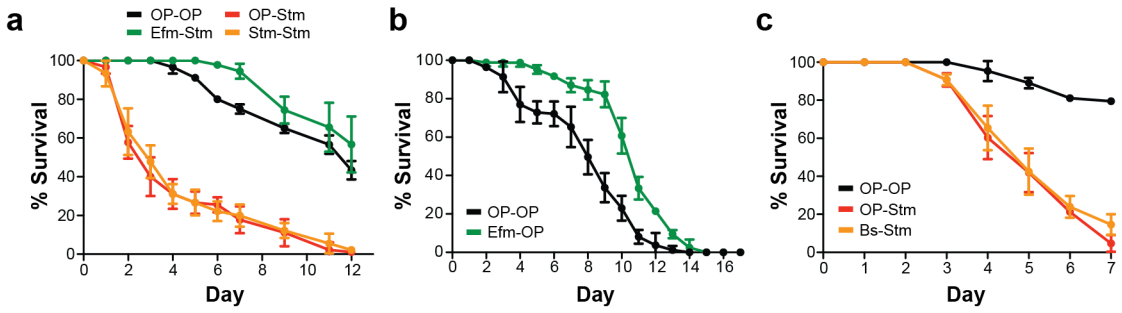

Figure 4.2. Contribution of *E. coli* OP50 pathogenesis.

a. Pulsed treatment-infection assay comparing 1 day *E. coli* OP50 treatment, 1 day *Salmonella* infection (OP-Stm) to a 2 day Salmonella infection (Stm-Stm). **b.** Pulsed treatment-infection assay showing *E. faecium* treatment inhibits *E. coli* OP50 pathogenesis. **c.** Pulsed treatment-infection assay showing that *B. subtlis* treatment does not inhibit *Salmonella* pathogenesis. Abbreviations: *E. coli* OP50 (OP); *S. typhimurium* (Stm); *E. faecium* (Efm), *B. subtilis* (Bs). For a-c, data points represent mean ± standard deviation for 3 plates of 30 worms each.

E. faecium is a genetically divergent species, with an abundance of mobile genetic elements and below 95% average nucleotide identity across some strains[189,190]. Nevertheless, we found that multiple strains of *E. faecium* were able to inhibit *Salmonella* pathogenesis, including a pig fecal isolate (NCTC 7171), two commensal human fecal isolates (Com12 and Com15), and a pathogenic human blood isolate (DO) (Figure 4.3a and b). These results suggest that despite genetic variation across the *E. faecium* strains tested, the mechanism of *E. faecium* protection is conserved. In our study, we chose to further characterize *E. faecium* strain Com15.

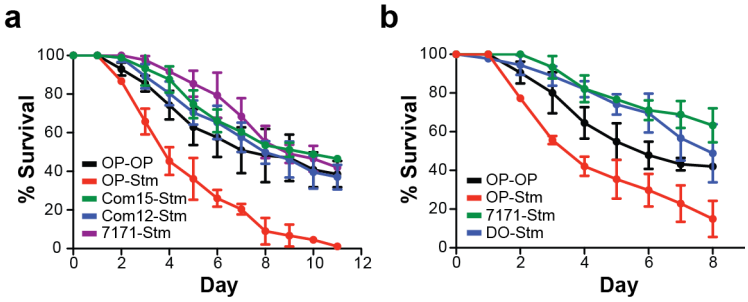

Figure 4.3. Inhibition of *Salmonella* pathogenesis by various *E. faecium* strains. **a.** Pulsed treatment-infection assay comparing treatment with *E. faecium* strains Com15, Com12, and NCTC 7171. **b.** Pulsed treatment-infection assay comparing treatment with *E. faecium* strains NCTC 7171 and DO. Abbreviations: *E. coli* OP50 (OP); *S. typhimurium* (Stm). For a and b, data points show mean ± standard deviation for 3 plates of 30 worms each.

Figure 4.4. Characterization and imaging of GFP- and mcherry-*Salmonella* infected *C. elegans*.

a. Continuous infection assay comparing wild type *Salmonella* to GFP-*Salmonella* (Stm, GFP) pathogenesis. **b.** Pulsed treatment-infection assay comparing wild type *Salmonella* to GFP-*Salmonella* pathogenesis. **c.** Fluorescence imaging of *C. elegans* infected with GFP-*Salmonella* (GFPStm) at day 6 in a continuous infection assay. The dotted lines indicate the outline of the worm body. Scale bar = 100 μm. **d.** Fluorescence imaging of *C. elegans* infected with GFP-*Salmonella* at day 3 in a pulsed infection assay. The images have been adjusted to show GFP auto-fluorescence of the gut. The lumen of the intestine is dark (top image). GFP-Salmonella appear to be ingested (bottom image) but do not subsequently colonize. The arrow indicates GFP-*Salmonella* in the isthmus of the pharynx. The dotted lines indicate the outline of the worm body. Scale bar = 50 μm. **e.** Continuous infection assay comparing wild type *Salmonella* (Stm, wt) to mcherry-*Salmonella* (Stm, mch) pathogenesis. **f.** Pulsed treatment-infection assay comparing wild type *Salmonella* to mcherry-*Salmonella* pathogenesis. **g.** Fluorescence images of *C. elegans* infected with mcherry-*Salmonella* (mcherryStm) at day 3 post-infection. The dotted lines indicate the outline of the worm body. Scale bar = 100 μm. Abbreviations: *E. coli* OP50 (OP); *S. typhimurium* (Stm); *E. faecium* (Efm). For a, b, d, and f, data points show mean ± standard deviation for 3 plates of 30 worms each.

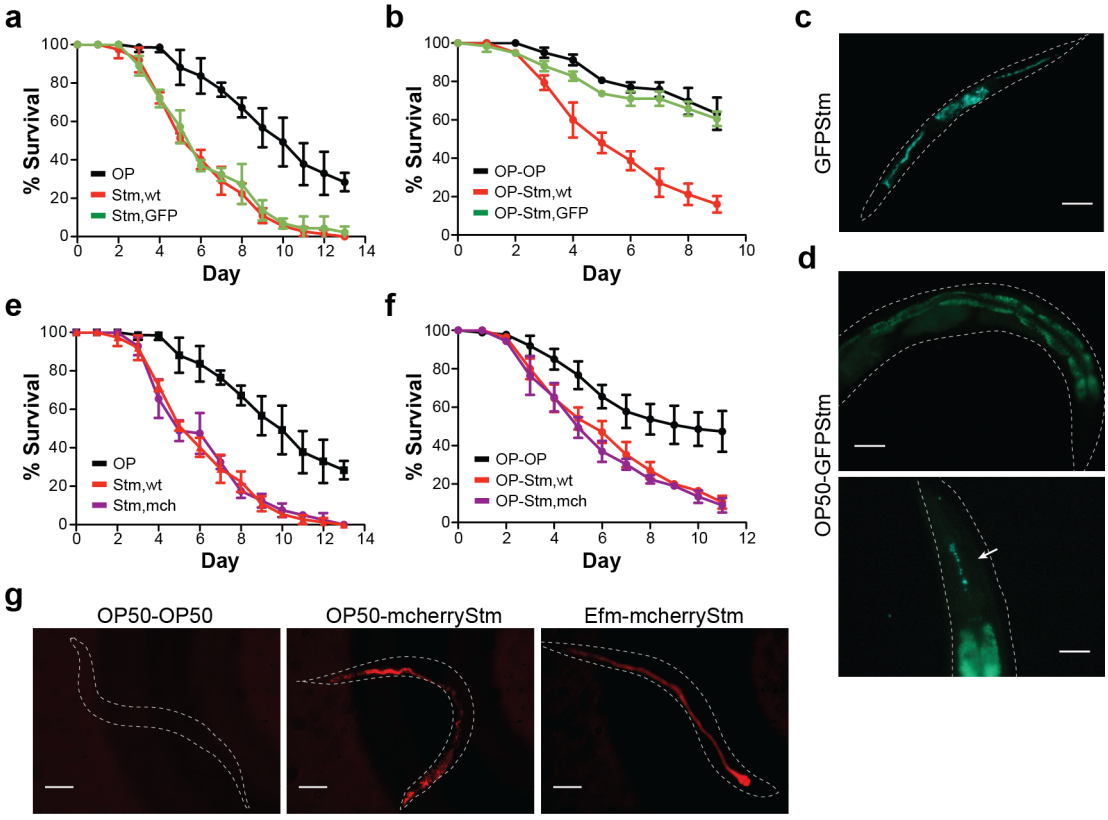

Figure 4.4. Characterization and imaging of GFP- and mcherry-*Salmonella* infected *C. elegans*.

To investigate the mechanism of *E. faecium*-mediated protection, we first analyzed the effect of *E. faecium* treatment on *S. typhimurium* colonization. Previous studies analyzing *Salmonella* colonization of worms have used *Salmonella* expressing GFP, although to our knowledge the relative pathogenicity of such strains has not been assessed. In mammalian cell culture models of *Salmonella* pathogenesis, certain strains of GFP-*Salmonella* exhibit attenuated virulence[191]. We found that GFP-*S. typhimurium* was pathogenic in a continuous infection model (Figure 4.4a), but non-pathogenic in the pulsed infection model (Figure 4.4b). This attenuation of pathogenicity seemed to be dependent on colonization, as GFP fluorescence imaging 3 days post-infection revealed little to no intestinal colonization (Figure 4.4c and d). For this reason, we instead used mcherry-*S. typhimurium*, which we found to be pathogenic in both a continuous and pulsed infection setting (Figure 4.4e and f). Fluorescence imaging of mCherry-*S. typhimurium* 3 days post-infection showed comparable *Salmonella* colonization of worms with or without *E. faecium*-treatment (Figure 4.4g).

Salmonella colony forming units (CFUs) recovered from lysed worms throughout the infection assay revealed robust initial *Salmonella* colonization of worms regardless of prior *E. faecium* treatment (Figure 4.5a). Interestingly, in *E. faecium*-treated worms, we observed a ~2 log decrease in *Salmonella* colonization 1 day post-infection. By 3 days post-infection, however, *Salmonella* titer was similar in OP50- and *E. faecium*-treated *Salmonella*-infected worms. The transient decrease in *Salmonella* CFUs may reflect niche competition between *Salmonella* and *E. faecium*, or an induced antimicrobial host response. To determine if this transient decrease in *Salmonella* colonization represented direct niche competition early in our assay, we monitored *E. faecium* CFUs throughout

the infection assay as well (Figure 4.5b). *E. faecium* initially colonized worms to ~10^5 CFUs/worm. After infection, however, *E. faecium* numbers decreased to ~10-10^2 per worm for the remainder of the assay. The decrease in *Salmonella* numbers 1 day post-infection did not coincide with an outgrowth of *E. faecium*, suggesting that this decrease is not due to simple niche competition.

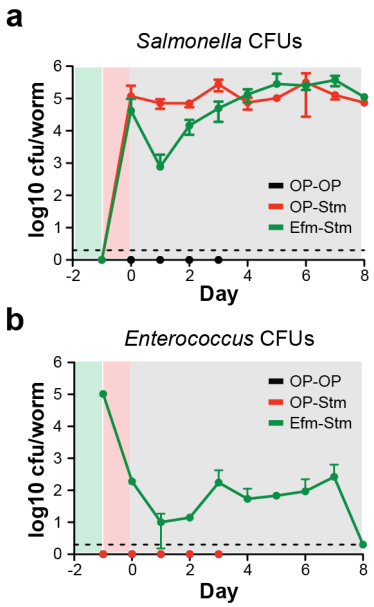

Figure 4.5. *E. faecium* transiently affects *Salmonella* colonization.
a. *Salmonella* CFUs measured in *C. elegans* throughout the pulsed treatment-infection assay. **b.** *Enterococcus* CFUs measured in *C. elegans* throughout the pulsed treatment-infection assay. For a and b, the background shading represents stages of the pulsed treatment-infection assay. Green indicated treatment, red indicates infection, and grey indicates *E. coli* OP50 feeding. The data points represent average CFUs from 5 worms ± standard deviation from two independent experiments. The dotted line indicates detection limit. Abbreviations: *E. coli* OP50 (OP); *S. typhimurium* (Stm); *E. faecium* (Efm).

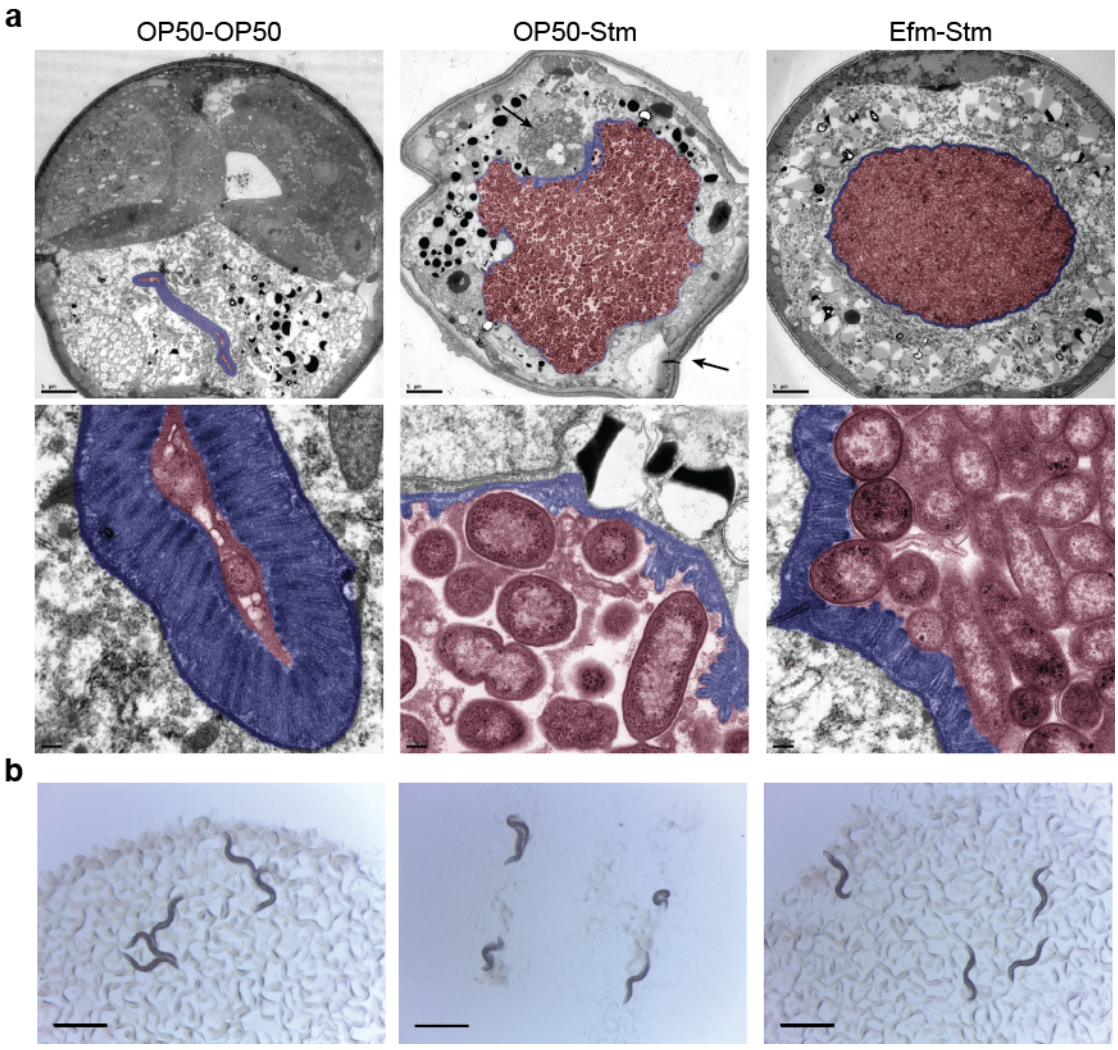

Figure 4.6. Electron microscopy of *Salmonella*-infected *C. elegans*.

a. Electron microscopy of transverse sections of *C. elegans* (top), and magnification of intestinal region (bottom) at day 4 post-infection in the pulsed treatment-infection assay. Conditions are as indicated on top. The blue coloring indicates the intestinal microvilli; the red coloring indicates the intestinal lumen. Arrows in the top middle panel indicate bacteria that have breached the epithelial barrier and escaped the lumen (top arrow) as well as loss of overall worm turgidity (bottom arrow). Scale bar (top row) = 5 μm. Scale bar (bottom row) = 200 nm. **b.** Images of worms from day 1 post-infection in the pulsed treatment-infection assay. Conditions are as indicated in (a.) Scale bar = 1mm. Abbreviations: *E. coli* OP50 (OP); *S. typhimurium* (Stm); *E. faecium* (Efm).

Electron microscopy of worm transverse sections 4 days post-infection revealed substantial degradation of the intestinal microvilli in OP50-treated *Salmonella*-infected worms compared to uninfected or *E. faecium*-treated worms (Figure 4.6a). In OP50-treated *Salmonella*-infected worms, we observed extensive tissue damage and bacteria transgressing the lumen (Figure 4.6a, middle panel). We do not believe this represents Type-3 secretion-mediated invasion, but rather bacterial outgrowth resulting from destruction of the intestinal barrier. In contrast, despite bearing a comparable bacterial load, *E. faecium*-treated worms appear to have contained the infection to the intestinal lumen and show no apparent tissue damage (Figure 4.6a, right panel), possibly indicating an enhancement in epithelial barrier function[21]. Consistent with these images, we observed that *E. faecium*-treated worms appeared less fragile and more motile than OP50-treated worms after infection (Figure 4.6b). Taken together, these results demonstrate that *E. faecium* does not prevent *Salmonella* colonization, and suggest that *E. faecium* is not acting through niche competition or a bactericidal mechanism.

To determine if *E. faecium* could inhibit pathogenesis when delivered *after* *Salmonella* infection, we inverted the order of our treatment-infection assay, and assessed *E. faecium*-mediated protection. When administered after infection, *E. faecium* was unable to inhibit pathogenesis (Figure 4.7a). We measured both *S. typhimurium* and *E. faecium* CFUs throughout the assay, to determine if differences in colonization efficiency could account for the difference we observed in survival (Figure 4.7b and c). Order of treatment and infection did not largely affect *Salmonella* colonization (Figure 4.7b). Regardless of treatment-infection order, we also observed a similar transient decrease in *Salmonella* CFUs (Figure 4.7b), suggesting that this decrease in *Salmonella* titer is not

key to the mechanism underlying *E. faecium*-mediated protection. In addition, infection with *Salmonella* did not inhibit subsequent *E. faecium* colonization (Figure 4.7c), indicating that *E. faecium* colonization alone is not sufficient for protection. This suggests that some sort of host priming may be necessary for *E. faecium*-mediated protection.

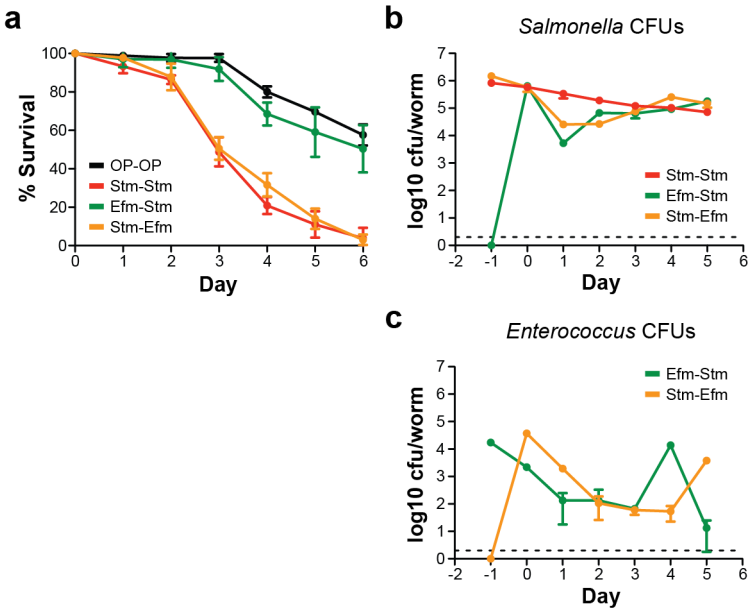

Figure 4.7. *E. faecium* cannot inhibit *Salmonella* pathogenesis when delivered after infection.

a. Pulsed treatment-infection assay showing that *E. faecium* administered after *Salmonella* infection cannot inhibit pathogenesis. **b.** *Salmonella* CFUs measured in *C. elegans* throughout the assay shown in (a.) **c.** *Enterococcus* CFUs measured in *C. elegans* throughout the assay shown in **a.** For a, data points represent mean ± standard deviation for 3 plates of 30 worms each. For b and c, data points represent average CFUs from 5 worms ± standard deviation of three technical replicates. The dotted line indicates detection limit. Abbreviations: *E. coli* OP50 (OP); *S. typhimurium* (Stm); *E. faecium* (Efm).

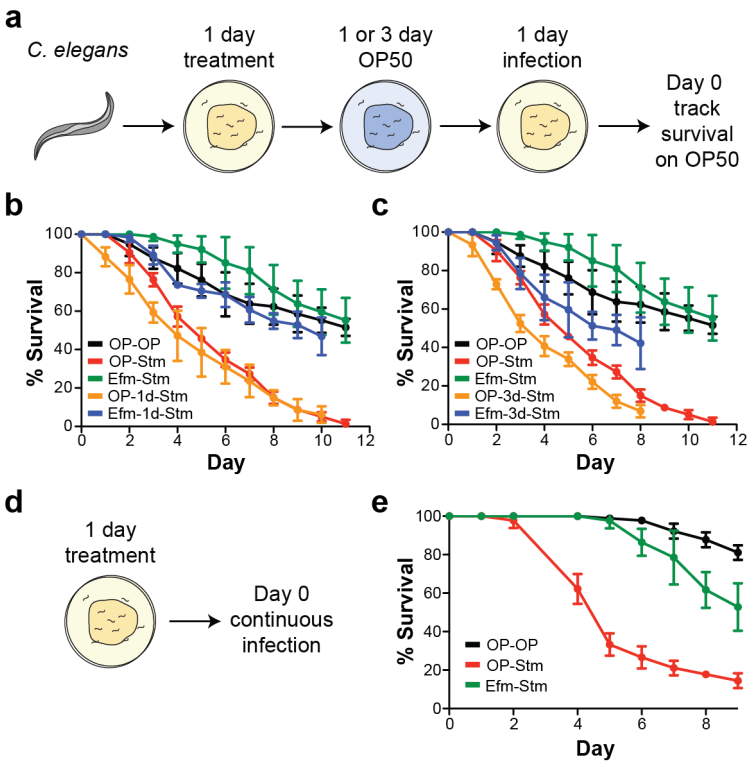

Figure 4.8. *E. faecium*-mediated protection is long-lasting.

a. Schematic of the pulsed treatment-infection assay with a 1 to 3 day delay introduced. See text for details. **b.** Pulsed treatment-infection assay with a 1 day delay. **c.** Pulsed treatment-infection assay with 3 day delay. **d.** Schematic of a treatment- continuous infection assay. See text for details. **e.** Survival curve showing that *E. faecium* can inhibit pathogenesis in a continuous infection assay. For b, c, and e, data points represent mean ± standard deviation for 3 plates of 30 worms. Abbreviations: *E. coli* OP50 (OP); *S. typhimurium* (Stm); *E. faecium* (Efm).

To assess the duration of protection afforded by *E. faecium* pre-treatment, we introduced a time delay between the treatment and infection steps of our assay (Figure 4.8a). After 1 day treatment, we transferred worms to *E. coli* OP50 plates for 1 or 3 days, before infection with *Salmonella*. We found that *E. faecium* was able to inhibit pathogenesis after a 1 or 3 day delay to infection (Figure 4.8b and c). Longer time delays were difficult to assess due to age-related mortality. We also evaluated *E. faecium*-

mediated protection against continuous *Salmonella* infection. In our continuous infection assay, worms were treated with either OP50 or *E. faecium* for 1 day, then transferred to *Salmonella* infection plates for the remainder of the assay (Figure 4.8d). In this continuous infection model, *E. faecium* still inhibited *Salmonella* pathogenesis (Figure 4.8e). Taken together, these data suggest that *E. faecium* employs a long-lasting protection mechanism that requires a priming phase, suggestive of an induced immune response.

We next explored whether specific factors produced by *E. faecium* were sufficient for protection against *S. typhimurium* pathogenesis. To do this, we developed a modified liquid treatment-infection assay (Figure 4.9a). In this assay, worms were bathed in different treatment wells for 2 hours, then transferred to *Salmonella* infection plates. After 1 day of infection, worms were transferred to *E. coli* OP50 plates for the remainder of the assay, and survival was scored. Using this assay, we found that *E. faecium* culture supernatant was as efficient as live *E. faecium* cultures in inhibiting *Salmonella* pathogenesis (Figure 4.9b), indicating that *E. faecium* colonization is not necessary for protection. Activity of the supernatant was sensitive to proteinase-K treatment (Figure 4.9c), trichloroacetic acid precipitation (Figure 4.9d), and 10-kDa size exclusion (Figure 4.9e), leading us to analyze the protein composition of *E. faecium* culture supernatant by mass spectrometry (Figure 4.10a). Proteomic analysis of *E. faecium* culture supernatant revealed 55 high-confidence secreted proteins and an enrichment of peptidoglycan remodeling factors (Figure 4.10b and Appendix 7). We focused on secreted antigen A (SagA), the most abundant protein identified from the supernatant (Figure 4.10b).

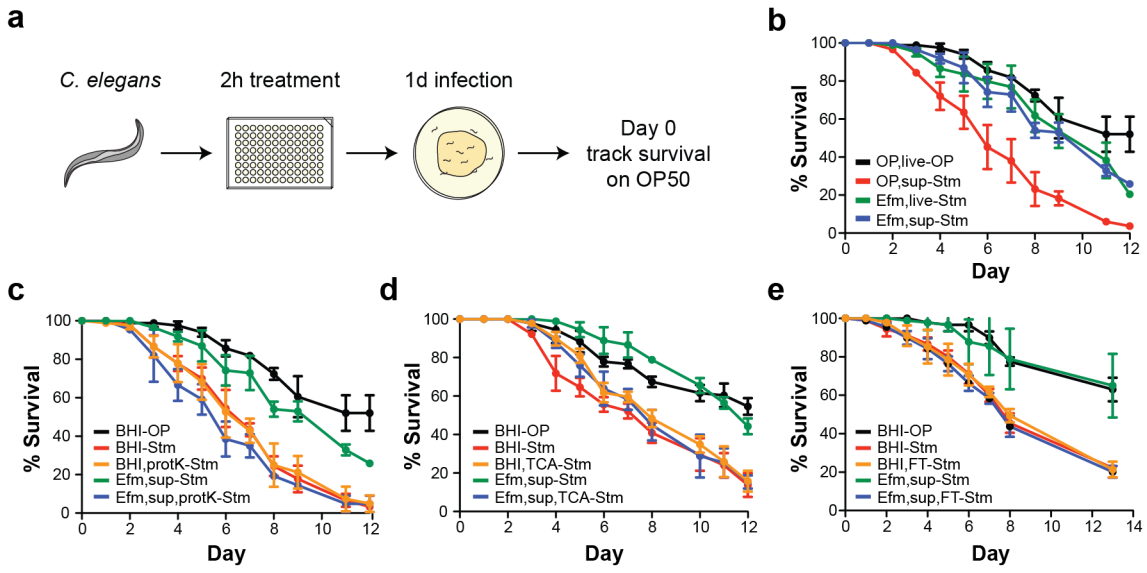

Figure 4.9. An *E. faecium* secreted protein can inhibit *Salmonella* pathogenesis. **a.** Schematic of liquid treatment-pulsed infection assay. See text for details. **b.** *E. faecium* culture supernatant (Efm,sup) inhibits *Salmonella*-induced death as well as live *E. faecium* culture (Efm,live). OP50 culture supernatant (OP,sup) is not protective. **c.** Proteinase-K-treated *E. faecium* culture supernatant (Efm,sup,protK) loses activity compared to untreated *E. faecium* culture supernatant (Efm,sup). Untreated media (BHI) and proteinase-K-treated media (BHI,protK) are inactive. **d.** Trichloroacetic acid (TCA) precipitated *E. faecium* culture supernatant (Efm,sup,TCA) loses activity. Untreated media (BHI) and TCA precipitated media (BHI,TCA) are inactive. **e.** 10-kDa MWCO column filtered *E. faecium* culture supernatant (Efm,sup,FT) is inactive. Untreated media (BHI) and 10-kDa MWCO column filtered media (BHI,FT) are inactive. For b-e, data points represent mean ± standard deviation for 3 plates of 30 worms each. Abbreviations: *E. coli* OP50 (OP); *S. typhimurium* (Stm); *E. faecium* (Efm).

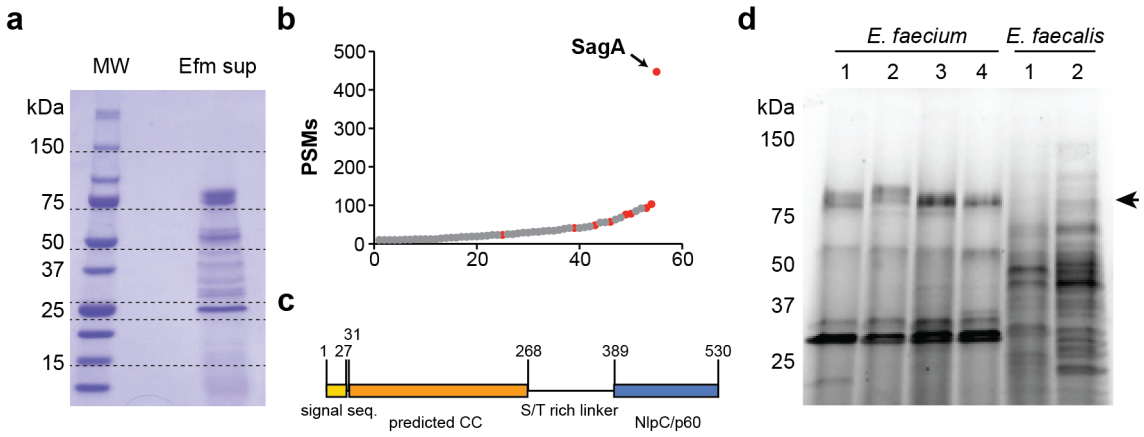

Figure 4.10. SagA is an abundantly secreted protein.

a. Coomassie stained SDS-PAGE of *E. faecium* Com15 culture supernatant (Efm sup) subsequently digested for mass spectrometry analysis. The dotted lines indicate gel slices made for trypsin digestion. **b.** Summary of proteins identified by mass spectrometry from *E. faecium* culture supernatant. Proteins shown were identified with at least 2 unique peptides and 10 peptide spectrum matches (PSMs). Proteins involved in peptidoglycan remodeling are highlighted in red. For the complete list of proteins identified, see Appendix 7. **c.** Schematic of SagA domain organization. The Type-1 signal peptide sequence is yellow, the predicted coiled-coil (CC) domain is orange, and the NlpC/p60 type hydrolase domain is blue. Amino acid number is as indicated. **d.** Stain-free imaging of culture supernatants from various *E. faecium* strains (1:Com15, 2:Com12, 3:NCTC 7171, and 4:DO) and *E. faecalis* strains (5:OG1RF, 6:V583) separated by SDS-PAGE. Arrow indicates a protein band corresponding to typical SagA migration.

SagA encodes a putative secreted peptidoglycan hydrolase that contains a Type-1 signal peptide, an uncharacterized N-terminal coiled-coil domain, a linker region with Ser/Thr-rich repeats, and a C-terminal NlpC/p60-type hydrolase domain (Figure 4.10c). While no hydrolase activity has been reported, SagA has been shown to bind extracellular matrix proteins *in vitro*[192]. The NlpC-p60-type hydrolase domain is a cysteine endopeptidase domain common amongst bacteria[193]. The regulation of this enzymatic

activity, however, is not well understood, and may be specified by other domains. Typically, NlpC-p60-type enzymes are involved in peptidoglycan remodeling during growth and division. The protein sequence of SagA is highly conserved within *E. faecium*, and it is regarded as an essential gene[192]. Although the function of SagA is unknown, SagA has high structural similarity to the CHAP-domain containing protein PcsB from S. pneumoniae (91% coverage, 34% sequence identity), which is required for normal cell septation[194].

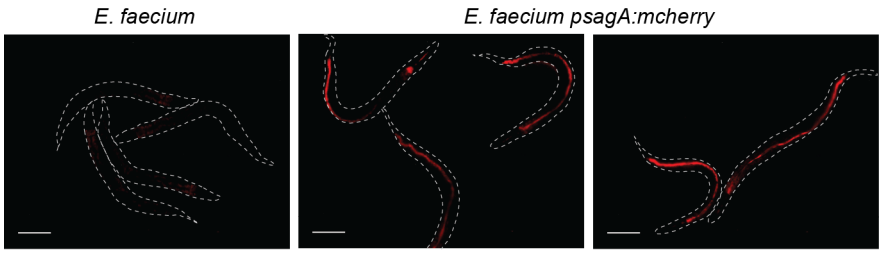

Figure 4.11. SagA is expressed by *E. faecium* in the *C. elegans* intestine. Fluorescence images of *C. elegans* treated for 1 day with *E. faecium* or *E. faecium* expressing *psagA:mcherry*. The dotted lines indicate the outline of the worm body. Scale bar = 200 μm.

To determine if SagA secretion was relevant to our treatment-infection assays with live *E. faecium*, we assessed whether *sagA* was expressed by *E. faecium* during colonization of *C. elegans*. To do this, we generated an *E. faecium* strain expressing mCherry under the *sagA* promoter (*psagA:mcherry*). Fluorescence imaging of worms treated for 1 day with *psagA:mcherry* suggested that SagA is indeed expressed during *E. faecium* colonization (Figure 4.11). To test SagA activity in worms directly, we expressed C-terminally His_6-tagged SagA from both *E. coli* BL21-RIL(DE3) and *E.*

faecium Com15 (Figure 4.12a). Cleavage of bacterial Type-1 signal peptides occurs upon secretion and can be required for proper protein activity[195]. For this reason, we purified SagA-His_6 from the culture supernatants of both *E. coli* and *E. faecium* rather than from cell lysates. Remarkably, treatment of worms with SagA-His_6 purified from either source was sufficient to inhibit *Salmonella* pathogenesis (Figure 4.12b).

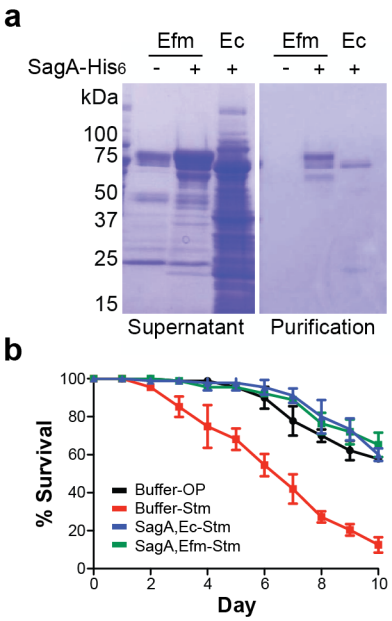

Figure 4.12. Purified SagA is sufficient to inhibit *Salmonella* pathogenesis.
a. Coomassie stained SDS-PAGE of culture supernatants and His_6 purifications of SagA-His_6 from *E. faecium* Com15 (Efm) and *E. coli* BL21-RIL(DE3) (Ec). **b.** SagA-His_6 purified from either *E. coli* BL21-RIL(DE3) (SagA, Ec) or *E. faecium* Com15 (SagA, Efm) is sufficient to inhibit *Salmonella* pathogenesis. Data points represent mean ± standard deviation for 3 plates of 30 worms each. Abbreviations: *E. coli* OP50 (OP); *S. typhimurium* (Stm); *E. faecium* (Efm).

We noticed that SagA-His_6 purified from *E. faecium* appeared as a smear of bands around 75 kDa, higher than the predicted molecular weight of 54 kDa (Figure 4.12a). This banding appearance is characteristic of glycosylation, which has been shown to regulate the activity of other peptidoglycan hydrolases[196]. Although SagA from *E. faecium* strain DO (which bears 91% identity to SagA from *E. faecium* Com15) was previously reported as not glycosylated[192], the abundance of serine and threonine residues present in the linker region of SagA are indicative of O-glycosylation. We used the periodic-acid-Schiff stain method to visualize the glycosylated proteins in *E. faecium* culture supernatant separated by SDS-PAGE (Figure 4.13a). Using this method, we detected a stained protein with a gel migration typical to SagA, and confirmed SagA identity by mass spectrometry of the excised gel band (Appendix 8). Interestingly, although SagA-His_6 purified from *E. coli* migrates higher than predicted, it appears as a crisp band, suggesting that it is not glycosylated (Figure 4.12a). We compared glycosylation of SagA-His_6 purified from *E. faecium* and *E coli*, and confirmed that SagA-His_6 purified from *E. coli* is indeed not glycosylated (Figure 4.13b). The unusual migration of SagA-His_6 purified from *E. coli* may be due to the stretch of charged and polar residues within the linker region, or to additional protein modifications. Nevertheless, the fact that SagA purified from either *E. coli* or *E. faecium* can inhibit *Salmonella* pathogenesis suggests that glycosylation is not necessary for SagA activity.

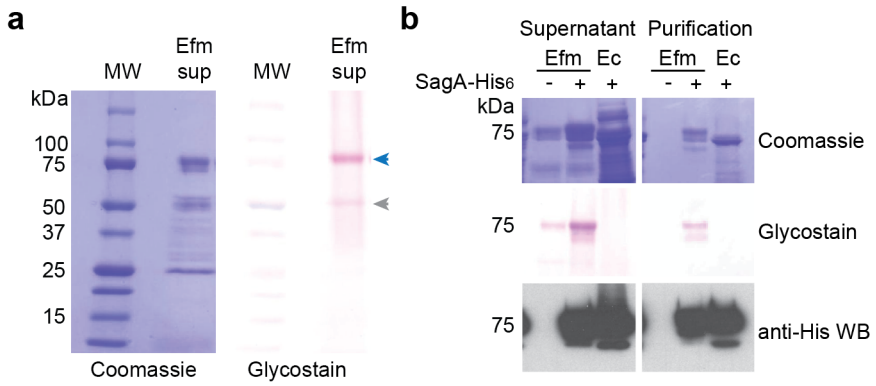

Figure 4.13. SagA is a glycosylated protein.

a. Coomassie blue staining and glycoprotein-staining of *E. faecium* Com15 culture supernatant (Efm sup). The blue arrow indicates a protein band corresponding to typical SagA migration. Both of the indicated stained bands were excised for mass spectrometry analysis presented in Appendix 8. **b.** SDS-PAGE of culture supernatants and SagA-His_6 purifications from *E. faecium* Com15 (Efm) and *E. coli* BL21-RIL(DE3) (Ec). Samples were visualized by Coomassie blue staining, glycoprotein-staining, and anti-His_6 Western blot (WB) as indicated. SagA is glycosylated in *E. faecium* but not *E. coli*.

In vitro, SagA can bind the extracellular matrix proteins fibrinogen, fibronectin, collagen type-I, collagen type-IV, and laminin[192], which are found in the intestinal basement membrane. *C. elegans* has homologues of both laminin and type-IV collagen[170]. We wondered if SagA could bind to the worm, possibly forming some sort of barrier to inhibit *Salmonella* pathogenesis. We measured binding of SagA-His_6 to worms by Western blot, and were unable to detect any SagA-His_6 in worms after pulsed S*almonella* infection (Figure 4.14). This suggests that SagA is only transiently associated with the worm, making the idea of a physical barrier to infection unlikely.

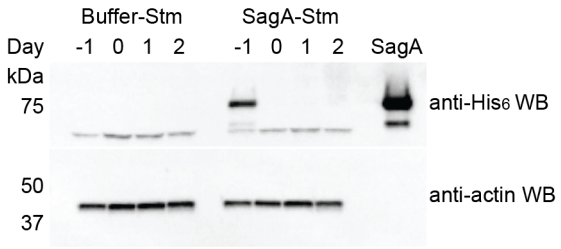

Figure 4.14. SagA does not robustly adhere to *C. elegans*.
Anti-His_6 Western blot (WB) for SagA-His_6 in infected worms at indicated days post *Salmonella* (Stm) infection. Anti-actin WB was used as a sample loading control. "SagA" lane shows typical His_6 blotting.

To determine if the NlpC/p60-type hydrolase domain of SagA is required for protection of *C. elegans,* we generated a deletion mutant of the entire C-terminal NlpC/p60-type hydrolase domain (ΔCterm) as well as an active site mutant of SagA (Figure 4.15a and b). To generate the active site mutant, we mutated the putative enzyme catalytic residues (Cys443, His494, and His506) to alanine. Both of these mutant proteins were expressed, secreted, and purified from *E. coli* BL21-RIL(DE3) (Figure 4.15c). We tested these mutant proteins for activity in *C. elegans*, and found that while wild type SagA inhibited *Salmonella* pathogenesis as well as *E. faecium* culture supernatants, the active site mutant and ΔCterm were not protective (Figure 4.15d), indicating that the NlpC/p60-type hydrolase domain is required for SagA activity.

Given that the hydrolase domain of SagA is required for its protective activity, we wondered if SagA could directly affect *Salmonella* growth or virulence. Fluorescence imaging of mCherry-*S. typhimurium* (Figure 4.16a and b) and *Salmonella* CFU measurements (Figure 4.16c) from untreated, SagA-treated, and active site mutant-treated

infected worms were comparable, indicating that SagA, like *E. faecium* treatment, does not affect *Salmonella* colonization of *C. elegans*. Additionally, exogenous addition of SagA had no effect on *Salmonella* growth rate in culture (Figure 4.16d). These results suggest that SagA does not act through a bactericidal mechanism.

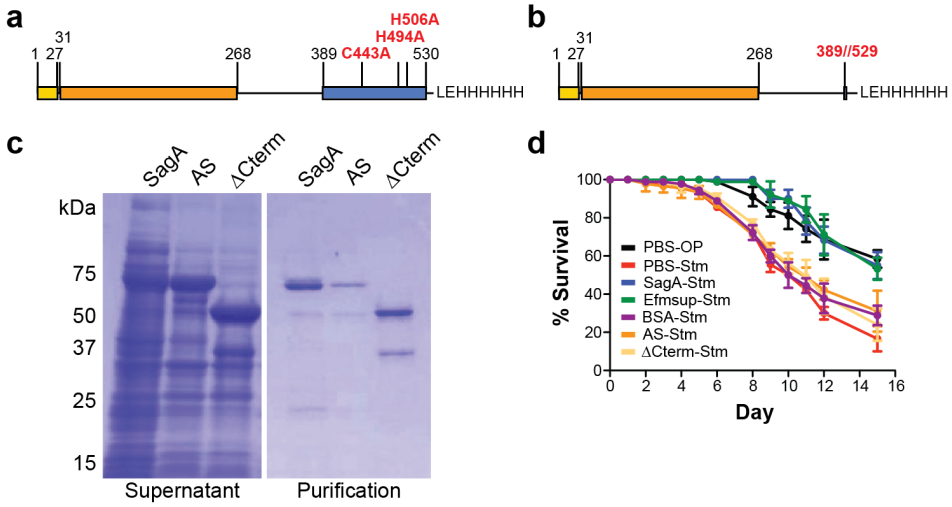

Figure 4.15. Enzymatic activity of SagA is required for inhibition of *Salmonella* pathogenesis.

a. Schematic showing the point mutations made to generate the active site mutant of SagA-His_6. **b.** Schematic showing the truncation made to generate the C-terminal domain deletion of SagA-His_6 (ΔCterm). **c.** Coomassie stained SDS-PAGE of culture supernatants and His_6 purifications of SagA-His_6, the active site mutant (AS), and ΔCterm from *E. coli* BL21-RIL(DE3). **d.** Survival curve showing that bovine serum albumin (BSA), the active site mutant (AS), and ΔCterm do not inhibit *Salmonella* pathogenesis, while SagA and *E. faecium* culture supernatants (Efmsup) do. Data points represent mean ± standard deviation for 3 plates of 30 worms each.

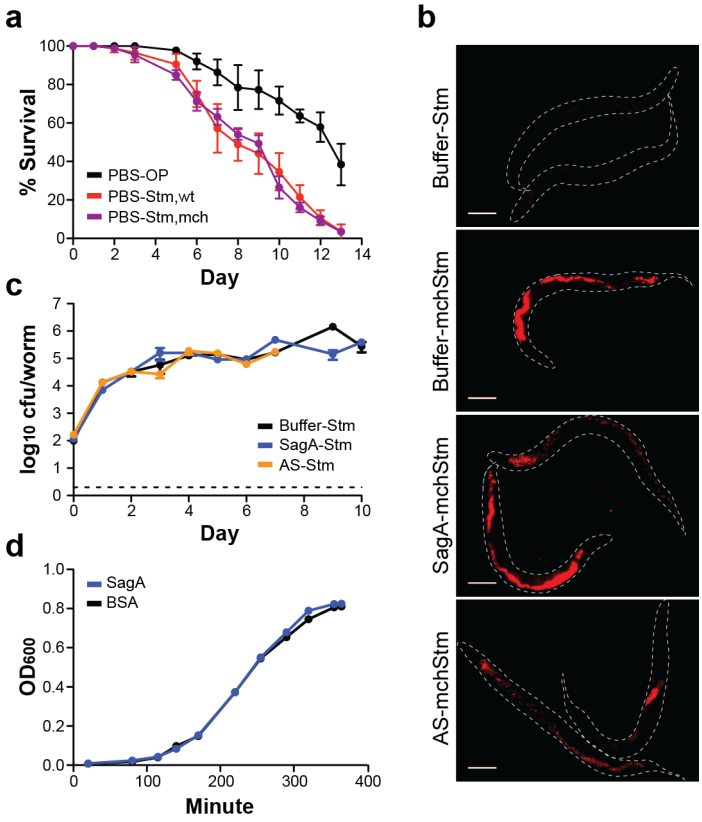

Figure 4.16. SagA treatment does not inhibit *Salmonella* colonization of *C. elegans* or growth in culture.

a. Survival curve showing that wildtype *S. typhimurium* (Stm, wt) and mcherry-*S. typhimurium* (Stm, mch) are equally pathogenic in a liquid treatment-pulsed infection assay. Data points represent mean ± standard deviation for 3 plates of 30 worms each. **b.** Fluorescence imaging of *C. elegans* infected with mcherry-*S. typhimurium* (mchStm) at day 5 post-infection. The dotted lines indicate the outline of the worm body. Scale bar = 200 μm. **c.** *Salmonella* CFUs measured in *C. elegans* throughout the liquid treatment pulsed infection assay. Data points represent average CFUS from 10-20 worms ± standard deviation of three technical replicates. The dotted line indicates detection limit. **d.** Growth curves of *S. typhimurium* in LB media + 10 μg/ml SagA or BSA.

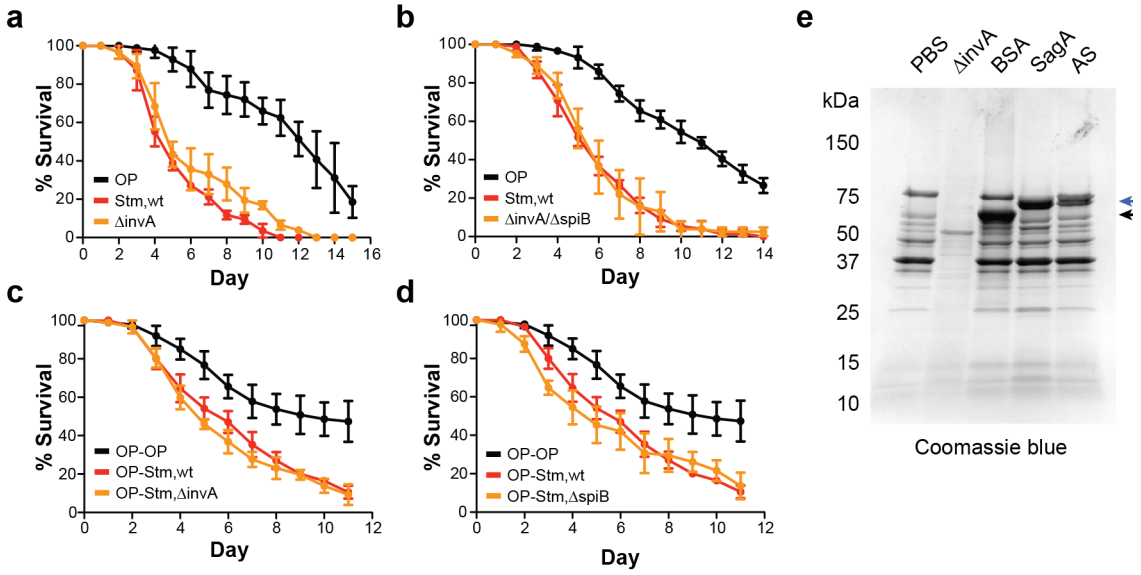

Figure 4.17. *Salmonella* Type-3 secretion systems are dispensible for *C. elegans* pathogenesis.

a. Wildtype *S. typhimurium* (Stm, wt) and a *ΔinvA* mutant are equally pathogenic to *C. elegans* in a continuous infection assay. InvA is a component of the SPI-1 needle complex required for effector secretion (see (e.)). **b.** Wildtype *S. typhimurium* and a *ΔinvA/ΔspiB* double mutant are equally pathogenic to *C. elegans* in a continuous infection assay. SpiB is a component of the SPI-2 needle complex required for effector secretion. **c.** Wildtype *S. typhimurium* and a *ΔinvA* mutant are equally pathogenic to *C. elegans* in a pulsed infection assay. **d.** Wildtype *S. typhimurium* and a *ΔspiB* mutant are equally pathogenic to *C. elegans* in a pulsed infection assay. **e.** SagA has no affect on SPI-1 secretion in culture. *Salmonella* cultures were grown in LB + 10 μg/ml BSA, SagA, or the active site mutant (AS). PBS indicates control treatment. For a-d, data points represent mean ± standard deviation for 3 plates of 30 worms each.

In mammals, *Salmonella* pathogenesis relies primarily on two Type-3 secretion systems for host cell invasion and subsequent intracellular replication[121]. In *C. elegans*, the role of Type-3 secretion in pathogenesis is unclear. Deletion mutants of several *Salmonella* Type-3 secretion factors have been reported to exhibit attenuated

virulence[161,163,197,198]. However, *Salmonella* does not appear to actively invade *C. elegans* intestinal cells, and instead remains extracellular. In both continuous and pulsed infection assays, we found no attenuation of *Salmonella* pathogenesis with SPI-1 or SPI-2 Type-3 secretion mutants (Figure 4.17a-d). This suggests that the virulence pathways involved in invasion and intracellular survival may not be required for pathogenesis in *C. elegans*, making them unlikely targets of SagA activity. In culture, addition of SagA had no effect on the secretion of *S. typhimurium* type III protein effectors (Figure 4.17e), suggesting that SagA does not target SPI-1 Type-3 secretion to inhibit pathogenesis.

As described earlier, *E. faecium* can inhibit the mild pathogenesis of *E. coli* OP50 (Figure 4.2b). We also found that *E. faecium*-treated worms were more resistant to pathogenesis caused by the Gram-positive intestinal pathogen *Enterococcus faecalis* strain V583[174] (Figure 4.18). This suggests that the mechanism of *C. elegans* protection can be generalized to other pathogens, making a *Salmonella*-specific mechanism unlikely.

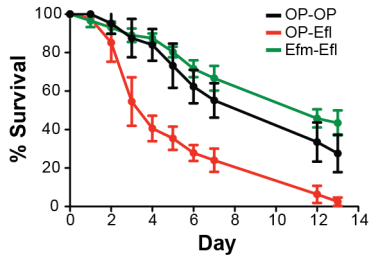

Figure 4.18. *E. faecium* can inhibit *E. faecalis* pathogenesis.
Survival curve showing that *E. faecium* can protect worms from *E. faecalis* V583 pathogenesis. Abbreviations: *E. coli* OP50 (OP); *S. typhimurium* (Stm); *E. faecium* (Efm); *E. faecalis* (Efl). Data points represent mean ± standard deviation for 3 plates of 30 worms each.

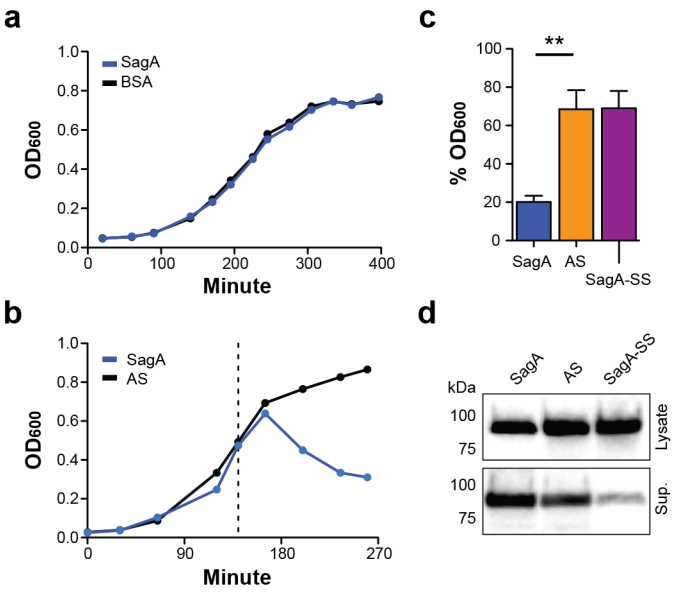

Figure 4.19. SagA expression and secretion by *E. coli* causes cell lysis.
a. Growth curves of *E. coli* BL21-RIL(DE3) in LB media + 10 μg/ml SagA or BSA. **b.** Growth curves of *E. coli* BL21-RIL(DE3) expressing SagA-His_6 or the active site mutant (AS) under an IPTG-inducible promoter. Dotted line indicates time of IPTG induction. **c.** OD_{600} of *E. coli* BL21-RIL(DE3) expressing SagA-His_6, the active site mutant (AS), or SagA-SS under an IPTG-inducible promoter. Measurements were taken 1 hour post-induction and normalized to the OD_{600} of a mock-induced non-expressing BL21-RIL(DE3) culture. Bars represent mean ± s.e.m. from three independent experiments. Significance was calculated by unpaired t test. For **, $p < 0.01$. **d.** Anti-His_6 Western blots of cell lysate or culture supernatant (Sup.) from *E. coli* BL21-RIL(DE3) expressing SagA-His_6, the active site mutant (AS), or Sag-SS after IPTG induction. SagA-SS is mostly retained in the cell lysates, while SagA and the active site mutant are secreted.

As with *Salmonella*, the addition of exogenous SagA had no effect on the growth rate of *E. coli* in culture (Figure 4.19a). However, we did notice that induction of SagA expression in *E. coli* led to a decrease in culture optical density (OD) (Figure 4.19b), indicating cell lysis. In contrast, expression of the active-site mutant of SagA or a signal

sequence mutant of SagA (SagA-SS) did not decrease culture OD (Figure 4.19b-d). This is consistent with our observations that leaky low-level constitutive expression of SagA, but not the active site mutant, in *E. coli* from the low-copy number plasmid, pAM401, strongly impaired *E. coli* growth on agar and in culture (data not shown). One explanation for the secretion-dependent toxicity of SagA expression in *E. coli* is that SagA is a functional hydrolase that can cleave *E. coli* peptidoglycan when properly targeted to the periplasm during secretion.

We generated additional mutant protein constructs to assess the function of the N-terminal domain and the linker region of SagA (Figure 4.20a-c). Interestingly, we were unable to express deletion mutants of the N-terminal domain, either with or without the signal sequence, in *E. coli*. Given that SagA expression causes cell death, this may suggest a regulatory function for this domain. We also generated a deletion mutant of the linker region (ΔLinker) (Figure 4.20c). The linker region of SagA is made up of an unusual series of serine, threonine, and glutamate-rich repeats, which might be involved in localizing SagA to specific sites in the intestine. We compared cell lysis resulting from ΔLinker induction as compared to wild-type SagA. ΔLinker induction did not lead to cell lysis, indicating reduced hydrolytic activity (Figure 4.20d). This suggests that the linker region is required for hydrolase function, and may reflect improper protein folding or substrate targeting. We assessed the ability of ΔLinker to inhibit *Salmonella* pathogenesis in *C. elegans*, and found that this mutant was not protective (Figure 4.20e). These results reinforce the correlation between SagA hydrolase activity and inhibition of *Salmonella* pathogenesis in *C. elegans*.

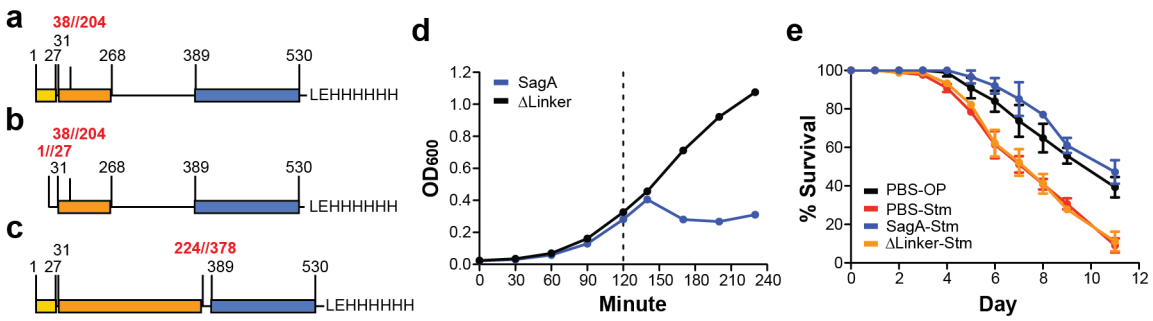

Figure 4.20. Characterization of the ΔLinker SagA mutant.

a and **b.** Schematics showing an two different N-terminal truncations made in SagA-His_6 that resulted in no protein expression in *E. coli* BL21-RIL(DE3). **c.** Schematic showing a truncation in the linker region of SagA to generate ΔLinker. **d.** Growth curves of *E. coli* BL21-RIL(DE3) expressing SagA-His_6 or ΔLinker under an IPTG-inducible promoter. Dotted line indicates time of IPTG induction. **e.** Survival curve showing that treatment with ΔLinker does not inhibit *Salmonella* pathogenesis. Data points represent mean ± standard deviation for 3 plates of 30 worms each.

Given that SagA does not attenuate *Salmonella* growth, we hypothesized that SagA may hydrolyze peptidoglycan fragments *in trans* to activate host immunity. Consistent with this hypothesis, we found that the flow-thru from 5 kDa-MWCO column-filtered culture supernatants of *E. coli* expressing SagA, but not the active site mutant, protected *C. elegans* from *Salmonella* pathogenesis (Figure 4.21a). We confirmed removal of SagA from the column flow-thru by Western blot (Figure 4.21b), suggesting that lower molecular weight products of SagA activity are sufficient for *C. elegans* protection. To test if SagA-generated *E. coli* peptidoglycan fragments can protect worms from *Salmonella* pathogenesis, we digested purified *E. coli* peptidoglycan with lysozyme and either SagA or the active site mutant, then filtered the digests through a 5 kDa-MWCO column to exclude protein. *C. elegans* treated with the SagA peptidoglycan

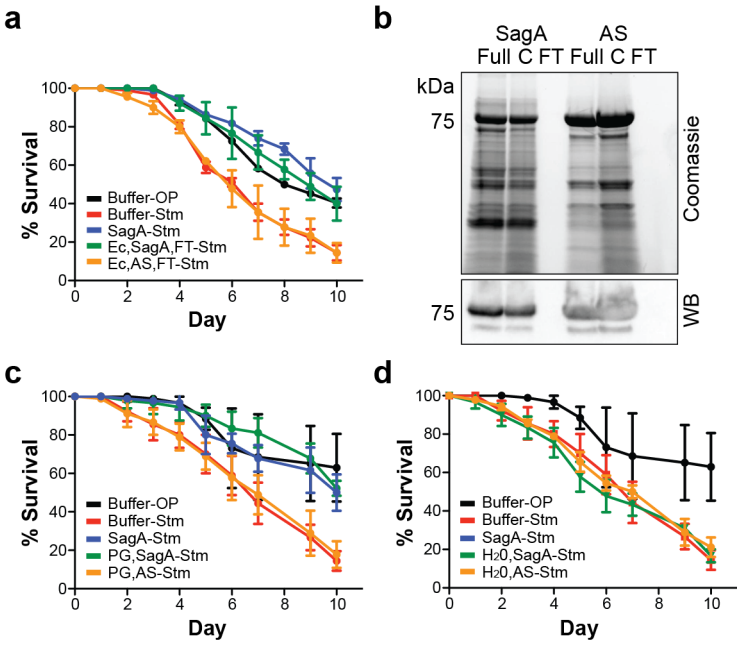

Figure 4.21. SagA-treated peptidoglycan can inhibit *Salmonella* pathogenesis. **a.** Survival curve showing that 5-kDa MWCO-column filtered *E. coli* culture supernatants expressing SagA-His_6 (Ec, sagA,FT) but not the active site mutant (Ec,AS,FT) can inhibit *Salmonella* pathogenesis. **b.** Coomassie blue staining and anti-His_6 WB of *E. coli* culture supernatants expressing SagA-His_6 or the active site mutant (AS). Supernatant was filtered through a 5-kDa MWCO column. Full unfiltered supernatant (Full), column concentrate (C), and column flow-through (FT) are as indicated. **c.** Survival curve showing that purified *E. coli* peptidoglycan treated with SagA then filtered through a 5-kDa MWCO-column (PG, SagA) can inhibit *Salmonella* pathogenesis. Peptidoglycan treated with the active site mutant (PG, AS) is not protective. **d.** Survival curve showing that water treated with either SagA (H20, SagA), or the active site mutant (H20, AS) then filtered through a 5-kDa MWCO-column, cannot inhibit *Salmonella* pathogenesis. For a, c, and d, data points represent mean ± standard deviation for 3 plates of 30 worms each.

digests survived similarly to SagA-treated worms, whereas active site mutant digests failed to attenuate *Salmonella* pathogenesis (Figure 4.21c). To control for column removal of SagA, we performed mock digests of water with SagA or the active site mutant, and confirmed that the filtered mock digests were non-protective (Figure 4.21d). These results suggest that SagA-generated peptidoglycan fragments, and not SagA itself, are responsible for protecting *C. elegans* from *Salmonella* pathogenesis. This hypothesis is consistent with the role of bacterial cell-wall components, including peptidoglycan, as activators of innate immunity in other animals[28,199].

In *E. faecium*, SagA is essential[192], suggesting that it likely has a cell intrinsic function in peptidoglycan remodeling. SagA expression in *E. coli*, however, causes cell lysis, suggesting that either the specificity or regulation of SagA enzymatic activity is altered. We previously showed that filtration of *E. faecium* culture supernatant through a 10kDa-size exclusion column abolishes activity (Figure 4.9e). This may be due to differences in the specific peptidoglycan fragments generated or to differences in the abundance of peptidoglycan shed into the supernatant. Different bacterial species recycle peptidoglycan during growth to varying extents[200,201]. For example, *E. coli* is thought to shed ~8% of its peptidoglycan during exponential growth[202], while *B. subtilis* sheds ~50%[203]. To our knowledge, the extent of peptidoglycan recycling in *E. faecium* has not been quantified, but this process could account for the differential activity of *E. faecium* and *E. coli* filtered culture supernatants. Another more attractive explanation comes from the differences in peptidoglycan structure between *E. faecium* and *E. coli* (Figure 4.22a and b). Peptidoglycan varies across species largely in the peptides linking the sugars together. As a putative D,L-endopeptidase, SagA is predicted to cleave

between D-iGln and L-Lys, which is in an area that differs between *E. faecium* and *E. coli*, and would result in different cleavage products. However, since *E. coli* peptidoglycan is an unnatural substrate for SagA activity, we do not know where SagA may optimally cleave in this structure, or what cleavage products may result.

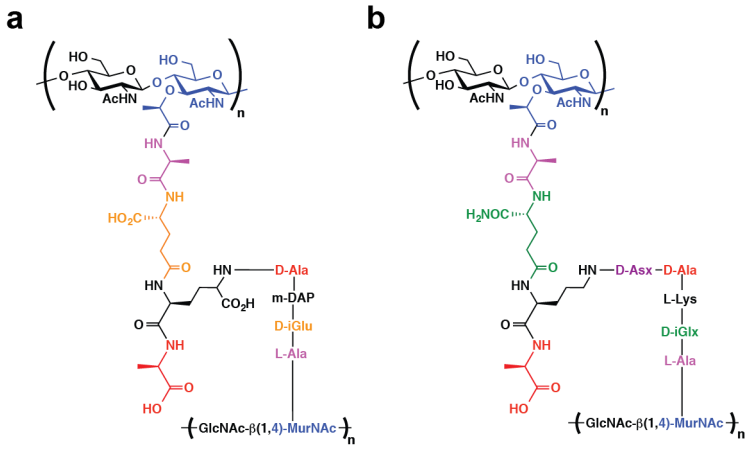

Figure 4.22. The structure of peptidoglycan.
a. Structure of *E. coli* (and *Salmonella*) peptidoglycan. D-isoglutamate (D-iGlu) can also be substituted by D-glutamate (D-Glu). **b.** Structure of *E. faecium* peptidoglycan. D-Asx indicates that both D-aspartate (Asp) and D-asparagine (Asn) at found at that position. D-iGlx indicates that both D-isoglutamate (D-iGlu) and D-isoglutamine (D-iGln) are found that position.

To determine what peptidoglycan fragment(s) are generated from SagA enzymatic activity, we used the UV-active compound 8-amino-naphthalene 1,3,6-trisulfonic acid (ANTS) to label and track peptidoglycan fragments[204,205]. ANTS covalently reacts with sugars through reductive amination, allowing for native gel separation and visualization of sugar-containing small molecules, such as peptidoglycan fragments (Figure 4.23a). With this method, we analyzed filtered culture supernatants of

E. coli cultures expressing either SagA-His_6 or the active site mutant (Figure 4.23b). We detected a SagA-specific UV-active band that migrated similarly to the ANTS-labeled synthetic peptidoglycan fragments MurNAc-L-Ala and GlcNac (Figure 4.23c). Interestingly, did not migrate similarly to MurNAc-L-Ala-D-Glu (MDP), which is the predicted monosaccharide cleavage product of SagA activity. We did not detect this fragment in filtered *E. faecium* culture supernatant (Figure 4.23c), suggesting that SagA activity results in different or more abundant peptidoglycan cleavage products in *E. coli* as compared to *E. faecium*.

Because *E. coli* culture supernatant contains additional cell wall components beyond peptidoglycan, we wanted to analyze SagA digests of purified peptidoglycan by the same method. *In vitro* digestion of purified *E. coli* peptidoglycan with lysozyme and either SagA or the active site mutant yielded a similar cleavage fragment (Figure 4.23d), suggesting that this fragment is indeed peptidoglycan derived. We suppose the identity of this fragment is most likely MurNAc-L-Ala rather than GlcNAc, given that SagA is predicted to be an endopeptidase. However, it is possible this fragment represents a different peptidoglycan fragment altogether. HPLC separation and mass spectrometry to determine the identity of this fragment is in progress.

We next assessed the activity of MurNAc-L-Ala, GlcNAc, and several other synthetic peptidoglycan fragments in protecting *C. elegans* from *Salmonella* pathogenesis. Treatment of *C. elegans* with 50 μM of MurNAc-L-Ala-D-Glu (MDP), MurNAc-L-Ala-D-Glu-mDAP (MTP(mDAP)), MurNAc-L-Aala-D-Gln-L-Lys (MTP(Lys)), MurNAc-L-Aala-D-Gln-L-Lys-D-Asn (MTP-D-Asn), Tri-Lys, Tri-DAP, iD-Glu-mDAP, or GlcNAc did not inhibit *Salmonella* pathogenesis (Figure 4.24a-d).

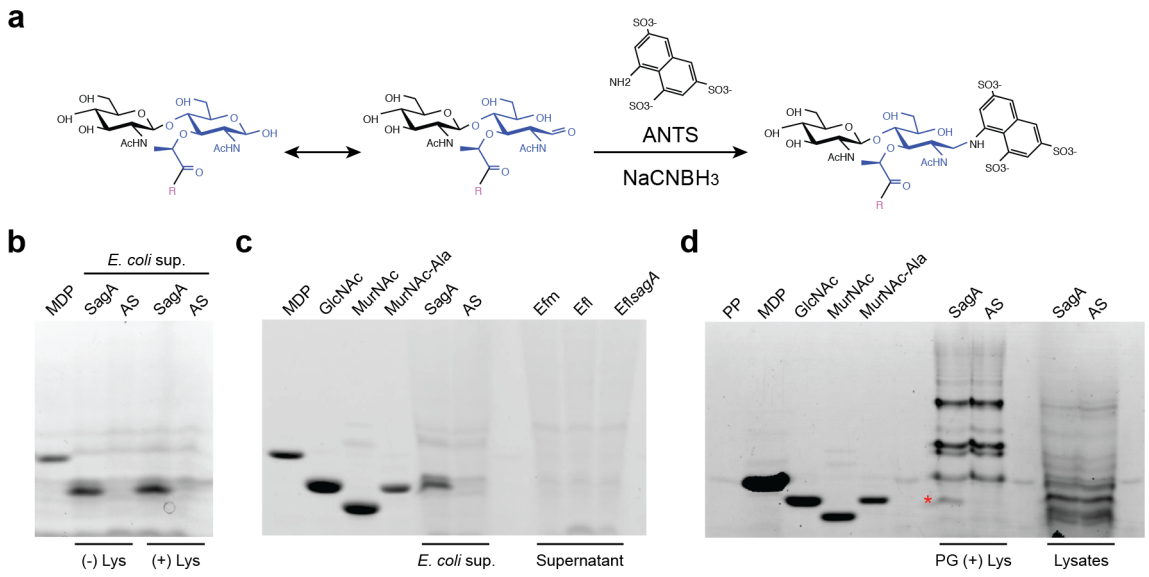

Figure 4.23. SagA hydrolase activity visualized by ANTS labeling.

a. Schematic of ANTS labeling reaction. See text for details. **b.** Culture supernatants (sup.) of *E. coli* expressing either SagA-His_6 or the active site mutant (AS). Supernatants were filtered through 10-kDa MWCO columns, dried, ANTS labeled, then separated by native PAGE. Gel was visualized by UV. Expression of SagA releases a unique ANTS-labeled fragment into the supernatant. Lysozyme treatment of the supernatant does not alter ANTS-labeling profile (+ Lys). **c.** Unique fragment found in the SagA-expressing *E. coli* supernatant co-migrates with GlcNAc and MurNAc-Ala. This fragment is not detected in *E. faecium* (Efm), *E. faecalis* (Efl), or *E. faecalis-sagA* (Efl*sagA*) culture supernatants. **d.** ANTS-labeled enzymatic digest of purified *E. coli* peptidoglycan (PG) with lysozyme and SagA yields a similar fragment (indicated with an asterix) as that found in SagA-expressing *E. coli* supernatant. ANTS-labeled cell lysates of *E. coli* expressing either SagA or the active site mutant (AS) are similar.

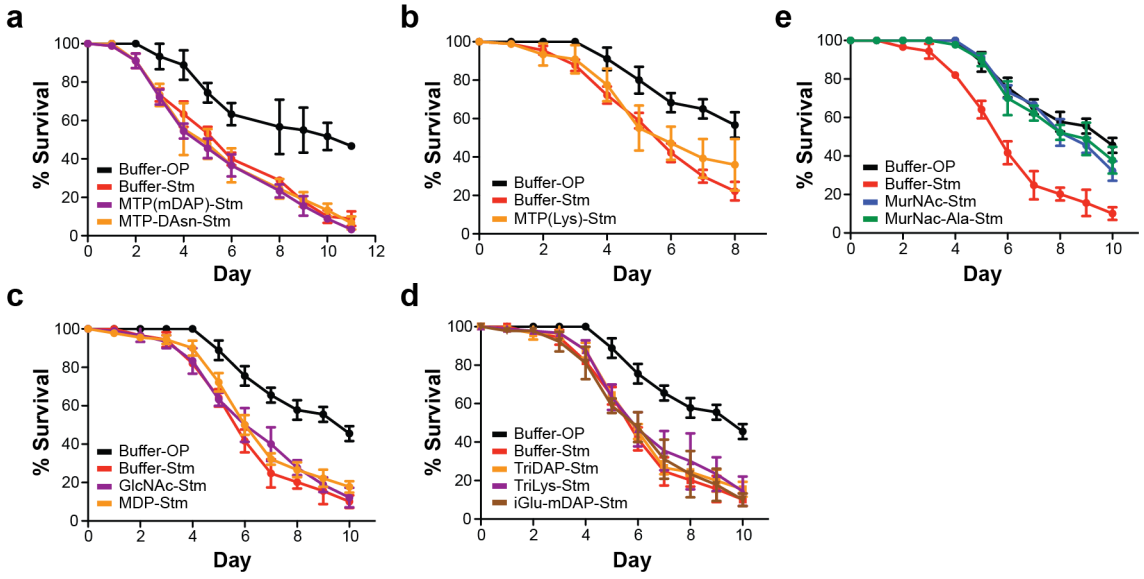

Figure 4.24. Small synthetic peptidoglycan fragments can inhibit Salmonella pathogenesis in *C. elegans*.

Survival curves showing that **a.** MTP(mDAP), MTP-D-Asn, **b.** MTP(Lys), **c.** MDP, GlcNAc, and **d.** TriDAP, TriLys, and iGlu-mDAP do not inhibit *Salmonella* pathogenesis, while **e.** MurNAc and MurNAc-Ala do. For a-e, data points represent mean ± standard deviation for 3 plates of 30 worms. Abbreviations: *E. coli* OP50 (OP); *S. typhimurium* (Stm).

However, treatment with either MurNAc or MurNAc-L-Ala inhibited *Salmonella* pathogenesis (Figure 4.24e). Correlating our *in vitro* ANTS-labeled peptidoglycan digest data to our *C. elegans* activity assays, we hypothesize that SagA hydrolysis of peptidoglycan generates MurNAc-L-Ala, which can activate innate immunity in *C. elegans*.

To determine if *E. faecium* acts through major *C. elegans* immune pathways to inhibit *Salmonella* pathogenesis, we surveyed *E. faecium*-mediated protection in the following immune-deficient worm strains: *pmk-1(km25)* (p38 MAPK/Pmk-1

pathway)[206,207], *dbl-1(nk3)* (TGF-β-like/Dbl-1 pathway)[208,209], *daf-16(mu86)* and *daf-2(e1370); daf-16(mgDf47)* (insulin-like receptor/Daf-2 pathway)[210,211], and *npr-1(ad609)* (Npr-1-mediated pathogen avoidance)[212]. In *pmk-1*, *dbl-1*, and *npr-1* mutants, survival of "uninfected", OP50-fed worms was greatly decreased as compared to wild-type worms (Figure 4.25a, b, and e). This suggests that these immune pathways are involved in mitigating the pathogenicity of OP50 grown on BHI. Nevertheless, in all mutants, we observed prolonged survival of *E. faecium*-treated infected worms (Figure 4.25a-e), indicating that these pathways are each not exclusively required for *E. faecium*-mediated protection against a pulsed *Salmonella* infection.

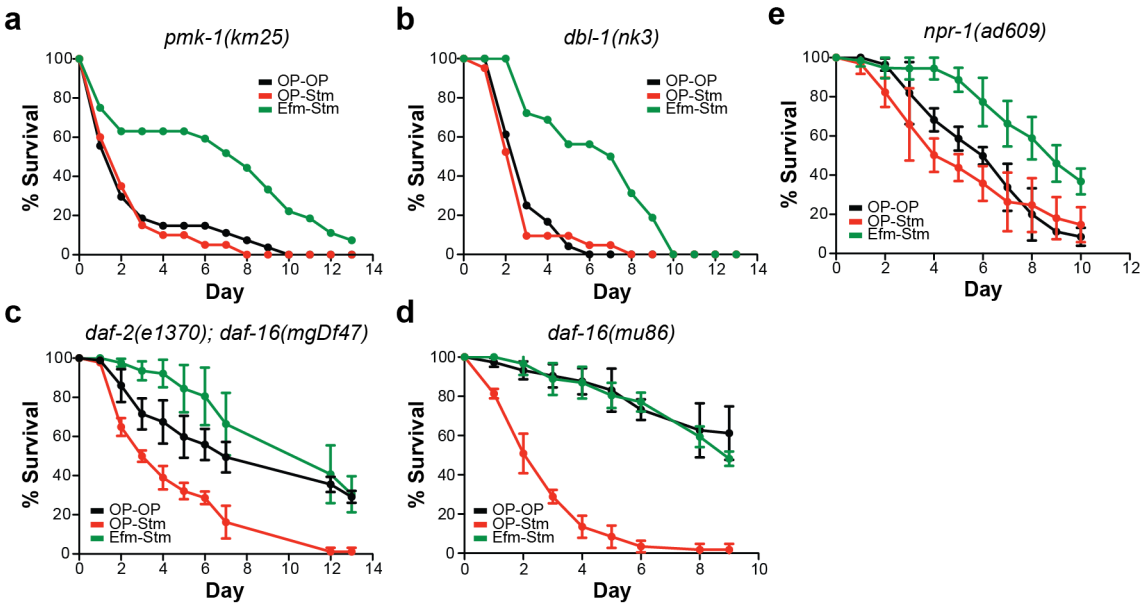

Figure 4.25. *E.* faecium activity in various *C. elegans* mutants.
Survival curves assaying *E. faecium*-mediated protection in **a.** *pmk-1(km25)* **b.** *dbl-1(nk3)* **c.** *daf-2(e1370);daf-16(mgDf47)* **d.** *daf-16(mu86)* and **e.** *npr-1(ad609)*. For c-e, each condition was tested with 3 plates of 30 worms each, and data points represent mean ± standard deviation. For a and b, each condition was tested with one plate of 30 worms. Abbreviations: *E. coli* OP50 (OP); *S. typhimurium* (Stm); *E. faecium* (Efm).

C. elegans encodes one predicted homologue of Toll-like receptor, *tol-1*[213]. Mammalian Toll-like receptors recognize various microbial-associated molecular patterns, including bacterial cell-wall components, leading to immune activation[27]. In *Drosophila*, Toll plays a role in both development and immunity, and does not function as a pattern recognition receptor[214]. Instead, bacterial or fungal infection leads to the proteolytic cleavage of Spaetzle, which binds Toll to promote downstream immune signaling. In *C. elegans,* a deletion of part of the extracellular domain in *tol-1(nr2013)* mutants, results in an embryonic lethal or larval arrest phenotype, suggesting that *tol-1* is required for proper development[213]. Deletion of the putative TIR signaling domain in *tol-1(nr2033)* mutants, however, does not apparently affect development or viability. Interestingly, *tol-1* is dispensable for *C. elegans* immunity against several pathogens including *P. aeruginosa*, *S. aureus*, and *D. coniospora*. However, *tol-1* mutants are defective in pathogen avoidance to *S. marsescens*[215]. A recent study from the Ringstad laboratory at NYU has found that *tol-1* is required for the differentiation of the CO_2-sensing BAG neurons[216] necessary for pathogen avoidance to *S. marsescens* (N. Ringstad, personal communication). In adult animals, *tol-1* expression has been reported in BAG neurons, 10 other neurons, and the head mesodermal cell; however, the extent of *tol-1* expression in other cells is unknown. We assessed SagA-mediated protection against *Salmonella* pathogenesis in *tol-1(nr2033)* and found that SagA was inactive in this mutant (Figure 4.26a). Similarly, we found that the peptidoglycan fragments MurNAc and MurNAc-L-ala were also inactive in *tol-1(nr2033)* (Figure 4.26b), suggesting that SagA activity is *tol-1*-dependent. It is unclear if TOL-1 is acting as a receptor for SagA or SagA-generated peptidoglycan fragments or if it has a more vague developmental role

that affects SagA activity, although we believe the latter is more likely. Nevertheless, the requirement of *tol-1* suggests that a host process is necessary for SagA activity (Figure 4.26c).

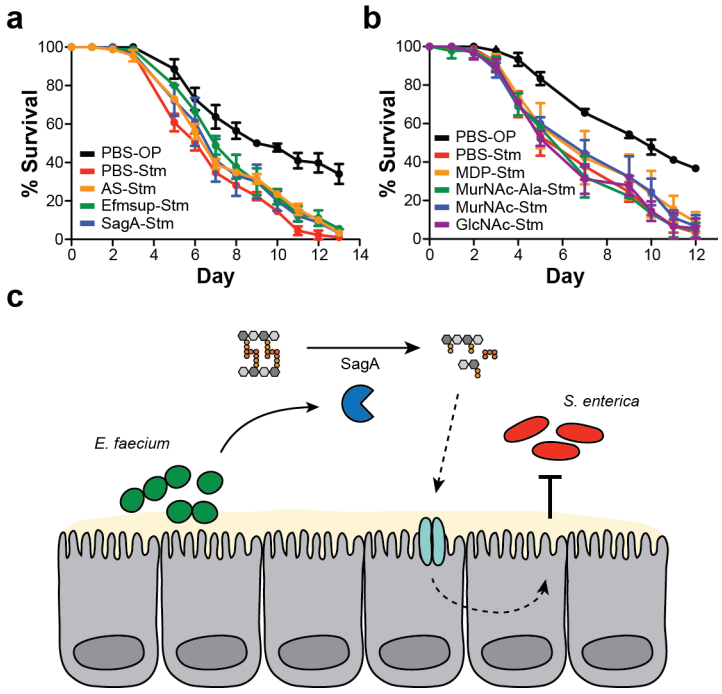

Figure 4.26. Inhibition of *Salmonella* pathogenesis by SagA requires *tol-1*

a. *E. faecium* culture supernatant (Efmsup) and purified SagA do not inhibit *Salmonella* pathogenesis in *tol-1(nr2033)* worms. **b.** MurNAc and MurNAc-Ala do not inhibit *Salmonella* pathogenesis in *tol-1(nr2033)* worms. **c.** Model of SagA activity. *E. faecium* (green cocci) secretes SagA (blue pac-man) in the intestinal lumen. SagA hydrolyzes *E. coli* peptidoglycan (PG) into smaller fragments. SagA-generated PG fragments stimulate a host response that leads to the inhibition of *Salmonella* (red bacilli) pathogenesis. The dashed arrows indicate processes that may require *tol-1*. For a and b, data points represent mean ± standard deviation for 3 plates of 30 worms each. Abbreviations: *E. coli* OP50 (OP); *S. typhimurium* (Stm).

Our hope in studying commensal-pathogen interactions in *C. elegans* was to more rapidly identify and characterize commensal factors relevant to mammalian infection. Having identified SagA as a protective factor in *C. elegans*, we sought to evaluate SagA activity against *Salmonella* pathogenesis in mice. *Salmonella* pathogenesis and invasion occurs in the mouse ileum, which is also a primary site of *E. faecium* colonization. Direct protein delivery to the small intestine, however, is difficult and requires the development of hydrogels to protect embedded protein from digestion[217]. Such methods are in development for insulin delivery, but they have not been used widely. In contrast, delivery of a SagA-expressing bacterial strain is a more tractable approach to directly target SagA to the small intestine. We decided to insert *sagA-his*$_6$ into the chromosome of *E. faecalis* OG1RF[218], a commensal human oral isolate that has been used extensively in mice.

In mammals, *E. faecalis* is an intestinal bacteria occupying a similar niche to *E. faecium*. *E. faecalis* OG1RF encodes three proteins with features similar to SagA, namely: F2MNS9, F2MN84, and F2MNY6 (Figure 4.27). Protein expression, however, has not been verified for any of these genes. Both F2MNS9 and F2MN84 are putative secreted NlpC/p60-type hydrolases. F2MNS9 has 35% sequence identity to SagA, as well as a similar overall protein domain architecture and relative chromosome location. F2MN84 has only 13% sequence identity to SagA and entirely lacks an N-terminal domain, consisting instead of only an NlpC-p60-type hydrolase domain. F2MNY6 is also predicted to be secreted, and has 31% sequence identity to SagA. F2MNY6 has an N-terminal domain most similar to SagA, but, interestingly, it lacks catalytic residues in its NlpC/p60-like domain. To determine whether any of these SagA-like proteins were

indeed secreted *in vitro*, we analyzed *E. faecalis* OG1RF culture supernatant by mass spectrometry (Figure 4.29a and b, Appendix 10). Interestingly, we detected only the non-enzymatic protein F2MNY6 as abundantly secreted in culture (Figure 4.29b). This suggests that *E. faecalis* OG1RF does not secrete high amounts of any protein functionally similar to SagA.

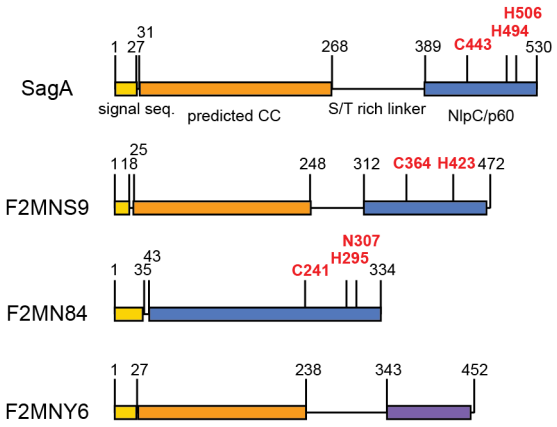

Figure 4.27. SagA-like proteins encoded by *E. faecalis* OG1RF.

a. Predicted domain architecture of the top three proteins in the *E. faecalis* OG1RF genome with significant alignment to SagA. By Needleman-Wunsch global alignment, F2MNS9 has 35.1% sequence identity and 50.6% sequence similarity to SagA; F2MNY6 has 35.6% identity and 54.5% similarity, and F2MN84 has 14.5% identity and 24.2% similarity. Amino acid number is as indicated, and putative catalytic residues are indicated in red bold type. F2MNY6 lacks any putative catalytic residues in its NlpC/p60 like domain, and F2MN84 lacks a predicted coiled-coil domain. As shown Figure 26a, both SagA and F2MNS9 are located after the mreCD operon in the chromosome.

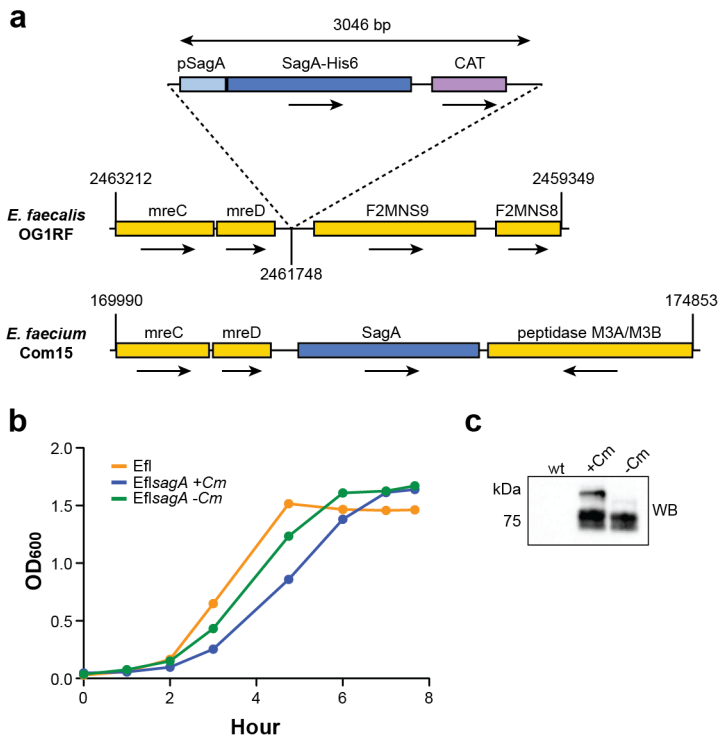

Figure 4.28. Construction of *E. faecalis-sagA*.

a. Schematic insertion of SagA-His$_6$ into the *E. faecalis* OG1RF chromosome to generate *E. faecalis-sagA* (top). CAT= chloramphenicol acyltransferase (chloramphenicol resistance gene). Also shown for comparison is a schematic of the SagA locus in *E. faecium* Com15 (bottom). **b.** Growth curves of *E. faecalis* OG1RF (Efl) and *E. faecalis-sagA* (Efl*sagA*). Cm+ and Cm- indicate ± 10 μg/ml chloramphenicol. **c.** Anti-His$_6$ Western blot (WB) of culture supernatants from the endpoint of the growth curve shown in b. SagA-His$_6$ is secreted by *E. faecalis-sagA* grown in the presence or absence of chloramphenicol (lanes +Cm and -Cm) but not by wild type *E. faecalis* (wt).

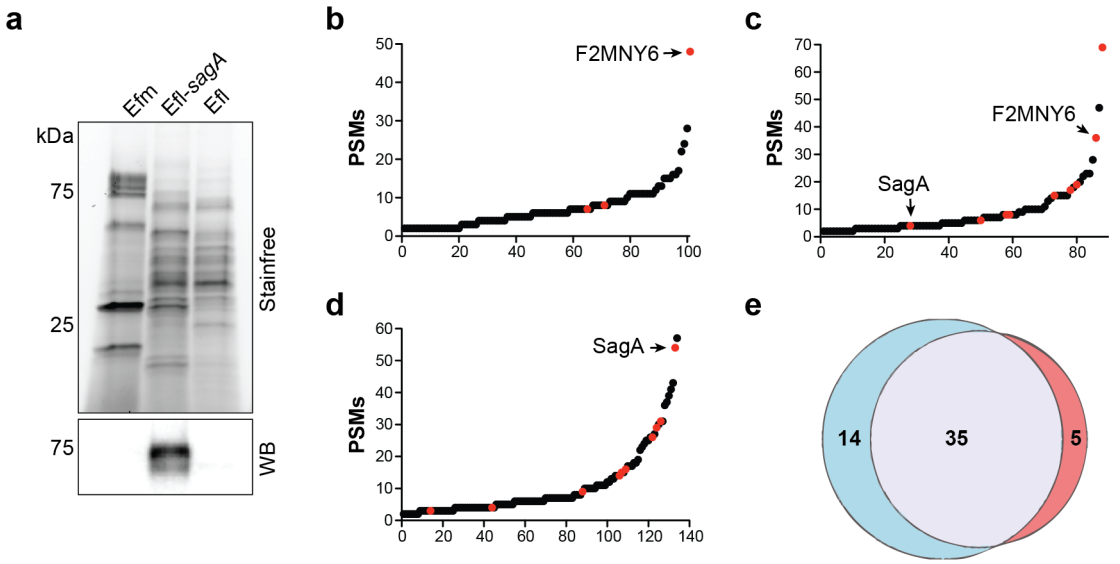

Figure 4.29. Secretome profiling of *E. faecium*, *E. faecalis*, and *E. faecalis-sagA*. **a.** Stain-free imaging and anti-His_6 Western blot (WB) of culture supernatants from *E. faecium* Com15 (Efm), *E. faecalis* OG1RF (Efl), and *E. faecalis-sagA* (Efl*sagA*). Remaining culture supernatant was trypsin digested in-solution for mass spectrometry analysis presented in b-e, and Appendices 9 and 10. **b.** Summary of proteins identified by mass spectrometry from *E. faecalis* OG1RF culture supernatant. Proteins shown were identified with at least 2 unique peptides. Proteins involved in cell-wall remodeling are highlighted in red. On the y-axis is peptide spectrum matches (PSMs); on the x-axis is arbitrary protein number. For the list of proteins identified, see Appendix 10. **c.** Summary of proteins identified by mass spectrometry from *E. faecalis-sagA* culture supernatant. Proteins shown were identified with at least 2 unique peptides. Proteins involved in cell-wall remodeling are highlighted in red. For the list of proteins identified, see Appendix 10. **d.** Summary of proteins identified by mass spectrometry from *E. faecium* Com15 culture supernatant. Proteins shown were identified with at least 2 unique peptides. Proteins involved in cell-wall remodeling are highlighted in red. For the list of proteins identified, see Appendix 9. **e.** Venn diagram comparing the proteins identified by mass spectrometry after in-gel trypsin digestion (blue) (See Figure 4.10a. and b., and Appendix 7) versus in-solution trypsin digestion (red). Proteins identified in both samples are indicated in the overlap (grey). Proteins included in this graph were identified with at least 2 unique peptides, and at least 10 PSMs.

Using a homologous recombination strategy developed by Nallapareddy et al.[219], we inserted *sagA-his6* into the chromosome of *E. faecalis*, generating the strain *E. faecalis-sagA* (Figure 4.28a). In culture, SagA-His_6 was expressed and secreted by *E. faecalis-sagA* (Figure 4.29a and Appendix 10). In culture, *E. faecalis-sagA* grew ~1.2 times slower as compared to wild-type *E faecalis* (Figure 4.28b and c). By Coomassie blue staining and Western blot, we observed that *E. faecalis-sagA* secreted qualitatively less SagA-His_6 as compared to *E. faecium* (data not shown). Reduced relative SagA secretion by *E. faecalis-sagA* was confirmed by mass spectrometry of *E. faecalis-sagA* culture supernatant (Figure 4.29c and Appendices 9 and 10). Interestingly, as compared to wild-type *E. faecalis*, *E. faecalis-sagA* secreted an abundance of additional cell wall remodeling enzymes, reminiscent of the secretion profile of *E. faecium* (Figure 4.29c and d). It may be that expression of SagA by *E. faecalis* necessitates the expression of compensatory peptidoglycan remodeling enzymes, which could explain the modest growth rate defect we observed in *E. faecalis-sagA*.

To assess the role of the hydrolase domain, we also wanted to generate an active site mutant insertion strain of *E. faecalis*. However, the active site mutant was not robustly expressed by *E. faecalis* when either plasmid-encoded (Figure 4.30a) or chromosomally inserted (Figure 4.30b). We hypothesize that the active site mutant might have a dominant negative effect on *E. faecalis* cell wall remodeling and growth, thereby selecting for no expression. Consistent with this, in *E. faecium* we observed reduced expression of plasmid-encoded active site mutant compared to wild type SagA (Figure 4.31a). *E. faecium* encodes an endogenous copy of SagA that could perhaps compete against the dominant negative effect of active site mutant expression, reducing its

deleterious effects. Interestingly, we found that SagA was almost entirely secreted by both *E. faecium* and *E. faecalis-sagA* (Figure 4.30b and 29a). In *E. faecalis-sagA*, we were unable to detect SagA by Western blot from cell lysates of unwashed stationary phase cells (Figure 4.30b), suggesting that SagA was not associated with the cell wall or envelope. We tracked SagA-His_6 secretion by *E. faecium* over growth by Coomassie and Western blot and found that SagA was abundantly secreted at all growth phases, with hardly any associated with the cell lysate (Figure 4.31b and c). Other NlpC/p60-type peptidoglycan hydrolases, including $PcsB^{220}$, are cell-wall associated, raising question as to the endogenous role of SagA in *E. faecium*.

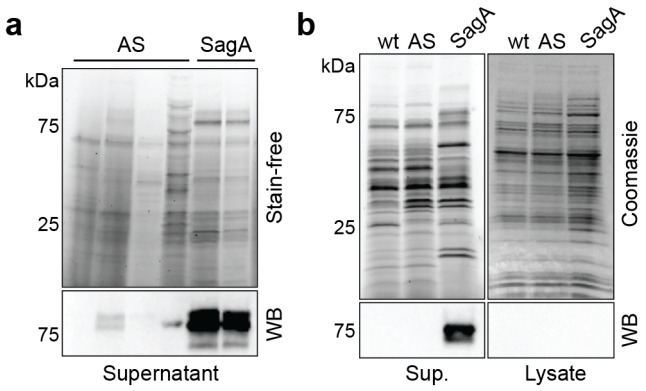

Figure 4.30. Expression of the SagA active site mutant is inhibited in *E. faecalis*. **a.** Stain-free imaging and anti-His_6 Western blot (WB) of culture supernatants from *E. faecalis* carrying plasmid-encoded SagA-His_6 or active site mutant. Four clones are shown for *E. faecalis* encoding the active site mutant (AS), and two clones are shown for *E. faecalis* encoding SagA. **b.** Coomassie blue staining and anti-His_6 WB of culture supernatants (Sup.) and cell lysates from *E. faecalis* expressing chromosomally-encoded SagA-His_6 or active site mutant. SagA is fully secreted, while the active site mutant (AS) is neither expressed nor secreted. Wildtype *E. faecalis* (wt) is shown as a control.

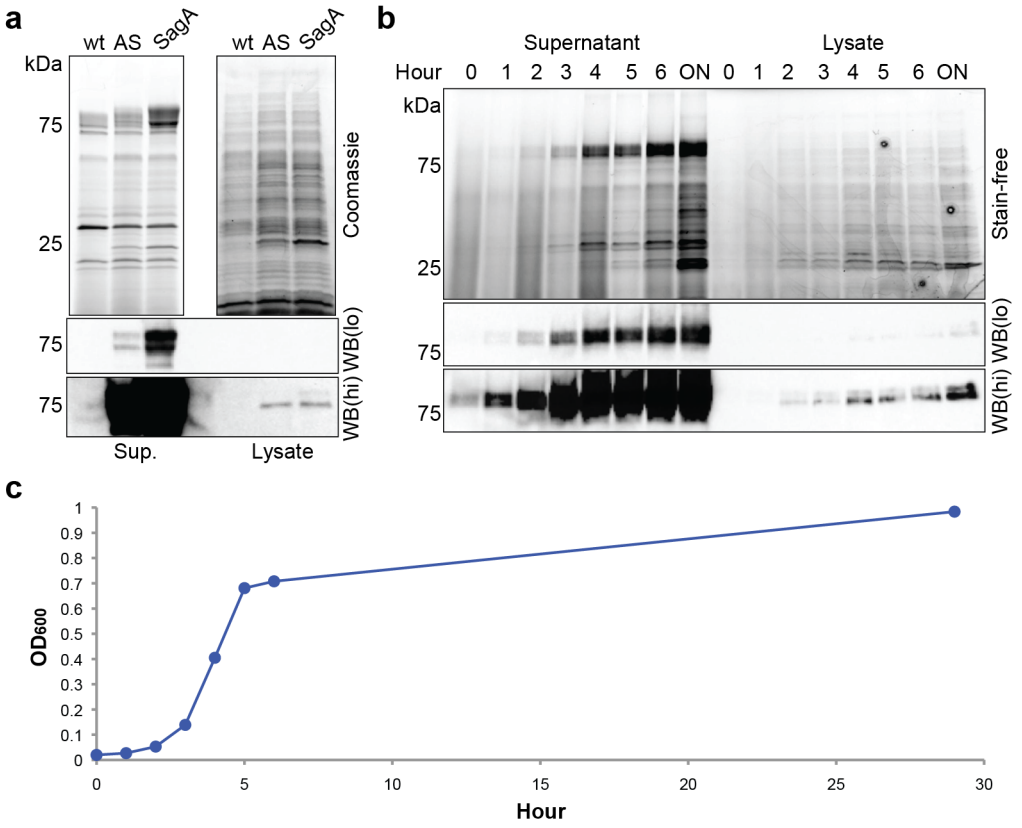

Figure 4.31. Abundant SagA secretion by *E. faecium*.

a. Coomassie blue staining and anti-His_6 Western blot (WB) of culture supernatants (Sup.) and cell lysates from *E. faecium* expressing plasmid-encoded SagA-His_6 or active site mutant (AS). The Commassie blue gel picture is split for individual contrast adjustment of the supernatants and lysates. For WB images, both low (WB(lo)) and high (WB(hi)) exposures are shown. **b.** Time course of SagA expression and secretion. *E. faecium* expressing plasmid-encoded SagA-His_6 was grown in culture and samples were taken at given hours throughout the growth curve. Stain-free imaging and anti-His_6 WB of the culture supernatant and cell lysates are shown. **c.** Growth curve associated with b.

Before testing the activity of *E. faecalis-sagA* against *S. typhimurium* pathogenesis in mice, we first assessed the activity of this strain in *C. elegans*. We were unable to meaningfully evaluate the protection of *E. faecalis-sagA* in the pulsed treatment-infection assay as wild type *E. faecalis* treatment was able to inhibit *Salmonella* pathogenesis (Figure 4.32a). CFU analysis throughout the pulsed infection assay revealed a marked drop in *Salmonella* CFUs 1 day post infection in worms treated with either *E. faecalis* or *E. faecium* (Figure 4.32b). In addition, *E. faecalis* persistently colonized worms to higher numbers than either *E. faecium* or *E. faecalis-sagA* (Figure 4.32c). The ability of *E. faecalis* to inhibit *Salmonella* pathogenesis in a pulsed infection assay may represent a more general protection strategy by *Enterococcus* that is reflected in the decrease in *Salmonella* CFUs observed at 1 day post-infection.

In the continuous infection assay, however, *E. faecalis* treatment was unable to inhibit pathogenesis, while *E. faecium* treatment was protective (Figure 4.32d). In this assay, *E. faecalis-sagA* attenuated *Salmonella* pathogenesis similarly to *E. faecium* (Figure 4.32d). CFU analysis revealed robust, persistent *Salmonella* colonization across all infected conditions (Figure 4.32e). In contrast, *Enterococcus* numbers dwindled by 3 days post treatment (Figure 4.32f) for all strains. Curiously, we observed a marked outgrowth of *E. faecium* in worms late in the assay (Figure 4.32f). A pulsed 2 hour liquid SagA treatment was insufficient to inhibit continuous *Salmonella* infection (Figure 4.33a), suggesting that prolonged delivery of SagA by either *E. faecium* or *E. faecalis-sagA* is required to mediate protection in this assay.

Figure 4.32. Analysis of *E. faecalis-sagA* treatment in pulsed and continuous infection assays.

a. Survival curve from a pulsed treatment-infection assay showing that treatment with wild type *E. faecalis* OG1RF inhibits *Salmonella* pathogenesis similarly to *E. faecium*. **b.** *Salmonella* CFUs measured in *C. elegans* throughout the pulsed treatment-infection assay. **c.** *Enterococcus* CFUs measured in *C. elegans* throughout the pulsed treatment-infection assay. **d.** Survival curve from a continuous infection assay showing that treatment with *E. faecalis-sagA* inhibits *Salmonella* pathogenesis similarly to *E. faecium*, while wild type *E. faecalis* does not protect. **e.** *Salmonella* CFUs measured in *C. elegans* throughout the continuous-infection assay. **f.** *Enterococcus* CFUs measured in *C. elegans* throughout the continuous-infection assay. For a and d, data points represent mean ± standard deviation for 3 plates of 30 worms each. For b and c, the background shading indicates stages of the pulsed treatment-infection. Green indicates treatment, red indicates infection, and grey indicates feeding on *E. coli* OP50. Data points represent average CFUs from 5 worms from one experiment without error bars. The dotted line indicates detection limit. For e and f, the background shading indicates stages of the treatment-continuous infection. Green indicates treatment and red indicates infection. Data points represent average CFUs from 5 worms ± standard deviation of two independent experiments. The dotted line indicates detection limit. Abbreviations: *E. coli* OP50 (OP); *S. typhimurium* (Stm); *E. faecium* (Efm); *E. faecalis* (Efl); *E. faecalis-sagA* (Efl*sagA*).

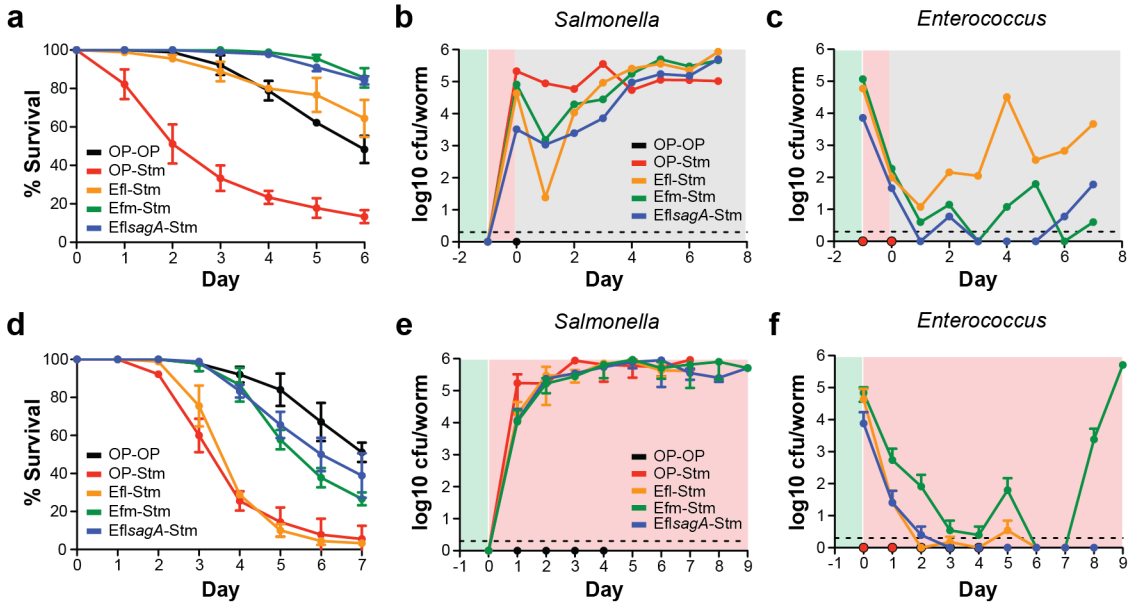

Figure 4.32. Analysis of *E. faecalis-sagA* treatment in pulsed and continuous infection assays.

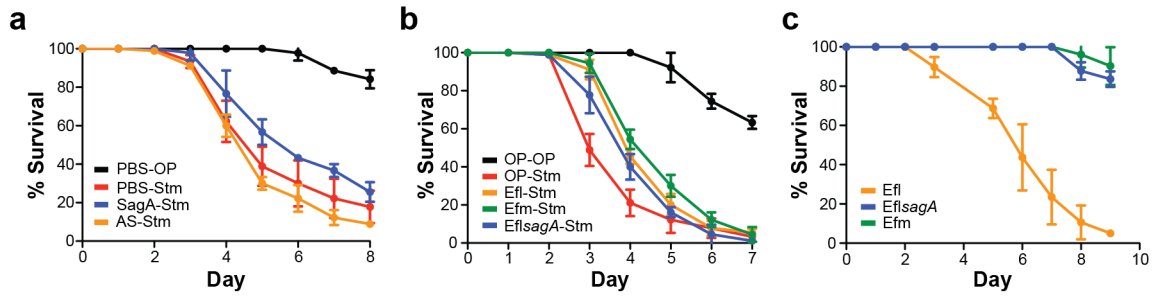

Figure 4.33. Characterization of SagA-mediated protection in various continuous infection assays.

a. Survival curve showing that SagA protein treatment cannot inhibit *Salmonella* pathogenesis in a continuous infection assay. **b.** Survival curve showing that *E. faecium* (Efm) and *E. faecalis-sagA* (Efl*sagA*) do not inhibit *Salmonella* pathogenesis in *tol-1(nr2033)* mutants in a continuous infection assay. **c.** Survival curve showing that Efl*sagA* is less pathogenic than wild type *E. faecalis* (Efl) in a continuous *E. faecalis* infection assay. For a-c, data points represent mean ± standard deviation for 3 plates of 30 worms each. Abbreviations: *E. coli* OP50 (OP); *S. typhimurium* (Stm); *E. faecium* (Efm); *E. faecalis* (Efl); *E. faecalis-sagA* (Efl*sagA*).

To determine if the SagA-dependent protection observed in the continuous infection assay relied on similar host factors as that observed in the pulsed infection assay, we assessed *E. faecalis-sagA* protection in *tol-1(nr2033)* mutant worms. Both *E. faecium* and *E. faecalis-sagA* were unable to inhibit continuous *Salmonella* pathogenesis in *tol-1(nr2033)* mutant worms (Figure 4.33b). This suggests that SagA-mediated protection in both the continuous and pulsed infection assays requires similar host factors, and is likely through a similar mechanism.

Continuous feeding on *E. faecalis*, but not *E. faecium,* is pathogenic to *C. elegans*[174]. We found that worms continuously fed *E. faecalis-sagA* survived similarly

those fed *E. faecium* (Figure 4.33c), suggesting that SagA expression counteracts the intrinsic pathogenesis of *E. faecalis* OG1RF.

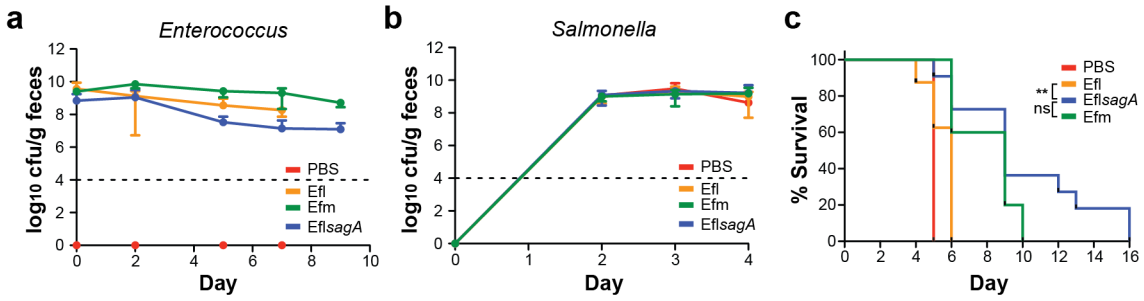

Figure 4.34. *E. faecalis-sagA* inhibits *Salmonella* pathogenesis in mice.
a. *Enterococcus* CFUs measured in mouse feces at indicated time-points during infection. Data points represent average CFUs ± standard deviation from three independent experiments. The dotted line indicates detection limit. **b.** *Salmonella* CFUs measured in mouse feces at indicated time-points during infection. Data points represent average CFUs ± standard deviation from three independent experiments. The dotted line indicates detection limit. **c.** Kaplan-Meier survival curve of *Salmonella* infected germ-free B6 mice. Pre-colonization with either *E. faecalis-sagA* (Efl*sagA*) or *E. faecium* (Efm) prolongs survival. Significance was calculated by log-rank test and p-values were adjusted for multiple comparisons. For **, $p < 0.01$; for ns, $p > 0.05$. Data were pooled from 3 independent experiments. For each condition: PBS, n=2; Efl, n=8; Efm, n=5; and Efl*sagA*, n=11.

To evaluate the protective activity of *E. faecalis-sagA* in mice, germ-free C57BL/6 mice were gavaged with PBS or 10^8 CFUs of *E. faecium, E. faecalis, or E. faecalis-sagA* 4 to 5 days prior to infection with *S. typhimurium*. *Enterococcus* and *Salmonella* load were measured in the feces, and mouse survival was tracked. All *Enterococcus* strains were similarly recovered from the feces after gavage, indicating efficient colonization of the intestine (Figure 4.34a). In addition, *S. typhimurium* CFUs in

the feces were similar across all conditions throughout infection (Figure 4.34b). Consistent with our results in *C. elegans*, this suggests that *E. faecium* does not inhibit *Salmonella* colonization. Germ-free mice are highly susceptible to *Salmonella*, requiring only tens of bacteria to cause pathogenesis and rapid death. Accordingly, PBS gavage prior to infection resulted in a median survival of 5 days (Figure 4.34c). Compared to *E. faecalis*, *E. faecium* treatment shifted median survival from 6 to 9 days (Figure 4.34c). Mice gavaged with *E. faecalis-sagA* prior to infection survived similarly to *E. faecium*-treated mice, and survived significantly longer than *E. faecalis*-treated mice (Figure 4.34c). These results indicate that SagA contributes to *E. faecium*-mediated protection in mice, and that SagA expression is sufficient to convert *E. faecalis* into a protective strain.

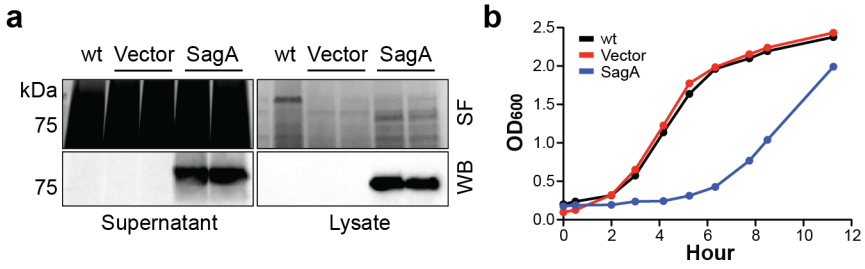

Figure 4.35. SagA expression and secretion by *Lactobacillus plantarum*.
a. Stain-free imaging (SF) and anti-His_6 Western blot (WB) of culture supernatants and cell lysates of *L. plantarum* WCSF1 carrying plasmid-encoded SagA-His_6 or empty vector. 2 clones each for SagA-His_6 and empty vector are shown. Wild type *L. plantarum* WCSF1 (wt) is shown as a control. The black smear in the stain-free imaging of the supernatant lanes is due to growing bacteria in MRS broth. **b.** Growth curves of *L. plantarum-sagA* or *L. plantarum*-vector as compared to wild type *L. plantarum*. SagA expression causes a ~ 2 hour extension of lag phase.

Our eventual goal is to engineer a safe probiotic prophylaxis against *Salmonella* pathogenesis. *E. faecalis* is not an ideal probiotic candidate, since it has pathogenic potential[189]. Therefore, we decided to develop *Lactobacillus plantarum* WCFS1[221] as a SagA-delivery strain. In general, *Lactobacilli* are safe commensal bacteria approved for use as probiotics in both humans and animals[222]. *L. plantarum* WCFS1 is a commensal human oral isolate that has been widely studied in mice as a probiotic. We constitutively expressed SagA-His_6 on a low-copy number plasmid to generate *L. plantarum-sagA*. In culture, SagA-His_6 was expressed and secreted by *L.plantarum-sagA* (Figure 4.35a). However, as compared to wild type *L. plantarum, L.plantarum-sagA* had a markedly protracted lag phase, and grew ~1.4 times slower during exponential phase (Figure 4.35b). Similar to *E. faecalis-sagA*, we hypothesize that this reflects compensatory peptidoglycan remodeling in response to SagA expression.

In preliminary mouse experiments, we have evaluated the protective activity of *L. plantarum-sagA* in a streptomycin-treatment *Salmonella* infection model as compared *E. faecium* or *L. plantarum* carrying an empty vector (*L. plantarum*-vector). Compared to germ-free rearing, streptomycin treatment prior to *Salmonella* infection results in a similar colitis phenotype, and is used extensively as a model for *Salmonella* pathogenesis[223]. We wanted to assess SagA activity in the streptomycin-colitis model, to determine if SagA could protect against *Salmonella* pathogenesis in mice with normally developed immune systems. In this assay, C57BL/6 mice were gavaged with streptomycin 24 hours before gavage with PBS or 10^8 CFUs of *E. faecium, L. plantarum*-vector, or *L. plantarum-sagA*. After 3 hours, mice were infected with *S. typhimurium*. Promisingly, treatment with *L. plantarum-sagA* or *E. faecium* significantly prolonged

survival as compared to PBS or *L. plantarum*-vector treatment (data not shown, V. Pedicord). This suggests that SagA can inhibit *Salmonella* pathogenesis after a brief treatment period, and within the context of a healthy immune background. Given this, we are now engineering an *L. plantarum* chromosomal SagA-insertion strain for future mouse studies.

SUMMARY.

In this study, we used *Caenorhabditis elegans* as a simplified model system to investigate the mechanisms underlying *E. faecium* probiotic function. We identified and characterized secreted antigen A (SagA) from *E. faecium* as a peptidoglycan hydrolase that is sufficient to protect *C. elegans* and mice from *Salmonella* pathogenesis. Our results in *C. elegans* suggest that SagA does not inhibit pathogen growth, but instead remodels peptidoglycan fragments *in vivo* to activate host immune pathways required for resistance to pathogenesis. We hypothesize that SagA promotes a strengthening of intestinal barrier integrity to confine *Salmonella* to the intestinal lumen. These results suggest that commensal bacterial factors can remodel microbial-associated molecular patterns to modulate host resistance to pathogens.

ACKNOWLEDGEMENTS AND CONTRIBUTIONS.

Thanks to Virginia Pedicord from the Hang and Mucida laboratories, who conducted the mouse experiments described in this study. Also, thank you to Yun Lu from the Shaham laboratory who performed the electron microscopy. In addition, I would like to thank Milica Tesic-Mark from The Rockefeller University Proteomics Resource Center for all LC/MS-MS analyses and Steven T. Chen from the Hang laboratory for cloning pET21a-SagA-SS. Thank you to Michael S. Gilmore for gifting the *E. faecium* Com15 and Com12 strains, Barbara E. Murray for *E. faecium* cloning vectors, John T. Singer for the p67mc1 plasmid, and Andreas J. Bäumler for the *ΔinvA* and *ΔinvA/ΔspiB S.typhimurium* strains. Thank you to Aneta Rogoz and Tomiko Rendon from the Mucida laboratory for assistance with germ-free mice, and to Steve Flavell from the Bargmann laboratory and Aaditya Rangan from the Courant Institute at NYU for advice on RNA-seq analysis not shown in this Chapter. I'd also like to thank Donovan Ventimiglia from the Bargmann laboratory for generating *C. elegans* transgenics not shown in this Chapter and providing invaluable advice, ideas, and support. Finally, thank you to Yen-Chih Wang and Byngchul Kim from the Hang laboratory, who are now following up on SagA enzymology studies**.** All *C. elegans* strains were provided by the CGC, which is funded by the NIH Office of Research Infrastructure Programs (P40 OD010440). This work was supported by the NIH-NIGMS 1R01GM103593 grant and the Lerner Trust to Howard C. Hang.

MATERIALS and METHODS.

Strains.

C. elegans were maintained as described by (Stiernagle 1999)[172]. *C. elegans* strains *npr-1(ad609)*, *daf-16(mu86)*, *daf-2(e1370)*; *daf-16(mgDf47), pmk-1(km25), dbl-1(nk3),* and *tol-1(nr2033)* were all provided by the *Caenorhabditis* Genetics Center.

E coli DH5α, *E. coli* BL21-RIL(DE3) (Agilent Technologies), and *Salmonella enterica* serovar *typhimurium* strain IR715 were grown in LB (BD Difco). *Enterococcus faecium* strains NCTC 7171 (ATCC 19434), Com15, Com12, and TX0016 (DO, ATCC BAA-472), *Enterococcus faecalis* strain OG1RF (ATCC 47077), and *Bacillus subtilis* strain 168 were grown in BHI (BD BBL). *Lactobacillus plantarum* WCFS1 (ATCC BAA-793) was grown in MRS (BD BBL). *E. faecium* strains Com15 and Com12 were a gift from Michael Gilmore. *S. typhimurium* strains Δ*invA* and Δ*invA*/Δ*spiB* were a gift from Andreas Baumler[85]. *S. typhimurium* strain Δ*spiB* was a gift from Helene Andrews-Polymenis[224].

When necessary, ampicillin was used at 100 μg/ml, gentamicin was used at 125 μg/ml, kanamycin was used at 50 μg/ml, and tetracycline was used at 15 μg/ml. Chloramphenicol was used at 25 μg/ml for *E. coli*, 10 μg/ml for *Enterococcus*, and 8 μg/ml for *L. plantarum.*

Cloning strategies:

Table 4.1. Plasmids used in this study.

SagA hydrolase domain prediction was determined using Phyre 2 software[225]. Coiled coil domain prediction were determined using COILS software[226]. Signal sequence prediction was determined using SignalP v4.1 software[227].

Name	Backbone	Description
pET21a-SagA	pET21a (Novagen)	Amp^R, SagA-His_6
pET21a-AS	pET21a	Amp^R, AS-His_6; C443A, H494A, H506A
pET21a-ΔCterm	pET21a	Amp^R, ΔCterm-His_6; Δ390-529
pET21a-SagA-SS	pET21a	Amp^R, SagA-SS-His_6; Δ2-27
pET21a-ΔLinker	pET21a	Amp^R, ΔLinker-His_6; Δ225-377
pET21a-ΔNterm+SS	pET21a	Amp^R, ΔNterm+SS-His_6; Δ39-203
pET21a-ΔNterm-SS	pET21a	Amp^R, ΔNterm-SS-His_6; Δ2-26; Δ39-203
pAM401-SagA	pAM401 (ATCC 37429)	Cam^R, psagA:SagA-His_6
pAM401-psagA:mcherry	pAM401	Cam^R, psagA:mcherry
pTEX5501ts-OG1RF-sagA	pTEX5501ts (Nallapareddy et al)[219]	Cam^R, Gen^R, *see below
p67MC1 (Singer et al 2010)[228]		Amp^R, mcherry
pSMC21 (Bloemberg et al 1997)[229]		Amp^R, Kan^R, GFP

All cloning was done in *E. coli* DH5α. pET21a constructs were transformed into *E. coli* BL21-RIL (DE3) for expression. pAM401 constructs were transformed into *i*, *E. faecium,* and *L. plantarum* for expression.

pET21a-SagA:

sagA was PCR amplified from the *E. faecium* Com15 genome using the following primers:

FW: GGACATATGAAAAAGAGTTTAATATCAGCAGTAATGG

RV: GGACTCGAGCATGCTGACAGCAAAGTCAGGTGCAAAC

Restriction sites for Nde1 and Xho1 are underlined. The PCR product was gel purified and subcloned into pGEMTeasy (Promega) for sequencing. Then, an internal Nde1 site was mutated using the Quikchange multi-site directed mutagenesis kit (Stratagene) using the following primer:

AAATATATCGGTACTCCtTATGTTTGGGGCGG

The site mutated is indicated in lowercase, resulting in a synonymous mutation in the SagA protein sequence. *sagA* was then excised from pGEMTeasy with Nde1 and Xho1 and was ligated into cut pET21a (Novagen).

pET21a-AS:

pET21a-SagA was mutagenized with the following primers to generate the indicated cysteine to alanine and histidine to alanine mutations in the SagA protein sequence:

C443A: CCAAGTGGATTTGACgcCTCAGGATTCACACG

H494A: TCACCAGGCGGAACTTACgcCGTAGCGATTGC

H506A: GGAGGACAATATATCgcTGCTCCTCAACCAGG

The mutated sites are indicated in lowercase.

pET21a-ΔCterm:

pet21a-SagA was mutagenized with the following primers to insert BamH1 sites flanking the hydrolase domain:

AACAGATCAAAGTGTgGATCCTGGGAACAGTACTGG

TGCACCTGACTTTGCgGatccCATGCTCGAGCACCAC

The BamH1 sites are underlined. The mutated sites are indicated in lowercase. The plasmid was then cut with BamH1 and re-ligated to form pET21a-ΔCterm, resulting in an in-frame excision of residues 390 through 529 in the SagA protein sequence.

pET21a-SagA-SS:

SagA-SS was PCR amplified from pET21a-SagA_BamH1 (see pAM401-SagA section below) using the following primers:

FW: CATCACCATATGGACGATTTTGATTCTCAGATA

RV: CATCACGGATCCTTTCGGGCTTTGTTA

The Nde1 and BamH1 sites are underlined. This PCR product was cut and ligated back into cut pET21a-SagA_BamH1, resulting in an in-frame excision of residues 2 through 27 in the SagA protein sequence.

pET21a-ΔLinker:

pet21a-SagA was mutagenized with the following primers to insert Kpn1 sites flanking the linker region:

CGCCAAAAAGCAGAAGgTaccGCAGAACAAGCACGCG

TCAACAACACCTGCGggTACcACACCATCAACAGATC

The Kpn1 sites are underlined. The mutated sites are indicated in lowercase. The plasmid was then cut with Kpn1 and re-ligated to form pET21a-ΔLinker, resulting in an in-frame excision of residues 225 through 377 in the SagA protein sequence.

pET21a-ΔNterm+SS:

pet21a-SagA was mutagenized with the following primers to insert Nhe1 sites flanking the N-terminal domain:

TTCTCAGATACAACAgCtAGcTCAAAAGATTGCAGAC

CGTACTGAAAACTTCgcTAGCTGCTGAACAAGCAAC

The Nhe1 sites are underlined. The mutated sites are indicated in lowercase. The plasmid was then cut with Nhe1 and re-ligated to form pET21a-ΔNterm+SS, resulting in an in-frame excision of residues 39 through 203 in the SagA protein sequence.

pET21a-ΔNterm-SS:

pet21a-ΔNterm was cut with Nde1 and SacII, the ends were blunted with Klenow, and the gel-purified plasmid was re-ligated. This resulted in a one base-pair frame shift. The frame shift was corrected by mutagenizing the plasmid with the following primer, restoring the Nde1 restriction site:

AAGGAGATATACAtATGGCGGACGATTTTG

The Nde1 site is underlined. The mutated site is indicated in lowercase. This resulted in an in-frame excision of residues 2 through 26 in the ΔNterm protein sequence, generating pET21a-ΔNterm-SS.

pAM401-psagA:mcherry:

The promoter region of *sagA* (*psagA*) was PCR amplified from the *E. faecium* Com15 genome using following primers:

FW: AAAGTCGACACGATGGTGGTCCAATTGAT

RV: TTTCATATGTCATTCCTCCGACTGGCTTA

Restriction sites for Sal1 and Nde1 are underlined. The PCR product was gel purified and subcloned into pGEMTeasy for sequencing. *psagA* was excised with Sal1 and Nde1, and ligated into cut pAM401-padd9:mcherry (**see below) to replace *paad9* with *psagA*.

pAM401-SagA:

pET21a-SagA was mutagenized to insert a BamH1 site after the 6X-His using the following primer to generate pET21a-SagA_BamH1:

TAACAAAGCCCGAAAGGAtccTGAGTTGGCTGCTGC

The BamH1 site is underlined. The mutated sites are indicated in lowercase. *sagA-his6* was then excised with Nde1 and BamH1, and ligated into cut pAM401-psagA:mcherry to replace mcherry with SagA-His_6. pAM401-SagA was transformed into *E. faecium* Com15, *E. faecalis* OG1RF, and *L. plantarum* WCFS1 as described below.

***Generating *E. faecalis-sagA*:**

pTEX5501ts-OG1RF-sagA:

pTEX5501ts was a gift from Barbara Murray. 986 bp of sequence "upstream" (on the minus strand) of the intended SagA insertion site was PCR amplified using the following primers:

FW: AAACGGCCGAGTGGGGCGTGTTATTGAAG

RV: TTTGTCGACGGGTAAGCTTCTCATCGTTTTG

The Eag1 and Sal1 sites are underlined. 1013 bp of sequence "downstream" (on the minus strand) of the intended SagA insertion site was PCR amplified using the following primers:

FW: AAACTGCAGTGGAGCCTTGAAGAAAGTTG

RV: TTTGGTACCATTGGCTGCTTTTGTTGCTT

The Pst1 and Kpn1 sites are underlined. The upstream and downstream PCR products were subcloned into pGEMTeasy and sequenced, then were excised and ligated into cut pTEX5501ts sequentially. (Note: For the Eag1/Sal1 double digest of pTEX4401ts, Sal1 was added first, then Eag1 because the restriction sites overlap in the vector, and Eag1 can cut more efficiently at the end of a linear DNA fragment). *psagA:sagA-his$_6$* was excised from pAM401-SagA with Sal1 and BamH1 and inserted into the cut vector, generating pTEX5501ts-OG1RF-sagA. OG1RF-*sagA-his$_6$* was generated using the protocol described by (Nallapareddy et al)[219]. Briefly, OG1RF was transformed with pTEX5501ts-OG1RF-sagA and single recombinants were selected after plasmid curing at 37 °C. Then colonies were passaged at 37 °C and screened for gentamicin sensitivity and chloramphenicol resistance until such a clone was identified. Chromosomal insertion was verified by PCR and sequencing.

****pAM401-paad9:mcherry:**

paad9:mcherry was designed by us and synthesized by Genewiz into pUC57. It encodes the synthetic promoter to *aad9*[230] flanked by Sal1 and Nde1 restriction sites, driving

mcherry flanked by Nde1 and BamH1 restriction sites. *paad9:mcherry* was excised from pUC57 with Sal1 and BamH1 and ligated into cut pAM401, inserting into the Tet^R gene.

Electroporation of *Enterococcus* and *Lactobacillus*:

Protocol for preparation of electrocompetent cells and electroporation was adapted from **(**Dunny et al. 1991)[231]. Briefly, *Enterococcus* or *Lactobacillus* were grown for 18 hours in M9YE (M9 media, 0.1% casamino acids, 0.3% yeast extract) + 2% glycine. Cultures were diluted in half with M9YE + 3% glycine, and grown for an additional 3 hours. Cultures were chilled, pelleted, and washed 3 times in sucrose wash buffer (0.625 M sucrose, 1 mM MgCl2, pH 4 with HCl), reducing the original culture volume by 1/2, 1/10, then 1/100 successively with each wash. Finally, cells were aliquoted, flash frozen in liquid nitrogen, and stored at -80 °C. Cells were electroporated in 2 mm cuvettes, 25 μF, 400 ohm, 2.5 kV. Cells were allowed to recover for 2 hours at room temperature without shaking in Todd-Hewitt Broth (BD Bacto) for *Enterococcus* or MRS broth (BD Bacto) for *Lactobacillus*, then with shaking at 37 °C for another 2 hours before plating on selective media.

Protein purification:

For *E. faecium* Com15 protein expression, plasmid-carrying strains were grown in BHI with appropriate antibiotics overnight. For *E. coli* BL21-RIL (DE3), LB cultures were inoculated with overnight cultures with appropriate antibiotics, grown for 2 hours or until $OD_{600} \sim 0.4$, induced with 1 mM IPTG, then grown for an additional 2 hours. His_6-tagged proteins were purified from culture supernatants using Ni-NTA agarose (Qiagen). Native

purifications were performed as recommended in the manufacturer's protocol. Purified protein was dialyzed into PBS at 4 °C overnight using 5 kDa or 7 kDa MWCO Slide-a-lyzers (Pierce Protein Biology). Protein concentration was estimated by BCA assay (Pierce Protein Biology) and protein was stored at -20 °C.

Protein gel methods and Western blotting:

Proteins were separated by SDS-PAGE on 4-20% Criterion Tris-HCl or Criterion TGX precast gels (Bio-Rad). Protein was visualized either by Coomassie blue (Bio-Rad) staining or stain-free imaging on a ChemiDoc MP system (Bio-Rad). Glycoproteins were visualized using the Pierce Glycoprotein staining kit (Thermo Scientific) as per the manufacturer's protocol. For Western blotting, proteins were transferred to nitrocellulose membrane. HRP conjugated polyclonal anti-His_6 (abcam ab1187) and monoclonal anti-actin (abcam ab14128) were used for His_6 and actin Western blots respectively. Western blots were visualized either by developing film or imaging on a ChemiDoc MP system.

Bacterial growth curves:

Growth of E. coli expressing SagA, AS, or SagA-SS:

Cultures were grown as described for protein purification, except that OD_{600} was monitored at given time points using a Spectromax M2e spectrophotometer.

Growth of E. coli and S. typhimurium in the presence of SagA:

LB media was inoculated with overnight cultures 1:100. Protein was added at 10 μg/ml and volumes were normalized across all conditions with PBS. OD_{600} was measured at given time points.

Growth of OG1RF-sagA:

BHI media was inoculated with overnight cultures 1:100. Chloramphenicol was added at 10 μg/ml as indicated. OD_{600} was measured at given time points.

***Salmonella* protein secretion assay:**

For each condition, 2 mL of LB was inoculated with overnight cultures 1:30. Protein was added to media at 10 μg/ml and volumes were normalized across all conditions with PBS. The Δ*invA*[63] strain was a gift from the Baumler lab. Cultures were grown for 4 hours, shaking at 37 °C, the pelleted at 7000 g for 5 minutes. 1 ml of culture supernatant was precipitated with trichloro acetic acid (TCA) at a final concentration of 10% overnight at 4 °C. Precipitated proteins were pelleted at 20,800 g for 30 minutes, rinsed 2 times in acetone, then air-dried. Proteins were then separated by SDS-PAGE and visualized by Coomassie blue staining.

***C. elegans* infection assays:**

For each condition, 3 plates of 30 worms each (total 90 worms) were scored, unless otherwise noted. Mean percent survival and standard deviation of the triplicate plates for a representative experiment is shown. *E. faecium* refers to strain Com15 unless otherwise

noted in the figure legends. Worms were handled using a Leica M60 microscope and imaged using a Leica IC80 HD camera.

Pulsed infection assay:

Worms were synchronized as described in (Powell and Ausubel 2010).[188] Synchronized young adult worms were washed in S buffer (129 ml 0.05 M K_2HPO_4, 871 ml 0.05 M KH_2PO_4, 5.85 g NaCl) and transferred to bacterial lawns grown on 2% agar BHI plates for colonization for 1 day. Then, worms were washed and transferred to lawns of OP50 or IR715 grown on BHI plates for infection for another day. Finally, worms were washed and transferred to lawns of OP50 grown on NGM plates (Day 0). Worms were maintained on OP50-NGM plates and survival was scored as described in (Powell and Ausubel 2010)[188].

Liquid-treatment pulsed infection assay:

Synchronized young adult worms were transferred to 96-well plate wells containing 32% BHI media, culture supernatant, or live cultures. For protein treatments, 10-20 µg/ml of protein in PBS was included in each well. For treatment with peptidoglycan digests, 100 µl of each digest was added to each well. For treatment with defined peptidoglycan fragments, 50 µM of each fragment in a mixture of PBS and water was included in each well. MTP(mDAP), MTP(L-Lys), MTP-D-Asn, TriDAP, TriLys, and D-iGlu-mDAP were purchased from Invivogen. MDP, GlcNAc, and MurNAc were purchased from Sigma-Aldrich. MurNAc-L-Ala was synthesized by Yen-Chih Wang. After 2 hours, worms were washed and transferred to lawns of IR715 grown on BHI plates for 1 day.

Then, worms were washed and transferred to lawns of OP50 grown on NGM plates (Day 0). Worms were maintained on OP50-NGM plates and survival was scored.

Continuous infection assay:

Synchronized young adult worms were washed and transferred to lawns of OP50 or IR715 grown on NGM plates (Day 0). Worms were maintained on OP50 or IR715 NGM plates and survival was scored. For liquid treatment prior to continuous infection, liquid treatments were performed as described above.

OG1RF pathogenesis assay:

This assay was performed as essentially as described by Garsin et al[174]. Briefly, synchronized young adult worms were transferred to Com15, OG1RF, or OG1RF-*sagA* bacterial lawns grown on BHI plates (Day 0). Worms were maintained on Com15, OG1RF, or OG1RF-*sagA* BHI plates, and survival was scored.

Worm CFU measurements:

Protocol for CFU measurements was adapted from Garsin et al[174]. Briefly, 5-20 worms were rinsed in drops of S buffer, and allowed to crawl free of bacteria on a sterile plate. These worms were then mechanically lysed in PBS using microtubes and pestles (Kimble-Chase). Serial dilutions of worm homogenate were plated on *Salmonella-Shigella* agar (BD BBL) or Enterococcosel (BD BBL) agar plates, and plates were incubated at 37 °C overnight.

Treatment of culture supernatants:

Proteinase K treatment: Culture supernatant or media was digested with 0.1 mg/ml of proteinase K in the presence of 1 mM CaCl2 for 2 hours at 37 °C. Then, 1 mM EGTA was added, and digestions were used in the liquid-treatment pulsed infection assay.

Trichloro acetic acid precipitation: Culture supernatant or media was precipitated with TCA (final concentration of 10%) overnight at 4°C. Precipitated proteins were pelleted and rinsed 2 times in acetone, then air-dried and resuspended in BHI media before use in the liquid-treatment pulsed infection assay.

10-kDa MWCO column filtration: *E. faecium* culture supernatant or media was filtered through 10-kDa MWCO columns (Vivaspin GE Healthcare), and the flow-thru was used in the liquid-treatment pulsed infection assay.

5-kDa MWCO column filtration of *E. coli* culture supernatants: *E. coli* BL21-RIL(DE3) expressing SagA-His or AS-His were induced in BHI media instead of LB as described above. Portions of the culture supernatants were filtered through 5-kDa MWCO columns (Vivaspin GE Healthcare), and the unfiltered supernatants, column concentrate, and column flow-thru were used in the liquid-treatment pulsed infection assay.

Peptidoglycan digests:

100 µg of *E. coli* peptidoglycan (Invivogen) was digested with 20 µg lysozyme (Sigma) and 20 µg of SagA-His or AS-His overnight in a mixture of PBS and water at 37 °C.

Digests were then filtered through 5-kDa MWCO columns (Vivaspin GE Healthcare), and the flow-thru was used in the liquid-treatment pulsed infection assay

Proteomics:

In-gel digestion:

1 ml of culture supernatant was precipitated with TCA as described above, resuspended in loading buffer and separated by SDS-PAGE. Proteins were processed for in-gel digestion with sequencing grade trypsin (Promega) as previously described[232] except that dried samples were resuspended in 5% acetonitrile, 2% formic acid in water.

In-solution digestion:

1 ml of culture supernatant was precipitated with TCA as described above, and proteins were digested with 0.2 µg of trypsin in 50 mM ammonium bicarbonate buffer overnight at 37 °C. Samples were dried by speed-vac, then resuspended in 5% acetonitrile, 2% formic acid in water. LC-MS was performed on digested peptides and peptide spectra were analyzed against the *E. faecium* Com15 proteome using Mascot v2.3 and Proteome Discoverer software.

8-aminonaphthalene 1,3,6 trisulfonic acid (ANTS) labeling assay:

E. coli supernatants were prepared by inoculating cultures 1:50 with an overnight culture of *E. coli* BL21-RIL(DE3) expressing SagA-His6 or AS-His6. Cultures were grown for 2 hours, then induced with 1 mM IPTG, and grown for an additional 2 hours. *Enterococcus* supernatants were prepared by growing cultures overnight. Cultures were

pelleted, and supernatant was filtered through 10 kDa MWCO columns (Millipore Microcon). For peptidoglycan digests, 100 µg of *E. coli* peptidoglycan was digested with 20 µg lysozyme and 20 µg of SagA-His or AS-His overnight in a mixture of PBS and water at 37 °C. Digests were filtered through 10 kDa MWCO columns. Culture supernatants, peptidoglycan digests, and defined peptidoglycan fragments were dried by speed-vac before ANTS labeling.

ANTS labeling was performed essentially as described by Young[205]. ANTS reaction mix was added to each tube of dried material (1:1 mixture of 0.2M ANTS (in 3:17 acetic acid:water): 1M $NaCNBH_3$ (in DMSO)). Reactions were incubated overnight at 37 °C. 0.5-3.5 µl of the ANTS labeled mixtures were mixed 1:1 with 40% glycerol and samples were separated by native PAGE on a hand-cast 37-40% Tris-glycine acrylamide gel (19:1 polyacrylamide:bisacrylamide, with a 20% acrylamide stack). at 150 V for ~ 3 hours or until the free ANTS front reached the bottom of the gel. Empty lanes adjacent to sample lanes were loaded with samples of ANTS labeled Ala-D-γ-Glu-Lys-D-Ala-D-Ala (Sigma). Remaining lanes were loaded with 20% glycerol.

Epifluorescence:

For imaging of mcherry-*Salmonella*, worms were treated as described for the pulsed infection assays except worms were infected with *S. typhimurium* carrying the plasmid p67MC1. For imaging of *E. faecium psagA:mcherry*, worms were fed *E. faecium* carrying the plasmid pAM401-mcherry for 1 day on BHI plates. Worms were mounted as described by Shaham 2006[233], except that worms were paralyzed in 1 mM tetramisole

(Sigma) instead of sodium azide. Worms were imaged on a Nikon Eclipse TS100 and pictures were taken using a Nikon Digital Sight DS-Fi1.

Electron Microscopy:

Animals were prepared for electron microscopy using standard methods[234]. Ultrathin serial sections (70 nm) were collected by using a Leica Ultracut UCT Ultramicrotome. Sections at two regions, 120 μm and 200 μm away from the head region, were examined for each condition. EM images were acquired using an FEI Tecnai G2 Spirit BioTwin transmission electron microscope operating at 80 kV with a Gatan 4K x 4K digital camera.

Mouse Experiments:

Mouse experiments were performed in accordance with NIH Animal Care guidelines, institutional guidelines, and animal protocols approved by the IACUC at The Rockefeller University. Germ-free C57BL/6 (B6) mice were bred and continuously housed in germ-free isolators and exported at 7-8 weeks of age. Exported germ-free mice were maintained in autoclaved cages with autoclaved food and water throughout all experiments.

Preparing bacterial cultures for gavage:

S. typhimurium and *Enterococcus* strains were grown overnight in LB and BHI respectively. For *Enterococcus* strains, BHI cultures were inoculated with overnight cultures at 1:50, and incubated at 37 °C for 3-4 hours. Cultures were diluted in PBS to

achieve a concentration of 10^9 CFU/ml. For *S. typhimurium*, LB cultures were inoculated with overnight cultures at 1:30, and incubated at 37 °C for 3-4 hours. Cultures were diluted in PBS to achieve a concentration of 10^3 CFU/ml. These cultures were serially diluted and plated on selective agar to confirm concentration.

Colonization-infection assay:

Upon export, mice were gavaged with PBS or ~10^8 CFUs (in 100 µl) of OG1RF, OG1RF-*sagA* or Com15. Mice were rested for 4-5 days, then infected with ~10^2 CFU (in 100 µl) of *S. typhimurium* per mouse by oral gavage. Infected mice were monitored daily for weight-loss, morbidity, and bacterial burden in the feces. Mice were euthanized upon overt signs of morbidity or loss of more than 20% of baseline body weight.

Mouse fecal CFU measurements:

Mouse feces were weighed and mechanically lysed in PBS using microtubes and pestles (Kimble-Chase). Serial dilutions of fecal homogenate were plated on Enterococcosel (BD BBL) and *Salmonella-Shigella* (BD BBL) agar plates, and plates were incubated at 37 °C overnight.

CHAPTER 5. Discussion and Outlook

Metagenomic[5,65] and metabolomic[235] profiling has revealed an abundance and diversity of bacterial biomolecules and metabolites present in the intestine. As described in Chapter 1, relatively few of these bacterial products have been characterized in the context of microbiota-mediated pathogen resistance. In this thesis, we describe two projects that explore the effects of commensal-derived metabolites in the context of *Salmonella* pathogenesis.

In Chapters 2 and 3, we use alkynyl-functionalized fatty acid chemical reporters to investigate how fatty acids modulate bacterial physiology and virulence. Genomic and proteomic profiling of intracellular *Salmonella* has revealed that this pathogen encodes an extensive metabolic capacity and exploits diverse host nutrients[96,97]. The specific contribution of fatty acids to *Salmonella* growth and virulence *in vivo*, however, is not clear. With our long-chain fatty acid reporter, alk-14, we show that *Salmonella* fully metabolizes exogenous long-chain fatty acids, and we track the covalent modification of metabolic enzymes labeled by alk-14 derived metabolites. We also show that alkynyl-short chain fatty acid reporters can recapitulate the inhibition of *Salmonella* virulence observed with natural short-chain fatty acids. These reporters covalently modify an abundance of *Salmonella* proteins, which may yet reveal the mechanisms underlying fatty-acid mediated attenuation of virulence. In general, our studies suggest that alkynyl-fatty acid reporters may be useful for tracking *Salmonella* metabolic flux and protein modifications in response to dietary or bacterial-derived fatty acids. Taken further,

alkynyl-fatty acid reporters could be used to follow the exchange of fatty acid derived metabolites between bacteria and host cells in more complex environments, such as the intestine.

In Chapter 4, we identify a peptidoglycan hydrolase (SagA) secreted by *Enterococcus faecium* that confers protection against *Salmonella* pathogenesis in *C. elegans* and mice. We hypothesize that SagA remodels peptidoglycan *in vivo* to enhance host resistance to pathogenesis. The conservation of SagA-mediated protection in *C. elegans* and mice is suggestive of a conserved mechanism. In *C. elegans*, SagA-activity appears to require *tol-1*-dependent host processes. Electron microscopy of *E. faecium*-treated worms revealed decreased degradation of the intestinal microvilli, despite robust *Salmonella* colonization, leading us to hypothesize that *E. faecium* may enhance epithelial barrier function. This is an attractive hypothesis since the secretion of antimicrobial peptides by intestinal epithelial cells constitutes a major arm of *C. elegans* immunity. Although little is known in *C. elegans* regarding epithelial barrier maintenance *per se*, in mammals, the secretion of mucins and antimicrobial peptides, most notably the C-type lectin Reg-IIIγ, by intestinal epithelial cells is required to segregate bacteria away from the intestinal border[45]. Preliminary experiments analyzing the inhibition of *Salmonella* pathogenesis by *E. faecium* in Rag2-deficient mice and Reg-IIIγ-deficient mice have indicated that *E. faecium*-mediated protection does not require adaptive immunity, but is dependent on Reg-IIIγ (data not shown, V. Pedicord). Although similar experiments using *E. faecalis-sagA* have yet to be performed, these data suggest that SagA-activity in mice leads to an enhancement in intestinal epithelial barrier function. If

true, the conserved action of SagA suggests a link between peptidoglycan recognition and innate immune enhancement of epithelial barrier function in both *C. elegans* and mice.

Peptidoglycan recognition and modification is a widely conserved aspect of innate immunity in animals. In mammals, NOD1 and NOD2 are the best characterized peptidoglycan recognition receptors[28]. Activation of downstream NF-κB and MAPK pathways upon peptidoglycan recognition leads to the expression of inflammatory cytokines, reactive oxygen species, and antimicrobial peptides, including Reg-IIIγ[236]. Peptidoglycan recognition by TLR2 has also been reported[237], although the specific peptidoglycan-derived ligand(s) recognized by TLR2 are unclear[238]. TLR2 activation leads to antimicrobial peptide production as well as an enhancement of tight junction integrity[239]. In the intestine, NOD1, NOD2, and TLR2 are involved in immune homeostasis and tolerance mechanisms, in part through the regulation of epithelial barrier function[21].

NOD1 and NOD2 respond to different peptidoglycan fragments; namely, NOD1 recognizes MTP(mDAP), TriDAP, and iGlu-DAP, while NOD2 recognizes MDP[240]. To our knowledge, the response to smaller peptidoglycan fragments, such as MurNAc and MurNAc-L-Ala, has not been assessed. Although various peptidoglycan fragments can stimulate NOD1 and NOD2, the endogenous ligands recognized *in vivo* remain unknown. Direct binding of peptidoglycan fragments to NOD1 or NOD2 has been suggested, but is confounded by the fact that these are cytoplasmic proteins. Hydrophobic peptidoglycan fragments could potentially diffuse through the cell membrane. However, various mechanisms to actively transport peptidoglycan to the cytoplasm have been suggested,

including endocytosis[241], peptide transporters[242], and injection by bacterial secretion systems[243].

The ligand specificity of NOD1 and NOD2 calls to question the role of peptidoglycan remodeling enzymes in modulating NOD-dependent responses. Besides the abundance of bacterially-encoded peptidoglycan remodeling enzymes likely expressed in the intestine, mammals express 4 peptidoglycan recognition receptors (PGRPs) in the intestine, namely: PGLYRP-1, -2, -3, and -4[199,244]. PGLYRP-1, -3, and -4 bind peptidoglycan and are bactericidal, possibly contributing to epithelial barrier function. In contrast, PGLYRP-2 has non-bactericidal peptidoglycan amidase activity, cleaving between MurNAc and L-Ala[245,246]. This activity could theoretically destroy NOD2 ligands, and decrease the uptake of NOD1 ligands (MTP --> tri-peptide). So far, the role of PGLYRP-2 *in vivo* is unclear, although in a *Salmonella* streptomycin-colitis model, PGLYRP-2-deficient mice exhibit enhanced caecal inflammation[247]. *Drosophila* encodes 20 PGRPs, of which 8 are known or predicted to have amidase activity. Several of the non-enzymatic PGRPS are involved in peptidoglycan recognition for immune activation, while those with amidase activity have been found to dampen excessive immune activation by cleaving and inactivating stimulatory peptidoglycan fragments. We hypothesize that SagA might function similarly to a PGRP, modulating the intestinal peptidoglycan pool to alter downstream host responses. A first step in addressing this hypothesis is to assess whether SagA-generated peptidoglycan fragments, or more specifically MurNAc and MurNAc-Lala, can activate NOD1, NOD2 or TLR2, given their well-characterized roles in epithelial barrier maintenance and innate immunity.

In *C. elegans*, no microbial-associated molecular patterns (MAMPs) or pattern recognition receptors (PRRs) have been characterized. In addition, *C. elegans* does not encode any obvious homologues to NOD-like receptors or PGRPs. Secreted intestinal lysozymes may be the only host-encoded peptidoglycan remodeling enzymes. C-type lectin domain (CTLD) containing proteins, which bind various monosaccharides and carbohydrates among other bacterial cell wall ligands[30], could be involved in *C. elegans* pattern recognition[159]. In addition, *C. elegans* also encodes 8 LysM domain-containing (LMD) proteins[248]. LysM domains are glycan/peptidoglycan-binding domains[249] that originated from bacteria, and are found in a variety of eukaryotes. However, whether LMD-containing proteins play a role in immunity is not known. Either CTLD- or LMD-containing proteins could potentially bind to SagA or SagA-derived peptidoglycan fragments to enhance immunity. The differential activity we observe between MurNAc and GlcNAc in *C. elegans* could be, for example, due to differences in the sugar-binding specificity of these domains. Future investigation into peptidoglycan recognition in *C. elegans*, and how downstream immune responses enhance epithelial barrier function could inform the evolution of these processes.

In the context of a diverse intestinal microbiome, we wonder: is the protective function of SagA actually unique? Peptidoglycan remodeling enzymes, including NlpC/p60 enzymes, are widespread amongst bacteria[193,250]. Nevertheless, the abundant secretion of SagA and other peptidoglycan remodeling enzymes by *E. faecium* may be an unusual property. It may be that our study has highlighted the activity of SagA through the use of simplified models, where a diverse microbiome is non-existent (as with *C. elegans* and germ-free mice) or severely compromised (as with streptomycin-treated

mice). It is possible, for example, that the protective activity of SagA is already partially reflected in the steady state resistance to *Salmonella* observed in wild-type mice. However, given that *E. faecium* is a minor member of the intestinal flora, one could imagine enhancing host resistance by increasing the abundance of SagA-producing bacteria. Future work assessing the roles of other secreted peptidoglycan remodeling enzymes could reveal an unappreciated tier of immune regulation in the intestine.

In mammals, innate immune recognition of bacterial cell wall components is balanced between mechanisms of tolerance versus immune activation. As microbivores, *C. elegans* could be under pressure to evolve functionally similar mechanisms of immune homeostasis. Host- and bacterial-encoded peptidoglycan remodeling enzymes may work in concert to promote this balance. If *E. faecium* is truly an "ancient" member of the microbiome, perhaps it played a part in generating the symbiosis that exists between host and microbiota.

APPENDIX 1. High confidence proteins identified from *E. coli* labeled with alk-14. Proteins listed were identified with at least 2 unique peptides and 10 fold enrichment in at least one sample over the DMSO control. Proteins that were enriched in the DMSO control of two of the three samples were omitted from this list, and included in Appendix 2. Predicted lipoproteins are highlighted in yellow.

						Expt 1: (-) IPTG		Expt 2: (+) IPTG		Expt 3		
Accession	**Uniprot ID**	**Gene Name**	**Description**	**LipoP**	**MW (kDa)**	**DMSO**	**alk-14**	**DMSO**	**alk-14**	**DMSO**	**alk-14**	**alk-2**
EG11504	METQ_ECOLI	metQ	Periplasmic methionine binding lipoprotein	SpII	29	0	514	0	25	0	0	0
EG14222	BAMD_ECOLI	bamD	Lipoprotein required for OM biogenesis	SpII	28	0	228	0	15	0	0	0
EG10684	PAL_ECOLI	pal	Lipoprotein associated with peptidoglycan	SpII	19	0	194	0	46	0	73	0
EG12271	YIAD_ECOLI	yiaD	Novel verified lipoprotein, function unknown	SpII	22	0	147	0	13	0	0	0
EG10658	BAMC_ECOLI	bamC	Lipoprotein required for OM biogenesis	SpII	37	0	140	0	37	0	0	0
EG12218	DCRB_ECOLI	dcrB	Probable lipoprotein required for phage C1 adsorption	SpII	20	0	130	0	15	0	24	0
EG13685	YBJP_ECOLI	ybjP	Novel verified lipoprotein, function unknown	SpII	19	0	113	0	0	0	64	0
EG13755	YDCL_ECOLI	ydcL	Novel verified lipoprotein, function unknown	SpII	24	0	113	0	0	0	0	0
EG14208	BAMB_ECOLI	bamB	Required for OM biogenesis, in BamABCD complex	SpII	42	0	99	0	31	0	0	0
EG12137	NLPE_ECOLI	nlpE	Lipoprotein activating Cpx in response to adhesion	SpII	26	0	92	32	3179	0	0	0
EG11703	ACRA_ECOLI	acrA	AcrAB-TolC multidrug efflux pump	SpII	42	0	85	2	47	0	0	0
EG13409	SLYB_ECOLI	slyB	Novel verified lipoprotein, function unknown	SpII	16	0	71	0	23	0	42	0
EG12182	YAJG_ECOLI	yajG	Probable lipoprotein, function unknown	SpII	21	0	69	0	10	0	19	0

EG12781	YRAP_ECOLI	yraP	OM lipoprotein, mutant is SDS-sensitive	SpII	20	0	68	0	5	0	16	0
EG10360	EFG_ECOLI	fusA	Elongation Factor EF-G	CYT	78	4	64	0	47	17	2	27
EG13431	LPOB_ECOLI	ycfM	Novel verified lipoprotein, function unknown	SpII	23	0	49	0	0	0	0	0
EG11384	AHPC_ECOLI	ahpC	Alkyl hydroperoxide reductase, subunit C	CYT	21	14	48	0	0	0	102	0
EG11291	LOIP_ECOLI	yggG	Heat shock protein binds Era	SpII	27	0	44	0	0	0	0	0
EG10701	PFLB_ECOLI	pflB	Pyruvate formate lyase I	CYT	85	0	33	0	6	3	2	7
EG11293	LOLB_ECOLI	lolB	Outer membrane lipoprotein required for lipoprotein localization	SpII	24	0	32	0	0	0	0	0
EG13081	YGDI_ECOLI	ygdI	Novel verified lipoprotein, function unknown	SpII	8	0	31	0	0	0	31	0
EG10657	NLPA_ECOLI	nlpA	Lipoprotein-28, inner membrane protein, function unknown	SpII	29	0	31	0	0	0	0	0
EG10855	LPTE_ECOLI	lptE	LPS assembly OM complex LptDE, lipopprotein component	SpII	21	3	28	0	0	0	22	0
EG10025	ODP2_ECOLI	aceF	Pyruvate dehydrogenase, dihydrolipoamide acetyltransferase E2	CYT	66	0	27	4	6	0	0	0
EG11502	RCSF_ECOLI	rcsF	Lipoprotein that signals increased capsule synthesis	SpII	14	0	25	0	0	0	0	0
EG14276	MLAA_ECOLI	vacJ	Surface-exposed lipoprotein	SpII	28	0	23	0	0	0	0	0
EG10954	SODF_ECOLI	sodB	Superoxide dismutase, Fe	CYT	21	16	21	0	0	0	18	0
EG12524	RIDA_ECOLI	yjgF	Function unknown	CYT	14	0	21	0	0	4	18	9
EG12778	LPOA_ECOLI	yraM	Probable lipoprotein, function unknown	SpII	73	0	19	0	0	2	0	0
EG11164	YGIB_ECOLI	ygiB	Probable lipoprotein, function unknown	SpII	23	0	17	0	14	0	0	0
EG12273	YIAF_ECOLI	yiaF	Probable lipoprotein, function unknown	SpII	26	0	17	0	3	0	0	0

EG13085	MLTA_ECOLI	mltA	Membrane-bound lytic transglycosylase A, murein hydrolase	SpII	40	0	17	0	0	0	0	0
EG10932	SDHB_ECOLI	sdhB	Succinate dehydrogenase (SQR) iron-sulfur protein	CYT	27	0	15	0	0	0	2	0
EG50003	ACP_ECOLI	acpP	Acyl carrier protein ACP	CYT	9	0	11	0	3	0	31	0
EG11117	YCEB_ECOLI	yceB	Novel verified lipoprotein, function unknown	SpII	21	0	10	0	0	0	0	0
EG12548	YJHF_ECOLI	yjhF	Putative GntP family transporter, function unknown	TMH	47	0	10	0	0	0	0	0
EG11890	SLP_ECOLI	slp	Outer membrane lipoprotein, stationary phase inducible	SpII	21	0	9	0	0	0	23	0
EG10872	RL11_ECOLI	rplK	50S ribosomal subunit protein L11	CYT	15	0	6	0	0	0	10	0
EG10868	RL5_ECOLI	rplE	50S ribosomal subunit protein L5	CYT	20	0	5	0	12	0	19	0
EG12040	YEJE_ECOLI	yejE	ABC transporter permease protein for microcin C uptake	TMH	38	0	0	0	10	0	0	0
EG10044	OSME_ECOLI	osmE	Osmotically inducible lipoprotein, function unknown	SpII	12	0	0	0	0	0	161	0
EG10544	LPP_ECOLI	lpp	Murein lipoprotein	SpII	8	0	0	0	0	0	28	0
EG12672	TPX_ECOLI	tpx	Lipid hydroperoxide peroxidase	CYT	18	0	0	0	0	0	16	0
EG11659	YEDD_ECOLI	yedD	Novel verified lipoprotein, function unknown	SpII	15	0	0	0	0	0	11	0
EG10912	RS13_ECOLI	rpsM	30S ribosomal subunit protein S13	CYT	13	0	0	0	0	0	10	0

APPENDIX 2. Medium confidence proteins identified from *E. coli* labeled with alk-14. Proteins listed were identified with at least 2 unique peptides, and 5 fold enrichment in at least one sample over the DMSO control. Predicted lipoproteins are highlighted in yellow.

						Expt 1: (-) IPTG		Expt 2: (+) IPTG		Expt 3		
Accession	**Uniprot ID**	**Gene Name**	**Description**	**LipoP**	**MW (kDa)**	**DMSO**	**alk-14**	**DMSO**	**alk-14**	**DMSO**	**alk-14**	**alk-2**
EG10671	OMPF_ECOLI	ompF	Outer membrane porin F	SpI	39	104	741	25	106	34	2	57
EG11036	EFTU1_ECOLI	tufA	EF-Tu, Elongation Factor-Translation, unstable	CYT	43	105	223	17	325	133	51	17
EG12316	ACON2_ECOLI	acnB	Aconitase B	CYT	94	11	128	2	0	9	0	14
EG10031	ADHE_ECOLI	adhE	Alcohol dehydrogenase, largely anaerobic	CYT	96	8	118	14	0	27	22	57
EG10703	PGK_ECOLI	pgk	Phosphoglycerate kinase	CYT	41	5	26	2	0	26	8	4
EG10489	IDH_ECOLI	icd	Isocitrate dehydrogenase, NADP+-specific	CYT	46	26	20	0	7	11	4	2
EG10423	GYRA_ECOLI	gyrA	DNA gyrase, subunit A	CYT	97	0	11	21	0	0	0	2
EG11015	TPIS_ECOLI	tpiA	Triosephosphate isomerase	CYT	27	0	10	0	0	8	0	6
EG10903	RS4_ECOLI	rpsD	30S ribosomal subunit protein S4	CYT	23	0	9	2	6	0	0	0
EG13637	BORD_ECOLI	borD	Lipoprotein in DLP12 prophage	SpII	10	0	9	0	3	0	0	0
EG10982	SUCD_ECOLI	sucD	Succinyl CoA synthase alpha-subunit	CYT	30	0	9	0	2	4	2	16
EG10979	ODO1_ECOLI	sucA	2-oxoglutarate dehydrogenase, E1 component	CYT	105	0	9	0	0	0	2	3
EG11325	ACON1_ECOLI	acnA	Aconitase A, stationary phase induced	CYT	98	0	8	2	3	2	0	0
EG10282	ALF_ECOLI	fbaA	Fructose-bisphosphate aldolase, class II	CYT	39	0	8	0	0	27	3	3
EG10511	KATG_ECOLI	katG	Catalase-hydrogen peroxidase I	CYT	80	0	8	0	0	0	0	0

EG12111	NLPD_ECOLI	nlpD	Lipoprotein, function unknown	SpII	40	0	7	0	0	0	0	0
EG10098	ATPA_ECOLI	atpA	ATP synthase subunit alpha, membrane-bound, F1 sector	CYT	55	0	7	0	0	0	0	0
EG10669	OMPA_ECOLI	ompA	Outer membrane protein A	SpI	37	0	6	0	0	0	0	0
EG11100	YBAB_ECOLI	ybaB	Function unknown, in recR operon	CYT	12	0	6	0	0	0	0	0
EG14091	ARNA_ECOLI	arnA	UDP-glucuronate dehydrogenase and UDP-ara4N formyltransferase	CYT	74	0	5	0	6	0	0	0
EG11390	USPA_ECOLI	uspA	Global regulatory gene for stress response	CYT	16	0	5	0	0	0	8	0
EG12367	CUSA_ECOLI	cusA	Silver and copper efflux, membrane transporter	TMH	115	0	5	6	0	5	0	4
EG12699	MLTB_ECOLI	mltB	Membrane-bound lytic transglycosylase B, murein hydrolase	SpII	40	0	5	0	0	0	0	0
EG13511	YEAY_ECOLI	yeaY	RpoE-regulated lipoprotein, function unknown	SpII	21	0	5	0	0	0	0	0
EG11506	FTSH_ECOLI	ftsH	ATP-dependent membrane protease, complexed with HflCK	SpI	71	0	5	0	0	0	0	0
EG13134	UUP_ECOLI	uup	DNA-binding ATPase involved in replication	CYT	72	0	5	0	0	0	0	0
EG10696	AMPN_ECOLI	pepN	Aminopeptidase N	CYT	99	0	5	0	0	0	0	0
EG13999	ASTC_ECOLI	astC	Succinylornithine transaminase, mutant cannot catabolize arginine, overproduction complements argD mutants	CYT	44	0	5	0	0	0	0	0
EG10886	RL28_ECOLI	rpmB	50S ribosomal subunit protein L28	CYT	9	0	5	0	0	0	0	0
EG10303	FHUB_ECOLI	fhuB	ABC transporter permease, Fe(3+)-ferrichrome uptake	TMH	70	0	4	0	8	0	0	0

EG12474	BLC_ECOLI	blc	Outer membrane lipoprotein, cell division and growth function	SpII	20	0	4	0	0	0	5	0
EG12606	FABF_ECOLI	fabF	beta-Ketoacyl-ACP synthase II	CYT	43	0	3	0	7	0	0	0
EG10869	RL6_ECOLI	rplF	50S ribosomal subunit protein L6	CYT	19	2	3	0	5	0	9	0
EG10274	FABB_ECOLI	fabB	beta-Ketoacyl-ACP synthase I	CYT	43	0	3	0	5	0	0	0
EG10356	FUMA_ECOLI	fumA	Fumarase A, aerobic	CYT	60	0	3	0	0	0	6	0
EG12094	SGRR_ECOLI	sgrR	Transcriptional activator of sgrS sRNA	CYT	64	0	2	0	5	0	0	0
EG13905	YCIT_ECOLI	yciT	Global regulator of transcription	CYT	28	0	0	0	9	0	0	0
EG12956	CUTC_ECOLI	cutC	Copper sensitivity	CYT	27	3	0	0	7	0	0	0
EG14161	MURR_ECOLI	murR	Repressor for murPQ, MurNAc 6-P inducible	CYT	31	2	0	0	6	0	0	2
EG10936	SECA_ECOLI	secA	Translocon ATPase	CYT	102	3	0	0	6	0	0	0
EG13226	FTSK_ECOLI	ftsK	DNA translocase at septal ring sorting daughter chromsomes	TMH	147	0	0	0	5	0	5	2
EG13689	YBJT_ECOLI	ybjT	Function unknown	CYT	54	0	0	0	5	4	2	5
EG11985	WBBK_ECOLI	wbbK	Involved in lipopolysaccharide biosynthesis	CYT	43	0	0	0	5	0	0	0
EG14215	HYFG_ECOLI	hyfG	Putative hydrogenase 4 component G	CYT	63	16	0	11	4	0	8	0
EG10938	SECD_ECOLI	secD	SecDFyajC inner membrane secretion protein trimeric complex	TMH	67	0	0	0	0	2	11	7
EG13253	YBAY_ECOLI	ybaY	Novel verified lipoprotein, function unknown	SpII	19	0	0	0	0	0	9	0
EG12585	YJIX_ECOLI	yjiX	Function unknown	CYT	8	0	0	0	0	0	9	0

EG13746	PAAX_ECOLI	paaX	Phenylacetic acid degradation	CYT	35	0	0	23	0	0	7	0
EG13484	YDJH_ECOLI	ydjH	Putative sugar kinase, function unknown	CYT	34	0	0	0	0	0	6	3
EG10349	FUCI_ECOLI	fucI	L-Fucose isomerase	CYT	65	0	0	0	0	0	6	0
EG10937	SECB_ECOLI	secB	Protein export chaperone	CYT	17	0	0	0	0	0	6	0

APPENDIX 3. Proteins identified from *E. coli* labeled with alk-2. Proteins listed were identified with at least 2 unique peptides. The peptide-spectral counts from alk-14 labeling in the same experiment are also listed for each protein. Proteins previously identified as acetylated in Zhang et al. 2013 are indicated in black, in Khun et al. 2014 are indicated in blue. No proteins were previously identified from Yu et al. 2008. Predicted lipoproteins are highlighted in yellow.

							Expt. 3		
Accession	**Uniprot ID**	**Gene Name**	**Description**	**LipoP**	**Acetyl-ation**	**MW (kDa)**	**DMSO**	**alk-2**	**alk-14**
EG14151	PTFX1_ECOLI	fryA	Putative fructose-like PTS system Enzyme I	CYT		92	0	12	0
EG11233	RSTB_ECOLI	rstB	Putative sensor kinase	TMH		49	0	8	0
EG11815	TORC_ECOLI	torC	c-Type cytochrome	TMH		44	0	4	0
EG11613	EPTA_ECOLI	eptA	Lipid A phosphoethanolamine transferase, associated with polymyxin resistance	TMH		62	0	4	0
EG11608	CLSA_ECOLI	cls	Cardiolipin synthase	TMH		55	0	4	0
EG12051	YEJO_ECOLI	yejO	Pseudogene reconstruction, autotransporter homolog	SpI		91	0	4	0
EG12775	YRAJ_ECOLI	yraJ	Putative outer membrane fimbrial subunit export usher protein	SpI		94	0	4	0
EG13217	YBAE_ECOLI	ybaE	Function unknown	CYT		65	0	4	0
EG11714	CBRA_ECOLI	cbrA	Function unknown, creBC regulon	CYT		40	0	4	0
EG10353	FUCR_ECOLI	fucR	Positive regulatory protein for fuc regulon	CYT		27	0	4	0
EG11667	ATOS_ECOLI	atoS	Transcriptional histidine protein kinase regulator of atoDAEB	TMH		68	0	3	0
EG10609	MREC_ECOLI	mreC	Cell division and growth	TMH		40	0	3	0
EG10167	CSTA_ECOLI	cstA	Starvation-induced protein involved in peptide utilization during carbon starvation	TMH		75	0	3	0
EG12077	NIKC_ECOLI	nikC	Nickel transport system permease	TMH		30	0	3	0
EG13863	PGAC_ECOLI	pgaC	Required for biofilm adhesin polysaccharide PGA synthesis	TMH		51	0	3	0
EG14095	YFBK_ECOLI	yfbK	Probable lipoprotein, function unknown	SpII		64	0	3	2
EG11347	FLIF_ECOLI	fliF	Flagellar basal body M-ring protein	SpI		61	0	3	0

EG12859	OPGD_ECOLI	opgD	Osmoregulated periplasmic glucan (OPG) biosynthesis	SpI		63	0	3	4
EG14082	YFAT_ECOLI	yfaT	Function unknown	SpI		24	0	3	0
EG13213	YPJA_ECOLI	ypjA	Overexpression increases adhesion, function unknown	SpI		157	0	3	0
EG10311	FIMD_ECOLI	fimD	Outer membrane fimbrial subunit export usher protein	SpI		96	0	3	0
EG13995	ASTE_ECOLI	astE	Probable succinylglutamate desuccinylase, arginine catabolism	CYT		36	0	3	0
EG12418	GATZ_ECOLI	gatZ	Tagatose bisphosphate aldolase GatYZ subunit	CYT	X	47	0	3	2
EG10686	PARC_ECOLI	parC	Topoisomerase IV, subunit A, ATP-dependent, type II	CYT		84	0	3	0
EG10660	RIR1_ECOLI	nrdA	Ribonucleoside diphosphate reductase, subunit alpha	CYT	XX	86	0	3	0
EG13506	DMLR_ECOLI	yeaT	Positive transcriptional regulator for yeaU	CYT		35	0	3	0
EG10435	HFLC_ECOLI	hflC	Membrane bound protease complex, with FtsH and HflK	CYT		38	0	3	0
EG13600	PRPR_ECOLI	prpR	Transcriptional regulator of prp operon	CYT		59	0	3	0
EG10631	NADB_ECOLI	nadB	Quinolinate synthase, B protein	CYT		60	0	3	0
EG10520	KDTA_ECOLI	waaA	3-deoxy-D-manno-octulosonate(Kdo)-lipid A transferase	CYT		47	0	3	0
EG13472	GSIA_ECOLI	gsiA	Glutathione transporter ATP-binding protein	CYT		69	0	3	0
EG12819	ZAPE_ECOLI	yhcM	Function unknown	CYT		43	0	3	0
EG10763	PRIA_ECOLI	priA	Primosome factor Y, also called protein n'	CYT		82	0	3	0
EG11558	CAIC_ECOLI	caiC	Crotonobetain/carnitine-CoA ligase	CYT		59	0	3	0
EG13695	MACB_ECOLI	macB	ABC-type macrolide efflux transporter, with MacA and TolC	CYT		71	0	3	0
EG12599	YJJW_ECOLI	yjjW	Putative YjjI activase, function unknown	CYT		31	0	3	0
EG10407	SYE_ECOLI	gltX	Glutamate--tRNA ligase	CYT	X	54	0	3	0
EG11481	TATD_ECOLI	tatD	Mg-dependent cytoplasmic DNase	CYT		29	0	3	0
EG10979	ODO1_ECOLI	sucA	2-oxoglutarate dehydrogenase, E1 component	CYT	XX	105	0	3	2
EG13484	YDJH_ECOLI	ydjH	Putative sugar kinase, function unknown	CYT		34	0	3	6

EG14044	YEDV_ECOLI	yedV	Probable histidine protein kinase sensor, function unknown	TMH		51	0	2	3
EG10018	CSRD_ECOLI	csrD	Targets csrB/C sRNAs for degradation by RNase E	TMH		73	0	2	0
EG11145	YFEA_ECOLI	yfeA	Putative c-di-GMP dual activity enzyme, function unknown	TMH		84	0	2	0
EG12256	YHJK_ECOLI	yhjK	Putative c-di-GMP dual activity enzyme, function unknown	TMH		73	0	2	0
EG11660	YEDE_ECOLI	yedE	Function unknown	TMH		44	0	2	0
EG10012	CYDC_ECOLI	cydC	Cysteine exporter CydDC	TMH		63	0	2	0
EG14075	YEIU_ECOLI	lpxT	Lipid A 1-diphosphate synthase	TMH		27	0	2	0
EG13987	YNIB_ECOLI	yniB	Function unknown	TMH		20	0	2	2
EG10344	FTSW_ECOLI	ftsW	Stabilizes FtsZ ring, membrane protein	TMH		46	0	2	0
EG13500	YEAN_ECOLI	yeaN	Putative transporter, function unknown	TMH		41	0	2	0
EG11753	CHAA_ECOLI	chaA	Ca2+/H+ and K+/H+ antiporter	TMH		39	0	2	0
EG11720	MDTL_ECOLI	mdtL	Multidrug resistance efflux protein	TMH		41	0	2	0
EG10476	HYCC_ECOLI	hycC	Formate hydrogenlyase complex inner membrane protein	TMH		64	0	2	0
EG12563	GNTP_ECOLI	gntP	Fructuronate and gluconate transporter	TMH		47	0	2	0
EG12625	DPPB_ECOLI	dppB	Dipeptide/heme transport, permease	TMH		37	0	2	0
EG13248	YBAT_ECOLI	ybaT	Mutant inhibits reduction of selenate, function unknown	TMH		46	0	2	0
EG13342	MMUP_ECOLI	mmuP	S-methylmethionine permease, CP4-6 putative prophage remnan	TMH		51	0	2	0
EG13665	YBHI_ECOLI	ybhI	Putative transporter, function unknown	TMH		51	0	2	0
EG14019	YEBQ_ECOLI	yebQ	Putative transporter, function unknown	TMH		48	0	2	0
EG13608	YAIW_ECOLI	yaiW	Required for swarming phenotype, probable lipoprotein	SpII		40	0	2	2
EG12258	GUN_ECOLI	bcsZ	Endo-1,4-D-glucanase	SpII		42	0	2	2
EG12875	YBHC_ECOLI	ybhC	Acyl-CoA thioesterase, verified lipoprotein	SpII		46	0	2	0
EG13687	AMID_ECOLI	amiD	1,6-anhydro-N-acetylmuramyl-L-alanine amidase, Zn-dependent	SpII		31	0	2	0

EG14007	YNJE_ECOLI	ynjE	Rhodanese-like protein, function unknown	SpI		48	0	2	0
EG20173	PTA_ECOLI	pta	Phosphotransacetylase. produces acetyl phosphate	SpI	XX	77	0	2	0
EG12969	YCIQ_ECOLI	yciQ	Function unknown	SpI		71	0	2	0
EG12334	BTUF_ECOLI	btuF	B12 uptake, ABC transporter periplasmic binding protein	SpI		29	0	2	0
EG13496	YEAJ_ECOLI	yeaJ	Probable diguanylate cyclase, function unknown	SpI		57	0	2	0
EG13635	LYSD_ECOLI	arrD	Phage lambda lysozyme R protein homolog, DLP12 prophage	SpI		18	0	2	0
EG13324	YBIS_ECOLI	ybiS	L,D-transpeptidase linking Lpp to murein, periplasmic	SpI		33	0	2	0
EG10674	OPPA_ECOLI	oppA	Oligopeptide transport, periplasmic oligopeptide binding protein	SpI	X	61	0	2	0
EG11227	FDNG_ECOLI	fdnG	Formate dehydrogenase-N, selenopeptide, anaerobic	SpI		113	0	2	2
EG12075	NIKA_ECOLI	nikA	Nickel-binding, heme-binding periplasmic protein	SpI		59	0	2	0
EG10306	FHUE_ECOLI	fhuE	Outer membrane receptor for ferric-rhodotorulic acid	SpI		81	0	2	0
EG13809	LSRB_ECOLI	lsrB	Autoinducer-2 (AI-2) uptake	SpI	XX	37	0	2	0
EG12676	BAMA_ECOLI	bamA	Outer membrane protein assembly factor, forms pores	SpI		91	0	2	0
EG13177	RSEB_ECOLI	rseB	Binds periplasmic domain of anti-RpoE sigma factor RseA	SpI		36	0	2	0
EG10232	DMSA_ECOLI	dmsA	DMSO reductase subunit A, anaerobic, periplasmic	SpI		90	0	2	0
EG11047	UGPB_ECOLI	ugpB	sn-Glycerol-3-phosphate transport system, periplasmic binding protein	SpI		48	0	2	0
EG11373	MLTF_ECOLI	mltF	Membrane-bound lytic transglycosylase F, murein hydrolase	SpI		58	0	2	0
EG13312	YBGP_ECOLI	ybgP	Putative periplasmic pilus chaperone, function unknown	SpI		27	0	2	0
EG10738	PA1_ECOLI	pldA	Outer-membrane phospholipase A	SpI		33	0	2	0
EG10155	CIRA_ECOLI	cirA	Colicin I receptor production	SpI		74	0	2	0
EG10895	RPOC_ECOLI	rpoC	rpoC RNA polymerase, beta' subunit	CYT	XX	155	0	2	0
EG11063	UVRC_ECOLI	uvrC	Excision nuclease subunit C	CYT	X	68	0	2	0
EG10605	PBPB_ECOLI	mrcB	Murein polymerase, PBP1B	CYT		94	0	2	0

EG10161	MANC_ECOLI	cpsB	Colanic acid (CPS) biosynthesis	CYT		53	0	2	0
EG12583	YJIV_ECOLI	yjiV	Pseudogene reconstruction, helicase-like, C-terminal fragment	CYT		112	0	2	2
EG10756	CAPP_ECOLI	ppc	Phosphoenolpyruvate carboxylase	CYT	X	99	0	2	0
EG10848	RHSC_ECOLI	rhsC	Function unknown, encoded within RhsC repeat	CYT		158	0	2	0
EG13493	YEAG_ECOLI	yeaG	Protein kinase, function unknown	CYT	X	74	0	2	4
EG13079	BGLA_ECOLI	bglA	Phospho-beta-glucosidase A	CYT	X	55	0	2	0
EG10795	PUR9_ECOLI	purH	Phosphoribosylaminoimidazolecarboxamide formyltransferase	CYT	X	57	0	2	0
EG10034	SYA_ECOLI	alaS	Alanine--tRNA ligase	CYT	XX	96	0	2	0
EG10866	RL3_ECOLI	rplC	50S ribosomal subunit protein L3	CYT	X	22	0	2	0
EG14011	YNJI_ECOLI	ynjI	Function unknown	CYT	X	40	0	2	0
EG10042	AMPE_ECOLI	ampE	Ampicillin resistance	CYT		32	0	2	0
EG10213	DDLA_ECOLI	ddlA	D-alanine:D-alanine ligase A, ADP-forming	CYT	X	39	0	2	0
EG10690	PCNB_ECOLI	pcnB	Poly(A) polymerase	CYT	X	54	0	2	0
EG10797	PUR4_ECOLI	purL	Phosphoribosylformylglycinamide synthase	CYT	X	141	0	2	2
EG10004	COABC_ECOLI	dfp	Coenzyme A biosynthesis, bifunctional enzyme	CYT		43	0	2	4
EG11929	ZUR_ECOLI	zur	Repressor for znuABC, the zinc high-affinity transport genes	CYT		19	0	2	0
EG10562	MALT_ECOLI	malT	ATP-dependent transcriptional activator for the mal regulon	CYT		103	0	2	0
EG11870	YIIM_ECOLI	yiiM	6-N-hydroxylaminopurine resistance, function unknown	CYT	X	25	0	2	0
EG10061	ARCA_ECOLI	arcA	Response regulator, represses aerobic genes anaerobically	CYT	X	27	0	2	0
EG11983	WBBI_ECOLI	wbbI	d-Galf:alpha-d-Glc beta-1,6-galactofuranosyltransferase	CYT	X	38	0	2	0
EG14219	HYFR_ECOLI	hyfR	Formate-sensing regulator for hyf operon	CYT		75	0	2	0
EG10841	FLID_ECOLI	fliD	Hook-associated protein 2, axial family	CYT		48	0	2	2
EG12531	YJGL_ECOLI	yjgL	Function unknown	CYT		70	0	2	3

EG11768	SELU_ECOLI	selU	tRNA 2-selenouridine synthase, selenophosphate-dependent	CYT		41	0	2	0
EG10923	RUVA_ECOLI	ruvA	Holliday junction recognition factor, recruits RuvB	CYT		22	0	2	0
EG11746	PANC_ECOLI	panC	Pantothenate synthase, dimeric	CYT	XX	32	0	2	0
EG12079	NIKE_ECOLI	nikE	Nickel transport ATP-binding protein	CYT		30	0	2	2
EG20080	MASZ_ECOLI	glcB	Malate synthase G	CYT	XX	80	0	2	3
EG10192	CYSK_ECOLI	cysK	Cysteine synthase A, O-acetylserine sulfhydrylase A	CYT	XX	34	0	2	0
EG10196	SYC_ECOLI	cysS	Cysteine--tRNA ligase	CYT	X	52	0	2	0
EG10080	AROH_ECOLI	aroH	3-deoxy-D-arabino-heptulosonate-7-phosphate (DAHP) synthase	CYT		39	0	2	0
EG10431	HEMH_ECOLI	hemH	Ferrochelatase	CYT		36	0	2	0
EG11025	TRPB_ECOLI	trpB	Tryptophan synthase, beta subunit	CYT		43	0	2	0
EG10550	AK3_ECOLI	lysC	Aspartokinase III	CYT		49	0	2	0
EG14228	YQIG_ECOLI	yqiG	Pseudogene reconstruction, FimD family, interrupted by IS2I	CYT		92	0	2	0
EG11609	EVGA_ECOLI	evgA	Response regulator for acid and drug resistance, cognate to EvgS	CYT		23	0	2	0
EG10372	DHE4_ECOLI	gdhA	Glutamate dehydrogenase	CYT	X	49	0	2	0
EG10458	T1MK_ECOLI	hsdM	DNA methyltransferase M, host modification of foreign DNA	CYT		59	0	2	0
EG10221	DEOC_ECOLI	deoC	2-deoxy-D-ribose 5-phosphate aldolase (DERA)	CYT	X	28	0	2	0
EG13262	YBBO_ECOLI	ybbO	Function unknown	CYT		29	0	2	0
EG11427	TKT1_ECOLI	tktA	Transketolase A	CYT	XX	72	0	2	0
EG10552	SYK1_ECOLI	lysS	Lysine--tRNA ligase, constitutive	CYT	XX	58	0	2	0
EG12105	YEIE_ECOLI	yeiE	Probable positive regulator of lysP transcription	CYT		33	0	2	0
EG14339	YIFN_ECOLI	yifN	Pseudogene reconstruction	CYT		17	0	2	0
EG13150	YAFM_ECOLI	yafM	Function unknown	CYT		20	0	2	0
EG10265	LPXC_ECOLI	lpxC	Lipid A synthesis, UDP-3-O-(R-3-hydroxymyristoyl)-N-acetylglucosamine deacetylase	CYT		34	0	2	0
EG12522	GARD_ECOLI	garD	D-galactarate dehydratase	CYT		56	0	2	0
EG13405	YECM_ECOLI	yecM	Function unknown, low abundance protein	CYT		21	0	2	0

EG11913	YIJO_ECOLI	yijO	AraC family transcriptional activator, function unknown	CYT		32	0	2	0
EG14226	YPJD_ECOLI	ypjD	Function unknown	CYT		29	0	2	0
EG50009	DCEA_ECOLI	gadA	Glutamate decarboxylase A	CYT	XX	53	0	2	0
EG20050	DGOD_ECOLI	dgoD	Galactonate dehydratase	CYT		43	0	2	0
EG11663	SLYD_ECOLI	slyD	FKBP-type peptidyl-prolyl cis-trans isomerase	CYT		21	0	2	0
EG13005	YGHU_ECOLI	yghU	Function unknown, glutathione S-transferase homolog	CYT	X	32	0	2	0
EG10013	MEPM_ECOLI	yebA	Putative metalloprotease, function unknown	CYT		49	0	2	0
EG10818	RBSK_ECOLI	rbsK	Ribokinase	CYT		32	0	2	0
EG11839	YIHM_ECOLI	yihM	Function unknown	CYT		37	0	2	0
EG11922	YJBD_ECOLI	pagB	Salmonella ortholog regulated by PhoP	CYT		11	0	2	0
EG12886	GSPG_ECOLI	gspG	Pseudopilin in H-NS-silenced gsp divergon, type II secreton	CYT		16	0	2	0
EG13997	ASTD_ECOLI	astD	Succinylglutamic semialdehyde dehydrogenase, NAD-dependent	CYT		53	0	2	0
EG13998	ASTA_ECOLI	astA	Probable arginine succinyltransferase, arginine catabolism	CYT	X	38	0	2	0
EG10423	GYRA_ECOLI	gyrA	DNA gyrase, subunit A	CYT	X	97	0	2	0
EG13226	FTSK_ECOLI	ftsK	DNA translocase at septal ring sorting daughter chromsomes	TMH		147	0	2	5
EG14161	MURR_ECOLI	murR	Repressor for murPQ, MurNAc 6-P inducible	CYT		31	0	2	0

APPENDIX 4. Proteins identified from *Salmonella typhimurium* after alk-14 labeling in LB media. Only proteins that were identified with 2 unique peptides, and 10 fold enrichment in at least one alk-14 sample as compared to the DMSO control are shown. Proteins previously identified as acetylated in Wang et al 2010 are indicated. Predicted lipoproteins are highlighted in yellow.

						Expt. 1		Expt. 2		Expt. 3	
Uniprot Accession	**Gene Name**	**LipoP**	**Acetyl-ation**	**Description**	**MW (kDa)**	**alk-14**	**DMSO**	**alk-14**	**DMSO**	**alk-14**	**DMSO**
D0ZIM1_SALT1	tuf_1	CYT		Elongation factor Tu	43	334	17	431	55	1102	55
D0ZTJ5_SALT1	ompA	SpI		Outer membrane protein A	38	325	6	266	22	35	7
D0ZQG7_SALT1	pal	SpII		Peptidoglycan-associated outer membrane lipoprotein	19	224	2	162	5	56	0
D0ZWQ1_SALT1	lpp	SpII		Murein lipoprotein	8	162	11	69	7	55	0
D0ZW45_SALT1	osmE	SpII		DNA-binding transcriptional activator OsmE	12	128	0	111	0	15	0
D0ZMZ4_SALT1	tsx	SpI		Nucleoside channel	37	119	0	121	5	0	0
D0ZNV0_SALT1	udp	CYT		Uridine phosphorylase	27	118	0	148	14	36	0
D0ZPK7_SALT1	ompC	SpI		Outer membrane porin protein C	41	111	6	148	25	872	45
D0ZN53_SALT1	ybaY	SpII		Putative uncharacterized protein ybaY	19	107	0	90	0	9	0
D0ZIM2_SALT1	fusA	CYT	X	Elongation factor G	78	89	0	134	8	83	0
D0ZIK3_SALT1	rplE	CYT		50S ribosomal protein L5	20	80	0	104	2	215	0
D0ZIC9_SALT1	mdh	SpI	X	Malate dehydrogenase	32	73	0	97	6	168	9
D0ZIK9_SALT1	rpsC	CYT	X	30S ribosomal protein S3	26	73	0	62	3	5	5
D0ZWX1_SALT1	slyB	SpII		Putative outer membrane lipoprotein	16	70	0	46	6	119	0
D0ZQV4_SALT1	rpoB	CYT		DNA-directed RNA polymerase subunit beta	151	68	0	87	0	10	2
D0ZXQ1_SALT1	ompD	SpI	X	Putative outer membrane porin	40	67	2	77	11	444	12
D0ZL00_SALT1	metQ	SpII		DL-methionine transporter substrate-binding subunit	29	67	0	69	0	14	0
D0ZJZ6_SALT1	acnB	CYT		Bifunctional aconitate hydratase 2	94	60	0	106	3	35	0
D0ZQF3_SALT1	sucC	CYT	X	Succinyl-CoA ligase [ADP-forming] subunit beta	41	59	7	79	7	124	10

D0ZRF0_SALT1	dps	CYT		DNA starvation/stationary phase protection protein	19	59	0	63	8	6	0
D0ZR81_SALT1	gpmA	CYT		2,3-bisphosphoglycerate-dependent phosphoglycerate-dependent phosphoglycerate mutase	28	56	2	53	0	0	0
D0ZJ71_SALT1		CYT		Putative glutamic dehyrogenase-like protein	48	56	0	44	0	38	0
D0ZJM1_SALT1		SpII		Putative uncharacterized protein	20	54	0	49	0	0	0
D0ZIX6_SALT1	acnA	CYT		Aconitate hydratase	98	53	0	79	2	17	0
D0ZW18_SALT1	gapA	CYT	X	Glyceraldehyde-3-phosphate dehydrogenase	36	51	0	45	5	231	10
D0ZRF5_SALT1	ompX	SpI		Outer membrane protein X	18	50	0	58	5	10	0
D0ZVT3_SALT1	ygdI	SpII		Putative lipoprotein	8	47	0	33	0	18	0
D0ZN75_SALT1	htpG	CYT		Chaperone protein htpG	72	46	0	56	0	3	0
D0ZJZ0_SALT1	aceE	CYT		Pyruvate dehydrogenase E1 component	100	45	0	61	2	18	0
D0ZIJ3_SALT1	rpsM	CYT		30S ribosomal protein S13	13	45	0	41	0	54	3
D0ZJ17_SALT1	adhE	CYT		Bifunctional acetaldehyde-CoA/alcohol dehydrogenase	96	42	0	59	0	30	0
D0ZN63_SALT1	acrA	SpII		Acridine efflux pump	42	42	0	39	0	6	0
D0ZTR4_SALT1	clpB	CYT		Protein disaggregation chaperone	95	41	0	72	0	22	0
D0ZKE5_SALT1	uspA	CYT		Universal stress protein A	16	41	2	12	0	59	0
D0ZQV5_SALT1	rpoC	CYT		DNA-directed RNA polymerase subunit beta	155	39	2	54	0	5	0
D0ZKX1_SALT1	rpsB	CYT		30S ribosomal protein S2	27	39	0	48	3	94	4
D0ZNK2_SALT1	cdd	CYT		Cytidine deaminase	32	38	0	51	2	0	0
D0ZWH3_SALT1	pgk	CYT	X	Phosphoglycerate kinase	41	37	3	56	4	226	2
D0ZWH2_SALT1	fbaA	CYT		Fructose-bisphosphate aldolase	39	37	3	51	3	43	0
D0ZW35_SALT1	argD_1	CYT		Bifunctional succinylornithine transaminase	44	37	0	48	0	30	0
D0ZRQ2_SALT1	nlpB	SpII		Lipoprotein	37	36	0	23	0	0	0
D0ZIQ6_SALT1	talB	CYT		Transaldolase B	35	34	0	35	7	56	5

D0ZX61_SALT1	yghA	CYT		Oxidoreductase	31	33	0	25	2	126	10
D0ZQF1_SALT1	kgd	CYT		Alpha-ketoglutarate decarboxylase	105	32	0	55	2	15	0
D0ZUE5_SALT1	deoC	CYT		Deoxyribose-phosphate aldolase	28	32	0	36	0	0	0
D0ZSC1_SALT1	ybjP	SpII		Putative lipoprotein	19	32	0	22	0	6	0
D0ZQQ1_SALT1	fadL	SpI		Long-chain fatty acid outer membrane transport	48	30	0	44	2	0	0
D0ZI13_SALT1		SpII		Putative outer membrane lipoprotein	24	30	0	42	0	0	0
D0ZIJ0_SALT1	rpoA	CYT		DNA-directed RNA polymerase subunit alpha	37	29	2	38	3	50	0
D0ZQF0_SALT1	sdhB	CYT	X	Succinate dehydrogenase iron-sulfur subunit	27	29	0	36	0	67	0
D0ZXW2_SALT1	yraP	SpII		Putative uncharacterized protein yraP	20	29	0	28	0	0	0
D0ZQE5_SALT1	gltA	CYT	X	Citrate synthase	48	27	0	99	3	88	21
D0ZL91_SALT1	yedD	SpII		Putative uncharacterized protein yedD	15	26	0	31	0	0	0
D0ZIK8_SALT1	rplP	CYT	X	50S ribosomal protein L16	15	26	0	30	0	2	0
D0ZIJ1_SALT1	rpsD	CYT		30S ribosomal protein S4	23	26	0	29	0	67	0
D0ZQF4_SALT1	sucD	CYT		Succinyl-CoA ligase [ADP-forming] subunit alpha	30	26	0	26	4	61	0
D0ZW75_SALT1	rplT	CYT		50S ribosomal protein L20	13	26	0	26	0	0	0
D0ZNF4_SALT1	fbaB	CYT		Fructose-bisphosphate aldolase	38	26	0	23	2	40	0
D0ZW92_SALT1	pps	CYT		Phosphoenolpyruvate synthase	87	25	0	42	0	12	0
D0ZIZ8_SALT1	yciE	CYT		Putative cytoplasmic protein	19	23	2	24	0	619	197
D0ZJZ1_SALT1	aceF	CYT	X	Dihydrolipoamide acetyltransferase	66	22	0	45	0	20	0
D0ZQE9_SALT1	sdhA	CYT		Succinate dehydrogenase flavoprotein subunit	64	22	0	26	3	33	0
D0ZMT9_SALT1	atpF	CYT		ATP synthase subunit b	17	22	0	24	0	21	28
D0ZRN4_SALT1	talA	CYT	X	Transaldolase A	36	22	0	21	0	86	9
D0ZUE8_SALT1	deoD	CYT		Purine nucleoside phosphorylase deoD-type	26	22	0	21	2	21	0
D0ZSH5_SALT1	pflB	CYT		Pyruvate formate lyase I	85	21	0	42	0	21	41
D0ZPY0_SALT1	lsrF	CYT		Uncharacterized aldolase lsrF	32	21	0	33	0	31	0

D0ZW53_SALT1	katE	CYT		Catalase	84	20	0	51	0	7	0
D0ZIJ8_SALT1	rpsE	CYT		30S ribosomal protein S5	18	20	0	26	0	2	0
D0ZXP4_SALT1	adhP	CYT		Alcohol dehydrogenase	36	20	0	18	0	61	0
D0ZHY7_SALT1	traT	SpII	X	Conjugative transfer: surface exclusion	26	20	0	18	0	36	16
D0ZJ54_SALT1	prsA	CYT		Ribose-phosphate pyrophosphokinase	34	20	0	18	0	14	0
D0ZN29_SALT1	yajG	SpII		Putative uncharacterized protein yajG	21	20	0	14	0	0	0
D0ZPA7_SALT1	ahpC	CYT		Alkyl hydroperoxide reductase subunit C	21	20	0	13	0	41	0
D0ZXZ2_SALT1	hflB	SpI		ATP-dependent metalloprotease	71	19	0	12	0	0	0
D0ZSK4_SALT1	aspC	CYT		Aromatic amino acid aminotransferase	44	18	0	29	0	13	0
D0ZWF1_SALT1	gcvP	CYT		Glycine dehydrogenase [decarboxylating]	104	18	0	22	0	11	0
D0ZQV2_SALT1	rplJ	CYT		50S ribosomal protein L10	18	18	0	19	0	96	0
D0ZK07_SALT1	minD	CYT		Cell division inhibitor MinD	30	18	0	19	0	13	0
D0ZQV0_SALT1	rplK	CYT	X	50S ribosomal protein L11	15	17	0	31	0	103	0
D0ZWI1_SALT1	tktA	CYT		Transketolase	72	17	0	23	2	3	0
D0ZMY7_SALT1	yajC	TMH		Preprotein translocase subunit YajC	12	17	0	17	0	0	0
D0ZTR7_SALT1	yfiO	SpII		Outer membrane protein assembly complex subunit	28	17	0	16	0	0	0
D0ZIL2_SALT1	rplB	CYT	X	50S ribosomal protein L2	30	17	0	14	0	5	0
D0ZR97_SALT1	ybhC	SpII		Putative pectinesterase	46	17	0	9	0	0	0
D0ZNW5_SALT1	fadB	CYT		Multifunctional fatty acid oxidation complex subunit	85	16	0	29	0	0	0
D0ZIK0_SALT1	rplF	CYT		50S ribosomal protein L6	19	16	2	15	0	138	6
D0ZMT6_SALT1	atpG	CYT		ATP synthase gamma chain	32	16	0	14	0	5	0
D0ZIZ7_SALT1	yciF	CYT		Putative cytoplasmic protein	19	16	0	10	0	400	8
D0ZWV7_SALT1	sodB	CYT	X	Superoxide dismutase	21	16	0	10	0	19	0
D0ZVP5_SALT1	eno	CYT	X	Enolase	46	15	5	59	6	241	5
D0ZWF3_SALT1	gcvT	CYT		Aminomethyltransferase	40	15	0	15	0	12	0
D0ZY43_SALT1	sspA	CYT		Stringent starvation protein A	24	15	0	10	0	24	0

D0ZIL5_SALT1	rplC	CYT	X	50S ribosomal protein L3	22	15	0	8	0	38	0
D0ZN37_SALT1	lon	CYT		ATP-dependent protease	87	14	0	26	2	8	8
D0ZRZ7_SALT1	acs	CYT	X	Acetyl-CoA synthetase	72	14	0	24	0	39	4
D0ZQT7_SALT1	cysK	CYT		Cysteine synthase	35	14	0	21	0	88	0
D0ZIK5_SALT1	rplN	CYT	X	50S ribosomal protein L14	14	14	0	17	2	22	0
D0ZII9_SALT1	rplQ	CYT		50S ribosomal protein L17	14	14	0	16	0	61	0
D0ZQ59_SALT1	lptE	SpII		LPS-assembly lipoprotein RplB	21	14	0	16	0	0	0
D0ZKR3_SALT1	yibF	CYT		Glutathione S-transferase	23	14	0	15	0	35	0
D0ZUP2_SALT1	fabG	CYT		3-ketoacyl-(Acyl-carrier-protein) reductase	26	14	0	13	2	44	0
D0ZRU1_SALT1	yfgL	SpII		Outer membrane protein assembly complex subunit	42	14	0	13	0	3	0
D0ZKZ9_SALT1	rcsF	SpII		Outer membrane lipoprotein	14	14	0	13	0	0	0
D0ZI65_SALT1	ynaF	CYT		Putative universal stress protein	16	14	0	11	0	62	0
D0ZMY2_SALT1		CYT		Putative thiol-alkyl hydroperoxide reductase	22	13	2	30	2	109	0
D0ZW11_SALT1	yeaG	CYT		Putative serine protein kinase	74	13	0	25	0	24	0
D0ZUV1_SALT1	alaS	CYT		Alanyl-tRNA synthetase	96	13	0	19	0	0	0
D0ZK25_SALT1	manX	CYT		Mannose-specific enzyme IIAB	35	13	0	15	0	0	0
D0ZKW6_SALT1	yaeH	CYT	X	UPF0325 protein yaeH	15	13	0	9	0	226	0
D0ZY47_SALT1	rplM	CYT		50S ribosomal protein L13	16	13	0	9	2	0	0
D0ZJD2_SALT1	ompR	CYT		Osmolarity response regulator	27	13	0	8	0	28	0
D0ZUE7_SALT1	deoB	CYT		Phosphopentomutase	44	12	0	25	0	17	0
D0ZP31_SALT1	ppiB	CYT		Peptidyl-prolyl cis-trans isomerase	18	12	0	10	0	26	0
D0ZIB8_SALT1	fabI	CYT		Enoyl-(Acyl carrier protein) reductase	28	12	0	9	0	6	0
D0ZW77_SALT1	pheS	CYT		Phenylalanyl-tRNA synthetase subunit alpha	37	12	0	7	0	0	0
D0ZS62_SALT1	groL	CYT		60 kDa chaperonin	57	11	24	157	62	642	11
D0ZIP4_SALT1	crp	CYT		cAMP-regulatory protein	24	11	0	24	0	64	0
D0ZRU8_SALT1	ndk	CYT		Nucleoside diphosphate kinase	16	11	0	21	0	76	0

D0ZKE8_SALT1	prlC	CYT		Oligopeptidase A	77	11	0	18	0	4	0
D0ZVA9_SALT1		CYT		Putative uncharacterized protein	40	11	0	15	0	0	0
D0ZJ50_SALT1	lolB	SpII		Outer membrane lipoprotein LolB	24	11	0	13	0	0	6
D0ZIL4_SALT1	rplD	CYT	X	50S ribosomal protein L4	22	11	0	13	0	0	0
D0ZT10_SALT1	hflC	CYT		FtsH protease regulator HflC	38	11	0	9	0	0	0
D0ZRN2_SALT1	maeB	CYT		Malic enzyme	82	10	0	22	0	17	0
D0ZTI0_SALT1	pepN	CYT		Aminopeptidase N	104	10	0	16	0	0	0
D0ZLX7_SALT1	gmhA	CYT		Phosphoheptose isomerase	21	10	0	15	0	7	0
D0ZLJ2_SALT1	kbl	CYT		2-amino-3-ketobutyrate coenzyme A ligase	43	10	0	15	0	7	0
D0ZQH3_SALT1	nuoG	CYT		NADH-quinone oxidoreductase	100	10	0	12	0	3	0
D0ZT42_SALT1	rpsR	CYT		30S ribosomal protein S18	9	10	0	10	0	35	0
D0ZUV5_SALT1	recA	CYT		Protein recA	38	10	0	7	0	5	0
D0ZN27_SALT1	cyoA	TMH		Cytochrome o ubiquinol oxidase subunit II	35	10	0	6	0	5	0
D0ZVH8_SALT1	pagC	SpI		Virulence membrane protein PAGC	20	10	0	6	0	0	0
D0ZTQ2_SALT1	wraB	CYT		TrpR binding protein WrbA	21	9	0	23	0	0	0
D0ZKL9_SALT1	yiaF	SpII		Putative outer membrane lipoprotein	26	9	0	15	0	8	0
D0ZWX7_SALT1	gst	CYT		Glutathionine S-transferase	22	9	0	14	0	23	0
D0ZI76_SALT1	ydaA	CYT		Universal stress protein UspE	36	9	0	11	0	3	0
D0ZX70_SALT1	dkgA	CYT		2,5-diketo-D-gluconate reductase A	31	9	0	11	0	2	0
D0ZSK6_SALT1	ompF	SpI		Outer membrane protein F	40	9	0	10	0	28	0
D0ZT67_SALT1	fbp	CYT	X	Fructose-1,6-bisphosphatase class 1	37	9	0	10	0	12	0
D0ZU91_SALT1		CYT		Putative NAD-dependent aldehyde dehydrogenase	50	8	0	69	5	158	5
D0ZUE6_SALT1	deoA	CYT	X	Thymidine phosphorylase	51	8	0	29	0	0	0
D0ZXX7_SALT1	pnp	CYT		Polyribonucleotide nucleotidyltransferase	77	8	0	17	0	2	0
D0ZJW7_SALT1	ftsZ	CYT		Cell division protein ftsZ	40	8	0	14	0	0	0
D0ZTS8_SALT1	rplS	CYT		50S ribosomal protein L19	13	8	0	14	0	0	0

D0ZR60_SALT1	qor	CYT		Quinone oxidoreductase, NADPH-dependent	35	8	0	13	0	2	0
D0ZPY3_SALT1	tpiA	CYT	X	Triosephosphate isomerase	27	8	0	12	0	88	0
D0ZKM7_SALT1	glyS	CYT		Glycyl-tRNA synthetase beta subunit	76	8	0	12	0	10	0
D0ZUK9_SALT1	grxB	CYT		Glutaredoxin 2	24	8	0	10	0	6	0
D0ZKL6_SALT1	yiaD	SpII		Putative outer membrane lipoprotein	22	8	0	10	0	0	0
D0ZQV3_SALT1	rplL	CYT		50S ribosomal protein L7/L12	12	8	0	10	0	0	0
D0ZIR2_SALT1	dnaK	CYT		Chaperone protein dnaK	69	8	0	7	3	66	0
D0ZTB4_SALT1	yjgF	CYT		Putative translation initiation inhibitor yjgF	14	8	3	7	4	38	0
D0ZV97_SALT1	icdA	CYT		Isocitrate dehydrogenase [NADP]	46	7	0	88	2	84	2
D0ZT09_SALT1	hflK	CYT		FtsH protease regulator HflK	46	7	0	21	0	0	0
D0ZL47_SALT1	cheA	CYT		Chemotaxis protein CheA	73	7	0	15	0	4	0
D0ZKX2_SALT1	tsf	CYT		Elongation factor Ts	30	7	0	12	3	14	0
D0ZW36_SALT1	astA	CYT		Arginine succinyltransferase	38	7	0	6	0	14	0
D0ZQN6_SALT1	fabB	CYT		3-oxoacyl-(Acyl carrier protein) synthase I	42	6	0	23	0	19	0
D0ZKR8_SALT1	yadF	CYT		Carbonic anhydrase	25	6	0	13	0	7	0
D0ZS90_SALT1	dacC	SpI		D-alanyl-D-alanine carboxypeptidase fraction C	44	6	0	12	0	5	6
D0ZXC6_SALT1	rpoD	CYT	X	RNA polymerase sigma factor	76	6	0	12	0	0	0
D0ZRN5_SALT1	tktB	CYT		Transketolase	73	6	0	11	0	7	0
D0ZSI1_SALT1	serC	CYT		Phosphoserine aminotransferase	40	6	0	10	0	4	0
D0ZQ92_SALT1	nagB	CYT		Glucosamine-6-phosphate deaminase	30	6	0	6	0	12	0
D0ZXS7_SALT1	yncB	CYT		Putative NADP-dependent oxidoreductase	39	6	0	6	0	12	0
D0ZQJ2_SALT1	pta	CYT		Phosphate acetyltransferase	77	5	0	15	0	9	0
D0ZNW4_SALT1	fadA	CYT		3-ketoacyl-CoA thiolase	41	5	0	12	0	10	0
D0ZKY0_SALT1	bamA	SpI		Outer membrane protein assembly factor YaeT	90	5	0	11	0	0	0

D0ZLJ3_SALT1	rfaD	CYT		ADP-L-glycero-D-mannoheptose-6-epimerase	35	5	0	11	0	0	0
D0ZY46_SALT1	rpsI	CYT		30S ribosomal protein S9	15	5	0	10	0	0	0
D0ZUS6_SALT1	ygaM	CYT		Putative uncharacterized protein ygaM	12	5	0	8	0	72	0
D0ZV78_SALT1	arcA	CYT		Two-component response regulator	27	5	0	8	0	10	0
D0ZI95_SALT1	tpx	CYT		Thiol peroxidase	18	5	2	5	0	80	0
D0ZIK1_SALT1	rpsH	CYT		30S ribosomal protein S8	14	5	0	5	0	51	0
D0ZSI6_SALT1	rpsA	CYT		30S ribosomal protein S1	61	5	0	5	2	18	0
D0ZXC4_SALT1	rpsU	CYT		30S ribosomal protein S21	9	5	0	2	0	13	0
D0ZQF2_SALT1	sucB	CYT		Dihydrolipoamide acetyltransferase	44	4	0	43	0	4	0
D0ZJ20_SALT1	hns	CYT	X	Global DNA-binding transcriptional dual regulator	16	4	0	12	2	180	0
D0ZIM3_SALT1	rpsG	CYT		30S ribosomal protein S7	18	4	0	10	0	0	0
D0ZRQ1_SALT1	purC	CYT		Phosphoribosylaminoimidazole-succinocarboxamide synthase	27	4	0	9	0	21	0
D0ZWV9_SALT1	ydhD	CYT		Putative uncharacterized protein ydhD	13	4	0	6	0	39	0
D0ZIK2_SALT1	rpsN	CYT		30S ribosomal subunit protein S14	11	4	0	6	0	26	0
D0ZUB5_SALT1		CYT		Putative glucosamine-fructose-6-phosphate aminotransferase	39	4	0	5	0	10	0
D0ZQH7_SALT1	nuoB	CYT		NADH dehydrogenase subunit B	25	4	0	0	0	10	0
D0ZMT5_SALT1	atpD	CYT		ATP synthase subunit beta	50	3	0	134	4	132	0
D0ZSP0_SALT1	glyA	CYT		Serine hydroxymethyltransferase	45	3	0	23	0	56	0
D0ZJ22_SALT1	galU	CYT		UTP--glucose-1-phosphate uridylyltransferase subunit	33	3	0	6	0	13	0
D0ZW43_SALT1	nadE	CYT		NH(3)-dependent NAD(+) synthetase	30	3	0	5	0	19	0
D0ZW73_SALT1	infC	CYT	X	Translation initiation factor IF-3	21	3	0	4	0	68	0
D0ZN77_SALT1	adk	CYT		Adenylate kinase	23	3	0	3	0	21	0
D0ZNJ0_SALT1	yohF	CYT		Acetoin dehydrogenase	27	3	0	2	0	14	0
D0ZUU5_SALT1	luxS	CYT	X	S-ribosylhomocysteine lyase	19	3	0	0	0	33	0
D0ZKB9_SALT1	aspS	CYT		Aspartyl-tRNA synthetase	66	2	0	15	0	0	0

D0ZRQ5_SALT1	bcp	CYT		Thioredoxin-dependent thiol peroxidase	18	2	0	2	0	30	0
D0ZMR9_SALT1	yieF	CYT		Putative oxidoreductase	20	2	0	0	0	12	0
D0ZQH5_SALT1	nuoE	CYT		NADH dehydrogenase subunit E	19	2	0	0	0	10	0
D0ZMT7_SALT1	atpA	CYT		ATP synthase subunit alpha	55	0	0	71	4	52	0
D0ZKQ9_SALT1	aldB	CYT		Aldehyde dehydrogenase B	56	0	0	56	3	54	5
D0ZMI7_SALT1	gnd	CYT		6-phosphogluconate dehydrogenase	51	0	0	40	0	29	0
D0ZJZ2_SALT1	lpdA	CYT		Dihydrolipoyl dehydrogenase	51	0	0	33	2	46	0
D0ZR32_SALT1	pgi	CYT	X	Glucose-6-phosphate isomerase	61	0	0	32	0	0	0
D0ZS57_SALT1	aspA	CYT		Aspartate ammonia-lyase	52	0	0	26	2	70	24
D0ZQY9_SALT1	aceA	CYT	X	Isocitrate lyase	48	0	0	26	0	56	0
D0ZMJ6_SALT1	rfbH	CYT		CDP-6-deoxy-D-xylo-4-hexulose-3-dehydrase	48	0	0	26	0	17	0
D0ZQB1_SALT1	pgm	CYT		Phosphoglucomutase	58	0	0	25	0	10	2
D0ZPY9_SALT1	glpK	CYT		Glycerol kinase	56	0	0	25	0	0	0
D0ZQH6_SALT1	nuoC	CYT		Bifunctional NADH:ubiquinone oxidoreductase subunit	69	0	0	24	0	0	0
D0ZV61_SALT1	yjjK	CYT		Putative ABC transporter ATP-binding protein	62	0	0	22	0	9	0
D0ZQU2_SALT1	ptsI	CYT		Phosphoenolpyruvate-protein phosphotransferase	63	0	0	22	0	8	0
D0ZSK8_SALT1	asnS	CYT		Asparaginyl-tRNA synthetase	53	0	0	21	0	6	0
D0ZJ14_SALT1	oppA	SpI		Oligopeptide transport protein	61	0	0	21	0	0	0
D0ZWD6_SALT1	lysS	CYT		Lysyl-tRNA synthetase	58	0	0	21	0	0	0
D0ZQY8_SALT1	aceB	CYT	X	Malate synthase	60	0	0	20	0	14	3
D0ZNP6_SALT1	rho	CYT		Transcription termination factor Rho	47	0	0	20	0	6	5
D0ZWZ8_SALT1	fumC	CYT	X	Fumarate hydratase	50	0	0	19	0	13	0
D0ZLY2_SALT1	pepD	CYT		Aminoacyl-histidine dipeptidase	52	0	0	17	0	6	3
D0ZU14_SALT1	gabD	CYT		Succinate-semialdehyde dehydrogenase I	52	0	0	16	0	19	0
D0ZW37_SALT1	astD	CYT		N-succinylglutamate 5-semialdehyde dehydrogenase	53	0	0	16	0	0	0

D0ZKZ7_SALT1	proS	CYT	X	Prolyl-tRNA synthetase	64	0	0	15	0	48	37
D0ZJ73_SALT1	treA	SpI		Trehalase	64	0	0	15	0	0	0
D0ZWZ4_SALT1	ydgA	SpI		Putative periplasmic protein	54	0	0	15	0	0	0
D0ZJ80_SALT1	dadA	SpI		D-amino acid dehydrogenase small subunit	48	0	0	13	13	13	0
D0ZL45_SALT1	cheM	CYT		Methyl accepting chemotaxis protein II	68	0	2	13	0	0	0
D0ZT13_SALT1	purA	CYT		Adenylosuccinate synthetase	47	0	0	12	0	11	0
D0ZKA0_SALT1	zwf	CYT		Glucose-6-phosphate 1-dehydrogenase	56	0	0	11	0	0	0
D0ZWG5_SALT1	rpiA	CYT		Ribose-5-phosphate isomerase A	23	0	0	10	0	47	0
D0ZWQ2_SALT1	pykF	CYT	X	Pyruvate kinase	51	0	0	8	0	22	0
D0ZIF4_SALT1	accC	CYT		Acetyl-CoA carboxylase biotin carboxylase subunit	49	0	0	6	0	34	0
D0ZIJ2_SALT1	rpsK	CYT		30S ribosomal protein S11	14	0	0	6	0	10	0
D0ZK97_SALT1	eda	CYT		Keto-hydroxyglutarate-aldolase/keto-deoxy-phosphogluconate aldolase	22	0	0	4	0	21	0
D0ZXN9_SALT1	osmC	CYT		Putative envelope protein	15	0	0	3	0	38	0
D0ZKX4_SALT1	frr	CYT	X	Ribosome-recycling factor	21	0	0	3	0	16	0
D0ZK08_SALT1	minE	CYT		Cell division topological specificity factor	10	0	0	2	0	21	0
D0ZRR3_SALT1	upp	CYT	X	Uracil phosphoribosyltransferase	23	0	0	0	0	42	0
D0ZJA6_SALT1	yhfL	SpII		Putative outer membrane lipoprotein	6	0	0	0	0	38	0
D0ZIZ9_SALT1		CYT		Putative catalase	32	0	0	0	0	30	0
D0ZLK0_SALT1	rfaJ	CYT		Lipopolysaccharide 1,2-glucosyltransferase	39	0	0	0	0	28	0
D0ZRR0_SALT1	yfgD	CYT		Putative arsenate reductase	13	0	0	0	0	20	0
D0ZN73_SALT1	ybaB	CYT		UPF0133 protein ybaB	12	0	0	0	0	20	0
D0ZS69_SALT1	efp	CYT		Elongation factor P	21	0	0	0	0	19	0
D0ZTK4_SALT1		CYT		Putative cytoplasmic protein	15	0	0	0	0	17	0
D0ZS77_SALT1	frdB	CYT		Fumarate reductase	27	0	0	0	0	14	0
D0ZWY4_SALT1	rsxC	CYT		Electron transport complex protein rnfC	79	0	0	0	0	13	0
D0ZK93_SALT1	yebE	CYT		Putative inner membrane protein	24	0	0	0	0	13	0

D0ZY25_SALT1	yhbL	CYT		Sigma cross-reacting protein 27A	23	0	0	0	0	12	0
D0ZXH9_SALT1	ydfG	CYT		NADP-dependent L-serine/L-allo-threonine dehydydrogenase	27	0	0	0	0	11	0
D0ZIN6_SALT1	yheS	CYT		Putative ATPase component of ABC transporter	72	0	0	0	0	11	0
D0ZT54_SALT1	cysQ	CYT		3'(2'),5'-bisphosphate nucleotidase cysQ	27	0	0	0	0	10	0
D0ZXW4_SALT1	yhbO	CYT		Putative intracellular proteinase	19	0	0	0	0	10	0

APPENDIX 5. Proteins identified from *Salmonella typhimurium* after alk-14 labeling in MgM+ media. Only proteins that were identified with 2 unique peptides, and 10 fold enrichment in at least one alk-14 sample as compared to the DMSO control are shown. Predicted lipoproteins are highlighted in yellow.

					Expt. 1		Expt. 2		Expt. 3	
Uniprot Accession	**Gene Name**	**Description**	**LipoP**	**MW (kDa)**	**alk-14**	**DMSO**	**alk-14**	**DMSO**	**alk-14**	**DMSO**
D0ZTJ5_SALT1	ompA	Outer membrane protein A	SpI	38	229	20	85	0	128	43
D0ZL00_SALT1	metQ	DL-methionine transporter substrate-binding subunit	SpII	29	202	0	6	0	399	0
D0ZW45_SALT1	osmE	DNA-binding transcriptional activator OsmE	SpII	12	188	0	14	0	69	0
D0ZQG7_SALT1	pal	Peptidoglycan-associated outer membrane lipoprotein	SpII	19	151	2	70	0	266	55
D0ZWQ1_SALT1	lpp	Murein lipoprotein	SpII	8	137	15	44	0	0	15
D0ZS62_SALT1	groL	60 chaperonin	CYT	57	108	31	218	5	675	404
D0ZN53_SALT1	ybaY	Putative uncharacterized protein ybaY	SpII	19	60	0	27	0	238	0
D0ZVT3_SALT1	ygdI	Putative lipoprotein	SpII	8	59	0	0	0	0	0
D0ZRF5_SALT1	ompX	Outer membrane protein X	SpI	18	58	4	36	0	28	29
D0ZL91_SALT1	yedD	Putative uncharacterized protein yedD	SpII	15	53	0	0	0	0	0
D0ZI13_SALT1		Putative outer membrane lipoprotein	SpII	24	48	0	0	0	37	0
D0ZWX1_SALT1	slyB	Putative outer membrane lipoprotein	SpII	16	47	0	22	0	0	9
D0ZJM1_SALT1		Putative inner membrane lipoprotein	SpII	20	46	0	4	0	53	0
D0ZPK7_SALT1	ompC	Outer membrane porin protein C	SpI	41	45	2	406	59	754	559
D0ZIM2_SALT1	fusA	Elongation factor G	CYT	78	45	0	54	0	245	105
D0ZW18_SALT1	gapA	Glyceraldehyde-3-phosphate dehydrogenase	CYT	36	44	4	124	2	316	138
D0ZSC1_SALT1	ybjP	Putative lipoprotein	SpII	19	44	0	4	0	39	0
D0ZTZ6_SALT1	iroN	Outer membrane receptor FepA	SpI	79	42	3	0	0	0	0
D0ZRQ2_SALT1	nlpB	Lipoprotein	SpII	37	41	0	25	0	116	0
D0ZUZ6_SALT1	sitA	Putative periplasmic binding protein	SpI	34	41	4	0	0	0	0

D0ZR81_SALT1	gpmA	2,3-bisphosphoglycerate-dependent phosphoglycerate-dependent phosphoglycerate mutase	CYT	28	38	0	2	0	0	0
D0ZIC9_SALT1	mdh	Malate dehydrogenase	SpI	32	33	6	43	4	193	138
D0ZNU5_SALT1	metE	5-methyltetrahydropteroyltriglutamate--homocysteine methyltransferase	CYT	85	33	0	0	0	0	0
D0ZJZ0_SALT1	aceE	Pyruvate dehydrogenase E1 component	CYT	100	30	0	76	2	316	164
D0ZHY7_SALT1	traT	Conjugative transfer: surface exclusion	SpII	26	28	0	60	0	262	0
D0ZTR7_SALT1	yfiO	Outer membrane protein assembly complex subunit	SpII	28	28	0	2	0	21	0
D0ZN63_SALT1	acrA	Acridine efflux pump	SpII	42	27	0	36	0	233	0
D0ZQV4_SALT1	rpoB	DNA-directed RNA polymerase subunit beta	CYT	151	27	2	4	0	102	50
D0ZIK9_SALT1	rpsC	30S ribosomal protein S3	CYT	26	26	0	0	0	10	0
D0ZIJ3_SALT1	rpsM	30S ribosomal protein S13	CYT	13	26	0	0	0	0	0
D0ZMT5_SALT1	atpD	ATP synthase subunit beta	CYT	50	25	0	39	0	232	30
D0ZXW2_SALT1	yraP	Putative uncharacterized protein yraP	SpII	20	25	0	9	0	39	0
D0ZN75_SALT1	htpG	Chaperone protein htpG	CYT	72	25	0	0	0	7	0
D0ZXQ1_SALT1	ompD	Putative outer membrane porin	SpI	40	24	2	43	2	651	430
D0ZQV5_SALT1	rpoC	DNA-directed RNA polymerase subunit beta	CYT	155	24	0	8	2	206	33
D0ZJZ1_SALT1	aceF	Dihydrolipoamide acetyltransferase	CYT	66	20	0	55	0	90	32
D0ZMI7_SALT1	gnd	6-phosphogluconate dehydrogenase	CYT	51	20	0	13	0	66	43
D0ZJ17_SALT1	adhE	Bifunctional acetaldehyde-CoA/alcohol dehydrogenase	CYT	96	19	0	84	0	283	96
D0ZQE5_SALT1	gltA	Citrate synthase	CYT	48	19	0	21	0	88	47
D0ZKX1_SALT1	rpsB	30S ribosomal protein S2	CYT	27	19	0	11	0	52	19
D0ZWH3_SALT1	pgk	Phosphoglycerate kinase	CYT	41	18	0	31	0	158	64
D0ZJN6_SALT1	carB	Carbamoyl phosphate synthase large subunit	CYT	118	18	0	7	3	35	16
D0ZTR4_SALT1	clpB	Protein disaggregation chaperone	CYT	95	17	0	35	0	152	50
D0ZSH5_SALT1	pflB	Pyruvate formate lyase I	CYT	85	16	0	49	0	197	155

D0ZRU1_SALT1	yfgL	Outer membrane protein assembly complex subunit	SpII	42	16	0	21	0	44	0
D0ZV97_SALT1	icdA	Isocitrate dehydrogenase [NADP]	CYT	46	16	2	17	0	150	48
D0ZIJ1_SALT1	rpsD	30S ribosomal protein S4	CYT	23	16	0	6	0	17	5
D0ZQV0_SALT1	rplK	50S ribosomal protein L11	CYT	15	15	0	8	0	0	0
D0ZR97_SALT1	ybhC	Putative pectinesterase	SpII	46	15	0	6	0	11	0
D0ZN29_SALT1	yajG	Putative uncharacterized protein yajG	SpII	21	15	0	0	0	16	0
D0ZQT7_SALT1	cysK	Cysteine synthase	CYT	35	14	0	49	0	71	39
D0ZMT7_SALT1	atpA	ATP synthase subunit alpha	CYT	55	14	0	31	0	181	91
D0ZIK3_SALT1	rplE	50S ribosomal protein L5	CYT	20	14	0	13	0	52	22
D0ZKZ9_SALT1	rcsF	Outer membrane lipoprotein	SpII	14	14	0	3	0	8	0
D0ZR32_SALT1	pgi	Glucose-6-phosphate isomerase	CYT	61	14	0	0	0	4	4
D0ZIR2_SALT1	dnaK	Chaperone protein dnaK	CYT	69	13	2	70	0	230	81
D0ZKE5_SALT1	uspA	Universal stress protein A	CYT	16	13	0	7	0	0	5
D0ZSK6_SALT1	ompF	Outer membrane protein F	SpI	40	13	0	0	0	3	9
D0ZSP0_SALT1	glyA	Serine hydroxymethyltransferase	CYT	45	12	0	30	6	91	43
D0ZJ80_SALT1	dadA	D-amino acid dehydrogenase small subunit	SpI	48	12	0	11	14	0	80
D0ZQF3_SALT1	sucC	Succinyl-CoA ligase [ADP-forming] subunit beta	CYT	41	12	0	3	0	156	116
D0ZWI3_SALT1	yggG	Putative Zn-dependent protease	SpII	27	12	0	0	0	0	0
D0ZJG1_SALT1	glpD	Glycerol-3-phosphate dehydrogenase	CYT	57	11	0	19	0	60	15
D0ZSK4_SALT1	aspC	Aromatic amino acid aminotransferase	CYT	44	11	0	10	0	40	30
D0ZQF4_SALT1	sucD	Succinyl-CoA ligase [ADP-forming] subunit alpha	CYT	30	11	0	7	0	45	6
D0ZXV9_SALT1	yraM	Putative transglycosylase	SpII	73	11	0	3	0	13	0
D0ZKL9_SALT1	yiaF	Putative outer membrane lipoprotein	SpII	26	11	0	0	0	28	0
D0ZVI8_SALT1		Putative outer membrane lipoprotein	SpII	11	11	0	0	0	0	0
D0ZMY7_SALT1	yajC	Preprotein translocase subunit YajC	TMH	12	11	0	0	0	0	0
D0ZSI6_SALT1	rpsA	30S ribosomal protein S1	CYT	61	10	0	35	0	125	11

D0ZIF3_SALT1	accB	Acetyl-CoA carboxylase biotin carboxyl carrier	CYT	17	10	6	22	0	58	81
D0ZPY9_SALT1	glpK	Glycerol kinase	CYT	56	10	0	16	0	113	56
D0ZWH2_SALT1	fba	Fructose-bisphosphate aldolase	CYT	39	10	2	16	0	82	43
D0ZIL5_SALT1	rplC	50S ribosomal protein L3	CYT	22	10	0	16	0	35	24
D0ZW92_SALT1	pps	Phosphoenolpyruvate synthase	CYT	87	10	0	11	0	20	7
D0ZQV1_SALT1	rplA	50S ribosomal protein L1	CYT	25	10	0	2	0	15	0
D0ZRN4_SALT1	talA	Transaldolase A	CYT	36	10	0	0	0	17	15
D0ZX99_SALT1	ygiB	Putative uncharacterized protein ygiB	SpI	23	9	0	13	0	22	0
D0ZWD6_SALT1	lysS	Lysyl-tRNA synthetase	CYT	58	7	0	3	0	8	0
D0ZUQ5_SALT1	ycfM	Putative outer membrane lipoprotein	SpII	23	7	0	0	0	20	0
D0ZXP4_SALT1	adhP	Alcohol dehydrogenase	CYT	36	6	0	28	0	58	14
D0ZRQ1_SALT1	purC	Phosphoribosylaminoimidazole-succinocarboxamide synthase	CYT	27	6	2	16	0	20	15
D0ZJZ2_SALT1	lpdA	Dihydrolipoyl dehydrogenase	CYT	51	6	0	14	0	134	55
D0ZPY3_SALT1	tpiA	Triosephosphate isomerase	CYT	27	6	0	12	0	19	29
D0ZMY2_SALT1		Putative thiol-alkyl hydroperoxide reductase	CYT	22	6	0	11	0	79	35
D0ZUV1_SALT1	alaS	Alanyl-tRNA synthetase	CYT	96	6	0	3	0	20	0
D0ZQ59_SALT1	lptE	LPS-assembly lipoprotein RplB	SpII	21	6	0	0	0	14	0
D0ZJ20_SALT1	hns	Global DNA-binding transcriptional dual regulator	CYT	16	5	0	18	0	0	6
D0ZW11_SALT1	yeaG	Putative serine protein kinase	CYT	74	5	0	16	0	12	8
D0ZQJ2_SALT1	pta	Phosphate acetyltransferase	CYT	77	5	0	11	0	35	10
D0ZUZ7_SALT1	sitB	Putative ATP-binding protein	CYT	30	4	0	18	0	0	0
D0ZXX7_SALT1	pnp	Polyribonucleotide nucleotidyltransferase	CYT	77	4	0	3	0	10	0
D0ZPA7_SALT1	ahpC	Alkyl hydroperoxide reductase subunit C	CYT	21	3	0	13	0	18	9
D0ZIB8_SALT1	fabI	Enoyl-(Acyl carrier protein) reductase	CYT	28	3	0	5	0	9	0
D0ZJZ6_SALT1	acnB	Bifunctional aconitate hydratase 2	CYT	94	3	0	0	0	73	4
D0ZSG4_SALT1	serS	Seryl-tRNA synthetase	CYT	49	3	0	0	0	15	0
D0ZJN5_SALT1	carA	Carbamoyl-phosphate synthase small chain	CYT	42	3	0	0	0	9	0

D0ZV78_SALT1	arcA	Two-component response regulator	CYT	27	3	0	0	0	6	0
D0ZQN6_SALT1	fabB	3-oxoacyl-(Acyl carrier protein) synthase I	CYT	42	2	0	12	0	44	15
D0ZT13_SALT1	purA	Adenylosuccinate synthetase	CYT	47	2	0	5	0	13	0
D0ZK14_SALT1	slp	Putative outer membrane protein	SpII	21	2	0	4	0	6	0
D0ZJ54_SALT1	prsA	Ribose-phosphate pyrophosphokinase	CYT	34	2	0	0	0	14	0
D0ZTQ2_SALT1		Flavoprotein wrbA	CYT	21	2	0	0	0	10	0
D0ZUE7_SALT1	deoB	Phosphopentomutase	CYT	44	2	0	0	0	10	0
D0ZNZ0_SALT1	glnA	Glutamine synthetase	CYT	52	0	0	34	3	69	25
D0ZW35_SALT1	argD	Acetylornithine/succinyldiaminopimelate aminotransferase	CYT	44	0	0	15	0	28	8
D0ZWC6_SALT1		Putative periplasmic protein	SpI	23	0	0	13	0	0	0
D0ZI53_SALT1	hrpA	ATP-dependent RNA helicase HrpA	CYT	146	0	5	12	0	0	0
D0ZJD2_SALT1	ompR	Osmolarity response regulator	CYT	27	0	0	10	0	6	0
D0ZNP6_SALT1	rho	Transcription termination factor Rho	CYT	47	0	0	8	0	13	0
D0ZMW7_SALT1	ilvE	Branched-chain amino acid aminotransferase	CYT	34	0	0	7	0	6	0
D0ZXY2_SALT1	infB	Translation initiation factor IF-2	CYT	97	0	0	5	0	25	0
D0ZUP3_SALT1	acpP	Acyl carrier protein	CYT	9	0	0	4	0	17	0
D0ZQ30_SALT1	ppc	Phosphoenolpyruvate carboxylase	CYT	99	0	0	4	0	14	0
D0ZUP4_SALT1	fabF	3-oxoacyl-(Acyl carrier protein) synthase II	SpI	43	0	0	4	0	14	0
D0ZUP2_SALT1	fabG	3-ketoacyl-(Acyl-carrier-protein) reductase	CYT	26	0	0	2	0	9	0
D0ZQH3_SALT1	nuoG	NADH-quinone oxidoreductase	CYT	100	0	0	0	0	50	0
D0ZUL5_SALT1	murJ	Virulence factor mviN	TMH	57	0	0	0	0	38	0
D0ZTL7_SALT1	sopB	Secreted effector protein	CYT	62	0	0	0	0	37	0
D0ZV19_SALT1	sipA	Secreted effector protein	CYT	74	0	0	0	0	36	0
D0ZKV8_SALT1	clcA	H(+)/Cl(-) exchange transporter clcA	CYT	50	0	0	0	0	26	0
D0ZK25_SALT1	manX	Mannose-specific enzyme IIAB	CYT	35	0	0	0	0	21	0
D0ZJ43_SALT1	kdsA	2-dehydro-3-deoxyphosphooctonate aldolase	CYT	31	0	0	0	0	21	0
D0ZV22_SALT1	sipB	Translocation machinery component	CYT	62	0	0	0	0	16	0
D0ZMZ4_SALT1	tsx	Nucleoside channel	SpI	37	0	0	0	0	16	0

D0ZRF0_SALT1	dps	DNA starvation/stationary phase protection pro	CYT	19	0	0	0	0	12	0
D0ZN27_SALT1	cyoA	Cytochrome o ubiquinol oxidase subunit II	TMH	35	0	0	0	0	9	0
D0ZSI9_SALT1	msbA	Lipid A export ATP-binding/permease protein	TMH	64	0	0	0	0	6	0
D0ZK23_SALT1	yoaE	Putative inner membrane protein	TMH	56	0	0	0	0	0	0

APPENDIX 6. Proteins identified from *Salmonella typhimurium* after alk-14 labeling in MgM media. Only proteins that were identified with 2 unique peptides, and 10 fold enrichment in at least one alk-14 sample as compared to the DMSO control are shown. Predicted lipoproteins are highlighted in yellow.

					Expt. 1		Expt. 2		Expt. 3	
Uniprot Accession	**Gene Name**	**Description**	**LipoP**	**MW (kDa)**	**alk-14**	**DMSO**	**alk-14**	**DMSO**	**alk-14**	**DMSO**
D0ZL00_SALT1	metQ	DL-methionine transporter substrate-binding subunit	SpII	29	219	0	58	0	251	0
D0ZTJ5_SALT1	ompA	Outer membrane protein A	SpI	38	203	17	64	0	102	14
D0ZWQ1_SALT1	lpp	Murein lipoprotein	SpII	8	182	15	35	11	58	11
D0ZW45_SALT1	osmE	DNA-binding transcriptional activator OsmE	SpII	12	150	0	45	0	173	0
D0ZQG7_SALT1	pal	Peptidoglycan-associated outer membrane lipoprotein	SpII	19	148	2	121	0	264	11
D0ZN53_SALT1	ybaY	Putative uncharacterized protein ybaY	SpII	19	128	0	150	0	270	0
D0ZPK7_SALT1	ompC	Outer membrane porin protein C	SpI	41	111	5	1234	62	893	420
D0ZRF5_SALT1	ompX	Outer membrane protein X	SpI	18	105	13	76	7	71	42
D0ZS62_SALT1	groL	60 kDa chaperonin	CYT	57	95	28	164	5	743	226
D0ZWX1_SALT1	slyB	Putative outer membrane lipoprotein	SpII	16	83	0	76	0	457	0
D0ZVT3_SALT1	ygdI	Putative lipoprotein	SpII	8	78	0	0	0	52	0
D0ZVP5_SALT1	eno	Enolase	CYT	46	63	14	43	3	340	90
D0ZJM1_SALT1		Putative inner membrane lipoprotein	SpII	20	56	0	37	0	76	0
D0ZI13_SALT1		Putative outer membrane lipoprotein	SpII	24	51	0	11	0	20	0
D0ZIM2_SALT1	fusA	Elongation factor G	CYT	78	39	0	108	6	166	33
D0ZSC1_SALT1	ybjP	Putative lipoprotein	SpII	19	39	0	8	0	32	0
D0ZN63_SALT1	acrA	Acridine efflux pump	SpII	42	37	0	69	0	265	0
D0ZHY7_SALT1	traT	Conjugative transfer: surface exclusion	SpII	26	34	0	60	0	176	0
D0ZRQ2_SALT1	nlpB	Lipoprotein	SpII	37	33	0	39	0	53	0
D0ZXW2_SALT1	yraP	Putative uncharacterized protein yraP	SpII	20	29	0	25	0	52	0
D0ZW18_SALT1	gapA	Glyceraldehyde-3-phosphate dehydrogenase	CYT	36	28	0	136	19	252	114

D0ZL91_SALT1	yedD	Putative uncharacterized protein yedD	SpII	15	28	0	0	0	0	0
D0ZTR7_SALT1	yfiO	Outer membrane protein assembly complex subunit	SpII	28	26	0	3	0	6	0
D0ZSH5_SALT1	pflB	Pyruvate formate lyase I	CYT	85	24	0	132	33	119	35
D0ZJZ0_SALT1	aceE	Pyruvate dehydrogenase E1 component	CYT	100	24	0	62	0	199	30
D0ZJ17_SALT1	adhE	Bifunctional acetaldehyde-CoA/alcohol dehydrogenase	CYT	96	21	0	155	0	262	33
D0ZJG1_SALT1	glpD	Glycerol-3-phosphate dehydrogenase	CYT	57	21	0	34	0	64	0
D0ZKL9_SALT1	yiaF	Putative outer membrane lipoprotein	SpII	26	19	0	5	0	14	0
D0ZKL6_SALT1	yiaD	Putative outer membrane lipoprotein	SpII	22	18	0	10	0	0	0
D0ZQV4_SALT1	rpoB	DNA-directed RNA polymerase subunit beta	CYT	151	17	2	15	0	58	3
D0ZNV0_SALT1	udp	Uridine phosphorylase	CYT	27	17	0	0	0	7	0
D0ZQT7_SALT1	cysK	Cysteine synthase	CYT	35	16	10	39	0	67	30
D0ZQV5_SALT1	rpoC	DNA-directed RNA polymerase subunit beta	CYT	155	16	0	26	0	101	3
D0ZWH3_SALT1	pgk	Phosphoglycerate kinase	CYT	41	16	0	21	0	175	30
D0ZJ50_SALT1	lolB	Outer membrane lipoprotein LolB	SpII	24	16	0	19	0	0	0
D0ZR81_SALT1	gpmA	2,3-bisphosphoglycerate-dependent phosphoglycerate-dependent phosphoglycerate mutase	CYT	28	16	0	0	0	7	0
D0ZN75_SALT1	htpG	Chaperone protein htpG	CYT	72	16	0	0	0	0	0
D0ZQ59_SALT1	lptE	LPS-assembly lipoprotein RplB	SpII	21	15	0	10	0	10	0
D0ZIC9_SALT1	mdh	Malate dehydrogenase	SpI	32	14	5	24	0	192	110
D0ZMI7_SALT1	gnd	6-phosphogluconate dehydrogenase	CYT	51	14	0	9	0	57	12
D0ZMY2_SALT1		Putative thiol-alkyl hydroperoxide reductase	CYT	22	13	2	71	3	65	32
D0ZWH2_SALT1	fba	Fructose-bisphosphate aldolase	CYT	39	13	2	17	0	78	46
D0ZR32_SALT1	pgi	Glucose-6-phosphate isomerase	CYT	61	13	5	9	0	0	0
D0ZRU1_SALT1	yfgL	Outer membrane protein assembly complex subunit	SpII	42	12	0	28	0	34	0
D0ZMT5_SALT1	atpD	ATP synthase subunit beta	CYT	50	12	0	9	0	247	10
D0ZUQ5_SALT1	ycfM	Putative outer membrane lipoprotein	SpII	23	12	0	6	0	8	0

D0ZKZ9_SALT1	rcsF	Outer membrane lipoprotein	SpII	14	12	0	6	0	8	0
D0ZV90_SALT1	phoP	DNA-binding transcriptional regulator PhoP	CYT	26	12	0	0	0	4	0
D0ZNY5_SALT1	hemN	Coproporphyrinogen III oxidase	CYT	53	12	0	0	0	0	0
D0ZUZ6_SALT1	sitA	Putative periplasmic binding protein	SpI	34	12	0	0	0	0	0
D0ZIR2_SALT1	dnaK	Chaperone protein dnaK	CYT	69	11	0	30	0	116	2
D0ZN29_SALT1	yajG	Putative uncharacterized protein yajG	SpII	21	11	0	5	0	18	0
D0ZXQ1_SALT1	ompD	Putative outer membrane porin	SpI	40	10	0	119	0	662	277
D0ZJZ1_SALT1	aceF	Dihydrolipoamide acetyltransferase	CYT	66	10	0	39	0	52	5
D0ZMT7_SALT1	atpA	ATP synthase subunit alpha	CYT	55	10	0	33	0	230	25
D0ZJN6_SALT1	carB	Carbamoyl phosphate synthase large subunit	CYT	118	10	0	13	5	17	0
D0ZS49_SALT1	phoN	Non-specific acid phosphatase	SpI	28	10	0	0	0	0	0
D0ZXP4_SALT1	adhP	Alcohol dehydrogenase	CYT	36	9	0	15	0	66	27
D0ZU91_SALT1		Putative NAD-dependent aldehyde dehydrogenase	CYT	50	8	0	21	0	66	11
D0ZMZ4_SALT1	tsx	Nucleoside channel	SpI	37	8	0	0	0	15	0
D0ZPY3_SALT1	tpiA	Triosephosphate isomerase	CYT	27	7	0	20	0	17	20
D0ZPA7_SALT1	ahpC	Alkyl hydroperoxide reductase subunit C	CYT	21	7	0	17	0	14	5
D0ZJZ2_SALT1	lpdA	Dihydrolipoyl dehydrogenase	CYT	51	7	2	15	0	157	13
D0ZK14_SALT1	slp	Putative outer membrane protein	SpII	21	7	0	10	0	21	0
D0ZQF4_SALT1	sucD	Succinyl-CoA ligase [ADP-forming] subunit alpha	CYT	30	7	0	2	0	23	0
D0ZLQ5_SALT1	mgtB	Mg2+ transporter	CYT	100	6	0	126	8	122	6
D0ZTR4_SALT1	clpB	Protein disaggregation chaperone	CYT	95	6	0	22	0	81	5
D0ZX99_SALT1	ygiB	Putative uncharacterized protein ygiB	SpI	23	6	0	11	0	13	2
D0ZPY9_SALT1	glpK	Glycerol kinase	CYT	56	6	0	9	0	91	6
D0ZTQ2_SALT1	wrbA	Flavoprotein wrbA	CYT	21	6	0	6	0	8	0
D0ZSQ2_SALT1	purG	Phosphoribosylformylglycinamidine synthase	CYT	141	6	0	4	0	6	0
D0ZR97_SALT1	ybhC	Putative pectinesterase	SpII	46	5	0	11	0	20	0
D0ZQQ2_SALT1	vacJ	Lipoprotein	SpII	28	5	0	11	0	3	0

D0ZSP0_SALT1	glyA	Serine hydroxymethyltransferase	CYT	45	5	0	8	0	74	4
D0ZW53_SALT1	katE	Catalase	CYT	84	5	0	7	0	0	0
D0ZSI6_SALT1	rpsA	30S ribosomal protein S1	CYT	61	4	0	25	0	114	0
D0ZWI1_SALT1	tktA	Transketolase	CYT	72	4	0	12	0	33	2
D0ZRQ1_SALT1	purC	Phosphoribosylaminoimidazole-succinocarboxamide synthase	CYT	27	4	2	10	0	14	2
D0ZQE5_SALT1	gltA	Citrate synthase	CYT	48	4	0	8	0	88	8
D0ZUE8_SALT1	deoD	Purine nucleoside phosphorylase deoD-type	CYT	26	4	0	2	0	10	0
D0ZJZ6_SALT1	acnB	Bifunctional aconitate hydratase 2	CYT	94	4	0	0	0	14	0
D0ZV97_SALT1	icdA	Isocitrate dehydrogenase [NADP]	CYT	46	3	0	5	0	159	8
D0ZUE7_SALT1	deoB	Phosphopentomutase	CYT	44	3	0	2	0	11	0
D0ZMJ6_SALT1	rfbH	CDP-6-deoxy-D-xylo-4-hexulose-3-dehydrase	CYT	48	3	0	0	0	43	3
D0ZUP3_SALT1	acpP	Acyl carrier protein	CYT	9	3	0	0	0	20	0
D0ZQ60_SALT1	leuS	Putative uncharacterized protein	TMH	106	2	0	6	0	17	0
D0ZXY2_SALT1	infB	Translation initiation factor IF-2	CYT	97	2	0	5	0	10	0
D0ZSK8_SALT1	asnS	Asparaginyl-tRNA synthetase	CYT	53	2	0	4	0	18	0
D0ZSK4_SALT1	aspC	Aromatic amino acid aminotransferase	CYT	44	2	0	0	0	47	2
D0ZKM7_SALT1	glyS	Glycyl-tRNA synthetase beta subunit	CYT	76	2	0	0	0	16	0
D0ZUV1_SALT1	alaS	Alanyl-tRNA synthetase	CYT	96	2	0	0	0	11	0
D0ZWQ2_SALT1	pykF	Pyruvate kinase	CYT	51	0	0	41	0	61	0
D0ZPB8_SALT1	rna	RNase I	SpI	30	0	0	22	0	0	0
D0ZIL5_SALT1	rplC	50S ribosomal protein L3	CYT	22	0	0	18	0	26	15
D0ZQN6_SALT1	fabB	3-oxoacyl-(Acyl carrier protein) synthase I	CYT	42	0	0	14	0	62	3
D0ZNZ0_SALT1	glnA	Glutamine synthetase	CYT	52	0	0	14	0	29	3
D0ZJ20_SALT1	hns	Global DNA-binding transcriptional dual regulator	CYT	16	0	0	12	0	10	3
D0ZN27_SALT1	cyoA	Cytochrome o ubiquinol oxidase subunit II	TMH	35	0	0	12	0	5	0
D0ZXM2_SALT1		Putative S-adenosylmethionine:tRNA-ribosyltransferase	CYT	40	0	0	12	0	0	0

D0ZV61_SALT1	yjjK	Putative ABC transporter ATP-binding protein	CYT	62	0	0	11	0	5	0
D0ZQ50_SALT1	rlpA	Rare lipoprotein A	SpII	39	0	0	6	0	6	0
D0ZT13_SALT1	purA	Adenylosuccinate synthetase	CYT	47	0	0	5	0	9	0
D0ZNP6_SALT1	rho	Transcription termination factor Rho	CYT	47	0	0	5	0	7	0
D0ZQU2_SALT1	ptsI	Phosphoenolpyruvate-protein phosphotransferase	CYT	63	0	0	4	0	6	0
D0ZLG6_SALT1	mtlD	Mannitol-1-phosphate 5-dehydrogenase	CYT	41	0	0	3	0	7	0
D0ZQH3_SALT1	nuoG	NADH-quinone oxidoreductase	CYT	100	0	0	2	0	40	0
D0ZQF7_SALT1	cydA	Cytochrome d terminal oxidase polypeptide subunit	TMH	58	0	0	0	0	90	0
D0ZJ71_SALT1		Putative homolog of glutamic dehydrogenase	CYT	48	0	0	0	0	61	5
D0ZIZ4_SALT1	trpB	Tryptophan synthase beta chain	CYT	43	0	0	0	0	55	0
D0ZQE9_SALT1	sdhA	Succinate dehydrogenase flavoprotein subunit	CYT	64	0	0	0	0	40	0
D0ZK25_SALT1	manX	Mannose-specific enzyme IIAB	CYT	35	0	0	0	0	23	0
D0ZQF2_SALT1	sucB	Dihydrolipoamide acetyltransferase	CYT	44	0	0	0	0	21	0
D0ZUP4_SALT1	fabF	3-oxoacyl-(Acyl carrier protein) synthase II	SpI	43	0	0	0	0	19	0
D0ZR44_SALT1	lamB	Maltoporin	SpI	51	0	0	0	0	19	0
D0ZVI4_SALT1		Putative molecular chaperone	CYT	18	0	0	0	0	18	0
D0ZIJ1_SALT1	rpsD	30S ribosomal protein S4	CYT	23	0	0	0	0	18	0
D0ZWJ6_SALT1	metK	S-adenosylmethionine synthase	CYT	42	0	0	0	0	17	0
D0ZME1_SALT1	pduC	Glycerol dehydratase large subunit	CYT	60	0	0	0	0	16	0
D0ZQJ1_SALT1	ackA	Acetate kinase	CYT	43	0	0	0	0	16	0
D0ZN77_SALT1	adk	Adenylate kinase	CYT	23	0	0	0	0	16	0
D0ZME0_SALT1	pduB	Propanediol utilization protein pduB	CYT	24	0	0	0	0	14	0
D0ZV13_SALT1	hilA	Transcriptional regulator hilA	CYT	63	0	0	0	0	14	0
D0ZIF4_SALT1	accC	Acetyl-CoA carboxylase biotin carboxylase subunit	CYT	49	0	0	0	0	14	0
D0ZWZ8_SALT1	fumC	Fumarate hydratase	CYT	50	0	0	0	0	13	0
D0ZQH6_SALT1	nuoC	Bifunctional NADH:ubiquinone oxidoreductase subunit	CYT	69	0	0	0	0	12	0

D0ZLJ2_SALT1	kbl	2-amino-3-ketobutyrate coenzyme A ligase	CYT	43	0	0	0	0	12	0
D0ZM37_SALT1	prpR	Propionate catabolism operon regulatory protein	CYT	60	0	0	0	0	11	0
D0ZME3_SALT1	pduE	Propanediol utilization dehydratase, small subunit	CYT	19	0	0	0	0	10	0
D0ZKA4_SALT1	pykA	Pyruvate kinase	CYT	51	0	0	0	0	10	0
D0ZQJ2_SALT1	pta	Phosphate acetyltransferase	CYT	77	0	0	0	0	9	0
D0ZMW7_SALT1	ilvE	Branched-chain amino acid aminotransferase	CYT	34	0	0	0	0	9	0
D0ZSI9_SALT1	msbA	Lipid A export ATP-binding/permease protein	TMH	64	0	0	0	0	8	0
D0ZTE2_SALT1		Gifsy-2 prophage protein	CYT	23	0	0	0	0	0	0
D0ZVL2_SALT1		Putative 3-polyprenyl-4-hydroxybenzoate decarboxylase	CYT	52	0	0	0	0	0	0
PUTA_SALTY	putA	Bifunctional protein putA	CYT	144	0	0	0	0	49	0

APPENDIX 7. Proteins identified from *E. faecium* Com15 culture supernatant by mass spectrometry. Proteins listed have at least 2 unique peptides identified. Proteins involved in peptidoglycan remodeling are highlighted in yellow. PSM = peptide spectrum match.

Uniprot Accession	Gene name	Description	# Unique Peptides	# PSMs
C9ASF4, C9ASF5	sagA	Secreted lipase	33	447
C9AS94		Mannosyl-glycoprotein endo-beta-N-acetylglucosamidase	16	103
C9AKY4		Peptidoglycan-binding protein LysM	8	93
C9AQS4		Extracellular solute-binding protein	18	92
C9AQL4		Basic membrane lipoprotein	24	85
C9ASJ4		N-acetylmuramoyl-L-alanine amidase	23	78
C9ATH2		Beta-1,4-N-acetylmuramoylhydrolase	16	76
C9AKY1		Periplasmic solute binding protein	21	68
C9AQT6		Periplasmic binding protein	16	63
C9ANP2		N-acetylmuramoyl-L-alanine amidase	10	57
C9APB3		Putative uncharacterized protein	16	56
C9ALQ1	eno	Enolase	23	55
C9APJ5		Penicillin-binding protein	23	48
C9AMB1		Sulfatase	20	45
C9ALP8		Glyceraldehyde-3-phosphate dehydrogenase	10	43
C9AQM8	tuf	Elongation factor Tu 2	13	41
C9ALW6		Glycosyl transferase	20	41
C9ARZ3		Extracellular solute-binding protein	12	41
C9AMG6	arcA	Arginine deiminase	17	39
C9AML5		Amino acid ABC transporter	8	36

C9ASF9		ErfK/YbiS/YcfS/YnhG family protein	16	34
C9AS22		FMN-binding protein	10	34
C9API8		Pyruvate kinase	19	33
C9ALP9	pgk	Phosphoglycerate kinase	13	31
C9AMK8	dnaK	Chaperone protein DnaK	23	31
C9AMB7	pgi	Glucose-6-phosphate isomerase	15	29
C9ALB5		Sulfatase	16	29
C9AMH5	tsf	Elongation factor Ts	11	27
C9AQB2		Fructose-bisphosphate aldolase class-II	10	25
C9ARP7		Glycine betaine/L-proline ABC transporter	9	25
C9AP18		D-alanyl-D-alanine carboxypeptidase	10	23
C9APP4		Transcriptional regulator	10	23
C9ANA8		Extracellular solute-binding protein	17	23
C9AL01		Extracellular solute-binding protein	12	21
C9ANQ7		Peptidyl-prolyl cis-trans isomerase	7	20
C9ARQ9	groEL	60 kDa chaperonin	15	19
C9ANB6		Extracellular solute-binding protein	9	19
C9ATA9		ATP-dependent Clp protease	14	18
C9AME5		Iron compound ABC transporter	11	18
C9AQM7	fusA	Elongation factor G	10	16
C9AS40		ABC transporter substrate binding protein	10	16
C9ANN9		NADH oxidase	10	15
C9AMN8	tig	Trigger factor	11	14
C9APM7		Phosphoenolpyruvate-protein phosphotransferase	11	12
C9AMG7		Ornithine carbamoyltransferase	7	12

C9AP95		Ribosomal protein S1	10	12
C9ARE8	prsA	PpiC-type peptidyl-prolyl cis-trans isomerase	8	12
C9ALQ0	tpiA	Triosephosphate isomerase	6	12
C9ASG0	ldh	L-lactate dehydrogenase 2	8	11
C9APR1		Predicted protein	5	11
C9AQP2	rplE	50S ribosomal protein L5	4	10
C9ANQ4		Glyceraldehyde-3-phosphate dehydrogenase	7	10
C9APA2		Peptidase M20A	8	10
C9ANB3		Putative uncharacterized protein	5	10
C9AR88		Peptidase S1	6	10
C9APC1	tuf	Elongation factor Tu 1	7	9
C9API4		6-phosphogluconate dehydrogenase, decarboxylating	8	9
C9AQB4		Glutamine synthetase	8	9
C9AN26		Heat shock protein	3	9
C9ARH9		Acyltransferase	6	8
C9AL54		NLPA lipoprotein	4	8
C9APP1		Chitin-binding protein	6	8
C9ALX9		Phosphoglucomutase/phosphomannomutase	7	7
C9AR81		Peptidase M20A	5	7
C9ASX8		Putative uncharacterized protein	4	7
C9ATI6		Extracellular solute-binding protein	5	7
C9ART9		Sulfatase	6	7
C9AQP7	rpsE	30S ribosomal protein S5	4	6

C9AQK7	guaA	GMP synthase [glutamine-hydrolyzing]	5	6
C9AS47		Ferritin	4	6
C9ANE7		Putative uncharacterized protein	2	6
C9ATD5		Intracellular protease	4	6
C9AQP5	rplF	50S ribosomal protein L6	5	6
C9AQI8		Oligopeptide binding protein	5	6
C9ARL2	rplK	50S ribosomal protein L11	4	5
C9ASH2	lysS	Lysine--tRNA ligase	4	5
C9AMH7	frr	Ribosome-recycling factor	5	5
C9AMC8		Predicted protein	5	5
C9AQQ1	adk	Adenylate kinase	5	5
C9ARL5	rplL	50S ribosomal protein L7/L12	4	5
C9AKW7		NAD(FAD)-dependent dehydrogenase	5	5
C9AM30		Putative uncharacterized protein	4	5
C9ALT5		Sigma 54 modulation protein/ribosomal protein S30EA	4	5
C9AN78		Putative uncharacterized protein	5	5
C9AL85	prsA	PpiC-type peptidyl-prolyl cis-trans isomerase	4	5
C9AN90		Cell envelope transcriptional attenuator	4	5
C9ASN4		Putative uncharacterized protein	3	5
C9AQM6	rpsG	30S ribosomal protein S7	2	4
C9APQ3		Superoxide dismutase	3	4
C9AP93		DNA binding protein HU	4	4
C9AQP4	rpsH	30S ribosomal protein S8	3	4
C9AS49	rpsI	30S ribosomal protein S9	2	4
C9API9	pfkA	6-phosphofructokinase	3	4

C9ASN2		Pyridoxal-dependent decarboxylase	3	4
C9AQQ7	rplQ	50S ribosomal protein L17	4	4
C9ANY2		Transketolase	4	4
C9ARX0		Signal peptidase I	3	4
C9AQP1	rplX	50S ribosomal protein L24	4	4
C9AQB3	pyrG	CTP synthase	4	4
C9ALR9	atpD	ATP synthase F1	4	4
C9AQM2	gpmA	2,3-bisphosphoglycerate-dependent phosphoglycerate mutase 2	2	4
C9ARX9	upp	Uracil phosphoribosyltransferase	3	4
C9APR6		Putative uncharacterized protein	4	4
C9ATB9		Cupin domain-containing protein	2	4
C9ASG5		Septum formation initiator	3	4
C9AKX7		Putative uncharacterized protein	2	4
C9ANY1		Dihydrolipoamide S-succinyltransferase	3	3
C9ALN5		Glyoxalase/bleomycin resistance protein/dioxygenase	3	3
C9ANP3		Transketolase	2	3
C9ARQ8	groES	10 kDa chaperonin	3	3
C9AQF3	guaB	Inosine-5'-monophosphate dehydrogenase	2	3
C9ARL3	rplA	50S ribosomal protein L1	3	3
C9AQN1	rplD	50S ribosomal protein L4	2	3
C9ALV5		UTP-glucose-1-phosphate uridylyltransferase	2	3
C9ARL4	rplJ	50S ribosomal protein L10	3	3
C9AMD1		Putative uncharacterized protein	2	3

C9APR5	greA	Transcription elongation factor greA	2	3
C9AS03	metG	Methionyl-tRNA synthetase	2	3
C9AP54	ppaC	Probable manganese-dependent inorganic pyrophosphatase	2	3
C9ARH5		Aldo/keto reductase	2	3
C9AR84		Glutamyl aminopeptidase	3	3
C9ALL0		Putative uncharacterized protein	3	3
C9AQN6	rpsC	30S ribosomal protein S3	3	3
C9ALV7		Putative uncharacterized protein	3	3
C9ANI8		HD domain-containing protein	3	3
C9AN38	prsA	Foldase protein prsA 2	2	3
C9AP35		Putative uncharacterized protein	3	3
C9AQM9	rpsJ	Ribosomal protein S10	2	2
C9AMH4	rpsB	30S ribosomal protein S2	2	2
C9AMN9	clpX	ATP-dependent Clp protease ATP-binding subunit ClpX	2	2
C9ASA9	gltX	Glutamate--tRNA ligase	2	2
C9AQZ1	pnp	Polyribonucleotide nucleotidyltransferase	2	2
C9AQP6	rplR	50S ribosomal protein L18	2	2
C9AL22		M13 family peptidase	2	2
C9ARB8		Predicted protein	2	2
C9ARX7	glyA	Pyridoxal-phosphate-dependent serine hydroxymethyltransferase	2	2
C9AQ30	ftsZ	Cell division protein ftsZ	2	2
C9AP56		Formate acetyltransferase	2	2
C9APC4		2,5-didehydrogluconate reductase	2	2
C9APL6		3-oxoacyl-[acyl-carrier-protein] synthase 2	2	2
C9AQA9	rpmE2	50S ribosomal protein L31 type B	2	2

C9AM29		D-alanyl-D-alanine carboxypeptidase	2	2
C9ASN3	tyrS	Tyrosine--tRNA ligase	2	2
C9ANP1		Cysteine synthase	2	2
C9AQ59	rpmA	50S ribosomal protein L27	2	2
C9AQN5	rplV	50S ribosomal protein L22	2	2
C9AQ61	rplU	50S ribosomal protein L21	2	2
C9APL9	acpP	Acyl carrier protein 1	2	2
C9AMM5		Putative uncharacterized protein	2	2
C9ARS4	nadE	NH(3)-dependent NAD(+) synthetase	2	2
C9ALC7		Putative uncharacterized protein	2	2
C9AP38		ABC transporter	2	2
C9ASJ8		Putative uncharacterized protein	2	2
C9ALI4		Putative uncharacterized protein	2	2
C9AN28		Predicted protein	2	2
C9ALC4		Lipoprotein YaeC	2	2
C9ASP9		Cell wall surface adhesion protein	2	2
C9APR0		Putative uncharacterized protein	2	2

APPENDIX 8. Proteins identified by mass spectrometry from the top and bottom bands as indicated in Figure 4.12a.

Uniprot Accession	Gene Name	Description	MW (kDa)	Unique Peptides	# PSMs Top Band	# PSMs Bottom band
C9ASF4,C9ASF5	sagA	Secreted lipase	53.6	17	104	13
C9ALL0		Putative uncharacterized protein	84.5	11	19	
C9APJ5		Penicillin-binding protein	78.3	10	18	
C9AQM7	fusA	Elongation factor G	76.7	9	17	
C9ASJ4		N-acetylmuramoyl-L-alanine amidase	77.3	8	12	
C9AQZ1	pnp	Polyribonucleotide nucleotidyltransferase	76.9	3	4	
C9ANP3		Transketolase	72.4	2	3	
C9ANY1		Dihydrolipoamide S-succinyltransferase	57.9	2	2	
C9ANA8		Extracellular solute-binding protein	45.7	12		25
C9AS94		Mannosyl-glycoprotein endo-beta-N-acetylglucosamidase	46.6	9		20
C9ALQ1	eno	Enolase	46.5	10		18
C9APP4		Transcriptional regulator	42.5	9		13
C9AQB4		Glutamine synthetase	50.6	7		11
C9AQM8	tuf	Elongation factor Tu 2	43.2	6		11
C9ATH2		Beta-1,4-N-acetylmuramoylhydrolase	71.0	4		9
C9AMB7	pgi	Glucose-6-phosphate isomerase	49.7	6		9
C9API4		6-phosphogluconate dehydrogenase, decarboxylating	52.7	4		7
C9ALB5		Sulfatase	79.1	3		6
C9AP95		Ribosomal protein S1	45.7	3		5
C9AMG6	arcA	Arginine deiminase	46.1	4		5
C9ART9		Sulfatase	70.9	3		5
C9ALR9	atpD	ATP synthase F1	51.0	2		4
C9AMB1		Sulfatase	80.4	3		4
C9ANE7		Putative uncharacterized protein	36.7	2		3
C9AQL4		Basic membrane lipoprotein	37.8	2		2

APPENDIX 9. Proteins in *E. faecium* Com15 culture supernatant identified by mass spectrometry, after in solution digestion. Proteins listed have at least 2 unique peptides. PSM = peptide spectrum match. Proteins involved in cell wall remodeling are highlighted in yellow.

Uniprot Accession	Gene Name	Description	# Unique Peptides	# PSMs
C9ALQ1	eno	Enolase	20	57
C9ASF4/C9ASF5	sagA	Secreted lipase	21	54
C9AKY1		Periplasmic solute binding protein	19	43
C9AQS4		Extracellular solute-binding protein	20	41
C9AMB1		Sulfatase	14	39
C9AQT6		Periplasmic binding protein	12	37
C9ARQ9	groEL	60 kDa chaperonin	17	36
C9APJ5		Penicillin-binding protein	16	31
C9API8		Pyruvate kinase	15	31
C9AQM7	fusA	Elongation factor G	11	30
C9ATH2		Beta-1,4-N-acetylmuramoylhydrolase	13	29
C9AQM8	tuf	Elongation factor Tu	13	27
C9ATA9		ATP-dependent Clp protease	15	26
C9AS94		Mannosyl-glycoprotein endo-beta-N-acetylglucosamidase	11	26
C9AMK8	dnaK	Chaperone protein	18	25
C9AMB7	pgi	Glucose-6-phosphate isomerase	11	25
C9ALP9	pgk	Phosphoglycerate kinase	11	24
C9ALP8		Glyceraldehyde-3-phosphate dehydrogenase	11	23
C9AMG7		Ornithine carbamoyltransferase	10	22
C9AMH5	tsf	Elongation factor Ts	12	19
C9APB3		Putative uncharacterized protein	9	18
C9AQB2		Fructose-bisphosphate aldolase class-II	8	18
C9AMN8	tig	Trigger factor	10	17
C9APW8		Putative uncharacterized protein	9	17

C9ASN3	tyrS	Tyrosine--tRNA ligase	7	17
C9AP18		D-alanyl-D-alanine carboxypeptidase	7	16
C9ASJ4		N-acetylmuramoyl-L-alanine amidase	9	15
C9AML5		Amino acid ABC transporter	6	15
C9ALB5		Sulfatase	8	14
C9ASF9		ErfK/YbiS/YcfS/YnhG family protein	7	14
C9AKY4		Peptidoglycan-binding protein LysM	6	14
C9ANA8		Extracellular solute-binding protein	8	13
C9ARE8	prsA	Foldase protein PrsA	6	13
C9APM7		Phosphoenolpyruvate-protein phosphotransferase	9	12
C9AQN3	rplB	50S ribosomal protein L2	5	12
C9AS40		ABC transporter substrate binding protein	7	11
C9ANB6		Extracellular solute-binding protein	6	11
C9AL01		Extracellular solute-binding protein	5	11
C9ARP7		Glycine betaine/L-proline ABC transporter	4	11
C9AQZ1	pnp	Polyribonucleotide nucleotidyltransferase	4	11
C9AQB4		Glutamine synthetase	6	10
C9APW3		Putative uncharacterized protein	5	10
C9APC1	tuf	Elongation factor Tu	5	10
C9APP1		Chitin-binding protein	4	10
C9ANY2		Transketolase	4	10
C9ATC6		Uncharacterized protein	3	10
C9ANP2		N-acetylmuramoyl-L-alanine amidase	5	9
C9ARY2		Cell wall surface adhesion protein	6	8
C9ATC3		Uncharacterized protein	6	8
C9ALV5		UTP-glucose-1-phosphate uridylyltransferase	4	8
C9AQ24	ileS	Isoleucine--tRNA ligase	3	8

C9ALL0		Putative uncharacterized protein	6	7
C9ASG0	ldh	L-lactate dehydrogenase	5	7
C9AMG6	arcA	Arginine deiminase	5	7
C9AQK7	guaA	GMP synthase [glutamine-hydrolyzing]	5	7
C9ARS4	nadE	NH(3)-dependent NAD(+) synthetase	5	7
C9APR1		Predicted protein	4	7
C9ARL2	rplK	50S ribosomal protein L11	4	7
C9AS47		Ferritin	4	7
C9ALR9	atpD	ATP synthase subunit beta	4	7
C9APW2		Predicted protein	3	7
C9APL9	acpP	Acyl carrier protein	3	7
C9ATD5		Intracellular protease	3	7
C9AS03	metG	Methionine--tRNA ligase	2	7
C9ANN9		NADH oxidase	2	7
C9AL85	prsA	Foldase protein PrsA	6	6
C9AQL4		Basic membrane lipoprotein	5	6
C9AS42	rpoC	DNA-directed RNA polymerase subunit beta'	5	6
C9AS49	rpsI	30S ribosomal protein S9	4	6
C9APA2		Peptidase M20A	4	6
C9ANY3		Pyruvate dehydrogenase	3	6
C9AQP6	rplR	50S ribosomal protein L18	3	6
C9AKW7		NAD(FAD)-dependent dehydrogenase	3	6
C9AR84		Glutamyl aminopeptidase	3	6
C9ALQ0	tpiA	Triosephosphate isomerase	3	6
C9ALX9		Phosphoglucomutase/phosphomannomutase	3	6
C9ATF4		Citrate lyase alpha subunit	3	6
C9AQP9	rplO	50S ribosomal protein L15	2	6
C9AN96		Alkyl hydroperoxide reductase	2	6

C9APR5	greA	Transcription elongation factor GreA	2	6
C9ALV9		Catabolite control protein A	4	5
C9ASA9	gltX	Glutamate--tRNA ligase	4	5
C9ANQ4		Glyceraldehyde-3-phosphate dehydrogenase	3	5
C9API9	pfkA	6-phosphofructokinase	3	5
C9ASH2	lysS	Lysine--tRNA ligase	3	5
C9AQ07		Predicted protein	3	5
C9ANY1		Dihydrolipoamide S-succinyltransferase	2	5
C9ASN4		Putative uncharacterized protein	2	5
C9ARP9		DegV family protein	2	5
C9ARL5	rplL	50S ribosomal protein L7/L12	4	4
C9ARQ8	groES	10 kDa chaperonin	4	4
C9AS41	rpoB	DNA-directed RNA polymerase subunit beta	4	4
C9AQF3	guaB	Inosine-5'-monophosphate dehydrogenase	4	4
C9AT02		Uncharacterized protein	3	4
C9AP93		DNA binding protein HU	3	4
C9AMH4	rpsB	30S ribosomal protein S2	3	4
C9ANQ7		Peptidyl-prolyl cis-trans isomerase	3	4
C9ART9		Sulfatase	3	4
C9AQ23	zwf	Glucose-6-phosphate 1-dehydrogenase	3	4
C9AQM2	gpmA	2,3-bisphosphoglycerate-dependent phosphoglycerate muta	2	4
C9AL78		Cell wall surface anchor family protein	2	4
C9AQN6	rpsC	30S ribosomal protein S3	2	4
C9APL6		3-oxoacyl-[acyl-carrier-protein] synthase 2	2	4
C9APQ3		Superoxide dismutase	2	4
C9AQP1	rplX	50S ribosomal protein L24	2	4
C9AR81		Peptidase M20A	2	4

C9AR88		Peptidase S1	2	4
C9AM29		D-alanyl-D-alanine carboxypeptidase	2	4
C9AP08	xpt	Xanthine phosphoribosyltransferase	2	4
C9AKX7		Putative uncharacterized protein	3	3
C9API4		6-phosphogluconate dehydrogenase, decarboxylating	3	3
C9ALU9		Putative uncharacterized protein	3	3
C9AP54	ppaC	Probable manganese-dependent inorganic pyrophosphatase	3	3
C9AQR6		Dak phosphatase	3	3
C9APV0		N-acetylmuramoyl-L-alanine amidase	2	3
C9ARH9		Acyltransferase	2	3
C9ANY0		Dihydrolipoyl dehydrogenase	2	3
C9ANP3		Transketolase	2	3
C9AS48	rplM	50S ribosomal protein L13	2	3
C9APV4		Putative uncharacterized protein	2	3
C9AP95		Ribosomal protein S1	2	3
C9AM30		Putative uncharacterized protein	2	3
C9AQ25		DivIVA protein	2	3
C9ANX7		GTP-binding protein TypA	2	3
C9APW1		Predicted protein	2	3
C9AS27		Cell surface protein (Fragment)	2	3
C9AQ61	rplU	50S ribosomal protein L21	2	2
C9AQZ7	rplY	50S ribosomal protein L25	2	2
C9AQQ1	adk	Adenylate kinase	2	2
C9ALR7	atpA	ATP synthase subunit alpha	2	2
C9ALT5		Sigma 54 modulation protein/ribosomal protein S30EA	2	2
C9AQN4	rpsS	30S ribosomal protein S19	2	2
C9ARJ0		Peptidase M3B	2	2
C9AMQ2	gatB	Aspartyl/glutamyl-tRNA(Asn/Gln) amidotransferase subunit	2	2

APPENDIX 10. Proteins in *E. faecalis* OG1RF and *E. faecalis-sagA* culture supernatants identified by mass spectrometry, after in solution digestion. Proteins listed have at least 2 unique peptides. PSM = peptide spectrum match. Proteins involved in cell wall remodeling are highlighted in yellow. F2MNY6 and SagA-His6 are highlighted in orange.

			E. faecalis		***E. faecalis-sagA***	
Uniprot Accession	**Gene Name**	**Description**	**# Unique peptides**	**# PSMs**	**# Unique Peptides**	**# PSMs**
F2MNY6		Secreted antigen	5	48	4	36
F2MPG2	pgk	Phosphoglycerate kinase	10	24	10	13
F2MPG0	eno	Enolase	9	22	8	15
F2MR31		Uncharacterized protein	8	16	14	47
F2MQS5	ptsI	Phosphoenolpyruvate-protein phosphotransferase	7	16	7	15
F2MPK1		Peptide ABC superfamily ABC transporter, binding protein	7	15	12	23
F2MNH6	gelE	Gelatinase	7	15	9	22
F2MQ41	npr	NADH peroxidase	4	15	4	4
F2MNQ3	htrA	Serine protease HtrA	4	13	3	4
F2MQL1	rpoC	DNA-directed RNA polymerase subunit beta'	7	12	5	7
F2MM76		ABC superfamily ABC transporter, binding protein	6	11	10	23
F2MNH5	sprE	SprE protein	4	11	5	20
F2MQ69	ackA	Acetate kinase	5	11	5	14
F2MR21	dnaK	Chaperone protein DnaK	9	11	8	11
F2MTS3	groEL	60 kDa chaperonin	7	11	7	10
F2MMD6	pepQ	Xaa-Pro dipeptidase	4	11	4	9
F2MSU5	pgi	Glucose-6-phosphate isomerase	4	11	4	9
F2MT66	oppA	Oligopeptide ABC superfamily ABC transporter, binding protein	7	11	6	8
F2MRX7	pdhA	Pyruvate dehydrogenase complex E1 component alpha subunit	3	11	2	5
F2MM98	tuf	Elongation factor Tu	7	10	5	6

F2MPU3		Transcriptional regulator	3	9	6	10
F2MQA4		ABC superfamily ABC transporter, binding protein	2	9	4	10
F2MST4	trxA	Thioredoxin	2	9	2	10
F2MQC6	glnA	Glutamine synthetase	5	9	4	7
F2MN33	ldh	L-lactate dehydrogenase	4	9	3	6
F2MR74		ABC superfamily ABC transporter, binding protein	3	8	9	15
F2MRQ5	lyzl6	Cell wall lysis protein	5	8	5	8
F2MPV9	tyrS	Tyrosine--tRNA ligase	5	8	2	7
F2MQH3	ubiD2	UbiD family decarboxylase	6	8	4	6
F2MQK7	dps	DNA starvation/stationary phase protection protein Dps	5	8	4	4
F2MML0	gnd	6-phosphogluconate dehydrogenase, decarboxylating	6	8	2	3
F2MSU4	gdhA	Glutamate dehydrogenase	4	7	6	10
F2MQH5		WxL domain surface protein	3	7	3	6
F2MQ03	fbaB	Fructose-bisphosphate aldolase	3	7	3	5
F2MRX1		Sugar ABC superfamily ABC transporter, sugar-binding protein	5	7	3	5
F2MMC3	adk	Adenylate kinase	3	7	2	4
F2MQX6		Sulfatase domain protein	5	6	8	15
F2MRL8	glnP	Amino acid ABC superfamily ABC transporter, binding/permease protein	3	6	4	8
F2MRY0	lpd	Dihydrolipoyl dehydrogenase	4	6	3	7
F2MN60	fabF	3-oxoacyl-[acyl-carrier-protein] synthase 2	3	6	3	5
F2MMK6	pfkA	6-phosphofructokinase	4	6	3	4
F2MQT2	fruK2	Tagatose-6-phosphate kinase	2	6	2	4
F2MTK3	ndh	NADH dehydrogenase	3	6	2	4
F2MMR7	ccpA	Catabolite control protein A	4	6	3	3
F2MTG7	hup	DNA-binding protein HU	3	6	2	2
F2MM84	deoB	Phosphopentomutase	3	5	4	6
F2MRY7		Hydroxymethylglutaryl-CoA synthase	2	5	2	5
F2MTV6	pflB	Formate acetyltransferase	4	5	3	4

F2MM91	adh3	Putative alcohol dehydrogenase (NADP(+))	2	4	3	7
F2MTA8	pta	Phosphate acetyltransferase	3	4	3	4
F2MRX8	pdhB	Pyruvate dehydrogenase complex E1 component beta subunit	3	4	2	2
F2MS34	frr	Ribosome-recycling factor	4	4	2	2
F2MS37	rpsB	30S ribosomal protein S2	3	4	2	2
F2MTE1		Uncharacterized protein	2	3	4	10
F2MRB6		Pheromone cAD1 lipoprotein	2	3	3	3
F2MT59	aad	Aldehyde-alcohol dehydrogenase	2	2	10	18
F2MRB5		Thiamine biosynthesis lipoprotein	2	2	3	5
F2MTQ5	atpA2	ATP synthase subunit alpha	2	2	2	3
F2MU99	ahpC	Peroxiredoxin	2	2	2	3
F2MM92	gpmA	2,3-bisphosphoglycerate-dependent phosphoglycerate mutase	2	2	2	2
F2MNI5		WxL domain surface protein	0	0	5	69
F2MNH1		Phosphatidylglycerol--membrane-oligosaccharide glycerophosphotransferase	0	0	9	28
F2MMF2	pbpC	Penicillin-binding protein C	0	0	9	19
F2MNV6		Chitin-binding protein/carbohydrate-binding protein	0	0	6	17
F2MUF4	penA	Penicillin-binding protein 2B	0	0	11	15
F2MRA7		Cell-envelope associated acid phosphatase	0	0	5	8
F2MTN5	pmi	Mannose-6-phosphate isomerase	0	0	4	8
F2MSL7	opuCC	Glycine/betaine/carnitine/choline ABC superfamily ABC transporter, binding protein	0	0	3	7
F2MU67		Transcriptional regulator	0	0	6	6
F2MS22	proS	Proline--tRNA ligase	0	0	2	5
F2MMR4	pbp1B	Penicillin-binding protein 1B	0	0	3	4
F2MMV9		ABC superfamily ABC transporter, substrate-binding protein	0	0	3	4
xxxxxx		SagA-His6	0	0	3	4
F2MTQ3	atpD2	ATP synthase subunit beta	0	0	2	4
F2MMX1	pabC	Aminodeoxychorismate lyase	0	0	3	3

F2MNF9		Uncharacterized protein	0	0	3	3
F2MQM9	pepV	Dipeptidase PepV	0	0	3	3
F2MTH6		Uncharacterized protein	0	0	3	3
F2MP85	dkgB	2,5-diketo-D-gluconate reductase	0	0	2	3
F2MQ25		Uncharacterized protein	0	0	2	3
F2MRN8		Acyltransferase	0	0	2	3
F2MTE4	gap	Glyceraldehyde-3-phosphate dehydrogenase	0	0	2	3
F2MU19		S41A family carboxy-terminal peptidase	0	0	2	3
F2MM97	fusA	Elongation factor G	0	0	2	2
F2MNV5	chiC	Chitinase C1	0	0	2	2
F2MPG1	tpiA	Triosephosphate isomerase	0	0	2	2
F2MSG8	arcA	Arginine deiminase	0	0	2	2
F2MT41	glyA	Serine hydroxymethyltransferase	0	0	2	2
F2MPW0		Decarboxylase	10	28	0	0
F2MR04		Uncharacterized protein	9	17	0	0
F2MMN0	pstS	Phosphate ABC superfamily ABC transporter, binding protein	6	13	0	0
F2MT47		Fumarate reductase	6	9	0	0
F2MMK7	pyk	Pyruvate kinase	5	7	0	0
F2MQL2	rpoB	DNA-directed RNA polymerase subunit beta	4	7	0	0
F2MTJ8	tkt	Transketolase	3	7	0	0
F2MMA5	rplB	50S ribosomal protein L2	3	6	0	0
F2MP87	gloA5	Lactoylglutathione lyase	3	6	0	0
F2MQH1	ubiD	UbiD family decarboxylase	2	6	0	0
F2MU24	coaC	Phosphopantothenoylcysteine decarboxylase	2	6	0	0
F2MRI2	rplI	50S ribosomal protein L9	4	5	0	0
F2MRM7	clpP	ATP-dependent Clp protease proteolytic subunit	4	5	0	0
F2MRQ6	leuS	Leucine--tRNA ligase	3	5	0	0
F2MMX0	greA	Transcription elongation factor GreA	2	5	0	0

F2MNZ2	pcp	Pyrrolidone-carboxylate peptidase	2	5	0	0
F2MU79	rplK	50S ribosomal protein L11	2	5	0	0
F2MMN1	aspC2	Aminotransferase	3	4	0	0
F2MQK0		Choline binding protein	3	4	0	0
F2MQK6	rplM	50S ribosomal protein L13	2	4	0	0
F2MQV8		Gfo/Idh/MocA family oxidoreductase	2	4	0	0
F2MT73	infC	Translation initiation factor IF-3	2	4	0	0
F2MMA3	rplD	50S ribosomal protein L4	3	3	0	0
F2MQQ0	prsA	Foldase protein PrsA	3	3	0	0
F2MR57	pepS	Aminopeptidase PepS	2	3	0	0
F2MSC3	purR	Purine operon repressor	2	3	0	0
F2MM66	guaA	GMP synthase [glutamine-hydrolyzing]	2	2	0	0
F2MM95	rpsL	30S ribosomal protein S12	2	2	0	0
F2MMA1	rpsJ	30S ribosomal protein S10	2	2	0	0
F2MMA2	rplC	50S ribosomal protein L3	2	2	0	0
F2MMA6	rpsS	30S ribosomal protein S19	2	2	0	0
F2MMA8	rpsC	30S ribosomal protein S3	2	2	0	0
F2MMB9	rpsE	30S ribosomal protein S5	2	2	0	0
F2MMD3	rpmA	50S ribosomal protein L27	2	2	0	0
F2MNV0	pepC	Aminopeptidase C	2	2	0	0
F2MPA1	rplS	50S ribosomal protein L19	2	2	0	0
F2MQT1	fruA	PTS family fructose porter, IIABC component	2	2	0	0
F2MRX9	aceF	Pyruvate dehydrogenase complex E2, dihydrolipoamide acetyltransferase	2	2	0	0
F2MTV4	ppaC	Probable manganese-dependent inorganic pyrophosphatase	2	2	0	0
F2MU40	pepF	Oligoendopeptidase F	2	2	0	0
F2MUA4	celM	M42 family glutamyl aminopeptidase	2	2	0	0

REFERENCES.

1 Chung, H. *et al*. Gut immune maturation depends on colonization with a host-specific microbiota. *Cell* **149**, 1578-1593, doi:10.1016/j.cell.2012.04.037 (2012).

2 Caballero, S. & Pamer, E. G. Microbiota-Mediated Inflammation and Antimicrobial Defense in the Intestine. *Annu Rev Immunol*, doi:10.1146/annurev-immunol-032713-120238 (2015).

3 Kamada, N., Chen, G. Y., Inohara, N. & Nunez, G. Control of pathogens and pathobionts by the gut microbiota. *Nat Immunol* **14**, 685-690, doi:10.1038/ni.2608 (2013).

4 Kamada, N., Seo, S. U., Chen, G. Y. & Nunez, G. Role of the gut microbiota in immunity and inflammatory disease. *Nat Rev Immunol* **13**, 321-335, doi:10.1038/nri3430 (2013).

5 Human Microbiome Project, C. Structure, function and diversity of the healthy human microbiome. *Nature* **486**, 207-214, doi:10.1038/nature11234 (2012).

6 Shreiner, A., Huffnagle, G. B. & Noverr, M. C. The "Microflora Hypothesis" of allergic disease. *Adv Exp Med Biol* **635**, 113-134, doi:10.1007/978-0-387-09550-9_10 (2008).

7 Wen, L. *et al*. Innate immunity and intestinal microbiota in the development of Type 1 diabetes. *Nature* **455**, 1109-1113, doi:10.1038/nature07336 (2008).

8 Turnbaugh, P. J. *et al*. An obesity-associated gut microbiome with increased capacity for energy harvest. *Nature* **444**, 1027-1031, doi:10.1038/nature05414 (2006).

9 Nell, S., Suerbaum, S. & Josenhans, C. The impact of the microbiota on the pathogenesis of IBD: lessons from mouse infection models. *Nat Rev Microbiol* **8**, 564-577, doi:10.1038/nrmicro2403 (2010).

10 Sekirov, I. *et al*. Antibiotic-induced perturbations of the intestinal microbiota alter host susceptibility to enteric infection. *Infect Immun* **76**, 4726-4736, doi:10.1128/IAI.00319-08 (2008).

11 Endt, K. *et al*. The microbiota mediates pathogen clearance from the gut lumen after non-typhoidal Salmonella diarrhea. *PLoS Pathog* **6**, e1001097, doi:10.1371/journal.ppat.1001097 (2010).

12 Buffie, C. G. & Pamer, E. G. Microbiota-mediated colonization resistance against intestinal pathogens. *Nat Rev Immunol* **13**, 790-801, doi:10.1038/nri3535 (2013).

13 Chu, H. & Mazmanian, S. K. Innate immune recognition of the microbiota promotes host-microbial symbiosis. *Nat Immunol* **14**, 668-675, doi:10.1038/ni.2635 (2013).

14 Gantois, I. *et al*. Butyrate specifically down-regulates salmonella pathogenicity island 1 gene expression. *Appl Environ Microbiol* **72**, 946-949, doi:10.1128/AEM.72.1.946-949.2006 (2006).

15 Hung, C. C. *et al*. The intestinal fatty acid propionate inhibits Salmonella invasion through the post-translational control of HilD. *Mol Microbiol* **87**, 1045-1060, doi:10.1111/mmi.12149 (2013).

16 Lawhon, S. D., Maurer, R., Suyemoto, M. & Altier, C. Intestinal short-chain fatty acids alter Salmonella typhimurium invasion gene expression and virulence through BarA/SirA. *Mol Microbiol* **46**, 1451-1464 (2002).

17 Pacheco, A. R. *et al*. Fucose sensing regulates bacterial intestinal colonization. *Nature* **492**, 113-117, doi:10.1038/nature11623 (2012).

18 Buffie, C. G. *et al*. Precision microbiome reconstitution restores bile acid mediated resistance to Clostridium difficile. *Nature* **517**, 205-208, doi:10.1038/nature13828 (2015).

19 Lebeer, S., Vanderleyden, J. & De Keersmaecker, S. C. Genes and molecules of lactobacilli supporting probiotic action. *Microbiol Mol Biol Rev* **72**, 728-764, Table of Contents, doi:10.1128/MMBR.00017-08 (2008).

20 Kleerebezem, M. *et al*. The extracellular biology of the lactobacilli. *FEMS Microbiol Rev* **34**, 199-230, doi:10.1111/j.1574-6976.2010.00208.x (2010).

21 Peterson, L. W. & Artis, D. Intestinal epithelial cells: regulators of barrier function and immune homeostasis. *Nat Rev Immunol* **14**, 141-153, doi:10.1038/nri3608 (2014).

22 Johansson, M. E. *et al*. The inner of the two Muc2 mucin-dependent mucus layers in colon is devoid of bacteria. *Proc Natl Acad Sci U S A* **105**, 15064-15069, doi:10.1073/pnas.0803124105 (2008).

23 Ivanov, II *et al*. Induction of intestinal Th17 cells by segmented filamentous bacteria. *Cell* **139**, 485-498, doi:10.1016/j.cell.2009.09.033 (2009).

24 Mazmanian, S. K., Round, J. L. & Kasper, D. L. A microbial symbiosis factor prevents intestinal inflammatory disease. *Nature* **453**, 620-625, doi:10.1038/nature07008 (2008).

25 Round, J. L. & Mazmanian, S. K. Inducible Foxp3+ regulatory T-cell development by a commensal bacterium of the intestinal microbiota. *Proc Natl Acad Sci U S A* **107**, 12204-12209, doi:10.1073/pnas.0909122107 (2010).

26 Mazmanian, S. K., Liu, C. H., Tzianabos, A. O. & Kasper, D. L. An immunomodulatory molecule of symbiotic bacteria directs maturation of the host immune system. *Cell* **122**, 107-118, doi:10.1016/j.cell.2005.05.007 (2005).

27 Akira, S. & Takeda, K. Toll-like receptor signalling. *Nat Rev Immunol* **4**, 499-511, doi:10.1038/nri1391 (2004).

28 Philpott, D. J., Sorbara, M. T., Robertson, S. J., Croitoru, K. & Girardin, S. E. NOD proteins: regulators of inflammation in health and disease. *Nat Rev Immunol* **14**, 9-23, doi:10.1038/nri3565 (2014).

29 de Zoete, M. R. & Flavell, R. A. Interactions between Nod-Like Receptors and Intestinal Bacteria. *Front Immunol* **4**, 462, doi:10.3389/fimmu.2013.00462 (2013).

30 Dambuza, I. M. & Brown, G. D. C-type lectins in immunity: recent developments. *Curr Opin Immunol* **32C**, 21-27, doi:10.1016/j.coi.2014.12.002 (2015).

31 Rakoff-Nahoum, S., Paglino, J., Eslami-Varzaneh, F., Edberg, S. & Medzhitov, R. Recognition of commensal microflora by toll-like receptors is required for intestinal homeostasis. *Cell* **118**, 229-241, doi:10.1016/j.cell.2004.07.002 (2004).

32 Lebeer, S., Vanderleyden, J. & De Keersmaecker, S. C. Host interactions of probiotic bacterial surface molecules: comparison with commensals and pathogens. *Nat Rev Microbiol* **8**, 171-184, doi:10.1038/nrmicro2297 (2010).

33 Mohamadzadeh, M. *et al*. Regulation of induced colonic inflammation by Lactobacillus acidophilus deficient in lipoteichoic acid. *Proc Natl Acad Sci U S A* **108 Suppl 1**, 4623-4630, doi:10.1073/pnas.1005066107 (2011).

34 Grangette, C. *et al*. Enhanced antiinflammatory capacity of a Lactobacillus plantarum mutant synthesizing modified teichoic acids. *Proc Natl Acad Sci U S A* **102**, 10321-10326, doi:10.1073/pnas.0504084102 (2005).

35 Macho Fernandez, E. *et al*. Anti-inflammatory capacity of selected lactobacilli in experimental colitis is driven by NOD2-mediated recognition of a specific peptidoglycan-derived muropeptide. *Gut* **60**, 1050-1059, doi:10.1136/gut.2010.232918 (2011).

36 Kinnebrew, M. A. *et al*. Interleukin 23 production by intestinal CD103(+)CD11b(+) dendritic cells in response to bacterial flagellin enhances mucosal innate immune defense. *Immunity* **36**, 276-287, doi:10.1016/j.immuni.2011.12.011 (2012).

37 Kinnebrew, M. A. *et al*. Bacterial flagellin stimulates Toll-like receptor 5-dependent defense against vancomycin-resistant Enterococcus infection. *J Infect Dis* **201**, 534-543, doi:10.1086/650203 (2010).

38 Konstantinov, S. R. *et al*. S layer protein A of Lactobacillus acidophilus NCFM regulates immature dendritic cell and T cell functions. *Proc Natl Acad Sci U S A* **105**, 19474-19479, doi:10.1073/pnas.0810305105 (2008).

39 Petersson, J. *et al*. Importance and regulation of the colonic mucus barrier in a mouse model of colitis. *Am J Physiol Gastrointest Liver Physiol* **300**, G327-333, doi:10.1152/ajpgi.00422.2010 (2011).

40 Mack, D. R., Ahrne, S., Hyde, L., Wei, S. & Hollingsworth, M. A. Extracellular MUC3 mucin secretion follows adherence of Lactobacillus strains to intestinal epithelial cells in vitro. *Gut* **52**, 827-833 (2003).

41 Macpherson, A. J. & Uhr, T. Induction of protective IgA by intestinal dendritic cells carrying commensal bacteria. *Science* **303**, 1662-1665, doi:10.1126/science.1091334 (2004).

42 Bevins, C. L. & Salzman, N. H. Paneth cells, antimicrobial peptides and maintenance of intestinal homeostasis. *Nat Rev Microbiol* **9**, 356-368, doi:10.1038/nrmicro2546 (2011).

43 Cash, H. L., Whitham, C. V., Behrendt, C. L. & Hooper, L. V. Symbiotic bacteria direct expression of an intestinal bactericidal lectin. *Science* **313**, 1126-1130, doi:10.1126/science.1127119 (2006).

44 Vaishnava, S., Behrendt, C. L., Ismail, A. S., Eckmann, L. & Hooper, L. V. Paneth cells directly sense gut commensals and maintain homeostasis at the intestinal host-microbial interface. *Proc Natl Acad Sci U S A* **105**, 20858-20863, doi:10.1073/pnas.0808723105 (2008).

45 Vaishnava, S. *et al*. The antibacterial lectin RegIIIgamma promotes the spatial segregation of microbiota and host in the intestine. *Science* **334**, 255-258, doi:10.1126/science.1209791 (2011).

46 Schlee, M. *et al*. Induction of human beta-defensin 2 by the probiotic Escherichia coli Nissle 1917 is mediated through flagellin. *Infect Immun* **75**, 2399-2407, doi:10.1128/IAI.01563-06 (2007).

47 Wehkamp, J. *et al*. NF-kappaB- and AP-1-mediated induction of human beta defensin-2 in intestinal epithelial cells by Escherichia coli Nissle 1917: a novel effect of a probiotic bacterium. *Infect Immun* **72**, 5750-5758, doi:10.1128/IAI.72.10.5750-5758.2004 (2004).

48 Kobayashi, K. S. *et al*. Nod2-dependent regulation of innate and adaptive immunity in the intestinal tract. *Science* **307**, 731-734, doi:10.1126/science.1104911 (2005).

49 Anderson, R. C. *et al*. Lactobacillus plantarum MB452 enhances the function of the intestinal barrier by increasing the expression levels of genes involved in tight junction formation. *BMC Microbiol* **10**, 316, doi:10.1186/1471-2180-10-316 (2010).

50 Karczewski, J. *et al*. Regulation of human epithelial tight junction proteins by Lactobacillus plantarum in vivo and protective effects on the epithelial barrier. *Am J Physiol Gastrointest Liver Physiol* **298**, G851-859, doi:10.1152/ajpgi.00327.2009 (2010).

51 Qin, H., Zhang, Z., Hang, X. & Jiang, Y. L. plantarum prevents enteroinvasive Escherichia coli-induced tight junction proteins changes in intestinal epithelial cells. *BMC Microbiol* **9**, 63, doi:10.1186/1471-2180-9-63 (2009).

52 Bansal, T., Alaniz, R. C., Wood, T. K. & Jayaraman, A. The bacterial signal indole increases epithelial-cell tight-junction resistance and attenuates indicators of inflammation. *Proc Natl Acad Sci U S A* **107**, 228-233, doi:10.1073/pnas.0906112107 (2010).

53 Shimada, Y. *et al*. Commensal bacteria-dependent indole production enhances epithelial barrier function in the colon. *PLoS One* **8**, e80604, doi:10.1371/journal.pone.0080604 (2013).

54 Yan, F. *et al*. Soluble proteins produced by probiotic bacteria regulate intestinal epithelial cell survival and growth. *Gastroenterology* **132**, 562-575, doi:10.1053/j.gastro.2006.11.022 (2007).

55 Yan, F. & Polk, D. B. Characterization of a probiotic-derived soluble protein which reveals a mechanism of preventive and treatment effects of probiotics on intestinal inflammatory diseases. *Gut Microbes* **3**, 25-28, doi:10.4161/gmic.19245 (2012).

56 Fukuda, S. *et al*. Bifidobacteria can protect from enteropathogenic infection through production of acetate. *Nature* **469**, 543-547, doi:10.1038/nature09646 (2011).

57 Fukuda, S., Toh, H., Taylor, T. D., Ohno, H. & Hattori, M. Acetate-producing bifidobacteria protect the host from enteropathogenic infection via carbohydrate transporters. *Gut Microbes* **3**, 449-454, doi:10.4161/gmic.21214 (2012).

58 Atarashi, K. *et al*. ATP drives lamina propria T(H)17 cell differentiation. *Nature* **455**, 808-812, doi:10.1038/nature07240 (2008).

59 O'Mahony, C. *et al*. Commensal-induced regulatory T cells mediate protection against pathogen-stimulated NF-kappaB activation. *PLoS Pathog* **4**, e1000112, doi:10.1371/journal.ppat.1000112 (2008).

60 Kamada, N. *et al*. Regulated virulence controls the ability of a pathogen to compete with the gut microbiota. *Science* **336**, 1325-1329, doi:10.1126/science.1222195 (2012).

61 Maltby, R., Leatham-Jensen, M. P., Gibson, T., Cohen, P. S. & Conway, T. Nutritional basis for colonization resistance by human commensal Escherichia coli strains HS and Nissle 1917 against E. coli O157:H7 in the mouse intestine. *PLoS One* **8**, e53957, doi:10.1371/journal.pone.0053957 (2013).

62 Fischbach, M. A., Lin, H., Liu, D. R. & Walsh, C. T. How pathogenic bacteria evade mammalian sabotage in the battle for iron. *Nat Chem Biol* **2**, 132-138, doi:10.1038/nchembio771 (2006).

63 Raffatellu, M. *et al*. Lipocalin-2 resistance confers an advantage to Salmonella enterica serotype Typhimurium for growth and survival in the inflamed intestine. *Cell Host Microbe* **5**, 476-486, doi:10.1016/j.chom.2009.03.011 (2009).

64 Deriu, E. *et al*. Probiotic bacteria reduce salmonella typhimurium intestinal colonization by competing for iron. *Cell Host Microbe* **14**, 26-37, doi:10.1016/j.chom.2013.06.007 (2013).

65 Donia, M. S. *et al*. A systematic analysis of biosynthetic gene clusters in the human microbiome reveals a common family of antibiotics. *Cell* **158**, 1402-1414, doi:10.1016/j.cell.2014.08.032 (2014).

66 Cotter, P. D., Hill, C. & Ross, R. P. Bacteriocins: developing innate immunity for food. *Nat Rev Microbiol* **3**, 777-788, doi:10.1038/nrmicro1273 (2005).

67 Bron, P. A., Grangette, C., Mercenier, A., de Vos, W. M. & Kleerebezem, M. Identification of Lactobacillus plantarum genes that are induced in the

gastrointestinal tract of mice. *J Bacteriol* **186**, 5721-5729, doi:10.1128/JB.186.17.5721-5729.2004 (2004).

68 Corr, S. C. *et al*. Bacteriocin production as a mechanism for the antiinfective activity of Lactobacillus salivarius UCC118. *Proc Natl Acad Sci U S A* **104**, 7617-7621, doi:10.1073/pnas.0700440104 (2007).

69 Rea, M. C. *et al*. Effect of broad- and narrow-spectrum antimicrobials on Clostridium difficile and microbial diversity in a model of the distal colon. *Proc Natl Acad Sci U S A* **108 Suppl 1**, 4639-4644, doi:10.1073/pnas.1001224107 (2011).

70 Rea, M. C. *et al*. Thuricin CD, a posttranslationally modified bacteriocin with a narrow spectrum of activity against Clostridium difficile. *Proc Natl Acad Sci U S A* **107**, 9352-9357, doi:10.1073/pnas.0913554107 (2010).

71 Marteyn, B. *et al*. Modulation of Shigella virulence in response to available oxygen in vivo. *Nature* **465**, 355-358, doi:10.1038/nature08970 (2010).

72 Kankainen, M. *et al*. Comparative genomic analysis of Lactobacillus rhamnosus GG reveals pili containing a human-mucus binding protein. *Proc Natl Acad Sci U S A* **106**, 17193-17198, doi:DOI 10.1073/pnas.0908876106 (2009).

73 Asahara, T. *et al*. Probiotic bifidobacteria protect mice from lethal infection with Shiga toxin-producing Escherichia coli O157:H7. *Infect Immun* **72**, 2240-2247 (2004).

74 de Sablet, T. *et al*. Human microbiota-secreted factors inhibit shiga toxin synthesis by enterohemorrhagic Escherichia coli O157:H7. *Infect Immun* **77**, 783-790, doi:10.1128/IAI.01048-08 (2009).

75 Ferreyra, J. A. *et al*. Gut microbiota-produced succinate promotes C. difficile infection after antibiotic treatment or motility disturbance. *Cell Host Microbe* **16**, 770-777, doi:10.1016/j.chom.2014.11.003 (2014).

76 Curtis, M. M. *et al*. The gut commensal bacteroides thetaiotaomicron exacerbates enteric infection through modification of the metabolic landscape. *Cell Host Microbe* **16**, 759-769, doi:10.1016/j.chom.2014.11.005 (2014).

77 Soares, J. A. & Ahmer, B. M. Detection of acyl-homoserine lactones by Escherichia and Salmonella. *Curr Opin Microbiol* **14**, 188-193, doi:10.1016/j.mib.2011.01.006 (2011).

78 Swearingen, M. C., Sabag-Daigle, A. & Ahmer, B. M. Are there acyl-homoserine lactones within mammalian intestines? *J Bacteriol* **195**, 173-179, doi:10.1128/JB.01341-12 (2013).

79 Hughes, D. T. *et al*. Chemical sensing in mammalian host-bacterial commensal associations. *Proc Natl Acad Sci U S A* **107**, 9831-9836, doi:10.1073/pnas.1002551107 (2010).

80 Dyszel, J. L. *et al*. Salmonella enterica serovar Typhimurium can detect acyl homoserine lactone production by Yersinia enterocolitica in mice. *J Bacteriol* **192**, 29-37, doi:10.1128/JB.01139-09 (2010).

81 Smith, J. N. *et al*. SdiA, an N-acylhomoserine lactone receptor, becomes active during the transit of Salmonella enterica through the gastrointestinal tract of turtles. *PLoS One* **3**, e2826, doi:10.1371/journal.pone.0002826 (2008).

82 Thompson, J. A., Oliveira, R. A., Djukovic, A., Ubeda, C. & Xavier, K. B. Manipulation of the Quorum Sensing Signal AI-2 Affects the Antibiotic-Treated Gut Microbiota. *Cell Rep*, doi:10.1016/j.celrep.2015.02.049 (2015).

83 Fabich, A. J. *et al*. Comparison of carbon nutrition for pathogenic and commensal Escherichia coli strains in the mouse intestine. *Infect Immun* **76**, 1143-1152, doi:10.1128/IAI.01386-07 (2008).

84 Lupp, C. *et al*. Host-mediated inflammation disrupts the intestinal microbiota and promotes the overgrowth of Enterobacteriaceae. *Cell Host Microbe* **2**, 204 (2007).

85 Winter, S. E. *et al*. Gut inflammation provides a respiratory electron acceptor for Salmonella. *Nature* **467**, 426-429, doi:10.1038/nature09415 (2010).

86 Thiennimitr, P. *et al*. Intestinal inflammation allows Salmonella to use ethanolamine to compete with the microbiota. *Proc Natl Acad Sci U S A* **108**, 17480-17485, doi:10.1073/pnas.1107857108 (2011).

87 Bertin, Y. *et al*. Enterohaemorrhagic Escherichia coli gains a competitive advantage by using ethanolamine as a nitrogen source in the bovine intestinal content. *Environ Microbiol* **13**, 365-377, doi:10.1111/j.1462-2920.2010.02334.x (2011).

88 Garsin, D. A. Ethanolamine utilization in bacterial pathogens: roles and regulation. *Nat Rev Microbiol* **8**, 290-295, doi:10.1038/nrmicro2334 (2010).

89 Winter, S. E. *et al*. Host-derived nitrate boosts growth of E. coli in the inflamed gut. *Science* **339**, 708-711, doi:10.1126/science.1232467 (2013).

90 Nedialkova, L. P. *et al*. Inflammation fuels colicin Ib-dependent competition of Salmonella serovar Typhimurium and E. coli in enterobacterial blooms. *PLoS Pathog* **10**, e1003844, doi:10.1371/journal.ppat.1003844 (2014).

91 MacIntyre, D. L., Miyata, S. T., Kitaoka, M. & Pukatzki, S. The Vibrio cholerae type VI secretion system displays antimicrobial properties. *Proc Natl Acad Sci U S A* **107**, 19520-19524, doi:10.1073/pnas.1012931107 (2010).

92 Fu, Y., Waldor, M. K. & Mekalanos, J. J. Tn-Seq analysis of Vibrio cholerae intestinal colonization reveals a role for T6SS-mediated antibacterial activity in the host. *Cell Host Microbe* **14**, 652-663, doi:10.1016/j.chom.2013.11.001 (2013).

93 Cummings, J. H., Pomare, E. W., Branch, W. J., Naylor, C. P. & Macfarlane, G. T. Short chain fatty acids in human large intestine, portal, hepatic and venous blood. *Gut* **28**, 1221-1227 (1987).

94 Verger, R. *et al*. Regulation of lumen fat digestion: enzymic aspects. *Proc Nutr Soc* **55**, 5-18 (1996).

95 Eisenreich, W., Dandekar, T., Heesemann, J. & Goebel, W. Carbon metabolism of intracellular bacterial pathogens and possible links to virulence. *Nat Rev Microbiol* **8**, 401-412, doi:10.1038/nrmicro2351 (2010).

96 Steeb, B. *et al*. Parallel exploitation of diverse host nutrients enhances Salmonella virulence. *PLoS Pathog* **9**, e1003301, doi:10.1371/journal.ppat.1003301 (2013).

97 Becker, D. *et al*. Robust Salmonella metabolism limits possibilities for new antimicrobials. *Nature* **440**, 303-307, doi:10.1038/nature04616 (2006).

98 Haraga, A., Ohlson, M. B. & Miller, S. I. Salmonellae interplay with host cells. *Nat Rev Microbiol* **6**, 53-66, doi:10.1038/nrmicro1788 (2008).

99 Fass, E. & Groisman, E. A. Control of Salmonella pathogenicity island-2 gene expression. *Curr Opin Microbiol* **12**, 199-204, doi:10.1016/j.mib.2009.01.004 (2009).

100 Buddelmeijer, N. The molecular mechanism of bacterial lipoprotein modification-How, when and why? *FEMS Microbiol Rev* **39**, 246-261, doi:10.1093/femsre/fuu006 (2015).

101 Nakayama, H., Kurokawa, K. & Lee, B. L. Lipoproteins in bacteria: structures and biosynthetic pathways. *FEBS J* **279**, 4247-4268, doi:10.1111/febs.12041 (2012).

102 Kovacs-Simon, A., Titball, R. W. & Michell, S. L. Lipoproteins of bacterial pathogens. *Infect Immun* **79**, 548-561, doi:10.1128/IAI.00682-10 (2011).

103 Stanley, P., Koronakis, V. & Hughes, C. Acylation of Escherichia coli hemolysin: a unique protein lipidation mechanism underlying toxin function. *Microbiol Mol Biol Rev* **62**, 309-333 (1998).

104 Jones, J. D. & O'Connor, C. D. Protein acetylation in prokaryotes. *Proteomics* **11**, 3012-3022, doi:10.1002/pmic.201000812 (2011).

105 Hu, L. I., Lima, B. P. & Wolfe, A. J. Bacterial protein acetylation: the dawning of a new age. *Mol Microbiol* **77**, 15-21, doi:10.1111/j.1365-2958.2010.07204.x (2010).

106 Grammel, M. & Hang, H. C. Chemical reporters for biological discovery. *Nat Chem Biol* **9**, 475-484, doi:10.1038/nchembio.1296 (2013).

107 Hirano, Y., Hossain, M. M., Takeda, K., Tokuda, H. & Miki, K. Structural studies of the Cpx pathway activator NlpE on the outer membrane of Escherichia coli. *Structure* **15**, 963-976, doi:10.1016/j.str.2007.06.014 (2007).

108 Yang, Y. Y., Grammel, M., Raghavan, A. S., Charron, G. & Hang, H. C. Comparative analysis of cleavable azobenzene-based affinity tags for bioorthogonal chemical proteomics. *Chem Biol* **17**, 1212-1222, doi:10.1016/j.chembiol.2010.09.012 (2010).

109 Yang, Y. Y. & Hang, H. C. Chemical approaches for the detection and synthesis of acetylated proteins. *Chembiochem* **12**, 314-322, doi:10.1002/cbic.201000558 (2011).

110 Juncker, A. S. *et al*. Prediction of lipoprotein signal peptides in Gram-negative bacteria. *Protein Sci* **12**, 1652-1662, doi:10.1110/ps.0303703 (2003).

111 Christopherson, M. R., Schmitz, G. E. & Downs, D. M. YjgF is required for isoleucine biosynthesis when Salmonella enterica is grown on pyruvate medium. *J Bacteriol* **190**, 3057-3062, doi:10.1128/JB.01700-07 (2008).

112 Yount, J. S., Charron, G. & Hang, H. C. Bioorthogonal proteomics of 15-hexadecynyloxyacetic acid chemical reporter reveals preferential targeting of fatty acid modified proteins and biosynthetic enzymes. *Bioorg Med Chem* **20**, 650-654, doi:10.1016/j.bmc.2011.03.062 (2012).

113 Ray, T. K. & Cronan, J. E. Acylation of Sn-Glycerol 3-Phosphate in Escherichia-Coli - Study of Reaction with Native Palmitoyl-Acyl Carrier Protein. *Journal of Biological Chemistry* **250**, 8422-8427 (1975).

114 Volz, K. A test case for structure-based functional assignment: the 1.2 A crystal structure of the yjgF gene product from Escherichia coli. *Protein Sci* **8**, 2428-2437, doi:10.1110/ps.8.11.2428 (1999).

115 Burman, J. D., Stevenson, C. E., Sawers, R. G. & Lawson, D. M. The crystal structure of Escherichia coli TdcF, a member of the highly conserved YjgF/YER057c/UK114 family. *BMC Struct Biol* **7**, 30, doi:10.1186/1472-6807-7-30 (2007).

116 Knapik, A. A. *et al*. Structure of Escherichia coli RutC, a member of the YjgF family and putative aminoacrylate peracid reductase of the rut operon. *Acta Crystallogr Sect F Struct Biol Cryst Commun* **68**, 1294-1299, doi:10.1107/S1744309112041796 (2012).

117 Parsons, L. *et al*. Solution structure and functional ligand screening of HI0719, a highly conserved protein from bacteria to humans in the YjgF/YER057c/UK114 family. *Biochemistry* **42**, 80-89, doi:10.1021/bi020541w (2003).

118 Lambrecht, J. A., Flynn, J. M. & Downs, D. M. Conserved YjgF protein family deaminates reactive enamine/imine intermediates of pyridoxal 5'-phosphate (PLP)-dependent enzyme reactions. *J Biol Chem* **287**, 3454-3461, doi:10.1074/jbc.M111.304477 (2012).

119 Lambrecht, J. A., Schmitz, G. E. & Downs, D. M. RidA proteins prevent metabolic damage inflicted by PLP-dependent dehydratases in all domains of life. *MBio* **4**, e00033-00013, doi:10.1128/mBio.00033-13 (2013).

120 Charron, G. *et al*. Robust fluorescent detection of protein fatty-acylation with chemical reporters. *J Am Chem Soc* **131**, 4967-4975, doi:10.1021/ja810122f (2009).

121 LaRock, D. L., Chaudhary, A. & Miller, S. I. Salmonellae interactions with host processes. *Nat Rev Microbiol* **13**, 191-205, doi:10.1038/nrmicro3420 (2015).

122 Watson, K. G. & Holden, D. W. Dynamics of growth and dissemination of Salmonella in vivo. *Cell Microbiol* **12**, 1389-1397, doi:10.1111/j.1462-5822.2010.01511.x (2010).

123 Jepson, M. A., Collares-Buzato, C. B., Clark, M. A., Hirst, B. H. & Simmons, N. L. Rapid disruption of epithelial barrier function by Salmonella typhimurium is associated with structural modification of intercellular junctions. *Infect Immun* **63**, 356-359 (1995).

124 Ellermeier, J. R. & Slauch, J. M. Adaptation to the host environment: regulation of the SPI1 type III secretion system in Salmonella enterica serovar Typhimurium. *Curr Opin Microbiol* **10**, 24-29, doi:10.1016/j.mib.2006.12.002 (2007).

125 Kato, A., Groisman, E. A. & Howard Hughes Medical, I. The PhoQ/PhoP regulatory network of Salmonella enterica. *Adv Exp Med Biol* **631**, 7-21 (2008).

126 Dalebroux, Z. D. & Miller, S. I. Salmonellae PhoPQ regulation of the outer membrane to resist innate immunity. *Curr Opin Microbiol* **17**, 106-113, doi:10.1016/j.mib.2013.12.005 (2014).

127 Bijlsma, J. J. E. & Groisman, E. A. The PhoP/PhoQ system controls the intramacrophage type three secretion system of Salmonella enterica. *Mol Microbiol* **57**, 85-96, doi:DOI 10.1111/j.1365-2958.2005.04668.x (2005).

128 Bajaj, V., Lucas, R. L., Hwang, C. & Lee, C. A. Co-ordinate regulation of Salmonella typhimurium invasion genes by environmental and regulatory factors is mediated by control of hilA expression. *Mol Microbiol* **22**, 703-714 (1996).

129 Behlau, I. & Miller, S. I. A PhoP-repressed gene promotes Salmonella typhimurium invasion of epithelial cells. *J Bacteriol* **175**, 4475-4484 (1993).

130 Perez, J. C. *et al*. Evolution of a bacterial regulon controlling virulence and Mg(2+) homeostasis. *PLoS Genet* **5**, e1000428, doi:10.1371/journal.pgen.1000428 (2009).

131 Viarengo, G. *et al*. Unsaturated long chain free fatty acids are input signals of the Salmonella enterica PhoP/PhoQ regulatory system. *J Biol Chem* **288**, 22346-22358, doi:10.1074/jbc.M113.472829 (2013).

132 Yu, B. J., Kim, J. A., Moon, J. H., Ryu, S. E. & Pan, J. G. The diversity of lysine-acetylated proteins in Escherichia coli. *J Microbiol Biotechnol* **18**, 1529-1536 (2008).

133 Zhang, J. *et al*. Lysine acetylation is a highly abundant and evolutionarily conserved modification in Escherichia coli. *Mol Cell Proteomics* **8**, 215-225, doi:10.1074/mcp.M800187-MCP200 (2009).

134 Wang, Q. *et al*. Acetylation of metabolic enzymes coordinates carbon source utilization and metabolic flux. *Science* **327**, 1004-1007, doi:10.1126/science.1179687 (2010).

135 Kuhn, M. L. *et al*. Structural, kinetic and proteomic characterization of acetyl phosphate-dependent bacterial protein acetylation. *PLoS One* **9**, e94816, doi:10.1371/journal.pone.0094816 (2014).

136 Thao, S., Chen, C. S., Zhu, H. & Escalante-Semerena, J. C. Nepsilon-lysine acetylation of a bacterial transcription factor inhibits Its DNA-binding activity. *PLoS One* **5**, e15123, doi:10.1371/journal.pone.0015123 (2010).

137 Garrity, J., Gardner, J. G., Hawse, W., Wolberger, C. & Escalante-Semerena, J. C. N-lysine propionylation controls the activity of propionyl-CoA synthetase. *J Biol Chem* **282**, 30239-30245, doi:10.1074/jbc.M704409200 (2007).

138 Peng, C. *et al*. The first identification of lysine malonylation substrates and its regulatory enzyme. *Mol Cell Proteomics* **10**, M111 012658, doi:10.1074/mcp.M111.012658 (2011).

139 Colak, G. *et al*. Identification of lysine succinylation substrates and the succinylation regulatory enzyme CobB in Escherichia coli. *Mol Cell Proteomics* **12**, 3509-3520, doi:10.1074/mcp.M113.031567 (2013).

140 Weinert, B. T. *et al*. Lysine succinylation is a frequently occurring modification in prokaryotes and eukaryotes and extensively overlaps with acetylation. *Cell Rep* **4**, 842-851, doi:10.1016/j.celrep.2013.07.024 (2013).

141 Zhang, Z. *et al*. Identification of lysine succinylation as a new post-translational modification. *Nat Chem Biol* **7**, 58-63, doi:10.1038/nchembio.495 (2011).

142 Weinert, B. T. *et al*. Acetyl-phosphate is a critical determinant of lysine acetylation in E. coli. *Mol Cell* **51**, 265-272, doi:10.1016/j.molcel.2013.06.003 (2013).

143 AbouElfetouh, A. *et al*. The E. coli sirtuin CobB shows no preference for enzymatic and nonenzymatic lysine acetylation substrate sites. *Microbiologyopen* **4**, 66-83, doi:10.1002/mbo3.223 (2015).

144 Beuzon, C. R., Banks, G., Deiwick, J., Hensel, M. & Holden, D. W. pH-dependent secretion of SseB, a product of the SPI-2 type III secretion system of Salmonella typhimurium. *Mol Microbiol* **33**, 806-816 (1999).

145 Lee, E. J., Pontes, M. H. & Groisman, E. A. A bacterial virulence protein promotes pathogenicity by inhibiting the bacterium's own F1Fo ATP synthase. *Cell* **154**, 146-156, doi:10.1016/j.cell.2013.06.004 (2013).

146 Soncini, F. C., Garcia Vescovi, E., Solomon, F. & Groisman, E. A. Molecular basis of the magnesium deprivation response in Salmonella typhimurium: identification of PhoP-regulated genes. *J Bacteriol* **178**, 5092-5099 (1996).

147 Zwir, I., Latifi, T., Perez, J. C., Huang, H. & Groisman, E. A. The promoter architectural landscape of the Salmonella PhoP regulon. *Mol Microbiol* **84**, 463-485, doi:10.1111/j.1365-2958.2012.08036.x (2012).

148 Yount, J. S. *et al*. Visible fluorescence detection of type III protein secretion from bacterial pathogens. *J Am Chem Soc* **132**, 8244-8245, doi:10.1021/ja102257v (2010).

149 Groisman, E. A., Kayser, J. & Soncini, F. C. Regulation of polymyxin resistance and adaptation to low-Mg2+ environments. *J Bacteriol* **179**, 7040-7045 (1997).

150 Stecher, B., Maier, L. & Hardt, W. D. 'Blooming' in the gut: how dysbiosis might contribute to pathogen evolution. *Nat Rev Microbiol* **11**, 277-284, doi:10.1038/nrmicro2989 (2013).

151 Keeney, K. M., Yurist-Doutsch, S., Arrieta, M. C. & Finlay, B. B. Effects of antibiotics on human microbiota and subsequent disease. *Annu Rev Microbiol* **68**, 217-235, doi:10.1146/annurev-micro-091313-103456 (2014).

152 Mattila, E. *et al*. Fecal transplantation, through colonoscopy, is effective therapy for recurrent Clostridium difficile infection. *Gastroenterology* **142**, 490-496, doi:10.1053/j.gastro.2011.11.037 (2012).

153 van Nood, E. *et al*. Duodenal infusion of donor feces for recurrent Clostridium difficile. *N Engl J Med* **368**, 407-415, doi:10.1056/NEJMoa1205037 (2013).

154 Irazoqui, J. E., Urbach, J. M. & Ausubel, F. M. Evolution of host innate defence: insights from Caenorhabditis elegans and primitive invertebrates. *Nat Rev Immunol* **10**, 47-58, doi:10.1038/nri2689 (2010).

155 Pukkila-Worley, R. & Ausubel, F. M. Immune defense mechanisms in the Caenorhabditis elegans intestinal epithelium. *Curr Opin Immunol* **24**, 3-9, doi:10.1016/j.coi.2011.10.004 (2012).

156 Irazoqui, J. E. *et al*. Distinct pathogenesis and host responses during infection of C. elegans by P. aeruginosa and S. aureus. *PLoS Pathog* **6**, e1000982, doi:10.1371/journal.ppat.1000982 (2010).

157 Pukkila-Worley, R., Ausubel, F. M. & Mylonakis, E. Candida albicans infection of Caenorhabditis elegans induces antifungal immune defenses. *PLoS Pathog* **7**, e1002074, doi:10.1371/journal.ppat.1002074 (2011).

158 Schulenburg, H. & Ewbank, J. J. The genetics of pathogen avoidance in Caenorhabditis elegans. *Mol Microbiol* **66**, 563-570, doi:10.1111/j.1365-2958.2007.05946.x (2007).

159 Schulenburg, H., Hoeppner, M. P., Weiner, J., 3rd & Bornberg-Bauer, E. Specificity of the innate immune system and diversity of C-type lectin domain (CTLD) proteins in the nematode Caenorhabditis elegans. *Immunobiology* **213**, 237-250, doi:10.1016/j.imbio.2007.12.004 (2008).

160 Aballay, A., Yorgey, P. & Ausubel, F. M. Salmonella typhimurium proliferates and establishes a persistent infection in the intestine of Caenorhabditis elegans. *Curr Biol* **10**, 1539-1542 (2000).

161 Labrousse, A., Chauvet, S., Couillault, C., Kurz, C. L. & Ewbank, J. J. Caenorhabditis elegans is a model host for Salmonella typhimurium. *Curr Biol* **10**, 1543-1545 (2000).

162 Stecher, B. *et al*. Salmonella enterica serovar typhimurium exploits inflammation to compete with the intestinal microbiota. *PLoS Biol* **5**, 2177-2189, doi:10.1371/journal.pbio.0050244 (2007).

163 Tenor, J. L., McCormick, B. A., Ausubel, F. M. & Aballay, A. Caenorhabditis elegans-based screen identifies Salmonella virulence factors required for conserved host-pathogen interactions. *Curr Biol* **14**, 1018-1024, doi:10.1016/j.cub.2004.05.050 (2004).

164 Jia, K. *et al*. Autophagy genes protect against Salmonella typhimurium infection and mediate insulin signaling-regulated pathogen resistance. *Proc Natl Acad Sci U S A* **106**, 14564-14569, doi:10.1073/pnas.0813319106 (2009).

165 McGhee, J. D. The C. elegans intestine. *WormBook*, 1-36, doi:10.1895/wormbook.1.133.1 (2007).

166 Labouesse, M. Epithelial junctions and attachments. *WormBook*, 1-21, doi:10.1895/wormbook.1.56.1 (2006).

167 Borgonie, G., Claeys, M., Vanfleteren, J., Dewaele, D. & Coomans, A. Presence of Peritrophic-Like Membranes in the Intestine of 3 Bacteriophagous Nematodes (Nematoda, Rhabditida). *Fund Appl Nematol* **18**, 227-233 (1995).

168 Borgonie, G. *et al*. Internal lectin binding patterns in the nematodes Caenorhabditis elegans, Panagrolaimus superbus and Acrobeloides maximus. *Fund Appl Nematol* **20**, 173-186 (1997).

169 Schimpf, J., Sames, K. & Zwilling, R. Proteoglycan distribution pattern during aging in the nematode Caenorhabditis elegans: An ultrastructural histochemical study. *Histochem J* **31**, 285-292, doi:Doi 10.1023/A:1003761817109 (1999).

170 Kramer, J. M. Basement membranes. *WormBook*, 1-15, doi:10.1895/wormbook.1.16.1 (2005).

171 Chauhan, V. M., Orsi, G., Brown, A., Pritchard, D. I. & Aylott, J. W. Mapping the Pharyngeal and Intestinal pH of Caenorhabditis elegans and Real-Time Luminal pH Oscillations Using Extended Dynamic Range pH-Sensitive Nanosensors. *Acs Nano* **7**, 5577-5587, doi:DOI 10.1021/nn401856u (2013).

172 Stiernagle, T. Maintenance of C. elegans. *WormBook*, 1-11, doi:10.1895/wormbook.1.101.1 (2006).

173 Felix, M. A. & Duveau, F. Population dynamics and habitat sharing of natural populations of Caenorhabditis elegans and C. briggsae. *BMC Biol* **10**, 59, doi:10.1186/1741-7007-10-59 (2012).

174 Garsin, D. A. *et al*. A simple model host for identifying Gram-positive virulence factors. *Proc Natl Acad Sci U S A* **98**, 10892-10897, doi:10.1073/pnas.191378698 (2001).

175 Lebreton, F., Willems, R. J. L. & Gilmore, M. S. in *Enterococci: From Commensals to Leading Causes of Drug Resistant Infection* (eds M. S. Gilmore, D. B. Clewell, Y. Ike, & N. Shankar) (2014).

176 Gilmore, M. S., Lebreton, F. & van Schaik, W. Genomic transition of enterococci from gut commensals to leading causes of multidrug-resistant hospital infection in the antibiotic era. *Curr Opin Microbiol* **16**, 10-16, doi:10.1016/j.mib.2013.01.006 (2013).

177 Staley, C., Dunny, G. M. & Sadowsky, M. J. Environmental and animal-associated enterococci. *Adv Appl Microbiol* **87**, 147-186, doi:10.1016/B978-0-12-800261-2.00004-9 (2014).

178 Tetlock, A., Yost, C. K., Stavrinides, J. & Manzon, R. G. Changes in the Gut Microbiome of the Sea Lamprey during Metamorphosis. *Appl Environ Microbiol* **78**, 7638-7644, doi:Doi 10.1128/Aem.01640-12 (2012).

179 Charrier, M., Combet-Blanc, Y. & Ollivier, B. Bacterial flora in the gut of Helix aspersa (Gastropoda Pulmonata): evidence for a permanent population with a dominant homolactic intestinal bacterium, Enterococcus casseliflavus. *Can J Microbiol* **44**, 20-27, doi:DOI 10.1139/cjm-44-1-20 (1998).

180 Hayashi, H., Takahashi, R., Nishi, T., Sakamoto, M. & Benno, Y. Molecular analysis of jejunal, ileal, caecal and recto-sigmoidal human colonic microbiota using 16S rRNA gene libraries and terminal restriction fragment length

polymorphism. *J Med Microbiol* **54**, 1093-1101, doi:10.1099/jmm.0.45935-0 (2005).

181 Tannock, G. W. & Cook, G. *The Enterococci: Pathogenesis, Molecular Biology, and Antibiotic Resistance*. 101-132 (ASM Press, 2002).

182 Maia, O. B., Duarte, R., Silva, A. M., Cara, D. C. & Nicoli, J. R. Evaluation of the components of a commercial probiotic in gnotobiotic mice experimentally challenged with Salmonella enterica subsp. enterica ser. Typhimurium. *Vet Microbiol* **79**, 183-189 (2001).

183 Franz, C. M., van Belkum, M. J., Holzapfel, W. H., Abriouel, H. & Galvez, A. Diversity of enterococcal bacteriocins and their grouping in a new classification scheme. *FEMS Microbiol Rev* **31**, 293-310, doi:10.1111/j.1574-6976.2007.00064.x (2007).

184 Cao, G. T. *et al*. Effects of a probiotic, Enterococcus faecium, on growth performance, intestinal morphology, immune response, and cecal microflora in broiler chickens challenged with Escherichia coli K88. *Poult Sci* **92**, 2949-2955, doi:10.3382/ps.2013-03366 (2013).

185 Jin, L. Z., Marquardt, R. R. & Zhao, X. A strain of Enterococcus faecium (18C23) inhibits adhesion of enterotoxigenic Escherichia coli K88 to porcine small intestine mucus. *Appl Environ Microbiol* **66**, 4200-4204 (2000).

186 Top, J., Willems, R. & Bonten, M. Emergence of CC17 Enterococcus faecium: from commensal to hospital-adapted pathogen. *FEMS Immunol Med Microbiol* **52**, 297-308, doi:10.1111/j.1574-695X.2008.00383.x (2008).

187 Arias, C. A. & Murray, B. E. The rise of the Enterococcus: beyond vancomycin resistance. *Nat Rev Microbiol* **10**, 266-278, doi:10.1038/nrmicro2761 (2012).

188 Powell, J. R. & Ausubel, F. M. Models of Caenorhabditis elegans infection by bacterial and fungal pathogens. *Methods Mol Biol* **415**, 403-427, doi:10.1007/978-1-59745-570-1_24 (2008).

189 Lebreton, F. *et al*. Emergence of epidemic multidrug-resistant Enterococcus faecium from animal and commensal strains. *MBio* **4**, doi:10.1128/mBio.00534-13 (2013).

190 Palmer, K. L. *et al*. Comparative genomics of enterococci: variation in Enterococcus faecalis, clade structure in E. faecium, and defining characteristics of E. gallinarum and E. casseliflavus. *MBio* **3**, e00318-00311, doi:10.1128/mBio.00318-11 (2012).

191 Knodler, L. A. *et al*. Cloning vectors and fluorescent proteins can significantly inhibit Salmonella enterica virulence in both epithelial cells and macrophages: Implications for bacterial pathogenesis studies. *Infect Immun* **73**, 7027-7031, doi:Doi 10.1128/Iai.73.10.7027-7031.2005 (2005).

192 Teng, F., Kawalec, M., Weinstock, G. M., Hryniewicz, W. & Murray, B. E. An Enterococcus faecium secreted antigen, SagA, exhibits broad-spectrum binding to extracellular matrix proteins and appears essential for E. faecium growth. *Infect Immun* **71**, 5033-5041 (2003).

193 Anantharaman, V. & Aravind, L. Evolutionary history, structural features and biochemical diversity of the NlpC/P60 superfamily of enzymes. *Genome Biol* **4**, R11 (2003).

194 Bartual, S. G. *et al*. Structural basis of PcsB-mediated cell separation in Streptococcus pneumoniae. *Nat Commun* **5**, 3842, doi:10.1038/ncomms4842 (2014).

195 Tuteja, R. Type I signal peptidase: an overview. *Arch Biochem Biophys* **441**, 107-111, doi:10.1016/j.abb.2005.07.013 (2005).

196 Rolain, T. *et al*. O-glycosylation as a novel control mechanism of peptidoglycan hydrolase activity. *J Biol Chem* **288**, 22233-22247, doi:10.1074/jbc.M113.470716 (2013).

197 Alegado, R. A. & Tan, M. W. Resistance to antimicrobial peptides contributes to persistence of Salmonella typhimurium in the C. elegans intestine. *Cell Microbiol* **10**, 1259-1273, doi:10.1111/j.1462-5822.2008.01124.x (2008).

198 Sahu, S. N. *et al*. Identification of virulence properties in Salmonella Typhimurium DT104 using Caenorhabditis elegans. *PLoS One* **8**, e76673, doi:10.1371/journal.pone.0076673 (2013).

199 Royet, J. & Dziarski, R. Peptidoglycan recognition proteins: pleiotropic sensors and effectors of antimicrobial defences. *Nat Rev Microbiol* **5**, 264-277, doi:10.1038/nrmicro1620 (2007).

200 Dworkin, J. The medium is the message: interspecies and interkingdom signaling by peptidoglycan and related bacterial glycans. *Annu Rev Microbiol* **68**, 137-154, doi:10.1146/annurev-micro-091213-112844 (2014).

201 Johnson, J. W., Fisher, J. F. & Mobashery, S. Bacterial cell-wall recycling. *Ann N Y Acad Sci* **1277**, 54-75, doi:10.1111/j.1749-6632.2012.06813.x (2013).

202 Goodell, E. W. & Schwarz, U. Release of cell wall peptides into culture medium by exponentially growing Escherichia coli. *J Bacteriol* **162**, 391-397 (1985).

203 Mauck, J., Chan, L. & Glaser, L. Turnover of the cell wall of Gram-positive bacteria. *J Biol Chem* **246**, 1820-1827 (1971).

204 Li, S. Y., Holtje, J. V. & Young, K. D. Comparison of high-performance liquid chromatography and fluorophore-assisted carbohydrate electrophoresis methods for analyzing peptidoglycan composition of Escherichia coli. *Anal Biochem* **326**, 1-12, doi:10.1016/j.ab.2003.11.007 (2004).

205 Young, K. D. A simple gel electrophoretic method for analyzing the muropeptide composition of bacterial peptidoglycan. *J Bacteriol* **178**, 3962-3966 (1996).

206 Kim, D. H. *et al*. A conserved p38 MAP kinase pathway in Caenorhabditis elegans innate immunity. *Science* **297**, 623-626, doi:10.1126/science.1073759 (2002).

207 Troemel, E. R. *et al*. p38 MAPK regulates expression of immune response genes and contributes to longevity in C. elegans. *PLoS Genet* **2**, e183, doi:10.1371/journal.pgen.0020183 (2006).

208 Mallo, G. V. *et al*. Inducible antibacterial defense system in C. elegans. *Curr Biol* **12**, 1209-1214 (2002).

209 Zugasti, O. & Ewbank, J. J. Neuroimmune regulation of antimicrobial peptide expression by a noncanonical TGF-beta signaling pathway in Caenorhabditis elegans epidermis. *Nat Immunol* **10**, 249-256, doi:10.1038/ni.1700 (2009).

210 Garsin, D. A. *et al*. Long-lived C. elegans daf-2 mutants are resistant to bacterial pathogens. *Science* **300**, 1921, doi:10.1126/science.1080147 (2003).

211 Evans, E. A., Chen, W. C. & Tan, M. W. The DAF-2 insulin-like signaling pathway independently regulates aging and immunity in C. elegans. *Aging Cell* **7**, 879-893, doi:10.1111/j.1474-9726.2008.00435.x (2008).

212 Reddy, K. C., Andersen, E. C., Kruglyak, L. & Kim, D. H. A polymorphism in npr-1 is a behavioral determinant of pathogen susceptibility in C. elegans. *Science* **323**, 382-384, doi:10.1126/science.1166527 (2009).

213 Pujol, N. *et al*. A reverse genetic analysis of components of the Toll signaling pathway in Caenorhabditis elegans. *Curr Biol* **11**, 809-821 (2001).

214 Valanne, S., Wang, J. H. & Ramet, M. The Drosophila Toll signaling pathway. *J Immunol* **186**, 649-656, doi:10.4049/jimmunol.1002302 (2011).

215 Pradel, E. *et al*. Detection and avoidance of a natural product from the pathogenic bacterium Serratia marcescens by Caenorhabditis elegans. *Proc Natl Acad Sci U S A* **104**, 2295-2300, doi:10.1073/pnas.0610281104 (2007).

216 Smith, E. S., Martinez-Velazquez, L. & Ringstad, N. A chemoreceptor that detects molecular carbon dioxide. *J Biol Chem* **288**, 37071-37081, doi:10.1074/jbc.M113.517367 (2013).

217 Bhattarai, N., Gunn, J. & Zhang, M. Chitosan-based hydrogels for controlled, localized drug delivery. *Adv Drug Deliv Rev* **62**, 83-99, doi:10.1016/j.addr.2009.07.019 (2010).

218 Bourgogne, A. *et al*. Large scale variation in Enterococcus faecalis illustrated by the genome analysis of strain OG1RF. *Genome Biol* **9**, R110, doi:10.1186/gb-2008-9-7-r110 (2008).

219 Nallapareddy, S. R., Singh, K. V. & Murray, B. E. Construction of improved temperature-sensitive and mobilizable vectors and their use for constructing mutations in the adhesin-encoding acm gene of poorly transformable clinical Enterococcus faecium strains. *Appl Environ Microbiol* **72**, 334-345, doi:10.1128/AEM.72.1.334-345.2006 (2006).

220 Barendt, S. M. *et al*. Influences of capsule on cell shape and chain formation of wild-type and pcsB mutants of serotype 2 Streptococcus pneumoniae. *J Bacteriol* **191**, 3024-3040, doi:10.1128/JB.01505-08 (2009).

221 Kleerebezem, M. *et al*. Complete genome sequence of Lactobacillus plantarum WCFS1. *Proc Natl Acad Sci U S A* **100**, 1990-1995, doi:10.1073/pnas.0337704100 (2003).

222 Bron, P. A., van Baarlen, P. & Kleerebezem, M. Emerging molecular insights into the interaction between probiotics and the host intestinal mucosa. *Nat Rev Microbiol* **10**, 66-78, doi:10.1038/nrmicro2690 (2012).

223 Kaiser, P., Diard, M., Stecher, B. & Hardt, W. D. The streptomycin mouse model for Salmonella diarrhea: functional analysis of the microbiota, the pathogen's virulence factors, and the host's mucosal immune response. *Immunol Rev* **245**, 56-83, doi:10.1111/j.1600-065X.2011.01070.x (2012).

224 Santiviago, C. A. *et al*. Analysis of pools of targeted Salmonella deletion mutants identifies novel genes affecting fitness during competitive infection in mice. *PLoS Pathog* **5**, e1000477, doi:10.1371/journal.ppat.1000477 (2009).

225 Kelley, L. A. & Sternberg, M. J. Protein structure prediction on the Web: a case study using the Phyre server. *Nat Protoc* **4**, 363-371, doi:10.1038/nprot.2009.2 (2009).

226 Lupas, A., Van Dyke, M. & Stock, J. Predicting coiled coils from protein sequences. *Science* **252**, 1162-1164, doi:10.1126/science.252.5009.1162 (1991).

227 Petersen, T. N., Brunak, S., von Heijne, G. & Nielsen, H. SignalP 4.0: discriminating signal peptides from transmembrane regions. *Nat Methods* **8**, 785-786, doi:10.1038/nmeth.1701 (2011).

228 Singer, J. T. *et al*. Broad-host-range plasmids for red fluorescent protein labeling of gram-negative bacteria for use in the zebrafish model system. *Appl Environ Microbiol* **76**, 3467-3474, doi:10.1128/AEM.01679-09 (2010).

229 Bloemberg, G. V., O'Toole, G. A., Lugtenberg, B. J. & Kolter, R. Green fluorescent protein as a marker for Pseudomonas spp. *Appl Environ Microbiol* **63**, 4543-4551 (1997).

230 Podbielski, A., Spellerberg, B., Woischnik, M., Pohl, B. & Lutticken, R. Novel series of plasmid vectors for gene inactivation and expression analysis in group A streptococci (GAS). *Gene* **177**, 137-147 (1996).

231 Dunny, G. M., Lee, L. N. & LeBlanc, D. J. Improved electroporation and cloning vector system for gram-positive bacteria. *Appl Environ Microbiol* **57**, 1194-1201 (1991).

232 Rangan, K. J., Yang, Y. Y., Charron, G. & Hang, H. C. Rapid visualization and large-scale profiling of bacterial lipoproteins with chemical reporters. *J Am Chem Soc* **132**, 10628-10629, doi:10.1021/ja101387b (2010).

233 Shaham (ed.), S. Methods in cell biology. *WormBook*, 1551-8507, doi:10.1895/wormbook.1.49.1 (2006).

234 Lundquist, E. A., Reddien, P. W., Hartwieg, E., Horvitz, H. R. & Bargmann, C. I. Three C. elegans Rac proteins and several alternative Rac regulators control axon guidance, cell migration and apoptotic cell phagocytosis. *Development* **128**, 4475-4488 (2001).

235 Matsumoto, M. *et al*. Impact of intestinal microbiota on intestinal luminal metabolome. *Sci Rep* **2**, 233, doi:10.1038/srep00233 (2012).

236 Natividad, J. M. *et al*. Commensal and probiotic bacteria influence intestinal barrier function and susceptibility to colitis in Nod1-/-; Nod2-/- mice. *Inflamm Bowel Dis* **18**, 1434-1446, doi:10.1002/ibd.22848 (2012).

237 Asong, J., Wolfert, M. A., Maiti, K. K., Miller, D. & Boons, G. J. Binding and Cellular Activation Studies Reveal That Toll-like Receptor 2 Can Differentially Recognize Peptidoglycan from Gram-positive and Gram-negative Bacteria. *J Biol Chem* **284**, 8643-8653, doi:10.1074/jbc.M806633200 (2009).

238 Travassos, L. H. *et al*. Toll-like receptor 2-dependent bacterial sensing does not occur via peptidoglycan recognition. *EMBO Rep* **5**, 1000-1006, doi:10.1038/sj.embor.7400248 (2004).

239 Cario, E., Gerken, G. & Podolsky, D. K. Toll-like receptor 2 enhances ZO-1-associated intestinal epithelial barrier integrity via protein kinase C. *Gastroenterology* **127**, 224-238 (2004).

240 Girardin, S. E. *et al*. Peptidoglycan molecular requirements allowing detection by Nod1 and Nod2. *J Biol Chem* **278**, 41702-41708, doi:10.1074/jbc.M307198200 (2003).

241 Lee, J. *et al*. pH-dependent internalization of muramyl peptides from early endosomes enables Nod1 and Nod2 signaling. *J Biol Chem* **284**, 23818-23829, doi:10.1074/jbc.M109.033670 (2009).

242 Vavricka, S. R. *et al*. hPepT1 transports muramyl dipeptide, activating NF-kappaB and stimulating IL-8 secretion in human colonic Caco2/bbe cells. *Gastroenterology* **127**, 1401-1409 (2004).

243 Viala, J. *et al*. Nod1 responds to peptidoglycan delivered by the Helicobacter pylori cag pathogenicity island. *Nat Immunol* **5**, 1166-1174, doi:10.1038/ni1131 (2004).

244 Dziarski, R. & Gupta, D. The peptidoglycan recognition proteins (PGRPs). *Genome Biol* **7**, 232, doi:10.1186/gb-2006-7-8-232 (2006).

245 Wang, Z. M. *et al*. Human peptidoglycan recognition protein-L is an N-acetylmuramoyl-L-alanine amidase. *J Biol Chem* **278**, 49044-49052, doi:10.1074/jbc.M307758200 (2003).

246 Gelius, E., Persson, C., Karlsson, J. & Steiner, H. A mammalian peptidoglycan recognition protein with N-acetylmuramoyl-L-alanine amidase activity. *Biochem Biophys Res Commun* **306**, 988-994 (2003).

247 Lee, J., Geddes, K., Streutker, C., Philpott, D. J. & Girardin, S. E. Role of mouse peptidoglycan recognition protein PGLYRP2 in the innate immune response to

Salmonella enterica serovar Typhimurium infection in vivo. *Infect Immun* **80**, 2645-2654, doi:10.1128/IAI.00168-12 (2012).

248 Buist, G., Steen, A., Kok, J. & Kuipers, O. P. LysM, a widely distributed protein motif for binding to (peptido)glycans. *Mol Microbiol* **68**, 838-847, doi:10.1111/j.1365-2958.2008.06211.x (2008).

249 Mesnage, S. *et al*. Molecular basis for bacterial peptidoglycan recognition by LysM domains. *Nat Commun* **5**, 4269, doi:10.1038/ncomms5269 (2014).

250 Vollmer, W., Joris, B., Charlier, P. & Foster, S. Bacterial peptidoglycan (murein) hydrolases. *FEMS Microbiol Rev* **32**, 259-286, doi:10.1111/j.1574-6976.2007.00099.x (2008).